

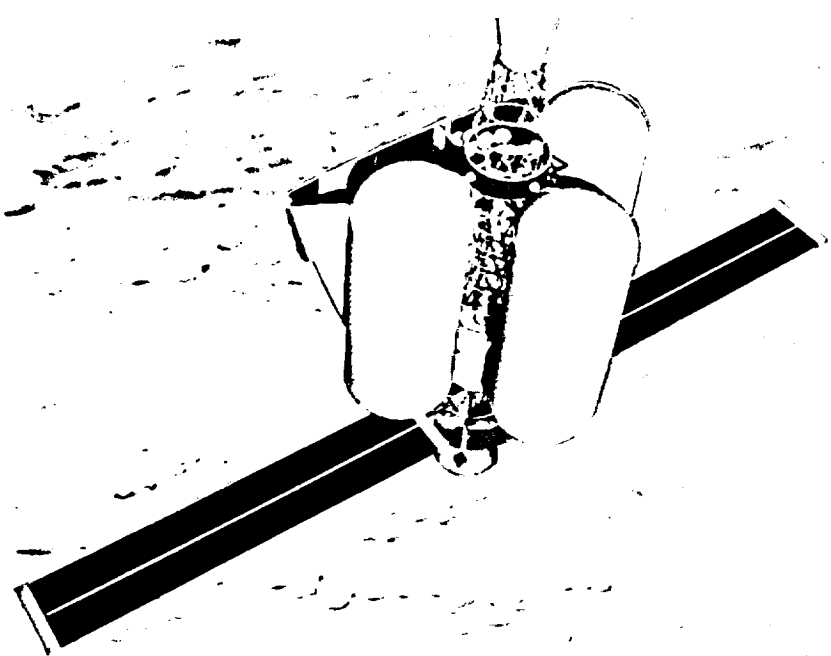
Space Transfer Concepts and Analysis for Exploration Missions



(NASA-CR-184301) SPACE TRANSFER CONCEPTS
AND ANALYSIS FOR EXPLORATION MISSIONS Final
Report (Boeing Co.) 237 p CSCL 22A

N92-22502

63/12 Unclas
0081280



Contract NAS8-37857
Final Report
December 1991

Boeing Defense & Space Group
Advanced Civil Space Systems
Huntsville, Alabama

D615-10045-2



BOEING

CAGE CODE

THIS DOCUMENT IS:

CONTROLLED BY Advanced Civil Space Systems
ALL REVISIONS TO THIS DOCUMENT SHALL BE APPROVED
BY THE ABOVE ORGANIZATION PRIOR TO RELEASE.

PREPARED UNDER CONTRACT NO.
 IR&D
 OTHER

PREPARED ON FILED UNDER
DOCUMENT NO. D615-10045-2 MODEL



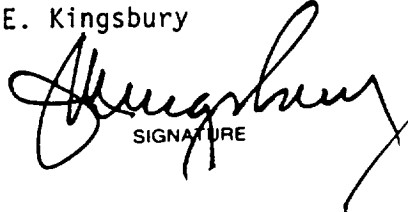
TITLE Space Transfer Concepts and Analysis for Exploration Missions,
Phase 2 Final Report

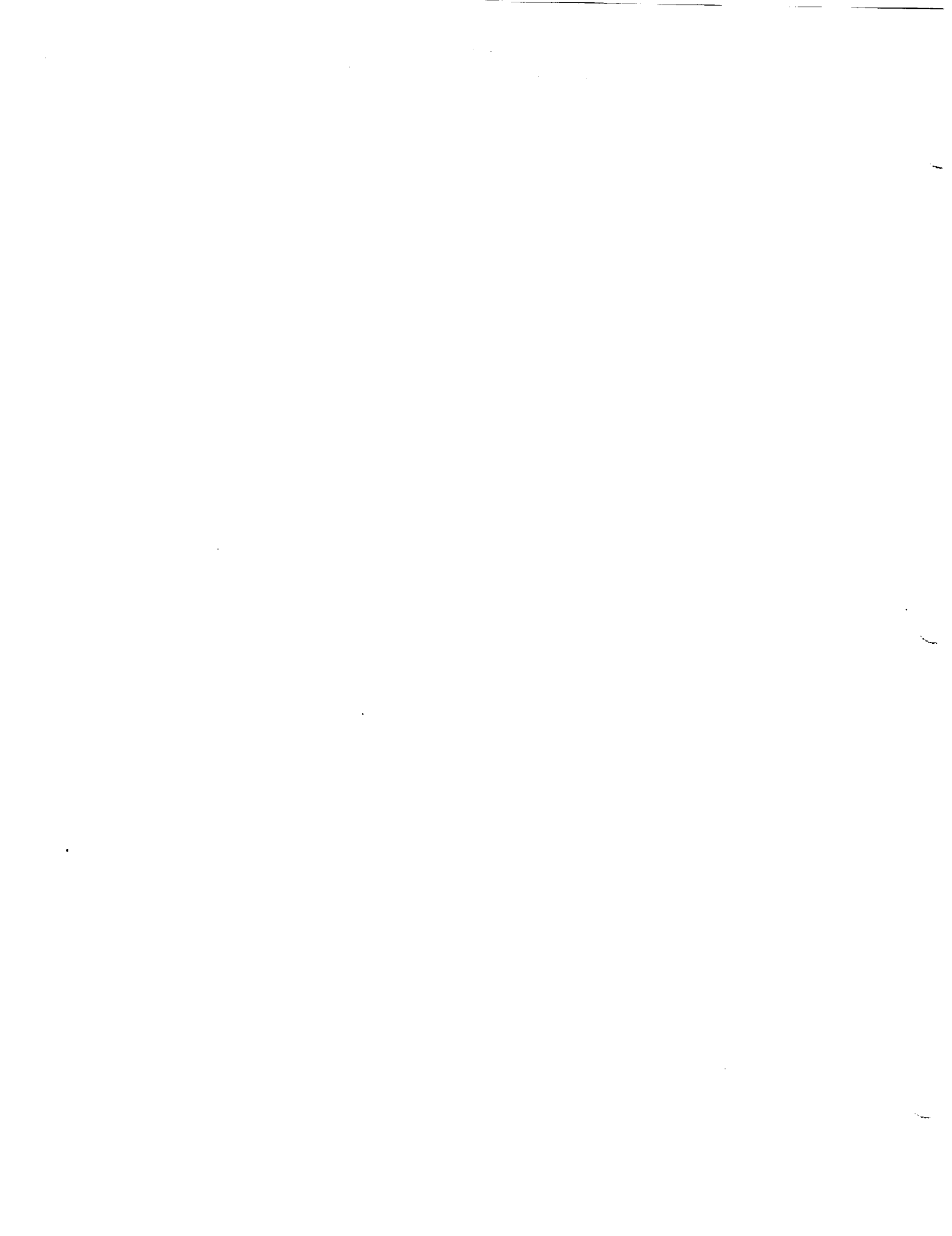
- THE INFORMATION CONTAINED HEREIN IS NOT PROPRIETARY.
 THE INFORMATION CONTAINED HEREIN IS PROPRIETARY TO THE BOEING COMPANY
AND SHALL NOT BE REPRODUCED OR DISCLOSED IN WHOLE OR IN PART OR USED FOR
ANY DESIGN OR MANUFACTURE EXCEPT WHEN SUCH USER POSSESSES DIRECT, WRITTEN
AUTHORIZATION FROM THE BOEING COMPANY.

ORIGINAL RELEASE DATE

ISSUE NO.	TO	DATE
-----------	----	------

ADDITIONAL LIMITATIONS IMPOSED ON THIS DOCUMENT
WILL BE FOUND ON A SEPARATE LIMITATIONS PAGE.

PREPARED BY	STCAEM Team	2-H895	91-12-20
CHECKED BY	Irwin E. Vas 	2-H895	91-12-20
SUPERVISED BY	Gordon R. Woodcock 	2-H895	91-12-20
APPROVED BY	J. E. Kingsbury 	2-H890	91-12-20
	SIGNATURE	ORGN	DATE



FOREWORD

The study entitled "Space Transfer Concepts and Analysis for Exploration Missions" (STCAEM) was performed by Boeing Missiles and Space, Huntsville, for the George C. Marshall Space Flight Center (MSFC). The current activities were carried out under Technical Directives 5 to 9 during the period February through September 1991. The Boeing program manager was Gordon Woodcock, and the MSFC Contracting Officer's Technical Representative was Alan Adams. Subcontractors to Boeing on this contract included: Aerojet Propulsion Division, Paul Hudson, Madison Research Corporation, and REMTECH, Incorporated. The task activities were led by M. Appleby, P. Buddington, B. Cothran, M. Cupples, B. Donahue, R. Fowler, J. Nordwall, B. Sherwood, and I. Vas, with technical support from J. Burrell, S. Capps, S. Doll, D. Eder, E. Fisher, M. Fouche, D. Harrison, S. LeDoux, J. McGhee, P. Ramsey, N. Rao, T. Ruff, A. Sane, R. Schorr, K. Stanley, R. Tanner, and B. Wallace.

ABSTRACT

This report covers the second phase of a broad-scoped and systematic study of space transfer concepts for human lunar and Mars missions. The study addressed issues that were raised during Phase 1, developed generic Mars missions profile analysis data, and conducted preliminary analysis of the Mars in-space transportation requirements and implementation from the Stafford Committee Synthesis Report.

ABBREVIATIONS AND ACRONYMS

a	Semi-major axis of an orbit
a0	Thrust Acceleration
A	Area
ACRV	Advanced Crew Recovery Vehicle
ACS	Attitude Control System
AFE	Aeroassist Flight Experiment
Al	Aluminum
ALARA	As Low as Reasonably Achievable
ALS	Advanced Launch System
ALSPE	Anomalous Large Solar Proton Event
ao	Thrust Acceleration
AOTV	Aeroassisted Orbit Transfer Vehicle
ASE	Airborne Support Equipment
AU	Astronomical Unit (=149.6 million km)
AXAF	Advanced X-Ray Astronomy Facility
BLAP	Boundary Layer Analysis Program
BFO	Blood-Forming Organs
BREM	Boeing Radiation Exposure Model
BRYNTRN	Baryon Transport Code
C	Temperature in Degrees Celsius
CAB	Cryogenic/Aerobrake
CAD/CAM	Computer-Aided Design/Computer-Aided Manufacturing
CAM	Computer Anatomical Man
CD	Drag Coefficient
CELSS	Closed Environmental Life Support System
CG	Center of Gravity
CHAP	Convective Heating and Ablation Program
CL	Life Coefficient
cm	Centimeter = 0.01 Meter
CM	Center of Mass
CMA	Charring Material Thermal Response and Ablation

CO ₂	Carbon Dioxide
COSPAR	Committee on Space Research of the International Council of Scientific Unions
C _p	Center of Pressure, specific heat at constant pressure
CREME	Cosmic Ray Effects on Micro-Electronics
CRV	Crew Recovery Vehicle, Crew Return Vehicle
CTV	Cargo Transfer Vehicle
C ₃	Hyperbolic Excess Velocity Squared (km ² /s ²)
d	Day
D	Drag
delta-V, ΔV	Velocity Change (m/s or km/s)
DLA	Declination of Launch Asymptote
DOD	Department of Defense
DRM	Design Reference Mission
DSN	Deep Space Network
ECLSS	Environmental Control and Life Support System
EMU	Extra-Vehicular Mobility Unit
EOC	Earth Orbit Capture
EOTV	Electric Orbit Transfer Vehicle
EP	Electric Propulsion
ET	External Tank
ETO	Earth-To-Orbit
EVA	Extra-Vehicular Activity
F	Temperature in Degrees Fahrenheit
FTS	Flight Telerobotic Servicer
F.T.	Flight Time
g	Acceleration in Earth Gravities (acceleration 9.80665m/s ²)
GCR	Galactic Cosmic Rays
GEO	Geosynchronous Earth Orbit
GOES	Geostationary Operational Environmental Satellite

HLLV	Heavy Lift Launch Vehicle
HLV	Heavy Launch Vehicle
HMEV	High Lift to Drag Mars Excursion Vehicle
H ₂	Hydrogen
h _s	Stagnation Enthalpy
HZE	High Atomic Weight and Energy Particles
HZETRN	Heavy-Ion Transport Code
IMLEO	Initial Mass in Low Earth Orbit
ISMU	<i>In-Situ</i> Materials Utilization
IVA	Internal Vehicular Activity
IR&D	Independent Research and Development
Isp	Specific Impulse (=thrust/mass flow rate)
J	Joule
JSC	Johnson Space Center
K	Temperature in Kelvin Units
kg	Kilograms
km	Kilometers
km/sec	Kilometers per Second
kWe	Kilo-watt Electric
L	Lift
L/D	Lift-To-Drag Ratio
LCV	Lunar Crew Vehicle
LEO	Low Earth Orbit
LET	Linear Energy Transfer
LEV	Lunar Excursion Vehicle
Level II	Space Exploration Initiative Project Office, Johnson Space Center
LH ₂	Liquid Hydrogen
LiOH	Lithium Hydroxide
LM	Lunar Module
LMEPO	Lunar Mars Exploration Program Office
LOR	Lunar Orbit Rendezvous
LSS	Life Support System

LTS	Lunar Transfer System
LTV	Lunar Transfer Vehicle
m	Meters
MAV	Mars Ascent Vehicle
M/C _D A	Ballistic Coefficient (mass/drag coefficient times area)
MEV	Mars Excursion Vehicle
MLI	Multilayer Insulation
MMU	Manned Maneuvering Unit
MOC	Mars Orbit Capture
MRCC	Mars Return Crew Capsule
m/s	Meters per Second
MSFC	Marshall Space Flight Center
mt	Metric Ton (1000kg)
MTA	Mars Transfer Habitat
MTH	Mars Transfer Habitat
MTV	Mars Transfer Vehicle
MWe	Megawatts Electric
M _∞	Free Stream Mach Number
N	Newton, Kilogram-Meters per Second Squared
n/a, N/A	Not Applicable
NASA	National Aeronautics and Space Administration
NCRP	National Council on Radiation Protection
NEP	Nuclear-Electric Propulsion
NERVA	Nuclear Engine for Rocket Vehicle Application
NLS	National Launch System
N(o)	Constant Related to the Size of the SPE
NOAA	National Atmospheric and Oceanic Administration
NRL	Naval Research Laboratory
NTP	Nuclear Thermal Propulsion
NTR	Nuclear Thermal Rocket
OTIS	Optimal Trajectories by Implicit Simulation Program
O ₂	Oxygen

P	Pressure
P _B	Base Pressure
P _c	Chamber Pressure
PDOSE	Proton Dose Code
P(o)	Characteristic Rigidity of the Particle Spectrum, MV
PT	Total Pressure Behind Normal Shock
PROMULGATE	Low-Thrust Interplanetary Trajectory Analysis Code
psi	Pounds per Square Inch
PSS	Planet Surface Systems
PVA	Photovoltaic Array
P _∞	Free Stream Pressure
q	Heat Flux (Watt per Square Centimeter)
Q	Heat Flux (Joules per Square Centimeter), Radiation Quality Factor
r	Planetary Radius to Vehicle
r ^Λ Z	Correlation Factor
RCS	Reaction Control System
Re	Reynolds Number
RF	Radio Frequency
RFC	Regenerative Fuel Cell
ROI	Return on Investment
RWA	Relative Wind Angle
R&D	Research and Development, Rendezvous and Docking
R _B	Body Radius, Aerobrake
s	Seconds
S	Planetocentric Unit Vector Pointing in the Direction of the V _{inf} Vector
SDIO	Strategic Defense Initiative Organization
sec	Seconds
SEI	Space Exploration Initiative
SEP	Solar-Electric Propulsion
sol	Solar Day (24.6 hours for Mars)
SPE	Solar Proton Events
SPESPEC	Solar Proton Event Spectrum

SSF	Space Station Freedom
SSME	Space Shuttle Main Engine
STCAEM	Space Transfer Concepts and Analysis for Exploration Missions
STME	Space Transportation Main Engine
STS	Space Transportation System
t	Metric Tons (1000kg)
TEI	Trans-Earth Injection
TEIS	Trans-Earth Injection Stage
TMI	Trans-Mars Injection
TPS	Thermal Protection System
T/W	Thrust to Weight Ratio
T _w	Wall Temperature
VECTRACE	Vector Trace
V _{hp}	Velocity, relative to a central body of a spacecraft a great distance from the central body
W	Weight
W/C _d A	Ballistic Coefficient
W/cm ²	Watts per Square Centimeter (also Wcm ⁻²)
WP	Work Package
zero-g	An Unaccelerated Frame of Reference, Free-fall
Δ	Delta
σ	Standard Deviation
μg	Microgravity
α	Angle of a Attack, Degrees Specific mass, power and propulsion dry mass divided by electric thruster input power, kg/kW _e
β	Ballistic Coefficient (m/C _D A, kg/m ²)
θ _s	Expansion Angle, Degrees
γ	Specific Heat Ratio
φ	Angle Between S and the Planetary Closest Approach Radius Vector
ε	Eccentricity of an Orbit
∞	Infinity, Free Stream Conditions

CONTENTS

	<u>Page</u>
1.0 EXECUTIVE SUMMARY	1
1.1 STUDY OVERALL SCOPE	1
1.2 ORGANIZATION OF THIS REPORT	1
1.3 SYNOPSIS OF PHASE 1 RESULTS	2
1.3.1 Lunar Missions	3
1.3.2 Mars Mission Profiles	4
1.3.3 Mars Transfer Propulsion Systems and Profile Considerations	4
1.3.4 Performance, Cost, and Evaluation Summary	7
1.4 PHASE 2 RESULTS	11
1.4.1 Summary of Issues	11
1.4.2 Issues from Phase 1	12
1.4.3 Synthesis Architecture Analyses	28
1.4.4 MEV Subsystems	36
1.4.5 Reference NTP Mission and Operations Scenarios	39
1.4.6 Appropriate Size of Heavy Lift Launch Vehicle	43
1.5 OVERVIEW OF STCAEM RESULTS TO DATE	44
1.5.1 Synthesis Architectures	44
1.5.2 Architecture Implementation from the Transportation Viewpoint	44
1.5.3 Lunar Missions and Lunar Transportation	45
1.5.4 Mars Transfer Propulsion and Aerobraking	46
1.5.5 MEV Lift-to-Drag Ratio	46
1.5.6 Cargo Requirements	46
1.5.7 ETO Transportation and HLV Size	47
2.0 VEHICLE INTEGRATION	48
2.1 INTRODUCTION	48
2.2 LUNAR CAMPSITE CONCEPTS	48
2.3 HIGH-L/D MARS EXCURSION VEHICLE (HMEV)	51
2.3.1 Mission Payloads	51
2.3.2 HMEV Design Drivers and Concept Evolution	53
2.4 NUCLEAR THERMAL PROPULSION MARS TRANSFER VEHICLE (NTP MTV)	61
2.4.1 NTP Design Drivers and Concept Evolution	62
2.4.2 Airlock	71
2.4.3 Cargo MTV Concepts	71
2.5 MICROGRAVITY-OPTIMIZED NUCLEAR ELECTRIC PROPULSION MARS TRANSFER VEHICLE (NEP MTV)	72
3.0 AEROBRAKE INTEGRATION	75
3.1 LUNAR CREW RETURN VEHICLE THERMAL PROTECTION SYSTEM ANALYSIS	75
3.1.1 Trajectory	75
3.1.2 Apollo Configuration Baseline	76
3.1.3 CHAP Ablative Materials Comparison	77
3.1.4 Lunar CRV TPS Mass Estimate	78
3.1.5 Summary	82

	<u>Page</u>
3.2 MARS CREW RETURN VEHICLE THERMAL PROTECTION	
SYSTEM ANALYSIS	82
3.2.1 Trajectory	82
3.2.2 Temperature Profile	85
3.3 HIGH L/D MARS EXCURSION VEHICLE	85
3.3.1 Aerodynamic Predictions	85
3.3.2 HMEV Concepts	86
3.4 AEROBRAKE STRUCTURES	90
3.5 LUNAR TRANSFER VEHICLE (LTV) WAKE ANALYSIS	94
3.5.1 Flight Conditions	96
3.5.2 Shear Layer Edge	96
3.5.3 Inviscid Flowfield Analysis	102
3.5.4 Wake Volumes	103
3.5.5 Wake Heating	104
3.6 MAIN ENGINE GIMBAL ANGLES	106
4.0 ASSEMBLY OPERATIONS	108
4.1 ON-ORBIT ASSEMBLY OPERATIONS	108
4.2 MADISON RESEARCH DATABASE	122
5.0 TRANSPORTATION CREW MODULES AND HABITAT	125
5.1 INTRODUCTION	125
5.2 MARS TRANSFER HABITAT	125
5.3 CREW RETURN VEHICLES	130
5.4 LUNAR EXCURSION MODULE	133
6.0 RADIATION ANALYSIS	135
6.1 INTRODUCTION	135
6.2 MODELS AND METHODS	135
6.2.1 Background and Description of the Analysis	135
6.2.2 Natural Radiation Environment Models	135
6.2.3 The Boeing Radiation Exposure Model	138
6.2.4 Solid Modeling	142
6.3 ANALYSIS RESULTS	143
6.3.1 Mars Transfer Habitat, Artificial Gravity	143
6.3.2 Mars Crew Return Vehicle	149
6.3.3 Mars Transfer Habitat, Zero-g	154
6.4 CONCLUSIONS AND RECOMMENDATIONS	157
7.0 ELECTRIC PROPULSION PERFORMANCE PARAMETRICS	162
7.1 INTERPOLATION SCHEME	163
7.2 SPECIFICATIONS DOCUMENT	167
7.3 DATA GENERATION	167
7.4 INTERPOLATION SUBROUTINE	167
8.0 FLIGHT MECHANICS SUPPORT	169
8.1 INTRODUCTION	169
8.2 THREE-BURN EARTH LAUNCH WINDOW ANALYSIS	169
8.2.1 Analysis Approach and Discussion	170

	<u>Page</u>
8.2.2 Earth Launch Window Analysis Results	172
8.3 CARGO MISSIONS DELTA-V ANALYSIS	174
8.4 EARTH/MARS LAUNCH WINDOWS	176
8.5 PARKING ORBIT ANALYSIS	183
8.6 MARS MISSIONS DELTA-V AND TIMELINE	184
8.6.1 2014 and 2016 Piloted Delta-V Comparison	184
8.6.2 Level II and Boeing Delta-V, Optimal Elliptical Parking Orbits	185
8.6.3 Mission Time Line	185
8.7 LANDING ANALYSIS FOR 2014 MISSION	187
8.8 NUCLEAR REACTOR DISPOSAL	192
9.0 VEHICLE APPLICATION AND ABORT OPTIONS	197
9.1 VEHICLE APPLICATIONS AND ABORT OPTIONS TO THE SYNTHESIS GROUP REPORT MARS ARCHITECTURES	197
9.2 VEHICLE DESCRIPTIONS	199
9.2.1 Flight One: 2010 Lunar Dress Rehearsal Mission	199
9.2.2 Flight Two: 2012 First Cargo Mission	200
9.2.3 Flight Three: 2014 First Piloted Mission-Opposition Class	201
9.2.4 Mars Crew Transportation System Operational Description	201
9.2.5 Launch Vehicle Flight 1	203
9.2.6 Launch Vehicle Flight 2	204
9.2.7 Launch Vehicle Flight 3	204
9.2.8 Launch Vehicle Flight 4 and 5	204
9.2.9 Flight Four: 2014 Second Cargo Mission	204
9.2.10 Flight Five: 2016 Second Manned Mission- Conjunction Class	204
9.3 MISSION OPTIONS DESCRIPTIONS	205
9.3.1 Option One: MEV Direct Entry vs MEV Descent Only Comparison	205
9.3.2 Option Two: MEV Accommodation	205
9.3.3 Option Three: Aborts Comparison	207
9.3.4 Option Four: Mars Flyby Abort Options	209
9.3.5 Option Five: Piloted MEV Placement	209
9.3.6 Mars Architecture Vehicle Fleet Development	211
9.3.7 Identifying Avenues to Fleet Cost	212
9.4 NTP BASELINE AND OPTIONS	214
10.0 CONCLUDING REMARKS	216

FIGURES

	<u>Page</u>
1-1 Representative Opposition and Conjunction Mars Round Trip Mission Profiles	5
1-2 Propulsion Applicability to Mars Mission Profiles	6
1-3 Opposition Profile Trip Time Trends for 120-Ton Payload	6
1-4 Propulsion Option Comparison for Resupply Mass and Reusability	8
1-5 In-Space Transportation DDT&E Comparison	8
1-6 Preferred Transportation Options for Range of Activity Levels	10
1-7 Alignment Requirements for Minimum Energy Elliptic Orbit MOC and TEI	13
1-8 Selected Orbit for 2014 Opposition Crew Mission	14
1-9 Orbit Parameters for 2014 Opposition Crew Mission, Showing Orbit Selection for Favorable Periapsis Lighting	15
1-10 Ground Tracks for High L/D Landing from 2014 Elliptic Orbit	16
1-11 Free-Flyer Assembly Platform for NTP	17
1-12 Integral-Launch Assembly Platform for NTP	18
1-13 Integral-Launch High L/D Mars Excursion Vehicle	19
1-14 Mars Cargo MEV and In-Space Transportation Integral Launch Options	20
1-15 Results of Preliminary Manifesting Analyses for Range of ETO Launch Vehicle Payload Capability	21
1-16 Calculated Integral Shield Distribution for Mars Crew Return Vehicles	22
1-17 Calculated Dose Equivalents Resulting from Third 12-Hour Period of 19 October 1989 Solar Flare	22
1-18 CRV Integrated Heat Load Comparison (Mars Return Entry Velocity 13.1 km/sec, Corresponds to $C3=50 \text{ km}^2/\text{sec}^2$)	23
1-19 Infrastructure Concept for Laser Power Beaming to the Moon and Electric Orbit Transfer Vehicles	25
1-20 Typical Laser Beam Power Electric Orbit Transfer Results	26
1-21 Trade and Option Tree for Analysis of Synthesis Architecture Implementations	29
1-22 Design Reference Delta-V Sets for Synthesis Mars Architecture Implementation	32
1-23 Mars NTP Configuration	33
1-24 Deployable Low L/D Landing Aerobrake Concept	37
1-25 Earth Orbit Assembly and Mission Timelines for 2014 Mars Mission	42

	<u>Page</u>
1-26 Launch Vehicle Sizing Rationale Summary	44
2-1 Lunar Campsite Mission Mode	49
2-2a Lunar Campsite Vehicle Concept	50
2-2b Lunar Crew Vehicle Concept (LCV)	50
2-3a Short-Stay Landed Payload Comparison	52
2-3b Long-Stay Landed Payload Comparison	52
2-4a L/D = 1.6 Mars Excursion Vehicle Concept (HMEV)	54
2-4b Cargo HMEV Lander on Mars	55
2-4c HMEV Crew-Carrying Vehicle Anatomy	56
2-5 Reference HMEV Mass Summary	56
2-6 Mars Ascent Vehicle (MAV)	57
2-7a Cargo Lander Anatomy	58
2-7b Crew Lander Anatomy	59
2-8 HMEV Aerobrake Jettison Scenario	60
2-9 HMEV Reference Launch Scenario	61
2-10a Nuclear Thermal Mars Transfer Vehicle Concept (NTP)	63
2-10b NTP Vehicle General Arrangement	64
2-11 NTP Concept Baseline Mass Summary	65
2-12a Hydrogen Tank Schematic	66
2-12b Nuclear Thermal Engine Schematic	67
2-13 Amidships Crossfeed Bay	68
2-14 Propulsion Subsystems Configuration	69
2-15 Forward Subsystems Superstructure	70
2-16 Reference Airlock Mass Summary	72
2-17a Nuclear Electric Microgravity Mars Transfer Vehicle Concept (μ g-NEP)	73
2-17b μ g-NEP Vehicle General Arrangement	74
3-1 CRV Lunar Return Entry Trajectory	76
3-2 CRV Lunar Return Heating Rates	76
3-3 Apollo Configuration Baseline	77
3-4 CHAP Output	79
3-5 CHAP Ablative Materials Comparison	80
3-6 Required Thickness Along Centerline	80
3-7 Equilibrium Wall Temperature	81
3-8 Lunar CRV TPS Mass Estimate	81

	<u>Page</u>
3-9 CRV Mars Return Earth Entry Trajectory	83
3-10 CRV Mars Return Heating Rates	84
3-11 CRV Integrated Stagnation Point Heat Load	84
3-12 HMEV Aerobrake Shape Concepts	86
3-13 Shape Parameters and Resultant Force Vectors for Concept 1	87
3-14 Shape Parameters and Resultant Force Vectors for Concept 2	88
3-15 Shape Parameters and Resultant Force Vectors for Concept 3	89
3-16 Concepts Lift to Drag Parameter	90
3-17 High L/D Mars Excursion Vehicle	91
3-18 Finite Element Model with Loads	92
3-19 Scaled Load Vectors, Left Side View	92
3-20 Aerobrake Structural Integration	93
3-21 Sandwich Configuration Cross-Section (Constant)	94
3-22 Composite Properties	94
3-23 Material Properties, 700°C and Room Temperature	95
3-24 Lunar Return Aerobrake Configurations	95
3-25 Flight Conditions at Peak Heating as a Function of Lift to Drag Ratio .	96
3-26 Peak Heating Condition Carpet Plot	97
3-27 Theoretical Expansion Angle Range	99
3-28 Expansion Angle Versus Mach Number for Gamma of 1.4	99
3-29 Measured Shear Layer Turning Angle Versus Theoretical Value	100
3-30 Measured Shear Layer Edge Angle Data to Theory Ratio	101
3-31 Base Pressure Effect on Wake Expansion Angle	101
3-32a Boundary Layer Edge Equilibrium Air Specific Heat Ratio at Lunar Return Peak Heating Conditions	102
3-32b Finite Rate Air Specific Heat Ratio at Lunar Return Peak Heating Conditions	103
3-33 Volumes of the Three Aerobrake Configurations	104
3-34 Wake Volumes of a Circular Body	105
3-35 Heating Sample Case	106
3-36 HLLV MEV Configuration STME Nozzle Angles	107
4-1 2nd NTP Platform Assessment	109
4-2 I-Beam on Typical NTP Configuration	110
4-3 Basic Truss Stowed Configuration	110
4-4 Basic NTP Platform Structure	111

	<u>Page</u>
4-5 Platform Translated Forward	112
4-6 General Platform Service System	112
4-7 Assembly Platform-A, Top View	113
4-7 Assembly Platform-B, Side View	113
4-8 Assembly Platform Parts List - A	114
4-8 Assembly Platform Parts List - B	114
4-8 Assembly Platform Parts List - C	115
4-8 Assembly Platform Parts List - D	115
4-8 Assembly Platform Parts List - E	116
4-9 NTP Platform Initial Deployment	117
4-10 NTP Platform Full-Up Configuration	117
4-11 Preliminary on Orbit Assembly "Walker"	118
4-12 NTP Assembly Sequence with Assembly Platform Deployment	120
4-13 NTP "Saddle" Assembly Platform	121
4-14 "Saddle" Platform on the New NTP Central Truss	122
4-15 Data Needs Catalog, Report Format 1	123
4-16 Data Needs Catalog, Report Format 2	124
4-17 Data Needs Catalog, Report Format 3	124
5-1 Induced Gravity Transfer Habitat, 6 Crew	126
5-2 Microgravity Hab Structural Concept	127
5-3 Microgravity Transit Hab	128
5-4 Shielding Strategy	129
5-5 Transit Hab Mass Analysis, 6 Crew	129
5-6 CRV Shape Options	130
5-7 Mars CRV Configuration	131
5-8 Mars CRV Mass Estimate	131
5-9 Lunar CRV Configuration	132
5-10 Lunar CRV Mass Estimate	132
5-11 Lunar Excursion Crew Module	133
5-12 Lunar Excursion Crew Module Mass Estimate	134
6-1 Radiation Sources	136
6-2 Zurich Smoothed Sunspot Number and Proton Fluence for Solar Cycles 19, 20, and 21	137
6-3 Flux/Energy Distributions for August '72 and October '89 Solar Proton Events	138

	<u>Page</u>
6-4 GCR Spectra and August '72 Solar Proton Event	139
6-5 The Boeing Radiation Exposure Model Analysis Method	140
6-6 VECTRACE Shield Distribution Analysis System	141
6-7 Listing of Materials Defined in Analysis	143
6-8 Current NCRP Recommended Exposure Limits	144
6-9 Analysis Grid Layout for Mars Transfer Habitat	144
6-10 Rem/Year to Blood Forming Organs	145
6-11 Rem/Hour to Blood Forming Organs	146
6-12 Habitat Proximity and Work Schedule	147
6-13 Mission Exposure from Galactic Cosmic Radiation	148
6-14 Galley Grid Layout	148
6-15 Iso-dose Contours of Dose Equivalent (rem) to BFO from August '72 SPE	149
6-16 Iso-dose Contours of Dose Equivalent (rem) to BFO for Oct. '89 SPE	150
6-17 NOAA 5 Minute Data Set for Initial 36 Hours of October 19, 1989 SPE	150
6-18 P(o) and N(o) and Generated 12 Hour Flux Energy Distributions	152
6-19 Cut-away Image of CRV and Crew Positions	152
6-20 Dose Equivalent Resulting From Initial 12 Hours of 19 Oct., '89 SPE ..	153
6-21 Dose Equivalent Resulting From Third 12 Hours of 19 Oct., '89 SPE ...	153
6-22 Differential Shield Distribution for Couch Positions 4 and 5	154
6-23 MTV Habitat Radiation Analysis Scope	155
6-24 Proximity of MOC and TMI Tanks to Habitat	156
6-25 Out-bound Exposure to BFO from GCR	157
6-26 In-bound Exposure to BFO from GCR	158
6-27 Out-bound Exposure to BFO August '72 SPE	159
6-28 In-bound Exposure to BFO August '72 SPE	160
7-1 Low Thrust Mars Mission Mapping Project Software Systems	162
7-2 Comparisons of (a) Linear and (b) Cubic Interpolations	164
7-3 Cubic Interpolations for Several Values of Flight Time and Thrust Acceleration	165
7-4 Variation of Costate Variable with Isp	165
7-5 Thrust Acceleration (mm/sec ²)	166

	<u>Page</u>
8-1 Three-Burn Departure Launch Window Diagram	170
8-2 Turn Angle Versus TMI C3	171
8-3 Plane Change Requirements for 2014 Mars Opportunity, 200-Day Transfer	172
8-4 Plane Change Requirements for 2014 Mars Opportunity, 150-Day Transfer	173
8-5 Plane Change Delta-Vs For Range of Elliptic Orbit Periods	173
8-6 Mars Cargo Missions Delta-V	175
8-7 2014 Cargo and Crew TMI Window	175
8-8 2014 Crew Return Window	177
8-9 2014 Crew Return Vhp at Earth	177
8-10 2014 Abort From Surface Window Analysis	178
8-11 2014 C3 Mars Departure Contour, Deep Space Maneuver	179
8-12 2014 Vhp Mars Departure Contour, Deep Space Maneuver	179
8-13 2016 Crew Return Window	180
8-14 2016 Crew Return Vhp at Earth	180
8-15 2016 Abort from Surface Window Analysis	181
8-16 2016 C3 Mars Departure Contour, Deep Space Maneuver	181
8-17 2016 Vhp Mars Departure Contour, Deep Space Maneuver	182
8-18 2014 Trajectory Trace and Parking Orbit	183
8-19 2014 Parking Orbit Periapsis Lighting and Departure Delta-V	184
8-20 Mars Piloted Mission Delta-Vs	185
8-21 Mission Delta-V Data	186
8-22 Reference Delta-V Set, Level II	186
8-23 Mars Missions Time Line, 2012-2018	187
8-24 2014 Descent Diagram	188
8-25 Relative Wind Angle Definition	189
8-26 Landing Analysis Results	189
8-27 Ground Trace	190
8-28 Altitude Time History	191
8-29 Velocity Time History	192
8-30 Bank Angle Time History	193
8-31 Relative Wind Angle Time History	194
8-32 Case 1 Descent Trajectory Dynamic Pressure	195
8-33 Case 2 Descent Trajectory Dynamic Pressure	195

	<u>Page</u>
8-34 Case 3 Descent Trajectory Dynamic Pressure	196
8-35 Case 4 Descent Trajectory Dynamic Pressure	196
9-1 Synthesis Report Mars Architecture Timeline	198
9-2 2012 Cargo and 2014 Piloted Vehicle Mission Profiles	198
9-3 Lunar Dress Rehearsal Vehicle Data Set	200
9-4 2014 Piloted Vehicle Data Set and Representative 150 Ton Launch Vehicle Manifest	201
9-5 2014 Second Cargo Mission, 3 MEV Transfer Vehicle	205
9-6 2012 Cargo Vehicle IMLEO Variation with Entry Mode and Earth Return Option	206
9-7 2014 Cargo Mission IMLEO Variation with Transfer Vehicle Number ..	206
9-8 2016 Conjunction Piloted Vehicle IMLEO Variation with Trip Time, Orbit Selection, and Surface Abort Period	208
9-9 2016 Conjunction Mission Abort Option Trip Reduction Analysis	209
9-10 2016 320-Day Transfer, Conjunction Mission, Flyby Abort Mode, IMLEO Variation with Earth Return Mode	210
9-11 2014 and 2016 IMLEO Variation with MEV Placement	210
9-12 Vehicle Fleet Application to Synthesis Report Mars Architecture	211
9-13 Avenues to Mars Architecture Fleet Cost: Trajectory Options 5	213
9-14 Avenues to Mars Architectures Fleet Cost: Non-trajectory Option 5 ..	214
9-15 Mars Nuclear Thermal Propulsion Baselines and Options	215

1.0 EXECUTIVE SUMMARY

1.1 STUDY OVERALL SCOPE

The Space Transfer Concepts and Analysis for Exploration Missions (STCAEM) study addresses in-space transportation systems for human exploration missions to the Moon and Mars. The subject matter includes orbit-to-orbit transfer vehicles, planetary landing/ascent vehicles, and the crew modules needed to form complete crew and cargo transportation systems. Also included are orbital assembly and operations facilities as needed for assembly, construction, recovery, storage in orbit, and processing in-space transportation systems for reuse, as well as significant impacts to, and new requirements for, ground processing capabilities are also included. All propulsion and systems technologies that can be technically quantified are considered and evaluated. Excluded from the study are Earth-to-orbit (ETO) and return transportation systems and their ground processing and launch facilities. Crew Earth entry vehicles (crew recovery vehicles, CRVs) intended for direct Earth atmosphere entry from a lunar or planetary return trajectory are included. Capabilities of, and constraints on, ETO systems and their operations were parametrically considered as a boundary condition on the in-space systems.

The previous work, STCAEM Phase 1, covered a wide range of transportation options, reference 1, and lunar rover concepts and technology needs. The current work, Phase 2, concentrated on Mars transportation using nuclear thermal propulsion. Both phases were trade study oriented.

1.2 ORGANIZATION OF THIS REPORT

This report begins with a synopsis of results from STCAEM Phase 1, followed by a summary of Phase 2 results, then followed by the main body of the report. Early in this phase, the Stafford Synthesis Report, *America at the Threshold*, was released (ref. 2); Phase 2 conducted preliminary Mars transportation analyses for the Synthesis architectures. The summary briefly describes results of work performed in response to issues raised by Phase 1 and the Synthesis architecture analysis results. The summary is not work breakdown structure oriented. The body of this report covers detailed results of the Phase 2 tasks according to the work breakdown structure specified in the applicable task directives.

1.3 SYNOPSIS OF PHASE 1 RESULTS

STCAEM Phase 1 performed parametric studies of lunar and Mars in-space transportation, emphasizing performance and cost considerations. The first 6 months of the study was mainly dedicated to supporting the NASA "90-Day Study" of Space Exploration Initiative (SEI) missions (ref. 3), and initiated trade studies of Mars transportation propulsion options; the following 12 months of Phase 1 conducted broad-scope trade studies. Phase 1 rover studies were separately reported.

Boeing postulated a range of mission activity levels for lunar and Mars missions, ranging from a few human trips to each body up to significant scales of permanent and continuous human operations on both. This range was intended to test the validity of transportation system analysis results over a wide range of requirements. After the Synthesis Report was released, the STCAEM study changed to the Synthesis architectures as the reference for analysis.

Lunar transportation analyses were a small part of the overall study since concurrent contracts were focused almost exclusively on lunar missions. This study surveyed lunar mission modes, traded vehicle staging and staging orbit locations, and reuse. Only cryogenic chemical and aerobraking technologies were evaluated. Lunar crew module concepts were developed with mass and cost estimates.

Mars transfer vehicle (MTV) analyses considered all relevant technologies, including cryogenic chemical (a) all-propulsive and (b) with aerobraking for Mars aerocapture; nuclear solid core thermal propulsion; nuclear gas core thermal propulsion; and nuclear and solar electric propulsion, all over plausible ranges of their performance capabilities. The study did not include solar sailing -- sail sizes required for crew missions are at least tens of square kilometers; nor magnetic sails -- more work is needed on the concept to establish technical characteristics information needed for mission/systems analysis; nor nuclear fusion propulsion -- valid technical characteristics of such a system are not available.

Mars excursion vehicle (MEV, performs Mars landing and ascent) propulsion options included oxygen-hydrogen cryogenic, Earth storable, metal-gel fuel Earth storable, and oxygen-methane cryogenic propulsion. All MEV concepts considered used aerobraking for Mars entry and descent, with transition to rocket propulsion for final deceleration to landing. Single-stage, partially staged, and two-stage systems were considered. MEV options for Phase 1 landed a crew and cargo mix for surface stays up to 60 days, with additional cargo-only landers to support long-duration stay missions.

The baseline crew for Mars missions was four people. Sensitivity studies were performed, evaluating the impact of crew sizes up to 32 on Mars mission propulsion

technology choice. A crew skills analysis late in the study highly recommended a crew of six as the minimum appropriate for Mars missions. Crew considerations analyzed for Mars missions included long-duration transfer habitat and excursion crew module designs, zero-g versus artificial-g transfer and space (natural environment) radiation shielding requirements.

Transfer mission profiles included:

- a. Conventional opposition and conjunction missions, with Venus swingby gravity assist where appropriate.
- b. Fast-transfer opposition and conjunction cases.
- c. Low-thrust profiles for electric propulsion.
- d. Cyclor orbit systems.
- e. "Mars direct" (a conjunction profile where the entire transfer vehicle lands on Mars and obtains return propellant from Mars resources).
- f. A "dash" opposition mode where the transfer system performs a Mars flyby, powered as needed, while the Mars excursion vehicle "dashes" ahead on the transfer path to arrive at Mars 10 to 30 days early. It rejoins the MTV by ascent to hyperbolic rendezvous as the MTV flies by Mars.
- g. Split mission options (separate crew and cargo) where this could enhance mission performance. Some split profiles deliver all or part of the crew transport Earth return propellant as cargo to Mars orbit, where it is transferred to the crew transportation system after a rendezvous.

The most important Phase 1 results are given below.

1.3.1 Lunar Missions

For low levels of lunar activity, in the range of one crew mission per year, expendable systems are the most cost effective; the crew returns by CRV direct entry to Earth landing. The STCAEM choice was a tandem-staged direct mode in which the lunar vehicle is landed on the Moon and returns direct to Earth without lunar orbit operations. A booster stage with the same propellant load and propulsion system is jettisoned in a highly elliptic Earth orbit. This mission profile is insensitive to lunar landing site latitude and does not require wait times for phasing. If landing sites are confined to the lunar equator, lunar orbit rendezvous (LOR) with a common-core vehicle offers a modest performance and cost advantage.

For higher levels of lunar activity, such as needed for any permanent human activities on the Moon beyond a very small base, reuse of the transfer part of the lunar

in-space transportation system by aerobraked return to low Earth orbit is favored. Recent studies of permanent base site selection favor a near-equatorial site because of astrophysics observatory sky-view needs; the LOR mode is not unduly constrained and has significant performance advantages. The lunar excursion vehicle is based on the lunar surface. This approach enables graceful growth to use of lunar oxygen to reduce ETO transportation requirements.

An evolutionary path is practical since the tandem-direct Lunar Transfer Vehicle (LTV) is approximately the right size and configuration for the reusable LOR system. It must, however, be designed with future addition of an aerobrake in mind.

1.3.2 Mars Mission Profiles

Opposition profiles offer total mission times about half those for conjunction profiles, i.e., 1.5 years versus 3 years. Figure 1-1 illustrates representative profiles. Mars stay time for opposition profiles ranges from 30 to 90 days; for conjunction profiles from 300 to 600 days. Opposition profiles in the 500-day class almost always use Venus swingbys to reduce delta-V. Opposition profiles can be forced to shorter transfer times and overall mission durations by propulsive effort (additional delta-V); Venus swingbys are usually not possible for round trip times less than 500 days. STCAEM investigated opposition round trips as short as 210 days (0.6 year).

Conjunction profile transfer times can similarly be reduced. Propulsive effort directed to shorter transfer times is more effective on conjunction profiles. Total mission durations are shortened about half as much as is the sum of transfer times; the balance of transfer time saved goes to increased Mars stay time. Short trips and transfers reduce mission risk, in part simply because of shorter duration and in part due to lesser crew radiation exposure because of shorter duration. The interest in conjunction profiles arises from the basic mission purpose of exploring Mars; longer stay time at Mars equates to more exploration opportunity. While the crew is on the surface of Mars they are relatively well shielded from space radiation by Mars' atmosphere and by the surface systems.

1.3.3 Mars Transfer Propulsion Systems and Profile Considerations

The major propulsion/profile tradeoffs consider mission delta-V, usually expressed as initial mass in low Earth orbit (IMLEO), transfer time, stay time at Mars, and split crew/cargo missions. The first-order trade filter is IMLEO. A value greater than 1000 metric tonnes is commonly taken as reason to reject a profile/propulsion option, since many profile/propulsion options offer values in the 500 to 700 t range.

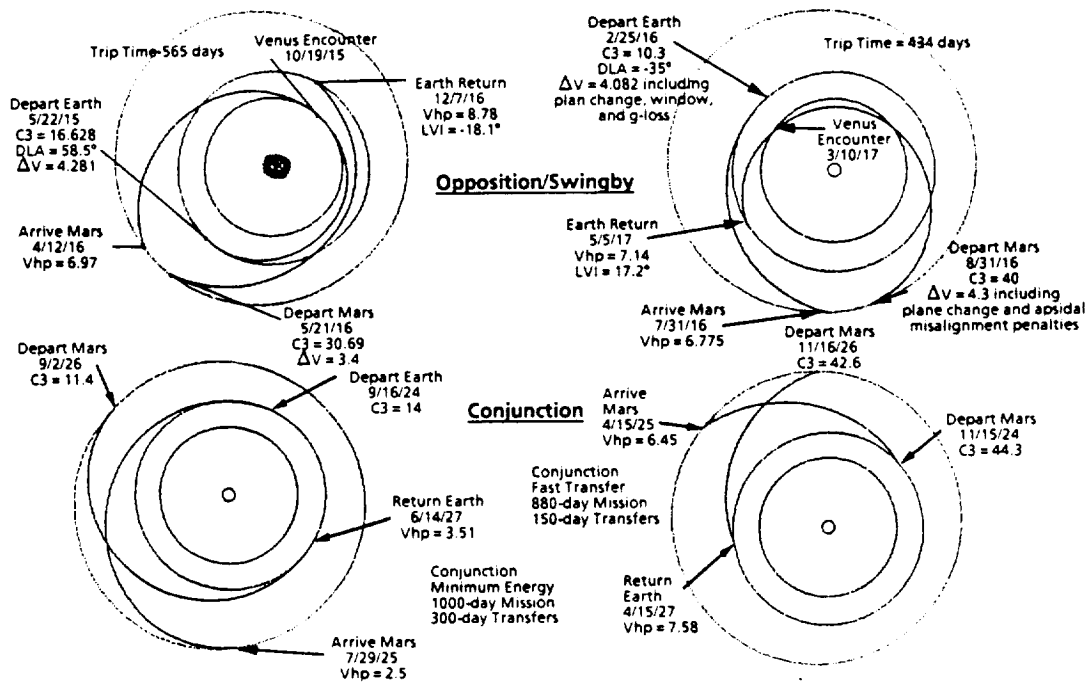


Figure 1-1. Representative Opposition and Conjunction Mars Round Trip Mission Profiles

A comparison of profiles and correlation with propulsion systems is shown in figure 1-2. Cryogenic all-propulsive systems are suited only for conjunction profiles with relatively slow (~6 months or more) transfers. Faster transfers cause IMLEO to exceed 1000 t. Cryogenic/aerobraking (CAB) systems are suitable for conjunction missions with somewhat faster transfers (120 to 150 days) and moderate energy opposition profiles. Nuclear thermal propulsion, (NTP), is suited to higher energy opposition profiles, with trip times as short as one year for "easy" Mars opportunity years and about 450 days for "difficult" years. Since the shorter opposition profiles, 450 days and less, have a high delta-V expense, these profiles are much aided by split missions which deliver Mars-Earth return propellant to Mars ahead of the "fast" mission on a low-energy profile or by electric propulsion (EP). (Mars opportunity flight mechanics demands that the low-energy mission use a prior opportunity, about 2 years in advance of the "fast" mission.) Electric propulsion systems can achieve interplanetary crew mission trip times competitive with all but the fastest high-thrust missions at about 10 megawatts or greater, with power-to-weight ratios of about 10 kg/kWe or less. Approximate trending data are shown in figure 1-3.

Mission Profile	Propulsion				Basing	
	Cryo/ All-Prop	Cryo/ Aerobrake	NTR	NEP/ SEP	Orbit	Surface
Conjunction Minimum Energy	✓	No advantage over propulsive capture	✓	✓	✓	Later
Conjunction Fast Transfer	Excessive IMLEO	✓	✓	✓	No. Reason for fast transfer is less GCR dose	✓
Opposition/ Swingby	Same	✓	✓	Note 1	✓	As a resupply mode
Opposition/ Fast	Same	Excessive IMLEO	✓	No able to make fast trips	✓	Same
Opposition/ Split Sprint	Same	Same	✓	Cargo only	✓	Same

Note 1: NEP flies an opposition/swingby-like-profile but does not benefit from Venus swingby.

Figure 1-2. Propulsion Applicability to Mars Mission Profiles

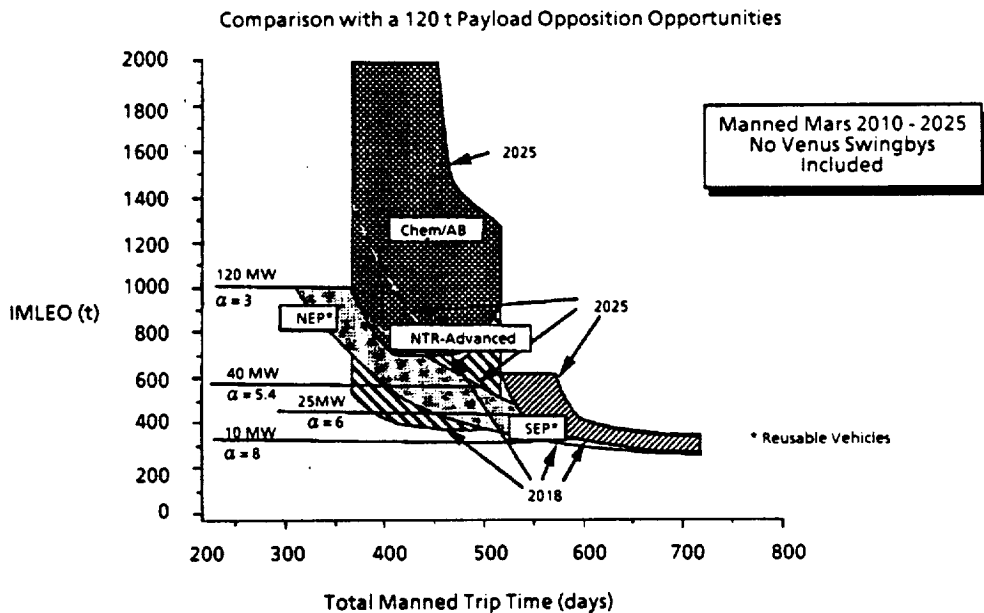


Figure 1-3. Opposition Profile Trip Time Trends for 120 + Payload

1.3.4 Performance, Cost, and Evaluation Summary

A summary of mass, reuse, and cost data are shown in figures 1-4 and 1-5. Each of the options investigated could become a preferred selection under plausible program circumstances.

- a. For a minimum lunar activity level, a simple tandem-staged direct expendable mode is attractive. While expendable systems require continuing hardware production, the production lines must be kept open in any case. For minimum activity levels, the cost of having open lines produce hardware is quite small. At two lunar missions per year, the return on investment (ROI) for developing a reusable lunar orbit rendezvous system is only about 5%. Programs with activity levels of four or more lunar missions per year benefit significantly from efficient reusable lunar transportation.
- b. For a minimum Mars activity level consisting of a half-dozen landings with two to three sites visited for a total of 30 to 90 days exploration time per mission, cryogenic all-propulsive minimum-energy missions with multiple landers, e.g., two or three per mission for two or three missions, are indicated as minimum cost. This offers the opportunity to briefly explore six sites at minimum cost and minimum technology risk. Carrying multiple landers per trip provides a desirable degree of rescue capability. While the STCAEM study was not oriented to judgements on mission profiles, the idea of spending 3 years in space for 3 months or less on Mars does not seem a sensible way to do Mars exploration.

A major concern with this implementation is the mission risk of having astronauts committed to almost 3 years in space, exposed to zero-g and cosmic rays, each Mars mission. While these concerns can presumably be dealt with, i.e., through zero-g countermeasures, artificial g, or suitable shielding, solutions may be costly in mass and complexity. Since (1) there is not much cost difference between the cryogenic/all propulsive and nuclear thermal propulsion, and (2) a technology decision must be made before the number of flights and the mission objectives are set, NTP (NERVA, etc.) is the wise choice.

- c. The performance potential of NTP leads to less initial mass than cryogenic/aerobraking for most mission profiles. A nuclear rocket can eliminate the need for high-energy areocapture at Mars; this is an important advantage. On the other hand, the development program for a nuclear rocket requires significant investment in effluent containment test facilities. Return on investment tradeoff of nuclear rocket versus cryogenic/aerobrake at a median Mars activity level favored the

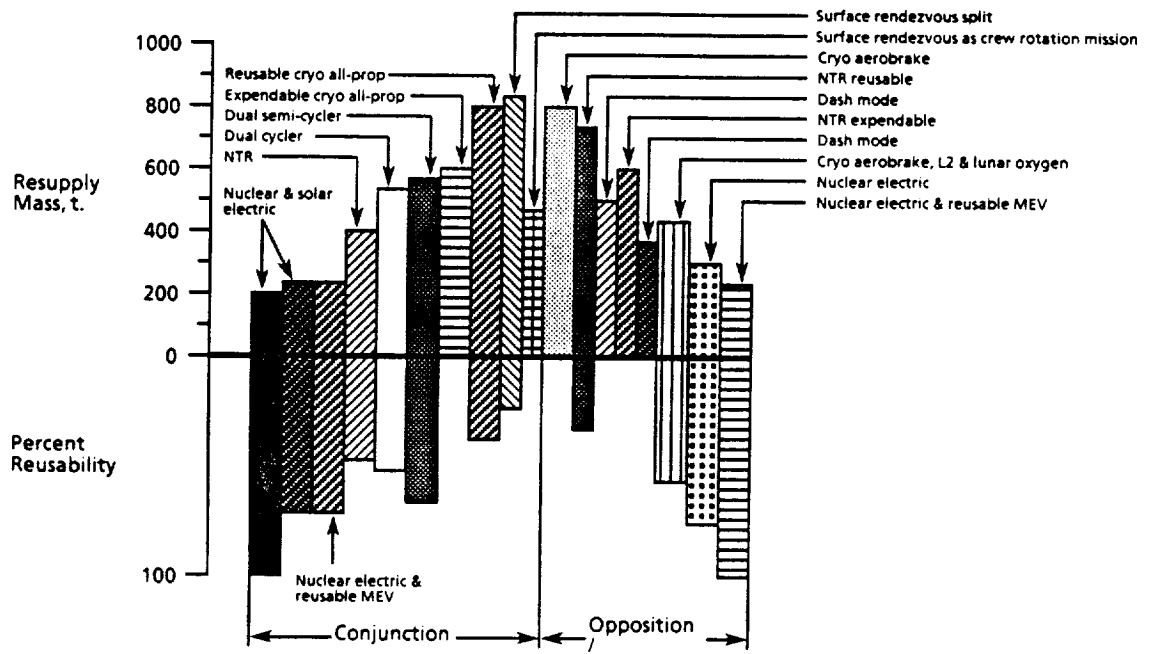


Figure 1-4. Propulsion Option Comparison for Resupply Mass and Reusability

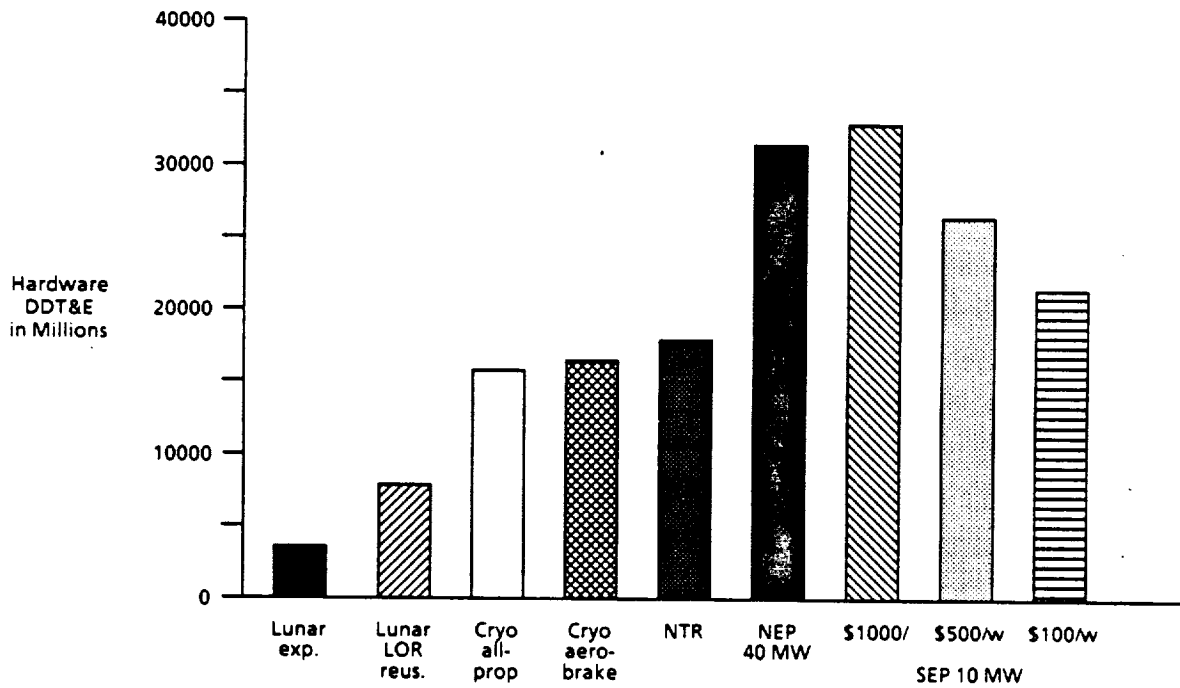


Figure 1-5. In-Space Transportation DDT&E Comparison

nuclear rocket. If Mars exploration progresses to a permanently occupied base, areocapture and NTR are complementary technologies in the NTR-dash mode; this traded favorably versus nuclear electric propulsion (NEP) in the ROI analysis.

The nuclear thermal rocket improves mission flexibility and reduces constraints on mission profiles. A nuclear rocket is the most promising propulsion system for fast Mars trips (a year or less). Fast trips, however, are indicated as expensive in terms of total mass and hardware expended.

- d. Electric propulsion systems are suitable for Mars crew transportation if (1) operated from high-altitude nodes such as L2 or (2) boarded by the mission crew at about lunar distance, where the crew fly to the electric propulsion vehicle on a lunar transfer vehicle. Trip times are competitive with all but fast-trip split-sprint nuclear thermal rocket systems, i.e., about 450 days for nuclear electric propulsion and 550 days for solar electric propulsion (SEP). On conjunction fast transfer profiles, NEP delivers 150 to 200 day transfers each way and SEP about 250.

The inherently high reusability and low resupply mass of electric systems offers life-cycle cost advantages at high activity levels. Development costs for NEP and array production costs for SEP are major issues. Resolution of the array production cost issue will require a manufacturing technology program. Costs and return on investment results show that estimated NEP development costs are not effectively amortized even at a settlement activity level when compared with a nuclear rocket operated in the dash mode. SEP at current array costs (~\$1000 per watt), is estimated as more expensive to develop than NEP. SEP becomes very attractive at \$100/watt, showing about 10% return on investment versus NTR at the median activity level. If a low-cost SEP is possible, it is also attractive for lunar cargo.

- e. Special architectures offer unique advantages in particular circumstances. For example, lunar libration point staging is attractive for low-thrust systems because spiral operations out from and into Earth's gravity well can be conducted by an electric orbit transfer vehicle in parallel with interplanetary transfers by the interplanetary SEP or NEP.

Lunar libration point operations offer reduced Earth launch mass for cryogenic/aerobraking profiles through use of lunar oxygen and to electric propulsion systems because the interplanetary vehicle need not execute low-thrust spirals out of and returning into Earth's gravity well. Neither of these potential advantages applies to nuclear thermal rockets; libration point operations for nuclear rockets were not considered.

Mars direct simplifies flight operations at Mars at the expense and risk of propellant production on Mars; it is more efficient than Mars orbit rendezvous in a crew transport mode after a base has been established, but not as efficient as NTR-dash. It appears too risky (lack of abort modes) for an initial mission. Mars direct offers potential advantages where galactic cosmic ray concerns dictate conjunction fast transfer profiles with long surface stays. It is not suitable for crew rotation and resupply of a permanent base because it is confined to the conjunction profile, and leads to gaps in crew presence at Mars.

A table of the basic types of operations for each activity level for lunar and Mars missions is presented in figure 1-6.

<u>Minimum</u>	<u>Median (full science)</u>	<u>Industrialization/ settlement</u>
<u>Lunar:</u> Expendable	<u>Lunar:</u> Start expendable, possible growth to LOR reusable, aerobraking	<u>Lunar:</u> LOR crew and tandem direct cargo, reusable, with lunar oxygen
<u>Mars:</u> <ul style="list-style-type: none"> • Cryogenic all-propulsive • Unless radiation environment requires reduced trip times; then nuclear rocket or cryo aerobrake conjunction fast transfer 	<u>Mars:</u> <ul style="list-style-type: none"> • Nuclear rocket, conjunction, multiple landers • Opposition or conjunction fast transfer options • Cryo/aerobraking backup • SEP "dark horse" 	<u>Mars:</u> <ul style="list-style-type: none"> • Early cryo/all-propulsive option • Electric propulsion for sustained growth (probably SEP) • Nuclear rocket/dash or Mars direct/Mars propellant, options for crew rotation and resupply

Figure 1-6. Preferred Transportation Options for Range of Activity Levels

Reusable MEVs using Mars oxygen, and methane or hydrogen if available, are interesting as an evolutionary development, mainly because their greater reusability may have significant life cycle cost benefit. In the STCAEM settlement scenario analysis, the reusable MEV came on line too late to have a net payoff. This concept needs further evaluation.

Cyclers may be advantageous if interplanetary transfer habitats need extensive radiation shielding or if large crews and consequent massive transfer habitats are needed to satisfy mission objectives. Early in a Mars program, cyclers do not have enough advantage over simple all-propulsive (cryogenic or nuclear) or aerobraking to merit their need for infrastructure pre-positioning, operational complexity and give-up of abort modes.

1.4 PHASE 2 RESULTS

The Phase 2 study effort was conducted based on a series of Technical Directives. The study addressed issues surfaced by Phase 1, developed generic Mars mission profile analysis data, and conducted preliminary analyses of the Mars in-space transportation requirements and implementations from the Synthesis Report architectures. Analyses of the first 8 of the 11 Phase 1 issues described below are directly pertinent to the Synthesis architecture implementation analyses performed by this study, and were so applied.

1.4.1 Summary of Issues

The principal issues passed from Phase 1 to Phase 2 were:

- a. Provision of reasonable Earth orbit launch windows for trans-Mars injection.
- b. Elliptic versus circular parking orbits at Mars (Phase 1 assumed elliptic orbits for all missions).
- c. Mars landing site access from elliptic orbits.
- d. Engine-out requirements for nuclear thermal propulsion systems.
- e. Assembly of Mars vehicles on orbit; especially assembly of capture and landing aerobrakes.
- f. Effects of ETO transportation lift capability on Mars transportation systems.
- g. Radiation shielding requirements for Mars transfer habitats, for anomalously large solar proton events (ALSPEs, commonly called flares) and galactic cosmic rays.
- h. Crew return vehicle heating and thermal protection requirements.
- i. Potential cost benefits from designing a cryogenic/aerobraking system for recapture in Earth orbit at the end of the mission for reuse.
- j. Potential benefits of laser power beamed from the surface of the Earth to Earth-Moon space to power photovoltaic electric orbit transfer vehicles.
- k. Wake closure angles and payload heating behind a low lift-to-drag ratio (L/D) lunar aerobrake.

During the Phase 2 study effort, the Synthesis Report, *America at the Threshold*, was released. The Synthesis Report recommended selection of nuclear thermal propulsion as the baseline technology for Mars transfer propulsion. As a result, the Phase 2 work focused almost exclusively on this propulsion means. The Synthesis report also raised several issues relevant to the Phase 2 work:

- a. Details of Mars mission profile design as regards cargo splits, means and timing of cargo delivery, and aborts. These issues are a normal consequence of developing more detailed mission profile design information for a particular propulsion system.
- b. Potential mass benefits of a zero-g Mars transfer crew habitat (the Phase 1 habitat was designed to be used either with zero-g or artificial g).
- c. Transportation requirements and options for attaining a long-duration stay capability at Mars early in the program, specifically on the second crew mission.
- d. Launch and on-orbit processing of the significant amounts of Mars surface cargo needed for the early long stay, at the same time as the first crew mission is sent to Mars.
- e. Appropriate MEV propulsion selection, considering that a long surface stay occurs as early as the second crew mission.

1.4.2 Issues from Phase 1

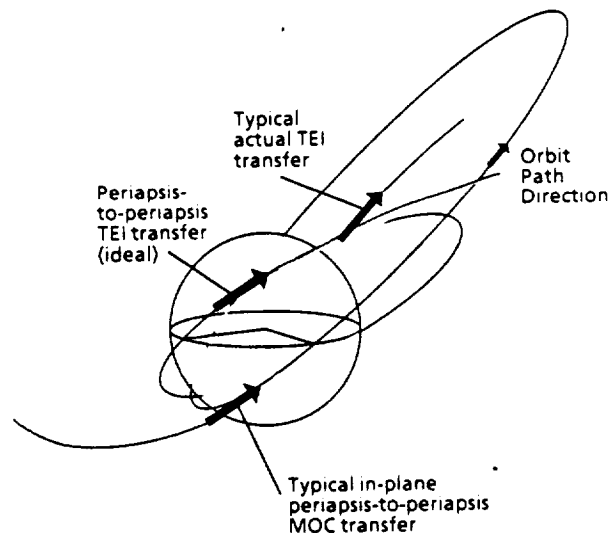
1.4.2.1 Launch Windows

The Phase 1 study effort did not consider launch windows for trans-Mars injection (TMI), since it was a broad-scoped trade of many profile and propulsion options. The launch window problem addressed by Phase 2 arises because of rapid nodal regression of low Earth orbits. A minimum delta-V TMI is only possible when the Earth assembly/parking orbit contains the trans-Mars departure vector. Over a reasonable launch window period, rapid regression of the orbit causes the departure vector to become far out of plane. Resulting plane change delta-V penalties can be thousands of meters per second. During Phase 2, a three-burn TMI strategy was developed. An intermediate elliptic Earth orbit enables the plane change to be made at a low apogee velocity. Plane change and impulsive delta-V requirements can be traded by proper positioning of the parking orbit so that the plane change penalty is reduced to 100-300 m/sec. These results were incorporated into mission profile analyses for the Synthesis architectures.

1.4.2.2 Mars Parking Orbits

The use of elliptic parking orbits at Mars reduces the ideal delta-V for Mars orbit capture and trans-Earth injection by about 1.2 km/sec each. This savings is just the difference between circular orbit velocity at 500 km altitude and the periapsis velocity of a 1-sol elliptic orbit (one sol is one Mars solar day of 24.6 hours). The savings is reduced in practice, because to obtain all of it, both MOC and TEI must be in-plane

periapsis-to-periapsis transfers. As shown in figure 1-7, the orbital alignment analysis includes regression of line of nodes and advance of periapsis during stay time and shows typical regression and advance. For opposition missions with their relatively short stay times, the mission design only has one degree of freedom, orbit inclination, with which to control the two variables of orbit line of nodes and line of apsides. The long stay time of a conjunction mission adds another degree of freedom, the orbit period combined with the secular perturbations of regression of the nodes and advance of periapsis (rates of both are a function of orbit period). On a conjunction profile, nearly ideal elliptic orbit MOC and TEI transfers can be obtained, but the orbit inclination, location of periapsis, and period are specified (periapsis moves during the stay). For an opposition profile, there is a "best" orbit with a specified inclination and location of periapsis, but significant apsidal misalignment penalties may be incurred. A typical opposition profile has reasonable apsidal alignment, with penalties of one to a few hundred meters per second, modest compared to the elliptic orbit savings. This is true of the reference Synthesis opposition profile for the year 2014. The IMLEO savings with elliptic orbits, including allowances for apsidal alignment penalties, are typically 25% for nuclear thermal propulsion. As a result, the STCAEM study recommended elliptic orbits as the baseline. Use of elliptic orbits has ramifications of landing site access and MEV L/D, discussed immediately following.



Note: Orbital alignment analysis includes regression of line of nodes and advance of periapsis during stay time; typical regression and advance shown.

Figure 1-7. Alignment Requirements for Minimum Energy Elliptic Orbit MOC and TEI

1.4.2.3 Mars Landing Site Access

The near-minimum-energy orbit (least apsidal alignment and plane change penalty) chosen for the 2014 opposition opportunity with return Venus swingby is illustrated in figure 1-8. This is the reference Synthesis opportunity and profile for the first piloted Mars mission for Architectures 1, 2, and 3. This orbit has inclination and periapsis location selected for the minimum energy compatible with a reasonable periapsis lighting angle. As shown in figure 1-9, a modest delta-V penalty is accepted in order to have daylight periapsis. Periapsis for this orbit is about 30° north latitude. Our investigations presumed that landing sites of interest would lie between 20° north and 20° south latitude. Longitudes of interest cover a wide range, but any longitude of interest can be reached by timing the mission to utilize Mars' rotation to position the desired landing site longitude at a reachable point.

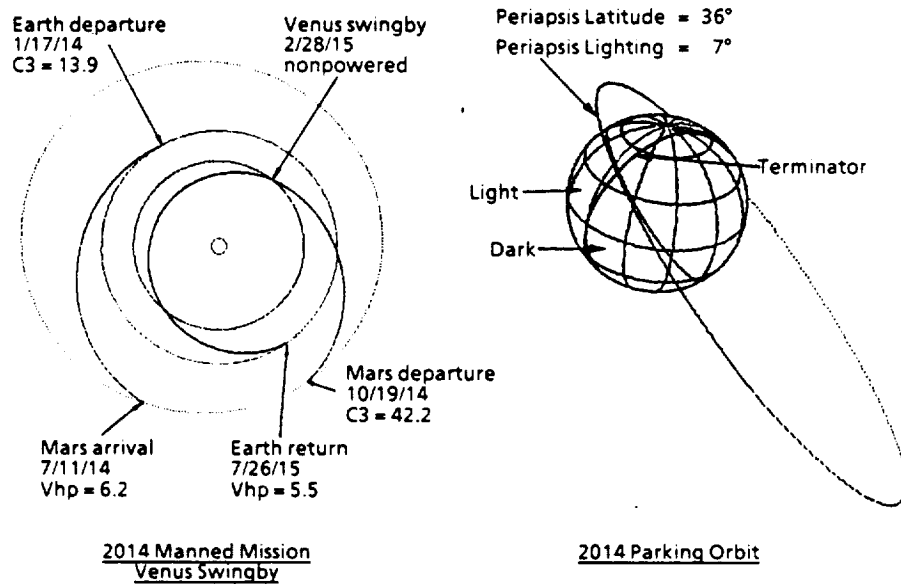


Figure 1-8. Selected Orbit for 2014 Opposition Crew Mission

A low-energy descent from an elliptic orbit performs the deorbit burn near apoapsis and enters Mars atmosphere about 18° central angle before periapsis. A nominal low L/D landing occurs near periapsis. The excess energy (above that of a low circular orbit) can be exploited to "stretch" the descent some distance downrange of periapsis but the path quickly crosses the evening terminator to the night side. Lift can be used to turn the path in a desired direction; at the same time drag slows the vehicle. Very little

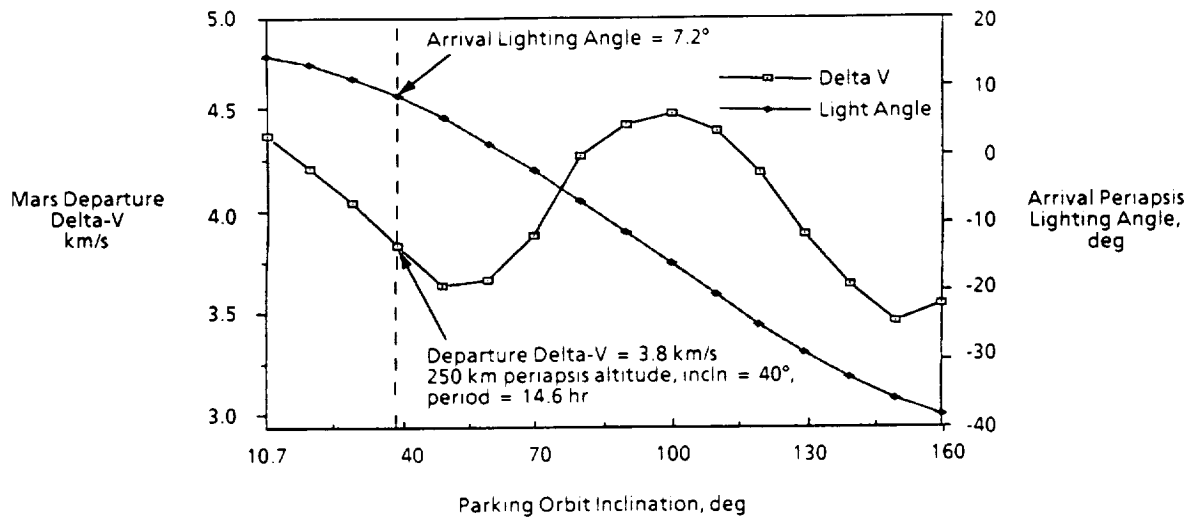


Figure 1-9. Orbit Parameters for 2014 Opposition Crew Mission, Showing Orbit Selection for Favorable Periapsis Lighting

cross-range (turning) is available to a low L/D lander. If the L/D is high enough to turn the path to the desired direction and retain near orbital velocity, high crossrange is attainable. Two landing trajectory design approaches were tried for the subject orbit: (1) sharp right turn at periapsis to a southerly path, staying on the light side of the terminator, and flying to the desired landing latitude; (2) a modest turn, partial skip-out, and flight path over the entire night hemisphere, crossing the morning terminator to the desired landing latitude. Typical landing ground tracks for L/D max = 1.6 are shown in figure 1-10. Design approach No. 1 was successful for 20° north latitude; No. 2 was best for 20° south latitude.

While circular orbits simplify access to low-latitude landing sites by not requiring high L/D, they severely restrict access to high inclination sites, e.g., near the Martian poles, because (1) circular orbits having in-plane arrival and departure are usually at moderate inclinations, and (2) plane changes entering or leaving circular orbits are very expensive, either for the MTV or the MEV. Descents from elliptic orbits with high L/D can reach polar latitudes; ascents require plane change to return to the MTV orbit but the plane change can be made at apoapsis where delta-V penalties are moderate.

1.4.2.4 Assembly of Mars Vehicles on Orbit

Concepts from Phase 1 required assembly of the MEV aerobrake and the NTP truss core from structural subassemblies. A variety of assembly facility concepts were conceived and analyzed, from facilities that fully enveloped the vehicle to use of the

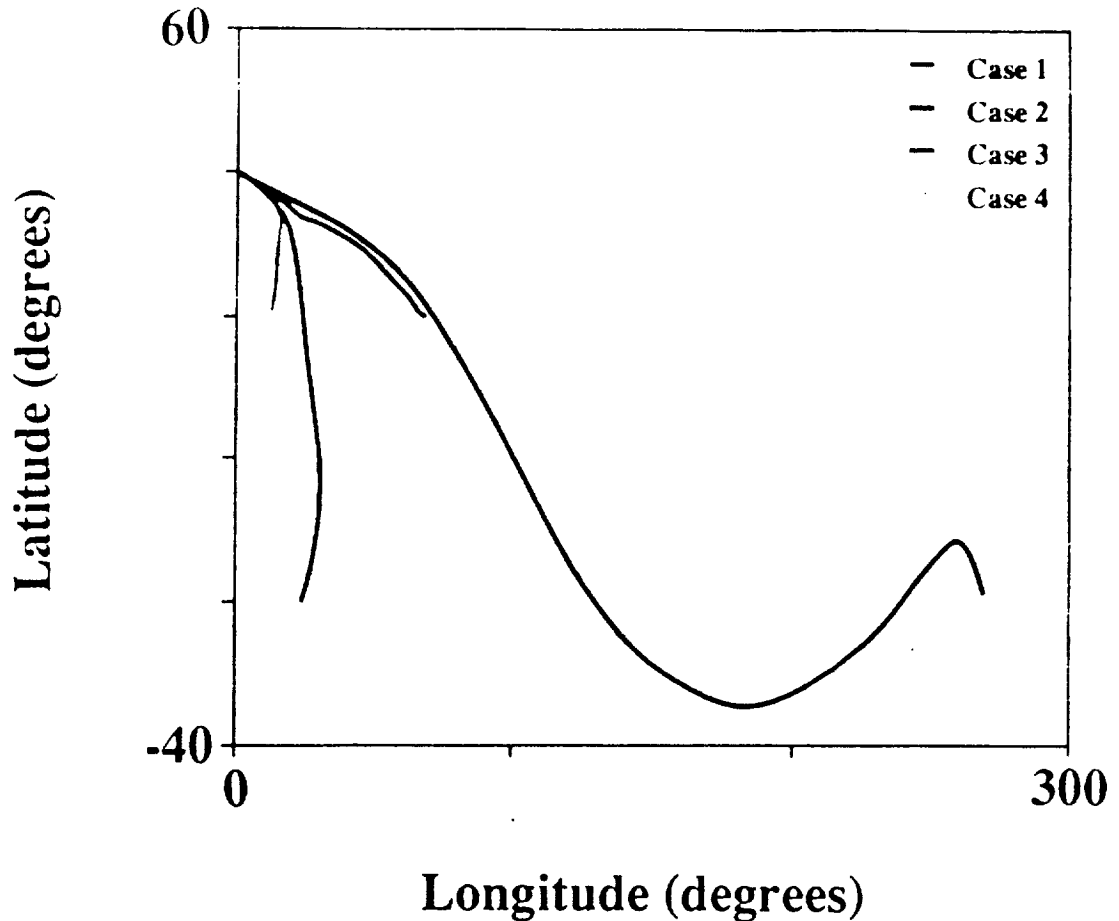


Figure 1-10. Ground Tracks for High L/D Landing from 2014 Elliptic Orbit

vehicle as its own assembly platform. Assembly issues were only partly reflected back into vehicle design. Phase 2 performed two iterations improving the assembly approach. The first provided a relatively simple platform for assembly of the reference NTP vehicle for Phase 1, shown in figure 1-11, while simultaneously redesigning the vehicle for simpler assembly. The second step used the redesign and a modified launch sequence to further simplify the assembly platform, as shown in figure 1-12.

Vehicle simplification took two significant steps: (1) the truss core was modified to be assembled from nestable sections with pre-integrated utilities, avoiding detailed truss assembly and utility installation; and (2) MEV/aerobrake concepts were developed that simplify or eliminate aerobrake assembly. Two options were considered: (1) the L/D 0.5 aerobrake was redesigned to be a monocoque structure that can be packaged as many small nesting sections for on-orbit assembly; the assembly operations would be similar to the EVA concept developed by McDonnell-Douglas for Langley Research Center; and



Figure 1-11. Free-Flyer Assembly Platform for NTP

(2) a high L/D MEV concept was developed for integral launch on the side of a launch vehicle shuttle Orbiter style, as depicted in figure 1-13.

These simpler vehicle concepts were exploited, along with a revised launch sequence to reduce the assembly platform to a strongback with manipulator arms that can be launched attached to the MTV habitat with its solar array/fuel cell power system and other utilities. This is the first launch in the sequence. After launch the array is deployed and the vehicle is an operable LEO spacecraft. The habitat can be used by assembly or test personnel if and when needed at the assembly site. The assembly process is designed to be remotely teleoperated except for contingencies.

1.4.2.5 Effects of ETO Transportation Lift Capability on Mars Transportation Systems

A range of ETO vehicle sizes was investigated, from 75 t to 250 t payload mass. The STCAEM study was concerned only with the effects of ETO capability on in-space transportation and operations; no design ETO concepts were made.

ETO capability affects in-space transportation and operations in three ways: (1) largest size single building block that can be transported to orbit, (2) complexity of on-orbit assembly operations, and (3) packaging and deployment requirements imposed by ETO launch shroud size limits. The number of launches required is also an important consideration, but more so to ETO ground operations than to in-space transportation.

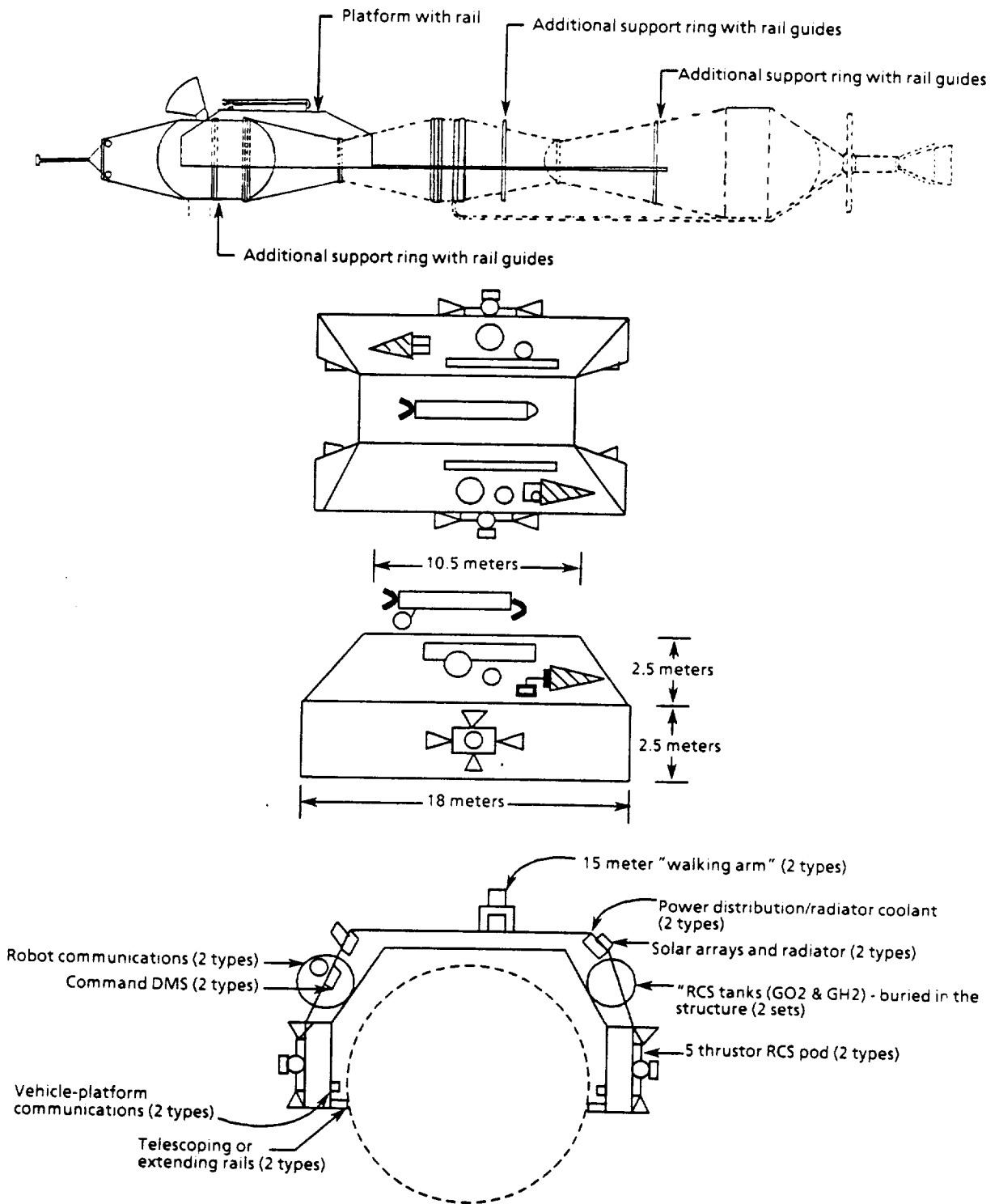
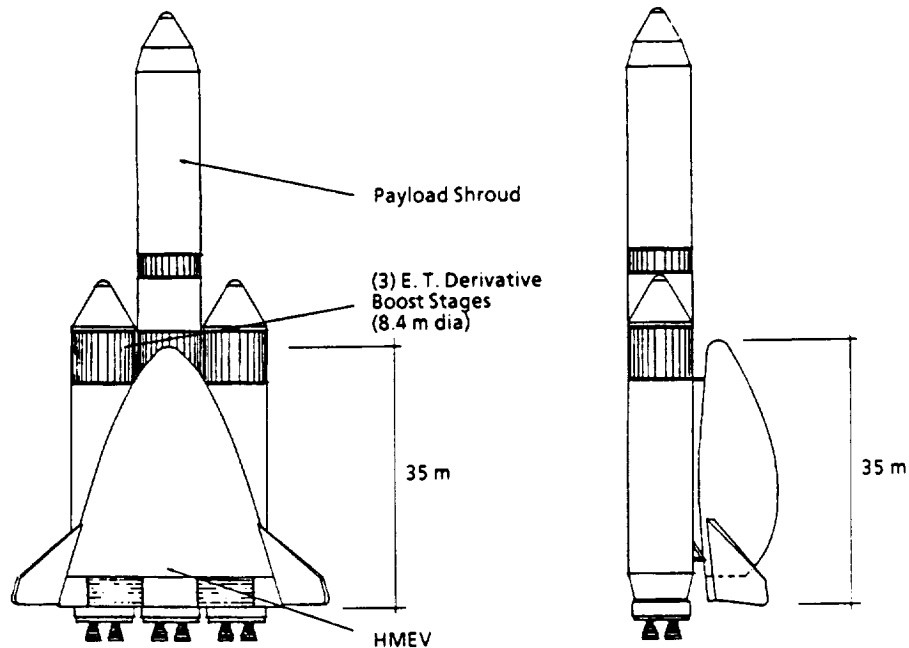


Figure 1-12. Integral-Launch Assembly Platform for NTP



Launch vehicle shown represents NLS with ~115 t lift capacity to SSF orbit. Mars-class HLV baselined for STCAEM manifesting purposes would throw ~150 t.

Figure 1-13. Integral-Launch High L/D Mars Excursion Vehicle

The largest single building block for Mars transportation is the transfer habitat. For six crew, the mass may be 60 t for an artificial-g habitat; a zero-g version is somewhat less. The size is about 7 m diameter by 12 to 16 m length. Neither the mass nor the size of this habitat was an issue for any of the ETO vehicles considered.

The MEV can be viewed as a single building block, or it can be assembled on orbit. The largest MEV was about 80 t, a probable constraint for the smallest ETO size. The physical size of the MEV aerobrake is the main concern, for which there are three options: assembly of the aerobrake on orbit, external launch of the aerobrake or complete MEV, and design of a deployable aerobrake that can be folded inside the launch shroud. The "bathtub-shape" L/D 0.5 aerobrake of Phase 1 is not well-suited to external launch. The design from Phase 1 was to be delivered to orbit in sections and assembled, but the rib/spar design did not package well for launch and required two launches just to get the aerobrake to orbit. In Phase 2, the brake was redesigned to use a monocoque structure that had no ribs or spars, so that it could be cut up into smaller sections for efficient launch packaging. Deployable concepts were not investigated in Phase 1, but were in Phase 2 as described below under Synthesis Architecture Analyses.

Complexity of on-orbit assembly was simplified at 150 t or larger. A few large subassemblies could be berthed together by a positioning arm. Little or no EVA is

needed except in contingency situations. As illustrated in figure 1-14, integral launch of Mars surface cargo becomes practical.

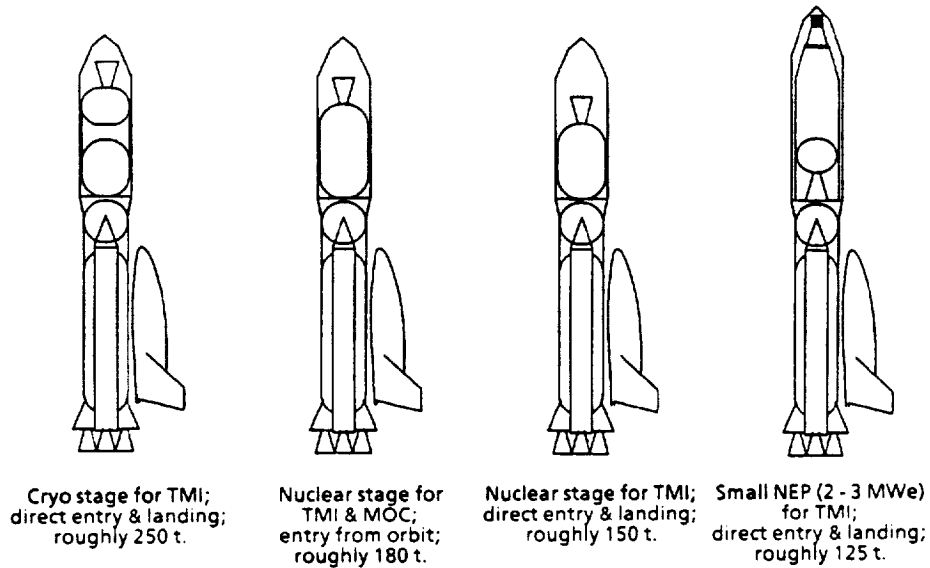


Figure 1-14. Mars Cargo MEV and In-Space Transportation Integral Launch Options

A preliminary manifesting analysis for the range of ETO sizes yielded the results presented in figure 1-15. The 150-t results were derived from a preliminary packaging analysis based on the current NTP configuration. The other results are deltas from the 150-t results but are believed accurate within ± 1 launch. The recommendation of 150-t is based on judgments that (1) the development cost difference between 150-t and 180-t ETO is much more important than one launch per Mars opportunity, and (2) also more important than the delta development cost to make the MEV capable of moderate energy ($C_3 \sim 15$) direct entry and landing at Mars.

Additional savings in numbers of launches are available at the 250-t level, but must be evaluated in light of an expensive, probably "clean sheet" design of a very large launch vehicle.

As the launch vehicle gets larger, the payload value at risk for each launch also gets larger. At the 150-t level, most of the cost of the piloted Mars mission (the habitat and crew MEV) are on one launch. Approaches to re-manifesting to reduce risk while not increasing the number of launches need to be investigated.

<u>80-t. Class</u>		<u>150-t. Class</u>		<u>180-t. Class</u>		<u>250-t. Class</u>	
<u>Launch No.</u>	<u>Payload</u>	<u>Launch No.</u>	<u>Payload</u>	<u>Launch No.</u>	<u>Payload</u>	<u>Launch No.</u>	<u>Payload</u>
1	AFT tank/ engine	1	AFT tank/ engine, part of truss	1	AFT tank/ engine, part of truss	1	Entire code
2	Hab	2	Hab + MEV, part of truss	2	Hab + MEV, part of truss	2, 3	Tanks
3	MEV	3-5	Tanks	3-5	Tanks	4-6	2016 cargo
4	Truss	6	Top-off tank	6-8	2016 cargo, entry from Mars orbit	(4 and 5)	if MEV sized larger)
5-7	Tanks	7-9	2016 cargo, direct entry				
8-10	Top-offs						
11-16	2016 cargo						
Smallest vehicle feasible for Mars missions without elaborate assembly on orbit.		Recommended reference as probable least cost.		Eliminates top-off and aerocapture-like maneuver for cargo MEVs.		Not much benefit over 150 - 180 t.; configuration impact to be assessed.	

Figure 1-15. Results of Preliminary Manifesting Analyses for Range of ETO Launch Vehicle Payload Capability

1.4.2.6 Radiation Shielding Requirements

The automated CAD-driven radiation analysis system "Brem" developed by Matthew Appleby of Boeing-Huntsville was used to analyze the Mars transfer habitat and the crew return vehicle, to estimate crew doses from galactic cosmic rays (GCR) and solar flares. Based on results from Phase 1, the habitat internal configuration was arranged to maximize shielding from equipment and stores. The CRV has relatively little shielding but is occupied only for the last 12 hours of the Mars mission, just before Earth entry. No special shielding was provided in either module. The CRV was analyzed only for a solar flare, using a 12-hour "worst case" period from the October 1989 flare. Results are shown in figures 1-16 and 1-17. Galactic cosmic ray annual exposure averaged over typical crew patterns for using the volume of the habitat module (some areas are better shielded than others) is predicted to be about half the annual astronaut exposure limit, assuming solar minimum which yields the highest GCR flux. If the crew stays in the galley region during a severe flare, the cumulative dose is about 5 rem.

The worst mission case is an opposition/swingby mission, during which the crew spends all but 30 to 70 days of a 1.5-year mission in the transfer habitat. The study estimates they will receive about half the exposure limit. The accuracy of these predictions in terms of delivered dose, calculated from quality factor and energy deposition, is thought to be about ± a factor of 2. The main uncertainties are (1) the

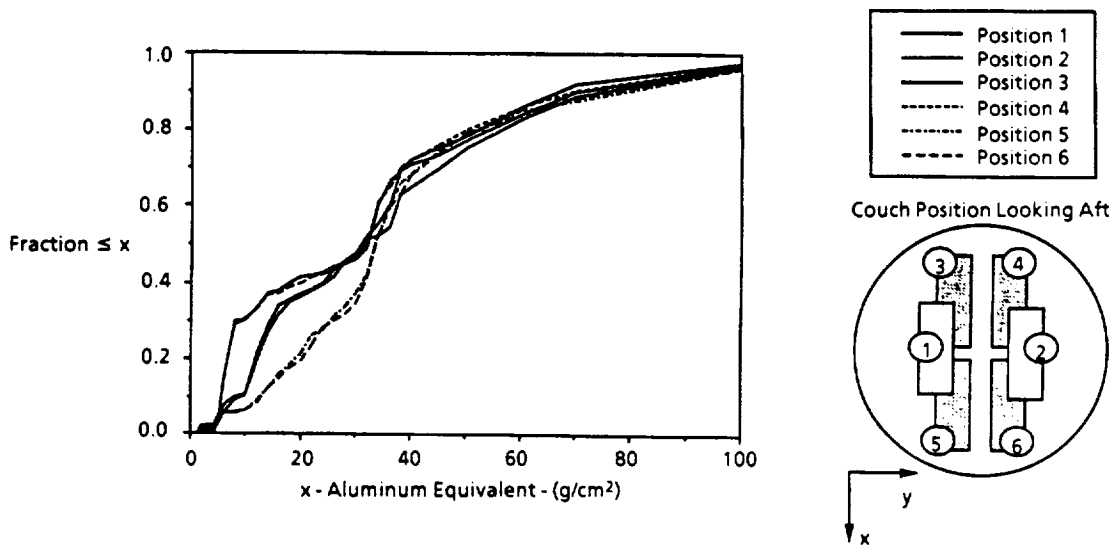


Figure 1-16. Calculated Integral Shield Distribution for Mars Crew Return Vehicles

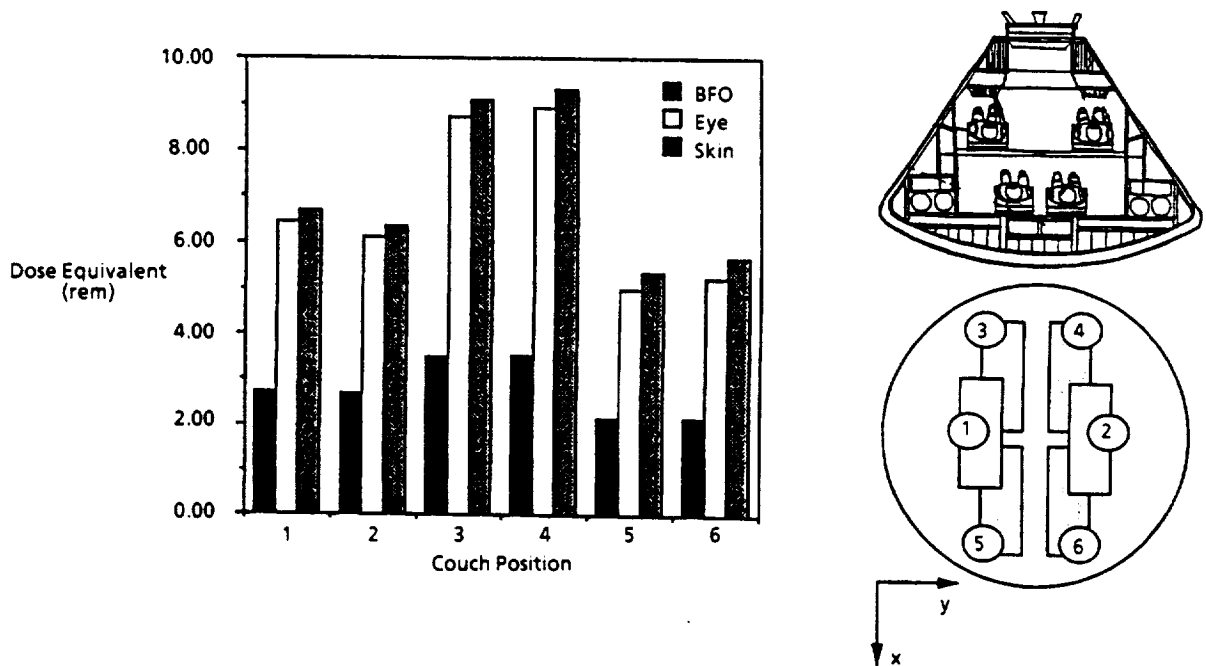


Figure 1-17. Dose Equivalent Resulting From Third 12 Hours of 19 October 1989 SPE

actual GCR flux, a major portion of the received dose is produced by heavy ions and their fragmentation products; and (2) the transport codes which use mainly theoretical nuclear cross sections. There is a further uncertainty in the quality factor for high LET particles; some analysts believe values presently in use are very conservative. If the estimates are low by a factor of 2 or more, the actual dose on this mission will exceed current exposure limits, unless additional shielding is provided.

Predictions for conjunction fast transfers, with long surface stays, are about half those for an opposition/swingby mission because the maximum in-space exposure time is less than half a year.

The predicted dose for 12 hours in the CRV, should the crew be unlucky enough to encounter a severe solar flare during the last few hours of the mission, is about 10 rem.

1.4.2.7 Crew Return Vehicle Heating and Thermal Protection Requirements

Crew return vehicle stagnation point heating was analyzed for a typical Mars return. Results are compared with Apollo data and predictions for the lunar CRV in figure 1-18. The peak Mars return heating is about twice that for lunar return, but only slightly more than the Apollo design. Plans to analyze heating rates with finite-rate chemistry away from the stagnation point were deferred because the chemistry tables in the computer codes (BLAP and BLIMP-K) do not go to high enough temperatures. Stagnation and non-stagnation heating will be revisited after the chemistry tables are extended.

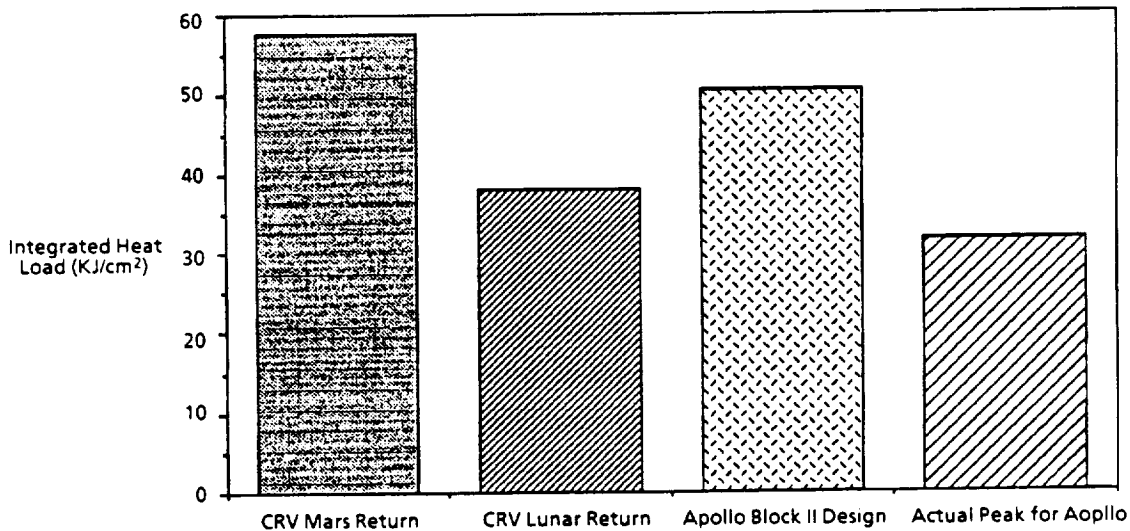


Figure 1-18. CRV Integrated Heat Load Comparison
(Mars Return Entry Velocity 13.1 km/sec,
Corresponds to $C3-50\text{km}^2/\text{sec}^2$)

1.4.2.8 Engine-Out Requirements for Nuclear Thermal Propulsion Systems

The Phase 1 NTP vehicle design used only one engine. During Phase 2, Aerojet performed a concept analysis for the particle-bed engine type; included in their analysis was a reliability and safety analysis for multiple engines. Over a plausible range of engine reliability and probability of fratricidal failure, two was the safety-optimal number of engines; a two-engine configuration was selected for Phase 2. Mission rule and abort analyses conducted by Level 2 (the Lunar-Mars Exploration Program Office, LMEPO) also indicated desirability of two engines to enable single engine out capability for propulsive maneuvers at Mars. A summary is as follows: If an engine fails during Earth departure or prior to Mars arrival, the mission is aborted without capture at Mars. If an engine fails during Mars capture early in the burn, the mission is diverted to an abort profile. Late in the burn or upon Mars departure, engine-out capability is provided; the maneuvers can be performed on one engine.

1.4.2.9 Potential benefits of laser power beaming

Sending power from the surface of the Earth to the Moon by laser beam, using SDIO technology, has been proposed as an option for lunar surface power. The concept is illustrated in figure 1-19, which points out that some of the power beaming stations are normally available for other use since they do not have a line of sight path to the Moon. One potential use is providing power to electric orbit transfer vehicles (EOTVs) in Earth-Moon space. Laser power, being monochromatic, can be converted to electricity at more than 50% efficiency if the laser frequency and the photovoltaic band gap are suitably matched. A beam expander "telescope" of reasonable aperture can provide several suns intensity on the array of an EOTV. The electrical power per unit area of EOTV array can be on the order of 10 times that derived from natural sunlight. This greatly ameliorates the cost issue associated with EOTV array cost, since the power-to-cost ratio is also increased by the same factor.

Laser power transfer to an EOTV would be intermittent since the EOTV is not continuously in line of sight with a ground station. A brief power beaming and flight mechanics simulation study assessed the severity of problems arising from (1) intermittent power, (2) asymmetric location of laser sites in longitude and at latitudes north of the equator, and (3) the possibility that intermittent power and asymmetric laser site locations would cause unacceptable orbit perturbations. This also briefly examined LEO to GEO transfers powered by laser. Typical results are shown in figure 1-20. The intermittency of power caused longer trip times, but times were generally acceptable, in the range 90 to 180 days. Asymmetries did not appear to cause

- Laser power beams from Earth to Moon.
- FEL with adaptive optics for tight beam.
- ~1 micron wavelength matched to receiver photovoltaics.
- Four sites on Earth for continuous view to Moon.
- Two sites are available for electric orbit transfer power beaming.
- Power per unit array area ~ ten times natural sunlight.

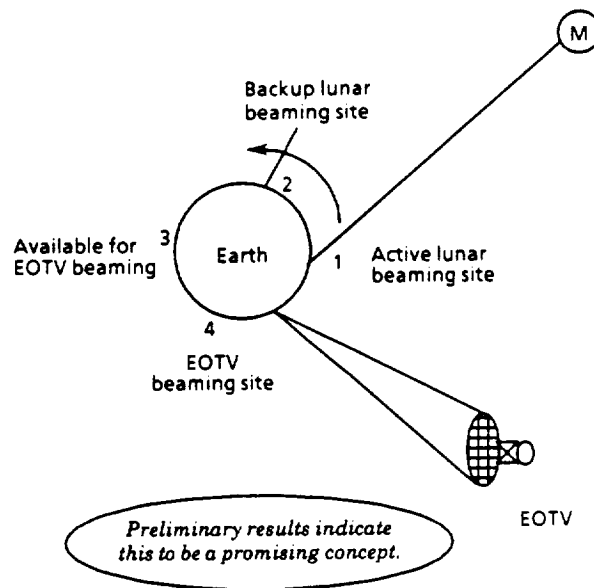


Figure 1-19. Infrastructure Concept for Laser Power Beaming to the Moon and Electric Orbit Transfer Vehicles

problems. The transfer orbits became moderately elliptical, but this tended to correct itself after a while. Simulations of transfers to GEO using a combined plane change and orbit raising steering law indicated that such a law would work, but here the intermittency and asymmetries caused the orbit plane to decrease to equatorial more rapidly than would have been the case for continuous thrusting. These investigations were only exploratory and much further work is needed in this area.

1.4.2.10 Lunar aerobrake wake closure angles and payload heating

Several studies of aerobrake wake flow have produced conflicting indications. In order to obtain some resolution, a wake flow analysis subcontract was issued to REMTECH. REMTECH reviewed the available data and predictions, including CFD and other analyses and wind tunnel tests, analyzed flow chemistry, and developed engineering correlations for wake closure and payload heating. The correlations show that greater closure angles (faster closure and smaller protected area behind the wake) occur with lower effective specific heat ratio in the flow around the shoulder of the brake. Rapid closure predictions arise from assuming chemical equilibrium flow, with specific heat ratio less than 1.2. However, finite chemistry analyses, performed with the Langley Research Center LAURA code and by REMTECH, indicate that the flow is essentially frozen at the low densities of a typical lunar return aerobrake. The effective specific heat ratio is about 1.6, and the predicted closure angle about 10 degrees. This provides a

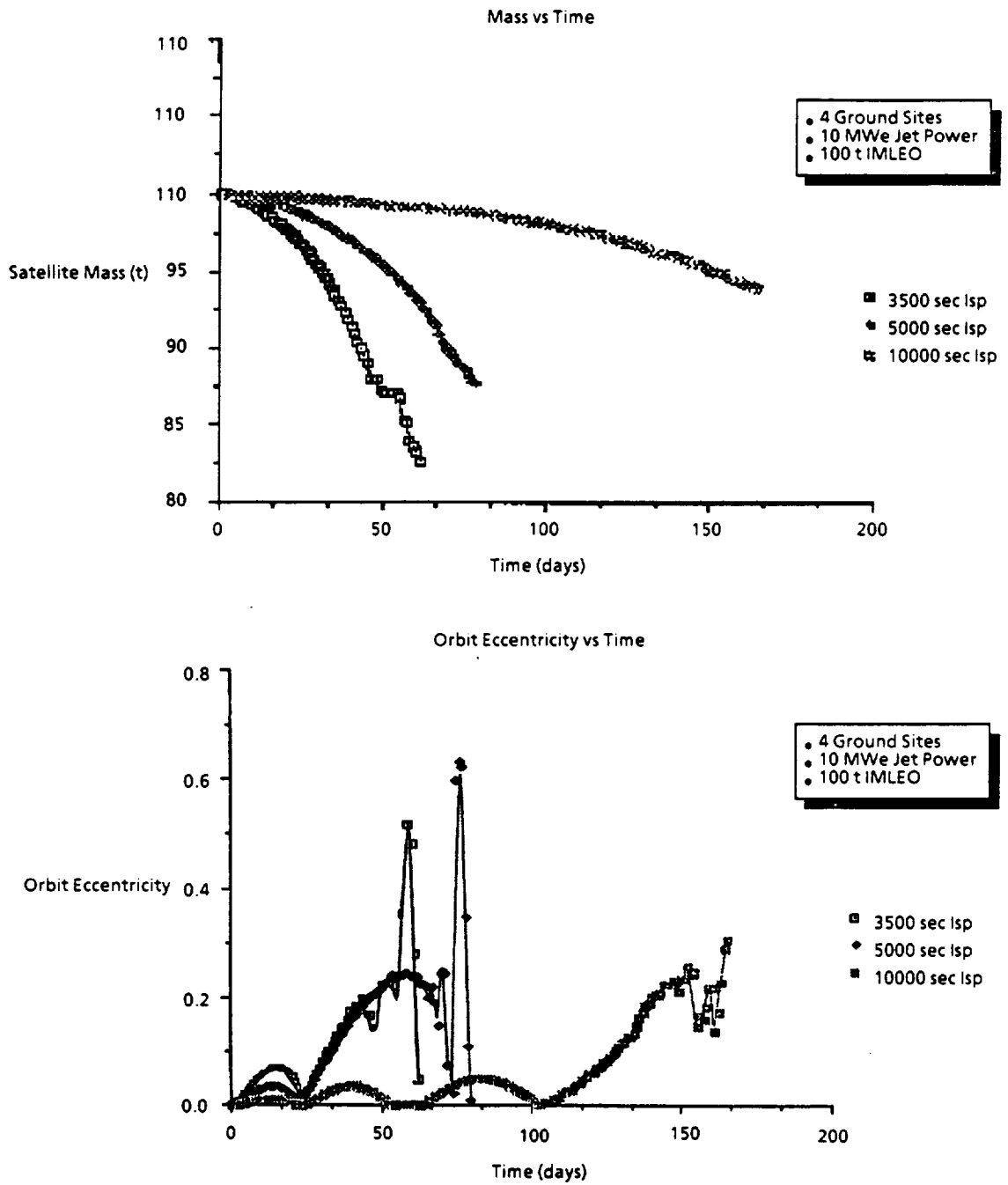


Figure 1-20. Typical Laser Beam Power Electric Orbit Transfer Results

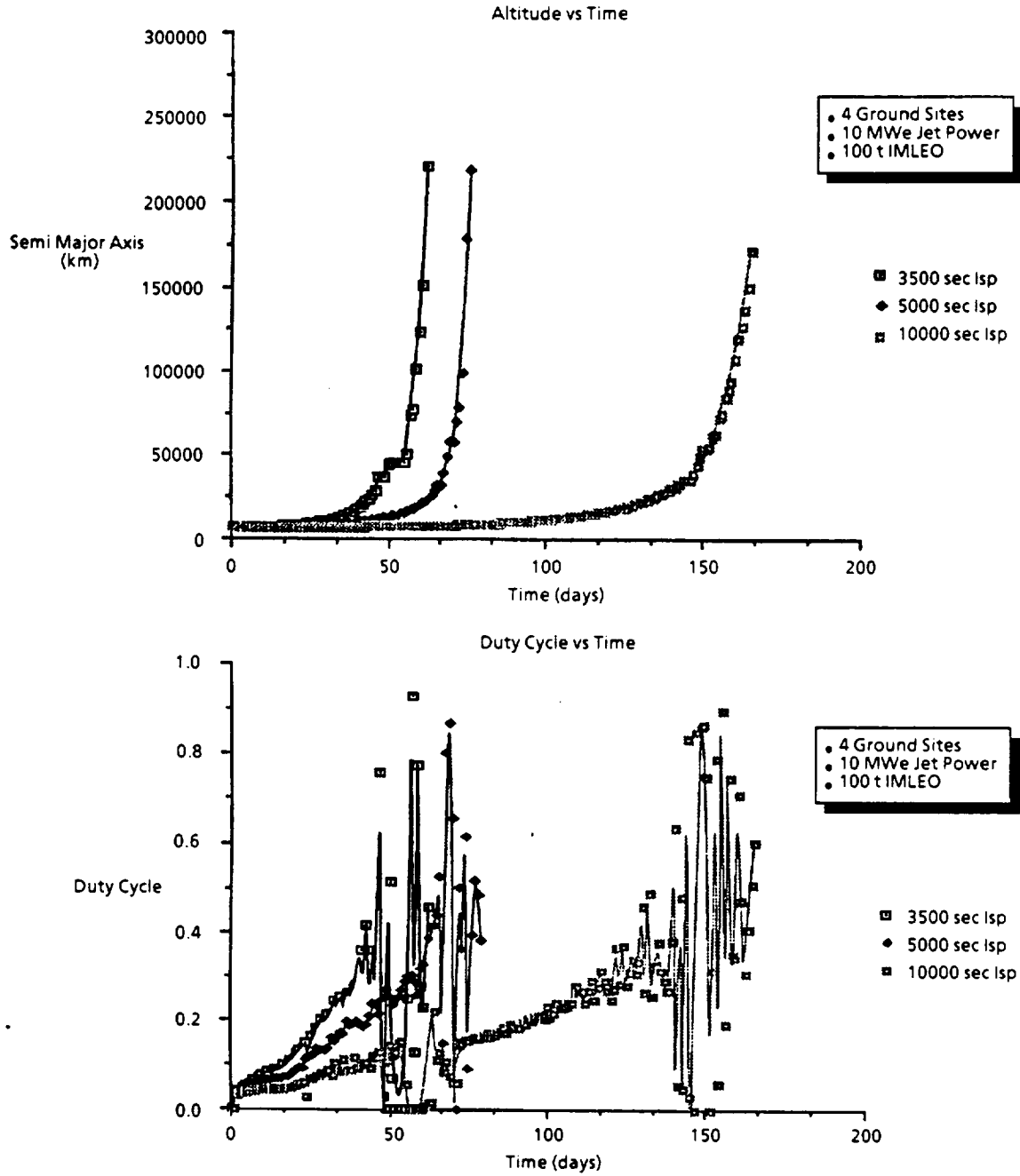


Figure 1-20. Typical Laser Beam Power Electric Orbit Transfer Results (Concluded)

much larger protected area than previously estimated. Estimates had tended to take the worst cases of the various predictions; these showed closure angles as high as 30 degrees.

1.4.3 Synthesis Architecture Analyses

For Mars, the four Synthesis architectures are similar. In all architectures, the first mission is an opposition/return swingby type, and the following missions use conjunction fast transfers. The conjunction fast transfers are all designed to permit an opposition return abort, at or soon after Mars arrival, if necessary. Mars surface cargo is always sent ahead on a prior opportunity. The Synthesis report selected nuclear thermal propulsion as the preferred implementation for the Mars transfer vehicle. The STCAEM Phase 2 effort concentrated on implementation analyses for the Synthesis architectures, and considered only nuclear thermal propulsion. Results of analysis of the Phase 1 issues were applied as described earlier.

1.4.3.1 Synthesis Reference Mars Missions

Architectures 1, 2, and 3 have a first piloted Mars mission in 2014, preceded by a cargo delivery in 2012. Architecture 4 defers the first piloted mission by 2 years to 2016, with the preceding cargo mission in 2014. The 2014 piloted mission is designed for 60 to 80 days on Mars. For Architecture 4, where the first piloted mission arrives in 2016, the surface stay is constrained to about 45 days by rapid increase in mission delta-V for longer stays. Cargo mass estimates indicate these stays can be accommodated by two cargo MEVs sent to Mars the prior opportunity. The second piloted mission is designed for 500 to 600 days on the surface. If the second piloted mission goes to a different place than the first, as recommended by Synthesis, three more MEVs are needed. If the second mission revisits the first site, two more MEVs may suffice. Since processing of cargo for the second piloted mission occurs during the same opportunity as the crew vehicle for the first piloted mission, the number of cargo MEVs has a significant impact on operational requirements.

1.4.3.2 Summary of Tradeoff Factors

The Synthesis architectures leave open a number of lower-level questions, issues and options. Representative trades and options needed to resolve these are depicted in the trade tree in figure 1-21. Cargo quantities were defined by Planet Surface Systems (PSS) at JSC. Total cargo for the first opposition mission is about 80 t; for subsequent conjunction missions about 120 t. The largest surface cargo elements are such that a common MEV can be used for crew and cargo. Two MEVs are needed for the first

mission and three for following ones. Surface transportation is to be provided by PSS to move the Mars surface base elements to a common location after landing. MEV landing precision is estimated as better than 1 km.

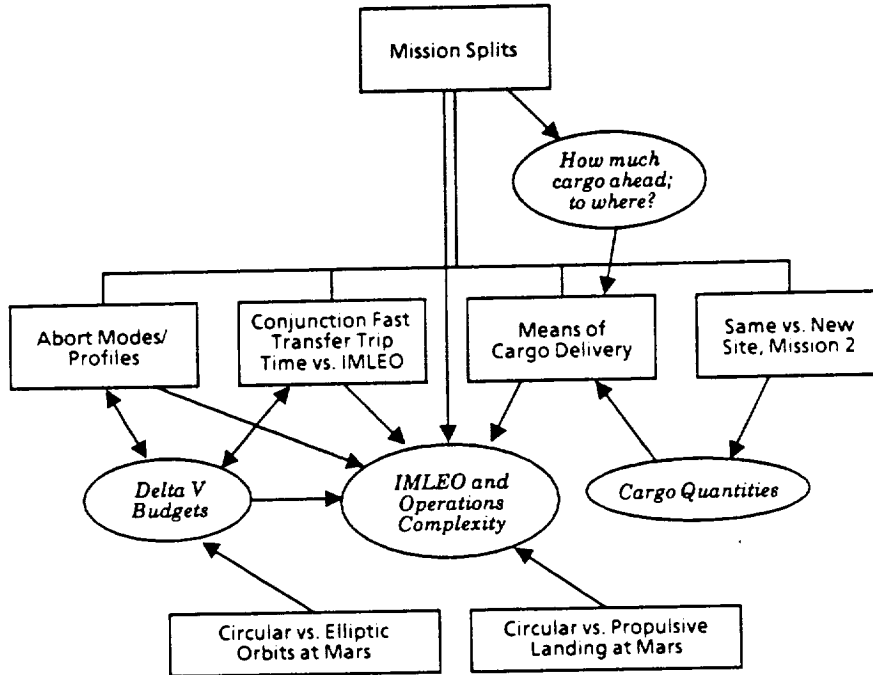


Figure 1-21. Trade and Option Tree for Analysis of Synthesis Architecture Implementations

The mission split recommended by Synthesis sends all cargo and crew MEVs ahead; sending some of the MTV return propellant is mentioned. STCAEM analyses of mission splits, abort modes, launch windows, and delta-V sets are described in the following paragraphs. Circular versus elliptic orbits and the implications on MEV L/D were discussed earlier; analysis led to recommendation of elliptic orbits as the minimum-cost approach. An all-propulsive MEV (no aerobrake for landing) was briefly investigated; the MEV mass is about three times that for an aerobraked MEV.

1.4.3.3 Cargo Splits and Means and Timing of Cargo Delivery

The current study investigated (1) sending all MEVs ahead as cargo, (2) sending MEVs and some return propellant ahead, (3) Mars surface cargo ahead and the crew MEV with the crew mission, and (4) all mission payload together (an all-up mission).

If all MEVs are sent ahead, with or without return propellant, the MEVs must be captured in a Mars orbit where a rendezvous is performed by the MTV when it arrives. To simplify operations, a single cargo mission vehicle with multiple MEVs would serve

each opportunity. This means that the cargo mission vehicle must be assembled during the same time period as the crew mission vehicle for the prior opportunity, e.g., cargo for the 2016 mission with the 2014 crew mission.

If only surface cargo MEVs are sent ahead, they can proceed to landing; rendezvous occurs on Mars. This simplifies operations by enabling integral launch of cargo MEVs, eliminating simultaneous on-orbit processing of crew and cargo missions. An all-up mission must include as many as four MEVs, posing difficult configuration and orbital assembly challenges.

Since there is little disadvantage to sending the single crew MEV with the crew mission, STCAEM recommends (3), the cargo MEVs ahead split option. The cargo MEVs are launched to Mars during the type II (more than 180° heliocentric arc) transfer window which opens several months prior to the piloted mission window. This has the advantage of (1) non-simultaneous orbital launch operations, (2) low energy, and (3) cargo arriving while the crew is there. The greater duration of the type II transfer makes it undesirable for a piloted mission.

1.4.3.4 Nominal profiles; Aborts

Abort analyses considered events in Mars' vicinity, to derive potential delta-V set requirements. For opposition/return swingby profiles, with short stay at Mars, an abort can only return earlier during the stay. The profile is similar to the basic mission profile. No delta-V impact was identified.

A powered swingby abort is possible upon Mars arrival; the delta-V required is much less than the normal capture mission. The decision to execute this abort is best made a few days before Mars arrival as optimal encounter conditions are different than for capture.

After Mars capture, a TEI abort may be executed earlier than the normal departure, usually beginning about halfway through the planned stay time, without delta-V penalty. The trip time for Earth return is essentially the same as for the normal mission. Since the nominal first mission plan has the long-duration base cargo arrive during the crew stay, it is possible (if the base comes, or can be delivered, to the first mission site) for the crew to activate the base and "winter over" until the later crew mission arrives; this mission would perform a rescue.

Synthesis fast-transfer conjunction profiles are designed to couple with an opposition-type return at or soon after arrival. The nominal stay is about 600 days at Mars. An abort can return much earlier by executing an opposition Venus swingby

return. This may be done either by a powered swingby at Mars or by early departure after capture.

The powered swingby abort delta-V is, as for the opposition mission, less than for the normal capture mission. After Mars capture, a TEI abort may be executed 30 or more days after arrival, but there is a delta-V penalty compared to a typical conjunction return. Up to about 30 days, the abort profile benefits from Venus swingby; after that time the abort requires a direct or deep space burn profile with much greater delta-V penalty. The trip time for Earth return is about 300 days. Based on consultation with Level 2 at JSC, STCAEM elected to enable abort up to 30 days after Mars capture (while the Venus swingby window is still open) and use the delta-V thus available to expedite the normal conjunction return.

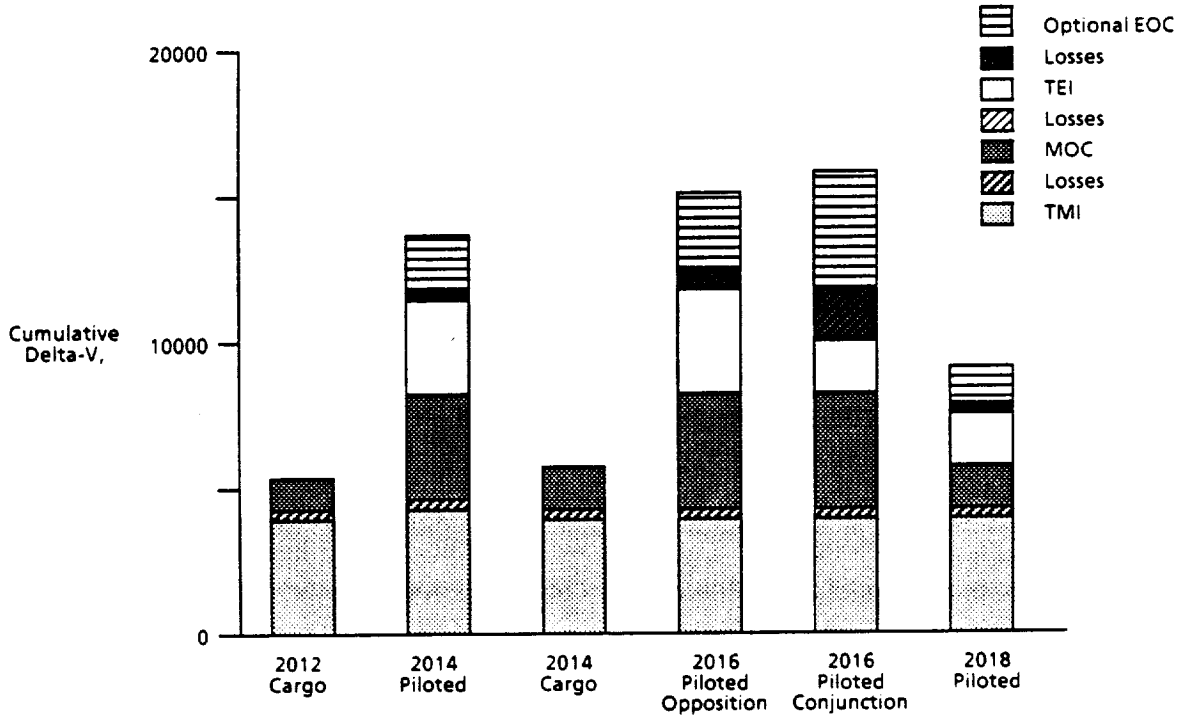
It is also possible for a conjunction mission to "winter over" at the surface base (the stay time is about 800 days) until a rescue can be performed during the next opportunity.

1.4.3.5 Delta-V Sets and Trip Times

Delta-V sets for Mars transportation baselines were defined to include: (1) impulsive delta-V for each maneuver; (2) finite-burn losses, calculated for the three-burn Earth departure and estimated for Mars orbit capture and departure; (3) plane change for Earth departure (made at apogee of the intermediate orbit in the 3-burn departure sequence) as needed to provide a 25-day launch window for launch from a 28.5° orbit; apsidal and nodal alignment penalties for Mars departure, based on the optimum elliptic parking orbit which minimizes these penalties. Mars descent delta-V is that required to decelerate from termination of the aerobraking landing maneuver to a soft landing, and includes a 1-minute hover allowance. Descent delta-V was based on numerically integrated descent simulations with the COSPAR low-density Mars atmosphere. Mars ascent delta-V was based on numerical integrations of ascent profiles, and assumes in-plane ascent to a 100-km phasing orbit followed by in-plane transfer to the MTV elliptic parking orbit. Design reference delta-V sets are summarized in figure 1-22.

1.4.3.6 Mission Requirements and Constraints Influence on Design Requirements

The Phase 1 study treated opposition and conjunction mission profiles generically to obtain comparisons of propulsion systems. The Synthesis architectures specify particular scenarios for transition from opposition to conjunction piloted mission profiles. Long-duration stay capability at Mars is required on the second crew mission. Selection of the MEV ascent propulsion system must consider that a 1.5 year surface stay occurs



Note: The 2016 piloted conjunction mission is designed to use the 2016 opposition profile as an early abort from Mars orbit. The 2016 opposition delta-V set is used to size the vehicle. The conjunction TEI delta-V is required assuming the vehicle uses a Mars parking orbit optimized for the abort case. If a conjunction-optimized parking orbit is used, the large TEI losses become small. The 2018 piloted mission is a conjunction mission, not including delta-V for early abort from Mars orbit.

Figure 1-22. Design Reference Delta-V Sets for Synthesis Mars Architecture Implementation

on its second operational use. While a cryogenic ascent stage is calculated to be the most efficient even for 600 days on Mars, cargo payload delivery requirements of 40 t per MEV define the size of the MEV aerobrake and descent system. This led to a decision to baseline storable ascent propulsion; the descent payload capability of the piloted MEV is less than with cryogenic ascent propulsion but the risk of maintaining adequate cryogenic storage on the surface of Mars is eliminated.

1.4.3.7 Reference NTP Vehicle

The Mars piloted vehicle uses nuclear thermal propulsion for all major maneuvers. The configuration, shown in figure 1-23, includes two NTP engines at 75,000 lb thrust each, a radiation shadow shield, an aft tank assembly, an interstage structure that includes expendable tank attachment and connect provisions, the Mars transfer crew habitat, power, thermal control, attitude control and communications utility services, and the Mars excursion vehicle. The core configuration is launched in two sections on

the 150-t payload capability HLV. Additional hydrogen propellant is provided by expendable hydrogen tanks launched separately and berthed to the core vehicle in low Earth orbit.

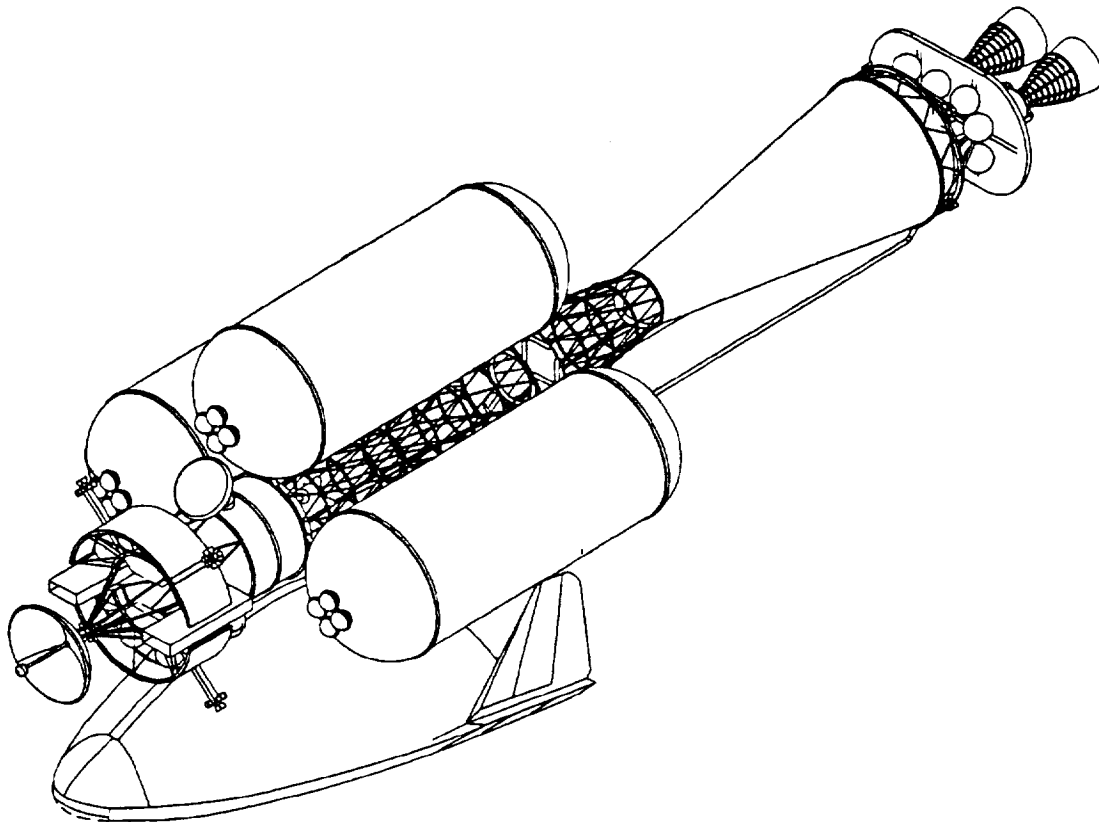


Figure 1-23. Mars NTP Configuration

1.4.3.8 Propulsion

The nuclear engines are advanced prismatic fuel or particle-bed engines with thrust-to-weight ratio of 10 or greater. Isp is baselined at 925 seconds. Liquid hydrogen propellant is provided by vehicle tanks; warm hydrogen gas is routed from the engines to the tanks for pressurization during burns. Vehicle tanks are thermally insulated with multilayer insulation and vapor-cooled shields; active refrigeration is not used. Both engines are operated for all maneuvers unless one is inoperable. Mission rules provide for return-to-Earth abort in the event an engine fails.

Attitude control propulsion is provided by mechanically compressed hydrogen gas obtained from main tank boiloff. Hydrogen gas accumulators provide sufficient storage for any one auxiliary propulsion maneuver; the accumulator capacity is sized by

Earth-Mars leg midcourse correction requirements. Accumulators are recharged during coast periods. Nuclear engines have low-rate gimbal capability for center of gravity tracking; the attitude control propulsion system provides attitude damping during thrust periods.

1.4.3.9 Structures

Propellant tanks use aluminum-lithium alloy. Intertank and other main structures employ advanced composites for reduced mass. The interstage is assembled on orbit from three nestable conic truss segments which are plugged together by a manipulator arm. One of these segments includes drop tank attachment provisions and propellant and pressurization manifolding. The extended length of this structure is sufficient to allow for attachment of the expendable hydrogen tanks.

The transfer habitat is a composite-reinforced aluminum pressure vessel with metallic interior secondary structures.

1.4.3.10 Thermal Control

Thermal control is provided for the transfer habitat and externally-mounted utility services. Cryogenics are insulated as noted above. Nuclear engines provide their own thermal control except after-heat removal which is provided by hydrogen bleed flow from the main propellant system.

1.4.3.11 Electrical Power

All electrical power is provided by a solar array/advanced battery system rated at 27 kWe average power. Batteries provide power during propulsive maneuvers and solar occultations. The system is operated at a de-rated level while parked in LEO so that LEO operations do not dictate power system capacity.

1.4.3.12 Avionics

The avionics system is located in the transfer habitat, except for MEV and CRV avionics, RF power amplifiers for the high-gain antennas, and distributed data acquisition and controllers. The avionics system is multistring and includes vehicle health management functions as well as crew controls and displays. Commonality across avionics systems is maintained to the extent practical, but each vehicle has special functions such as approach ranging for the interplanetary vehicle and landing radar for the MEV.

1.4.3.13 ECLSS

The environmental control and life support system for the transfer habitat is a physico-chemical two-gas system closed on oxygen and water. Food is supplied in shelf-stable and frozen forms. A greenhouse is provided for fresh vegetable supply, but its products are not required for crew health/survival. The ECLSS is redundant as is the pressurized volume of the habitat so that a depressurization only affects half the pressurized volume; recovery and repressurization means are provided. The ECLSS systems for the MEV and CRV are open-loop in view of the short mission duration for these vehicles. The MEV is capable of supporting its crew for up to 5 days while the surface base is checked out and during ascent to Mars orbit at the end of the mission.

1.4.3.14 Crew Systems

The transfer habitat provides full-service crew systems with private quarters, a galley/wardroom, command and control area, health maintenance, exercise and recreational equipment and space. Dedicated radiation shielding is not provided; radiation dose calculations indicate that the shielding provided by the transfer habitat structure, systems and consumables is adequate to protect the crew from galactic cosmic rays and solar proton events assuming the crew uses the galley as a storm shelter during severe SPEs. Radiation analyses indicate the MEV and CRV do not require radiation shielding; this assumes a warning system capable of forecasting approximately 36-hour SPE "safe" periods for MEV ascent. Crew system provisions in the MEV and CRV are similar to those provided by the Apollo command module.

Mars cargo vehicles use the same nuclear engine as the crew vehicles, with one per vehicle since engine-out is not required. Each cargo vehicle consists of a nuclear stage which delivers the cargo MEV to Mars orbit and one cargo MEV. The cargo vehicle is derived from the crew vehicle, applying subsystems as needed. The cargo MEV is the same as the crew MEV with substitution of landed cargo for the ascent stage and crew module.

The Mars Excursion Vehicle performs the descent and ascent maneuvers for the piloted Mars missions, and the descent cargo delivery for cargo-only missions. For the cargo-only missions, the MEV does not have an ascent stage. Descent from Mars parking orbit is performed using an aerobrake to slow down from entry speed to about 600 m/sec; final deceleration and descent use rocket propulsion. Descent and ascent propulsion systems are separate, using storable propellants. The same engine design is used for descent and ascent. The MEV cargo delivery capability is 38 t in the all-cargo mode and 5.6 t in the crew mode.

The propulsion characteristics of the MEV are:

Descent propellant	Earth storables, N ₂ O ₄ + MMH, Isp 340
Ascent propellant:	Earth storables, N ₂ O ₄ + MMH, Isp 340
Rated thrust:	133 kN (30,000 lb.)
Number of descent engines:	4 (derived from lunar LEV engines)
Number of ascent engines:	3
Type of engines:	Pump-fed gas generator, regeneratively cooled

The MEV is designed with an L/D > 1.5 aerobrake. The aerobrake is used during the descent maneuver to decelerate the vehicle and lessen the propulsive requirements. The high L/D provides enough cross-range to reach landing sites at any longitude and any latitude within 20° of Mars' equator, from an optimal elliptic Mars parking orbit. The MEV is designed to be launched external to the launch vehicle in the manner of the Space Shuttle Orbiter to eliminate assembly on orbit. Launch vehicle aero/performance analysis was performed to ascertain that this launch configuration does not pay excessive performance penalties and does not lead to excessive engine gimbal angles.

If a large shroud is available, a deployable aerobrake is an option. STCAEM developed the "flower-petal" rigid deployable configuration shown in figure 1-24 for a low-L/D descent-only brake to be launched in a 14-m diameter shroud. This concept needs further exploration towards smaller shrouds and higher L/Ds.

With either option orbital assembly is eliminated. Cargo MEVs can be integrally launched on a single ETO launch and do not require manned or man-tended orbital operations.

1.4.4 MEV Subsystems

1.4.4.1 Descent Main Propulsion

The MEV descent main propulsion system uses cryogenic engines derived from the lunar program to maximize cargo descent payload; descent propellant does not pose a Mars surface storage problem. The descent propulsion engines are distributed around the periphery of the descent stage to permit cargo to be close to the surface of Mars after landing. This leads to a limited engine out capability; if an engine fails, a balancing engine must also be shut down. The presumed piloted mission rule will be that unless all engines start successfully for the initial deorbit burn, a landing will not be attempted. If an engine fails during or after landing engine restart, an abort to orbit is possible with the ascent stage.

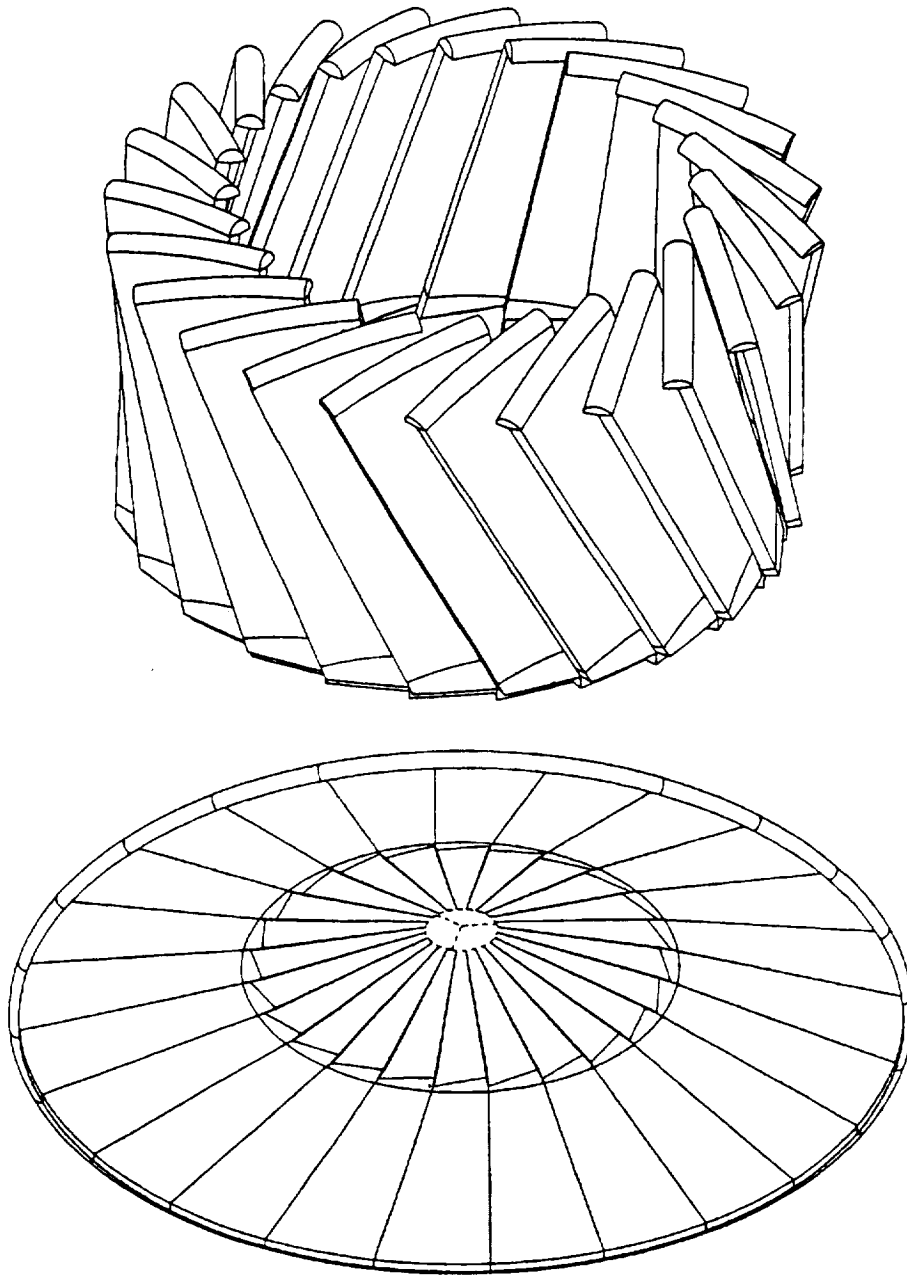


Figure 1-24. Deployable Low L/D Landing Aerobrake Concept

1.4.4.2 RCS

The ascent propulsion system uses storable propellant engines (as noted earlier), clustered beneath the ascent stage center of gravity for full engine-out capability. Each stage of the MEV has its own RCS/auxiliary propulsion system; these consist of self-contained pressure-fed storable propellant/thruster modules.

1.4.4.3 Aerobrake

The aerobrake is a high L/D integral design. Advanced composite materials are used for minimum mass. The heat shield/outer shell is titanium-aluminide with a zirconia overspray. The relatively mild heating environment for deorbit/descent requires modest thermal protection. During Mars descent, after the entry heat and aerodynamic pressure pulse, doors in the brake open and descent engines are started. As the MEV slows down under rocket thrust and aerodynamic pressure continues to decline, the aerobrake is jettisoned. Landing occurs on rocket thrust.

1.4.4.4 Thermal Control

Thermal control of the crew module is provided by a simple single-loop system with body-mounted radiators. The system has limited water-boiler heat-sink capabilities for the descent period when the wake heating fairing is in place. MLI and electrical heaters are used to maintain storable propellants in the desired temperature range.

1.4.4.5 Structures

Propellant tanks are aluminum; the advantages of advanced tank materials are very limited for this small vehicle. Dry structures use advanced composites for minimum mass. The descent stage structure is designed around the cargo-version payload envelope (8 m diameter x 11 m length) and the aerobrake, with a removable section at one end, such that the payload can be lowered onto a transporter and moved from under the MEV. The ascent stage structure is a simple truss arrangement that interconnects the propellant tanks, propulsion system, and crew module.

1.4.4.6 Electrical Power

Electrical power for active periods (descent and ascent) is provided by advanced primary batteries. During dormant, powered-down periods on Mars, health maintenance power is provided by a small solar array/battery system.

1.4.4.7 Avionics

All avionics except descent-unique functions and distributed sensors, effectors and data multiplex/control units, are contained in the crew module. The avionics system is multistring and includes vehicle health management functions as well as crew controls and displays. RF communications links with the MTV and surface base are provided; a backup voice-only and low-rate telemetry link direct to Earth is also provided.

1.4.4.8 ECLSS

The ECLSS is a simple two-gas open-loop system with LiOH CO₂ absorption. Food is provided in ready-to-eat form. Hygiene is Apollo-style. The crew wear EVA suits during decent and ascent; these provide backup for accidental cabin depressurization. All cabin systems (except the obvious ECLSS functions) are designed to operate normally in vacuum. The entire cabin can be depressurized for egress and ingress; if an IVA crew transport module is available on Mars for later missions, a hatch connection for it can be added to the MEV.

1.4.4.9 Crew Systems

Interior crew systems consist of seats, windows for descent piloting, and flight controls and displays. The ascent stage crew module is used for descent to enable descent abort to orbit. An ingress-egress hatch at the top of the crew module includes a berthing adaptor for IVA transfer to and from the MTV crew habitat; a similar hatch and stairway in the side of the module near the planet surface provide for on-surface ingress and egress. No solar flare shielding is provided. Since the ascent and rendezvous sequence can require up to 36 hours, a limited capability to predict flare-safe periods is assumed.

1.4.5 Reference NTP Mission and Operations Scenarios

Flight operations of the Mars crew transportation system begins with the first launch to low Earth orbit. This launch delivers the aft tank/engine assembly loaded with propellant, and part of the intertank truss. The second launch delivers the transfer habitat, the rest of the intertank, the MEV and the CRV. The third launch delivers both MOC tanks. The fourth and fifth launches deliver trans-Mars injection (TMI) tanks. Depending on the specific mission profile and delta-V set, one or more additional launches may be needed for top-off propellant. If human presence aboard the vehicle is needed for assembly assistance or test and checkout, the transfer habitat can be used by an assembly/test crew. This crew will bring their own consumables and provisions so as not to disturb the provisions for the Mars mission.

The part of the vehicle launched first includes a mini-assembly platform with teleoperation arms for berthing the following vehicle elements. These are transferred from the launch vehicle delivery orbit to the assembly area by a cargo transfer vehicle (CTV) equipped with automated rendezvous and proximity operations packages. Vehicle assembly occurs autonomously, assisted by ground-based teleoperation as needed. Debris shields are launched attached to collision-sensitive parts of the vehicle such as propellant tanks, and removed before TMI by the CTV.

About one month before the TMI window opens, a test crew will board the vehicle for final tests and pre-orbital-launch checkout. One week before the window opens the mission crew will board; after a tie-in period the test crew will return to Earth on the shuttle that delivered the mission crew.

Trans-Mars injection occurs in three burns of the NTP system. The first burn places the vehicle in a 72-hour elliptic orbit with apogee about halfway to the Moon's orbit. The second burn occurs at apogee and makes the plane change required to access the trans-Mars velocity vector; orbit period is not changed by this burn. The third burn starts just before perigee and increases the vehicle velocity to that required for TMI. The crew spends the time during the first and third burns in the galley area to reduce radiation dose from van Allen belt passage.

Trans-Mars injection tanks are retained during the coast to Mars for their radiation shielding value. Midcourse corrections during trans-Mars are divided into three maneuvers to reduce total delta-V, improve targeting, and also reduce the amount of hydrogen that must be stored in the attitude control propulsion system accumulators.

A few days before Mars arrival, terminal navigation and maneuvering begin. Navigation can use satellites in Mars orbit or radar ranging of Mars itself for approach state vector update. A test of the nuclear engines assures that both are ready for operation; if a failure is detected, or if other mission/equipment anomalies dictate, the approach path is retargeted by the attitude control system for a Mars flyby abort.

The Mars phase of the mission begins with a single-burn orbit insertion into an elliptic orbit. The state vector is updated by Earth track, and descent preparations begin, including orbital high-resolution imagery and viewing of the planned landing site. The Mars Excursion Vehicle is checked out. Separation and de-orbit of the MEV occurs near apoapsis of the parking orbit. Atmosphere entry occurs 6 to 12 hours later, depending on the parking orbit period, and atmosphere braking begins. The MEV maneuvers towards the landing site and acquires one of the landing beacons delivered with the surface cargo mission. At about 10 km altitude, landing engines are started and the aerobrake is jettisoned. Terminal maneuvering to the landing site is done on rocket propulsion. The final approach is on a 15° descent "glide" slope so that the landing site is visible to the crew on approach. Touchdown occurs within 1 km of the base.

During the descent, the crew occupies the crew module of the ascent stage to enable abort. Abort is possible during the terminal phase of the aerodescent or after descent engines start; the ascent stage can start engines, separate and return to Mars orbit.

After landing the crew performs an ascent stage checkout, powers down and secures the MEV and initiates the surface mission. The MEV health management system remains active during the surface stay to alert the crew of any problem that might call for an abort to Mars orbit.

Upon completion of the surface mission, the crew returns to the MEV, boards the ascent stage, and prepares for ascent. Ascent windows occur at least twice per Mars day, whenever the surface base is in the parking orbit plane. At the first opportunity, ascent is initiated. The MEV ascent stage flies to a 100 km circular phasing orbit coplanar with the parking orbit. Upon arrival at periapsis, burn to a transfer ellipse (apoapsis coincident with the parking orbit) occurs. At apoapsis the final phasing burn occurs followed by rendezvous and docking with the interplanetary vehicle. The crew transfers and the MEV ascent stage is jettisoned. This nominal ascent occurs about 10 days before the return-to-Earth window closes to allow contingency time.

Trans-Earth injection occurs on a single burn. The coast to Earth is similar to the coast to Mars, with multiple midcourse corrections. Terminal navigation for Earth return is provided by the DSN.

About 16 hours before Earth arrival, the crew enters the CRV with the Earth return science. At entry minus 12 hours the CRV separates from the rest of the vehicle. Since the interplanetary vehicle is not on an Earth atmosphere intercept path, the CRV makes a burn of about 20 m/sec to place it on its entry path. The interplanetary vehicle passes by Earth and is abandoned. Earth gravity assist and final attitude control propulsion maneuvers place the vehicle on a trajectory which avoids a later Earth impact. The CRV enters Earth's atmosphere, decelerates, deploys parachutes, and makes a water landing to complete the mission.

The timeline of figure 1-25 depicts Earth orbit assembly operations assuming 150-t ETO capacity. Six launches are required to deliver the 2014 piloted mission vehicle, with three additional for the 2016 mission cargo. The cargo missions are shown scheduled during the cargo window, although they could be launched on a more leisurely schedule and loiter in Earth orbit. Four assembly crew launches are shown. It is presumed that these are regular Space Station Freedom (SSF) logistics/crew launches; the crews reside at SSF and fulfill other duties in addition to supporting Mars vehicle assembly.

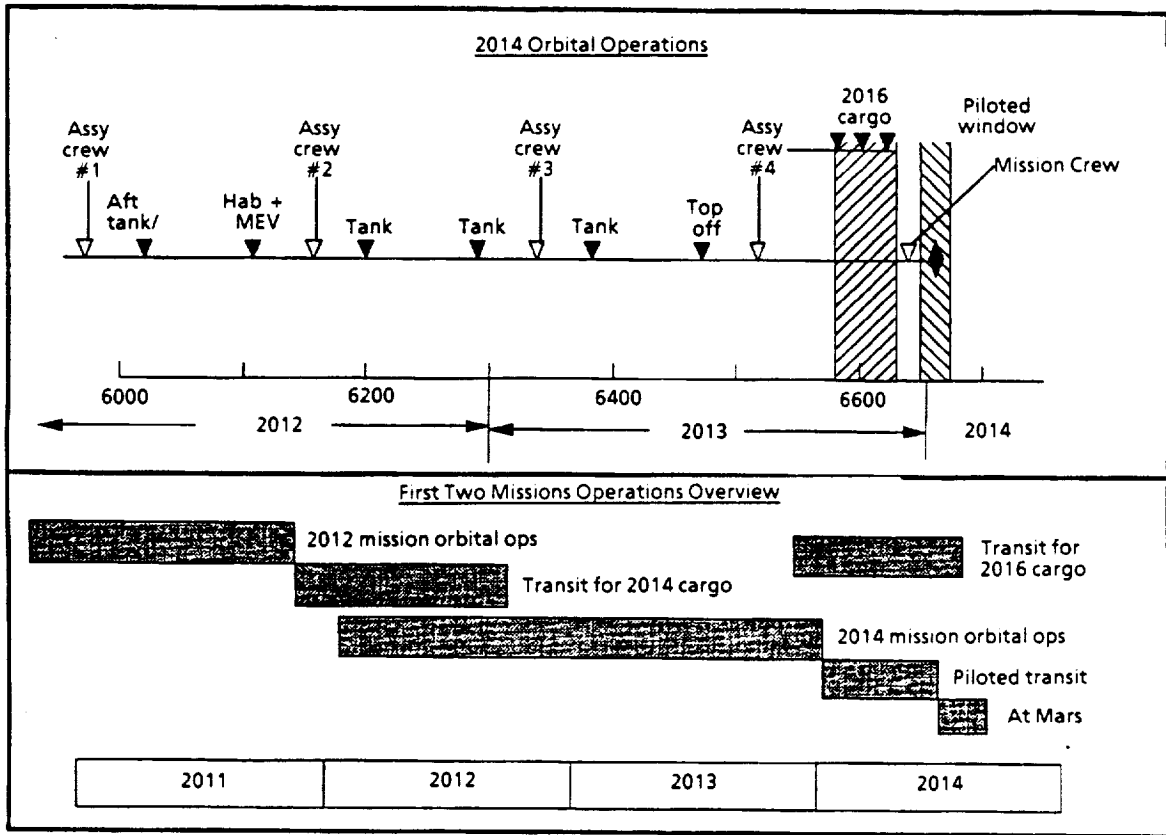


Figure 1-25. Earth Orbit Assembly and Mission Timelines for 2014 Mars Mission

The lower part of the figure shows the 2014/2016 mission activities in the context of the earlier 2012 cargo mission, and that the 2016 mission cargo arrives while the 2014 crew is at Mars. This timeline also shows that if more than six launches were required for the 2014 piloted mission, a higher average launch rate must be sustained to accomplish the 2014 mission in the time available after the 2012 mission is launched from Earth orbit.

The simplification of operations achieved through direct launch of cargo MEVs is premised on the idea that these MEVs land independently after arrival at Mars. Rendezvous of crews and cargo occurs on Mars surface; crew MEVs go to Mars as a part of the crew missions.

1.4.6 Appropriate Size of Heavy Lift Launch Vehicle

STCAEM analyzed the important issue of appropriate heavy lift launch vehicle size for the Mars exploration period. The Synthesis report gives a range of 150 t LEO capability to 250 t. The lower end of this range appears reachable by evolution of the NLS vehicle, while the upper end is probably a "clean sheet" design.

Historical payload mass/volume ratios are approximately the density of liquid hydrogen. This is true, for example, of the shuttle. The study found that lower densities were needed for Mars in-space transportation systems. An effective shroud size for a 150-t vehicle, for example, was 12 m diameter by 32 m cylinder length. This equates to 60% of hydrogen density, about 40 kg/m³. A 14 m by 30 m shroud for a 250-t vehicle was too small; the lift mass capability could not be effectively used.

For Mars missions, an ETO capacity less than 150 t leads to high launch rates and parallel on-orbit processing of crew and cargo missions. Too small a heavy lift capacity will cause bottlenecks in the most intense and complex parts of Mars transportation operations.

The 150-t size enables single-launch direct Mars surface cargo delivery missions as described earlier. Cargo missions need not be processed through an orbital assembly and checkout facility. Each cargo MEV travels to Mars and executes a precision landing at the selected base site.

At 180 t, a toff launch may be eliminated. The added capacity also permits a larger nuclear stage for the cargo missions, enabling propulsive capture into Mars orbit before landing. Designing cargo MEVs for direct entry and landing (arrival C₃ is low on a cargo mission) is expected to prove more cost effective than increasing launch capacity to 180 t, but these cost trades remain to be accomplished.

The study did not identify significant break points above 180 t. In-space transportation vehicle design impacts are anticipated as necessary to effectively use larger launch capacity, but this assessment is incomplete. Further, the hardware loss potential and associated program recovery provisions to accommodate a launch failure grow with greater launch capacity.

STCAEM recommends 150 t as the preferred launch system capacity, with continuing evaluation of capacity up to 180 t. The rationale is summarized in figure 1-26.

- | |
|---|
| <ul style="list-style-type: none"> • Less than 150 t <ul style="list-style-type: none"> - Parallel on-orbit assembly processing of crew and cargo missions - High launch rates indicate launch facilities cost impact • 150 t <ul style="list-style-type: none"> - Process on 90-d. launch centers with some surge capability - Mars cargo - Lunar missions • 180 t <ul style="list-style-type: none"> - Eliminates top-off launch - Enables single-launch delivery of MEV to Mars orbit (rather than TMI) - Impact on launch vehicle development cost estimated greater and earlier than these penalties • 250 t <ul style="list-style-type: none"> - Fewer launches - No significant break points in operations complexity - Mars vehicle configuration impact not yet assessed - Large impact on launch vehicle development cost |
|---|

Figure 1-26. Launch Vehicle Sizing Rationale Summary

1.5 OVERVIEW OF STCAEM RESULTS TO DATE

This section presents considerations of overall lunar/Mars transportation evolution that were developed during the STCAEM study, broader than any particular task or phase of work.

1.5.1 Synthesis Architectures

STCAEM found the Synthesis architectures to be a sound basis for Mars transportation analysis. The Synthesis mission profile strategy begins with an opposition mission, grows quickly to conjunction fast transfer, delivers surface cargo separately, and always includes abort requirements in the profile design. This makes sense from the transportation point of view and leads to practical and flexible implementations. The Synthesis architectures for Mars, however, include so few missions that they do not support a long-range view of transportation needs for Mars.

1.5.2 Architecture Implementation from the Transportation Viewpoint

Lunar and Mars missions are of different character, seen from the transportation viewpoint. Lunar missions can be accommodated by one or two launches of a reasonably sized ETO launcher. Lunar mission profiles remain quite constant over time. Lunar mission trip times are brief, although stay times on the Moon can be long. Risks are modest and well understood. Piloted missions to Mars require many launches, even for the largest ETO systems considered. Trip times are long, performance achievable with advanced propulsion has high leverage, and mission profiles are more complex and varied. Risks are greater and not as well understood.

Eventual purposes are also different. STCAEM touched on this in Phase 1, and Synthesis touched on it in Architecture 4. A number of potential industrial applications of lunar missions have been identified, from energy resources for Earth to exotic laboratories exploiting the extensive very high vacuum, and remoteness and stability of the Moon as a platform. Industrial uses have not been identified for Mars but it is seen as a more attractive site for eventual human settlement because it is more Earthlike than the Moon. From the transportation view, however, these long-range purposes have similar impact, i.e., needs for delivery of massive amounts of cargo.

1.5.3 Lunar Missions and Lunar Transportation

Human lunar missions are an early development target for exploration. A modest beginning with few and simple development projects is needed for budget compatibility. At the same time, provisions for growth to more ambitious activities need to be built in to the systems. STCAEM found that a simple tandem-staged expendable system flying a direct lunar profile had the attributes of (1) fewest development projects for initial return to the Moon, (2) simplest operations, (3) easy access to any lunar landing site, (4) feasibility with a single 150-t-class ETO launch with modest cargo capability, (5) compatibility with a "campsite" early lunar surface mission system, and (6) straightforward evolutionary path to an efficient, economic reusable LOR system.

Because lunar missions are practical with one or two ETO launches, operating efficiency and simplicity demands that lunar missions be designed so that the transportation system operates efficiently. This turns around the usual process of setting somewhat arbitrary requirements and forcing the transportation system to adapt. The recommended process is (1) select an ETO system compatible with reasonable budget expectations, such as an NLS-derived 150-t vehicle; (2) select the most economic in-space transportation system based on a match to ETO capability, i.e., fully use the capacity of one or two ETO launches, balance between development and operating cost for the early lunar program traffic level, operational simplicity, ability to perform initial crew missions, and identified evolutionary path to economic operations at later lunar program traffic levels; and (3) determine the derivative cargo delivery capability of this system and fit the lunar surface missions to that capability. Not following this process leads to a lunar transportation system that does not use the ETO system efficiently and is therefore more expensive to field and operate than it should be.

1.5.4 Mars Transfer Propulsion and Aerobraking

STCAEM has consistently identified nuclear thermal propulsion (NTP) as the best choice for Mars transfer propulsion, based on current estimates of performance and cost. Uncertainties associated with NTP performance and cost justify one or more backup technologies until technology advancement efforts reduce the uncertainties. SEP technology needs to be brought along for cargo delivery as discussed below; this is a potential backup for Mars transfer propulsion depending on its cost and performance outcomes which are also highly uncertain. Aerobraking in some forms is essential to exploration missions: Mars precursors, crew return vehicles for Earth entry, and Mars excursion vehicles, both crew and cargo. Aerobraking technology must be brought along for these needs. One of the major perceived issues with aerobraking for Mars is assembly of large aerobrakes on orbit. STCAEM identified three avenues to eliminate assembly: (1) integral side-mount launch of a high L/D MEV, (2) integral launch (12-m or larger shroud size) of a bent biconic median L/D MEV, (3) a rigid deployable "flower petal" low to median L/D aerobrake. While all of these concepts need much more work, it is judged that aerobraking is a viable technology backup to NTP for Mars transfer application provided that aerobraking technology is advanced appropriate to its other uses.

1.5.5 MEV Lift-to-Drag Ratio

STCAEM investigated high L/D MEV concepts while the prevailing thrust of the aerobraking community has been directed to ascertaining how low the L/D could be and still achieve a successful aerocapture. From the system design point of view, low L/D concepts are well in hand. The current study effort was motivated by the view that Mars landing site access has not been adequately addressed as a mission requirement, and when it is, high L/D will be needed to meet the requirement. Mars scientists have expressed the need for access to varied targets including the polar regions, which are of very high priority for the search for traces of ancient life. The STCAEM high L/D concepts and analyses provide an initial data base for highly flexible landing site access.

1.5.6 Cargo Requirements

The current trend in exploration mission understanding shows continuing increase in cargo delivery requirements relative to crew transportation. This trend merges with (1) recent advances in solar array technology, now being explored for Space Station Freedom growth and application to potential DOD electric orbit transfer applications; and (2) recent emergence of concepts and supporting technology for transmission of

megawatt-class power by laser from Earth to cislunar space. The resulting indication is that electric propulsion for cargo transfer to lunar and Mars orbits needs review and update. The levels of cargo delivery associated with longer-range lunar and Mars missions would benefit in a major way from the high efficiency of electric propulsion.

1.5.7 ETO Transportation and HLV Size

One area where the Synthesis report recommendations are contrary to indications of other studies is in the focus on very large ETO vehicles. The idea of simplifying orbital operations is meritorious, but at what cost? Launch vehicle studies during the Apollo era associated low cost with very large payload capacity, but everything learned in the last 20 years points to an urgent need for routineness and simplicity of ETO operations. A very large ETO vehicle has no other mission but exploration; the exploration program must fund its entire development. A vehicle derived from a general-purpose vehicle is better; using the general-purpose vehicle itself would be still better.

There are a number of U. S. activities, from the National Aerospace Plane and Single Stage to Orbit to a variety of projectile launch concepts, targeted for dramatically lower unit cost (dollars per pound) in small sizes. High launch rates are a common and sometimes unstated assumption in these schemes. Whether any of them will come to realization or be successful in delivering on low cost is not yet known. Whether a success in this area could serve exploration missions, and how, certainly merits analysis.

STCAEM made significant advances in understanding how to simplify on-orbit operations for Mars vehicle assembly without reliance on very large launch vehicles; in fact little on-orbit operations payoff in going larger than 150 t was identified. The concept engineering work has just commenced; there is much more to be done in this area. Exploration missions and transportation systems need to be designed to fit into the national ETO launch strategy without creating singular, and very expensive, requirements and systems with no other users.

2.0 VEHICLE INTEGRATION

2.1 INTRODUCTION

The current study includes the development and detailing of the following vehicle concepts, listed in order of priority: (1) the Nuclear Thermal Propulsion archetype described in Phase 1, reference 1 (2) a new Mars lander (HMEV) with $L/D = 1.6$; (3) a simple, cost-effective solution to the return-to-the-Moon problem, called the Lunar Campsite; and (4) a revision of the microgravity version of the nuclear electric Mars transfer vehicle (NEP) described in Phase 1. The discussion below reports these vehicle integration results, beginning with the lunar systems and then moving on the Mars systems.

2.2 LUNAR CAMPSITE CONCEPTS

The lunar campsite approach uses two versions of a single in-space transportation vehicle type to enable an early, cost-effective surface-operations capability on the Moon. Two tandem LTV-type chassis (75 t cryogenic propellant capacity each) deliver the Campsite, unmanned, to the lunar surface. Two more deliver the Lunar Crew Vehicle (LCV) nearby, and the crew inhabit the Campsite for surface missions lasting for one or two months at a time. The mission profile is shown in figure 2-1. Lunar surface construction equipment, lunar orbit rendezvous, LEO assembly, SSF rendezvous upon return, aerocapture, refurbishment, in-space transfer of propellants, cargo and crew, and the development of a separate (LEV) vehicle are all avoided by this architecture.

Several mission-mode and configuration variants of the basic idea were explored. The campsite mission capability and architecture were first investigated in the earlier study, reference 1. Initial hardware concepts for the Campsite surface module were developed under Boeing 1990 IR&D. Early in this investigation, a "mini-campsite" alternative was investigated which baselined an LEV-type chassis (25 t propellant load) to perform a "single-shot" campsite mission and avoid multiple HLV launches. That mission type was found to be marginally feasible, with one caveat (a high-energy, SSME-based upper stage was required for the HLV) and two major penalties: weight limitations prohibited delivery of 30 d-class lunar surface science payloads, and drove selection of an open-loop ECLSS requiring resupply of life support consumables on each crew flight.

The effort reported here returned to the "full-size" Campsite, regenerable ECLSS, and tandem-direct mission mode. Fundamental goals remained early accomplishment, simple and robust systems, self-deployment and self-sufficiency. Six critical, unresolved

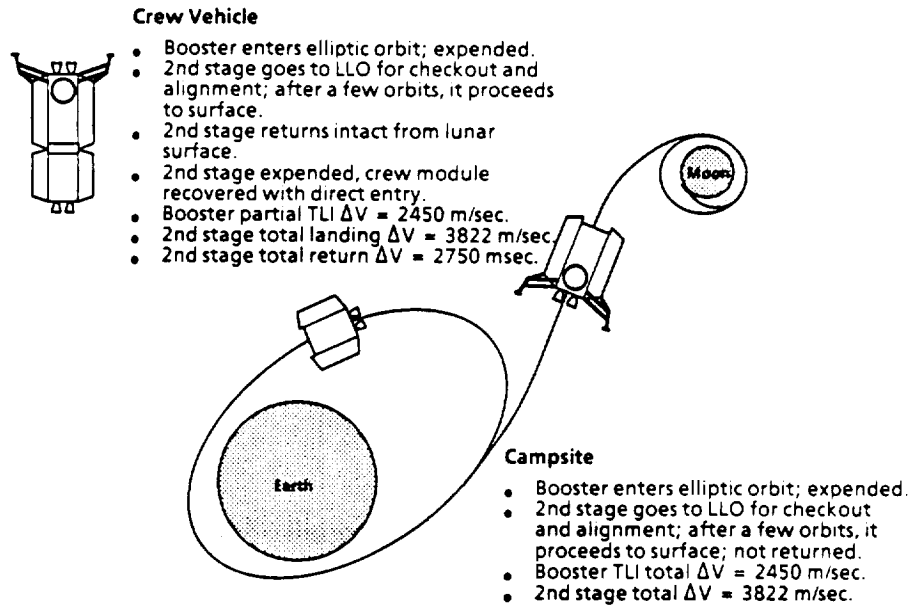
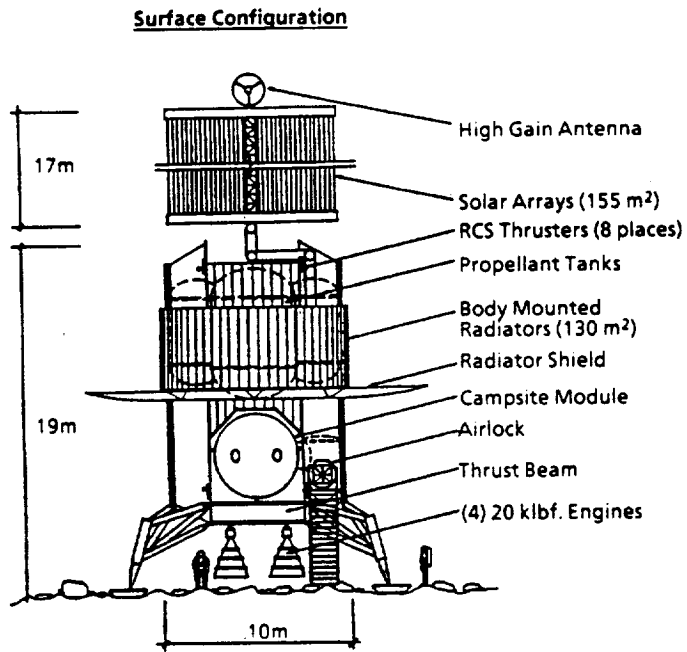


Figure 2-1. Lunar Campsite Mission Mode

areas were used as the starting point: (1) the type of CRV to be integrated into the LCV; (2) the specific nature of that integration, especially location and orientation; (3) the best way to scar the design for later *in situ* system upgrades and growth; (4) the integration of the surface module with the Campsite vehicle bus; (5) the surface relationship between the two landers; and (6) requirements for robotic capability, especially provisions for external manipulation. Major areas of accomplishment were: (1) science manifest refinement, including provision of a tele-rover preceding crew arrival; (2) propellant tank sizing to fit the driving case (the LCV); (3) thermal control system detailing, and regenerable fuel cell sizing based on careful nighttime power budgeting; (4) scrubbed volume and area requirements for the Campsite interior, with matching resupply requirements; and (5) definition of health care provisions.

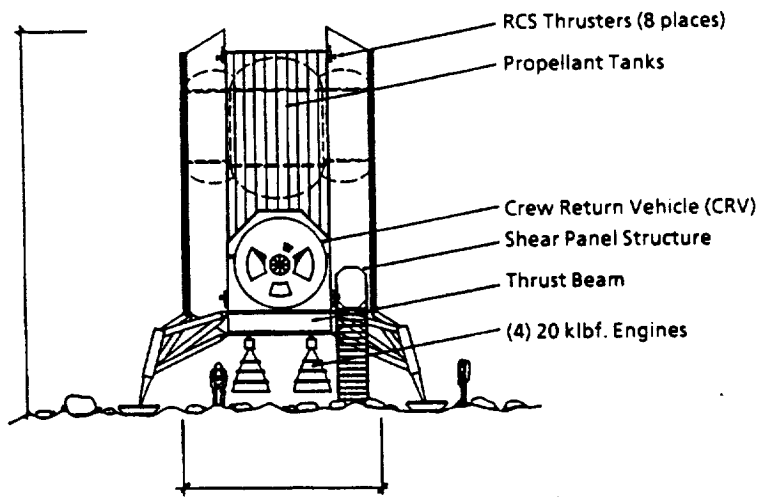
Integrated vehicle concepts fitted within a 10-m shroud for both the Campsite and the LCV were produced (figure 2-2). A descent-stage vehicle geometry was selected with the payload located above the propulsion subsystem and below the tankage; this keeps the number of redundant engines required to one. Four clustered 20 klbf engines are used. The Campsite and LCV both use the same vehicle chassis. A shear-panel structure system supports the cryogenic propellant tanks and leaves outboard "corner" spaces for subsystems integration. Maintenance access to the subsystems is then from the outside.



Mass Statement

Boost LTV	
Inerts	10.6
Propellant	<u>71.7</u>
	82.3 mt
Lander	
Inerts	10.6
Propellant	57.1
Campsite	<u>31.6</u>
	99.3 mt

Figure 2-2a. Lunar Campsite Vehicle Concept



Mass Statement

Boost LTV	
Inerts	10.6
Propellant	<u>72.0</u>
	82.6 mt
Lander	
Inerts	10.6
Propellant	74.4
CRV	8.2
Crew & Supplies	3.9
Rover and Science	<u>2.7</u>
	99.8 mt

Figure 2-2b. Lunar Crew Vehicle Concept (LCV)

On the Campsite, a tracking solar array is stowed in one of these utility spaces, and deploys above the vehicle after touchdown. Body-mounted radiators with deployable surface-view shields are wrapped around the upper half of the vehicle. Below, a clear-through payload bay accommodates either the surface module (for the Campsite) or the CRV (for the LCV). A simple berthing carriage facilitates controlled separation of the CRV from the LCV after the TEI burn. On the LCV, a surface-staged airlock in front of the CRV allows an upright posture for the crew during landing and ascent, and avoids months-long depressurization of the CRV. Small external viewing ports are provided in each end of the Campsite surface module, and a growth port is located in one side, opposite the airlock. The LCV is landed uprange and to the side of the Campsite, no closer than 500 m away. The tele-rover delivered and unloaded by the Campsite can then meet the crew upon their arrival and transfer them to the Campsite.

2.3 HIGH-L/D MARS EXCURSION VEHICLE (HMEV)

The HMEV concept was planned as the reference destination payload for the integrated NTP Mars transfer ship discussed below. Knowledge about Mars aerobraking has evolved substantially over the last 3 years, and attention in the exploration community has vacillated throughout the entire range of L/D ratios practical for Mars aerobraking, from roughly 0.2 to over 1.5. Because the integration details have significant effects on vehicle size, mass and performance, it is important to understand the implications of L/D selections throughout this whole range. In the previous study, integrated concepts for Mars landers with $L/D = 0.5$ and $L/D = 1.1$ were developed. An integrated vehicle concept with an $L/D = 1.6$, the highest yet studied, has now been developed. The basic characteristics of this vehicle are improved maneuverability, reduced heating, and the achievement of greater cross-range upon entry to allow greater site access around the globe of Mars. The cross-range capability is especially important for crew landings, given current emphasis on high-thrust propulsion for Mars transfer (NTP, or CAB backup).

2.3.1 Mission Payloads

The HMEV integration effort began by taking a fresh look at down-cargo capacity to match Synthesis and LMEPO mission designs. Payload drives transportation system design, and Mars lander mass is amplified back through the entire transportation system to Earth's surface, so special attention was paid to the HMEV payloads. LMEPO provided a strawman manifest in March 91 for cargo to be delivered to the surface of Mars. Initial work began with those data, and later responded to the analysis of a new

cargo manifest data set provided by the LMEPO Design Reference Mission for Synthesis Architecture 1 in August 91. A comparison was made between the numbers provided and those available directly from other relevant sources (prior contracts, Space Station Freedom WP-01 and WP-02 mass properties databases, Phase 1 STCAEM, PSS Level III, specialists from Level IV and several noted Mars scientists), tempered by an assessment of mission risk. A summary of the LMEPO guidelines for the 2014 and 2016 surface missions is shown in figure 2-3, as are the recommended departures from them, and supporting rationale. "Mission margins" have not been included.

Element	Level II 4/8/91	Level II Arch-I DRM	STCAEM 8/91	Comments
Habitat	25.70	18.02	26	Original estimate more credible 2.5 kg/man-d + LSS + EVA 2, adapted from SSF WP-02
Consumables	3.46	3.00	2.4	
Airlock	2 (4.9)	5.50	6.0	
Open rover	2 (1.67)	1.5	2 (1.5)	Smaller estimate more credible; 2 required for rescue
Press. rover	---	5.7	---	Not needed for 90 d stay
25kW power cart	---	5.22	---	Not required
Trailer	---	3.00	---	Not required
Construction vehicle	---	2.5	---	Not required
PVA/RFC	4.00 (50 kW)	2.3	4.0	25kW only; Boeing parametrics
SP-100	---	5.20	---	Not required
Surface science	3.15	3.18	3.2	As given
	49.45 t	55.12 t	44.6 t	

No mission margin included

46 t total design down-capacity available

Figure 2-3a. Short-Stay Landed Payload Comparison

Element	Level II 4/8/91	Level II Arch-I DRM	STCAEM 8/91	Comments
Habitat	36.28	35.50	36.4	Long duration unitary module; ambient gravity and spares Function provided by lander Food, gases, supplies 2, adapted from SSF WP-02
Hab chassis	0.65	0.65	---	
Consumables	23.17	18.00	14.2	
Airlock	---	5.5	6.0	
Open rover	1.67	1.5	1.5	Smaller estimate more credible
Press. Rover	6.5	5.7	2 (6.0)	2 required
25 kW power cart	5.22	5.22	2 (5.22)	As given; required for each rover
Trailer	3.00	3.0	3.0	As given
Construction vehicle	---	2.50	---	Function provided by lander
SP-100	---	5.2	5.2	As given
PVA/RFC	2.00 (25 kW)	2.3	4.0	Boeing parametrics for 25 kWe
Science (incl. ISMU)	4.80	5.88	10	Long-duration-class science
	83.29 t	90.95 t	102.7 t	

No mission margin included

43 t down-capacity available per cargo HMEV

Figure 2-3b. Long-Stay Landed Payload Comparison

Basically our reviews have confirmed the overall picture of delivery requirements for Mars surface missions as satisfactory, although there are three specific suggestions: (1) consumables allocations should be based on reusing clothing, linens and utensils -- 2.5 kg/man-d adequately covers a reasonable mix of hydrated and dehydrated packaged food, repressurization gases, life support and EVA consumables, and miscellaneous supplies like paper, personal hygiene materials, and disposable supplies; (2) sensible risk management dictates taking a backup for whichever surface mobility system has the longest range -- in this case the pressurized rover and its support; and (3) 3000 man-d on the surface enables a different kind of science than the 540 man-d available to the 2014 mission -- appropriate science equipment will have to include provision for enhanced site access technologies. With an HMEV delivery capacity of roughly 45 t, one vehicle can deliver the 2014 manifest, but in general three will be required to support 600 d Mars surface missions.

To drive the payload bay size, an 8 m diameter, unitary habitat module sized for six crew in a gravity field was used as cargo, of the same type selected for the Mars transfer long-duration habitat trade study, reference 1. This represents the least-mass solution, as well as the one most amenable to long-duration habitability and eventual growth.

2.3.2 HMEV Design Drivers and Concept Evolution

The purpose of the study was to design a single vehicle type that could accommodate either unmanned cargo or crew-carrying missions, that would be sized to accomplish the 2014 mission with just one cargo and one crew landing, that would be expendable and staged, and that would address directly and in an integrated fashion the perennial problem of landing proximity, cargo offloading, and surface positioning.

Three categories of design drivers were addressed. First was the accommodation of three different kinds of payload manifests: (1) bulky and heavy cargo, e.g., surface habitat systems; (2) mixed cargo, e.g., collections of rovers, science equipment, power systems and supplies; and (3) the ascent vehicle (MAV) for crew-carrying missions. Second was the integration, ETO launch, use and finally shedding (after engine-start but prior to terminal descent) of a sleek, closed aeroshell. Third was the provision, intrinsic to the lander, of sufficient surface mobility to position properly the cargo it lands. The response to these drivers resulted in a vehicle concept, (fig. 2-4) with a large, adaptable payload bay; limited surface mobility able to bring separate landers together, maneuvering, depositing and manipulating their payloads; and a lightweight, segmented, fully enclosing aerobrake. The cargo version can deliver 41 t (including ASE) to the

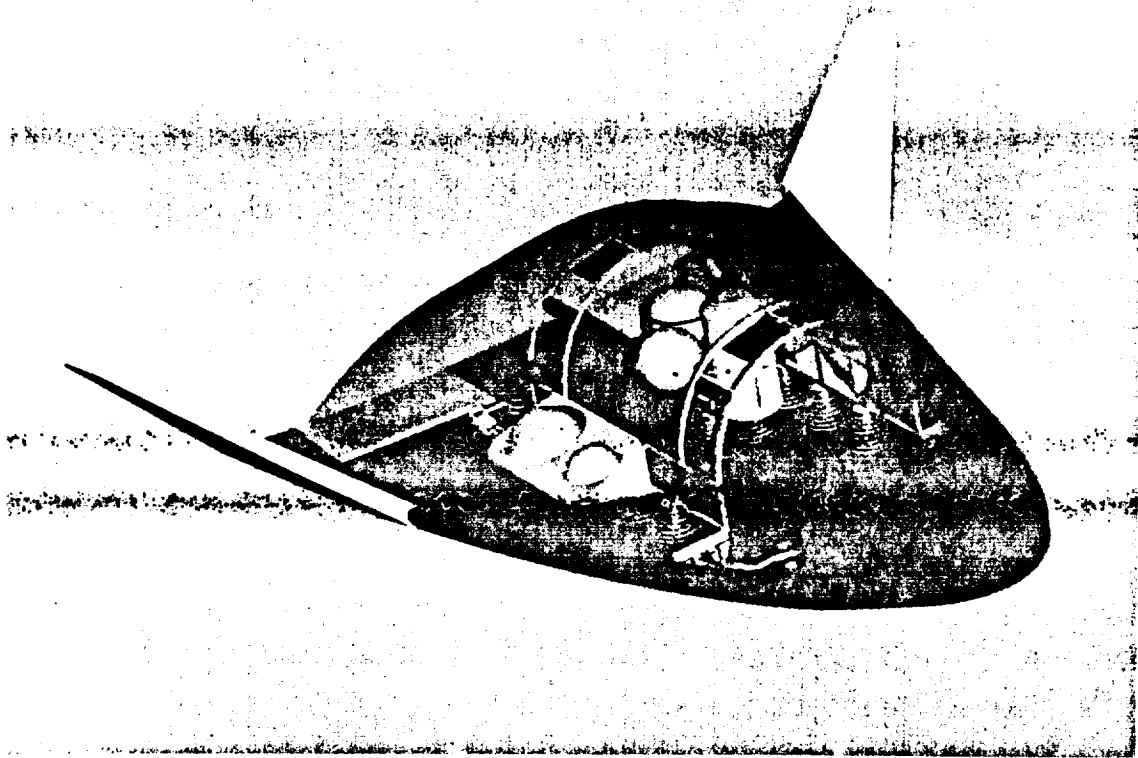


Figure 2-4a. LID = 1.6 Mars Excursion Vehicle Concept (HMEV)

surface, while the crew version can deliver 9 t (including ASE) in addition to the complete MAV. Together, this delivery capacity can accommodate the STCAEM 2014 surface payload manifest mass with about 10% allowance for ASE and mission margin, figure 2-5.

Storable propellants were baselined for the ascent vehicle (MAV). Three 30 klbf engines are used. Although cryogenic propulsion has marginally superior performance even for conjunction-class surface stays, it requires absolute integrity of vacuum-jacketing in the Mars atmosphere for the entire surface interlude. The minutes-to-hours warning for an abort-to-orbit incurred by this system was incompatible with a mission design incorporating multi-day, pressurized-rover crew excursions away from the MAV.

The MAV is arranged to allow a short stack and good crew visibility for touchdown (fig. 2-6). A modest nominal engine cant allows full CM tracking with any engine out during any mission phase (the slight, permanent steering loss caused by the cant is taken into account in the propellant budget). A new crew cab concept is baselined, derived

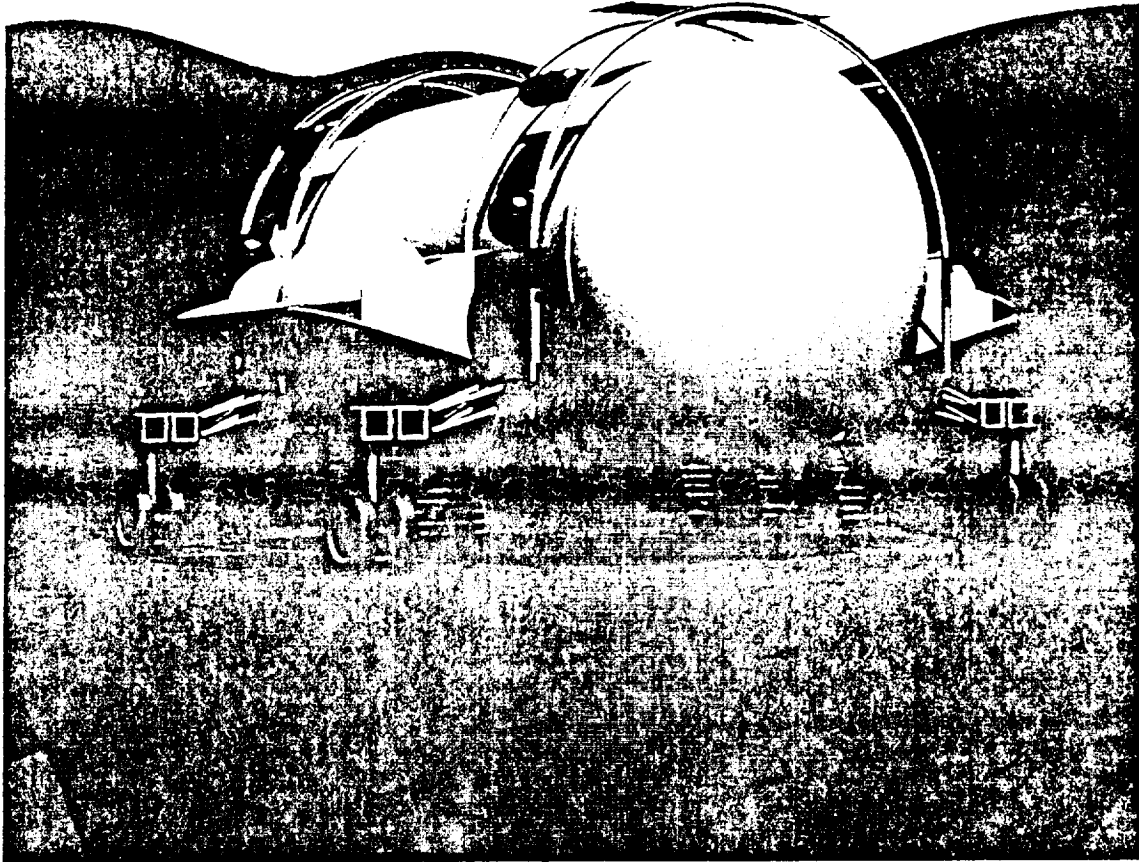


Figure 2-4b. Cargo HMEV Lander on Mars

specifically for this MAV concept but appears to have good applicability across architectures. It responds directly to two key drivers, volume and shape. Pressurized volume/crew is commensurate with the Apollo LM, and with current JSC man-systems baseline values, for a total of 24 m^3 . The vertically-oriented, 2.5 m diameter cylinder integrates well with excursion vehicle geometry; allows a two-deck arrangement analogous to the shuttle with good visibility for the flight crew; and permits both a small hatch on top for berthing to the MTV habitat and a submarine-type door hatch for EVA egress on the surface. The entire cab is depressurized for surface egress.

The initial HMEV brake shape selected to attain $L/D = 1.6$ was a wide delta wing, because it seemed to allow the smallest overall dimensions. A radially pseudo-symmetrical lander concept was developed which would use six legs, each capable of lifting off the ground and pivoting laterally through a small angle, to walk the lander

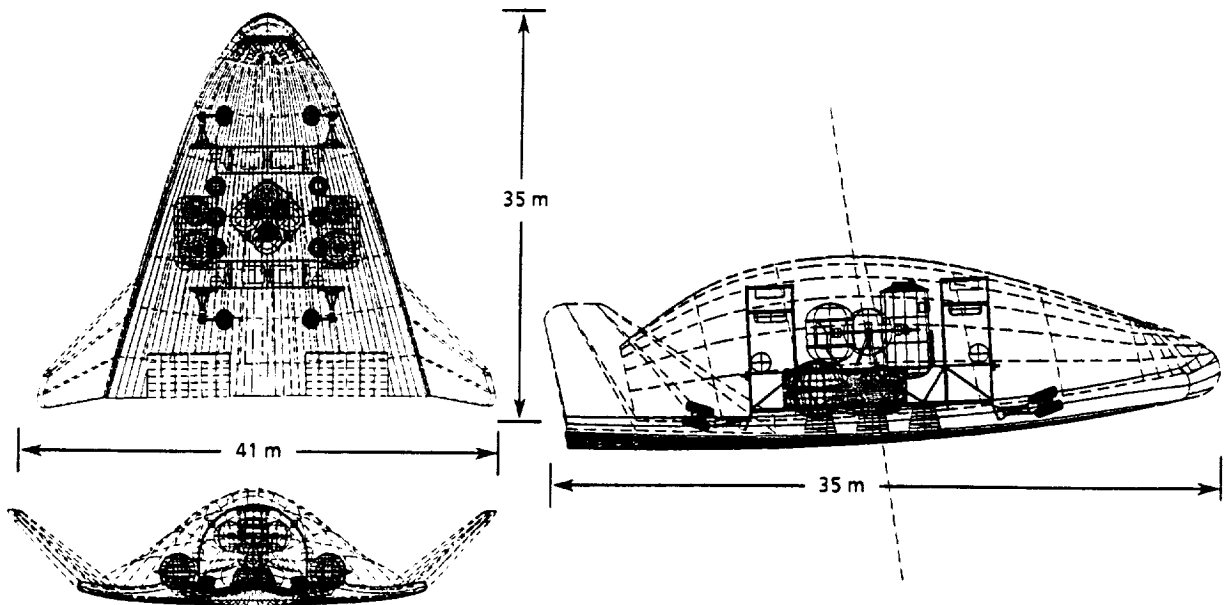


Figure 2-4c. HMEV Crew-Carrying Vehicle General Arrangement

Systems	Cargo Version		Cargo Version	
Ascent Stage			X	
Crew Cab	4,250			
N ₂ O ₄ (includes 3% steering loss)	17,281			
MMH (includes 3% steering loss)	9,095			
RCS Propellant	244			
Propellant tanks	1,567			
Propulsion System (engines, lines, etc.)	649			
Structure	391			
Stage total	33,477			
Descent Stage	(Cryo)	(Storable)	(Cryo)	(Storable)
Cargo	8,904	5,646	40,939	37,681
LH ₂ (MMH)	1,709	5,399	1,709	5,399
LO ₂ (N ₂ O ₄)	10,252	10,259	10,252	10,259
RCS Propellant	1,103	1,087	1,103	1,087
Propellant Tanks	1,969	1,576	1,969	1,576
Propulsion System (engines, lines, etc.)	1,296	1,296	1,296	1,296
Structure	1,316	1,316	1,316	1,316
Wheels	-----	-----	331	331
Drive System (motors, susp., etc.)	-----	-----	675	675
Power System (10 kWe arrays and battery)	-----	-----	285	285
Landing Legs	817	817	-----	-----
Robotic Manipulator System	1,000	1,000	1,000	1,000
Aerobrake	10,644	10,644	11,612	39,040
Stage Total	38,010	39,040	72,487	72,517
Total (kg)	72,487	72,517	72,487	72,517
All values except cargo and propellant mass include 15% growth				

Figure 2-5. Reference HMEV Mass Summary

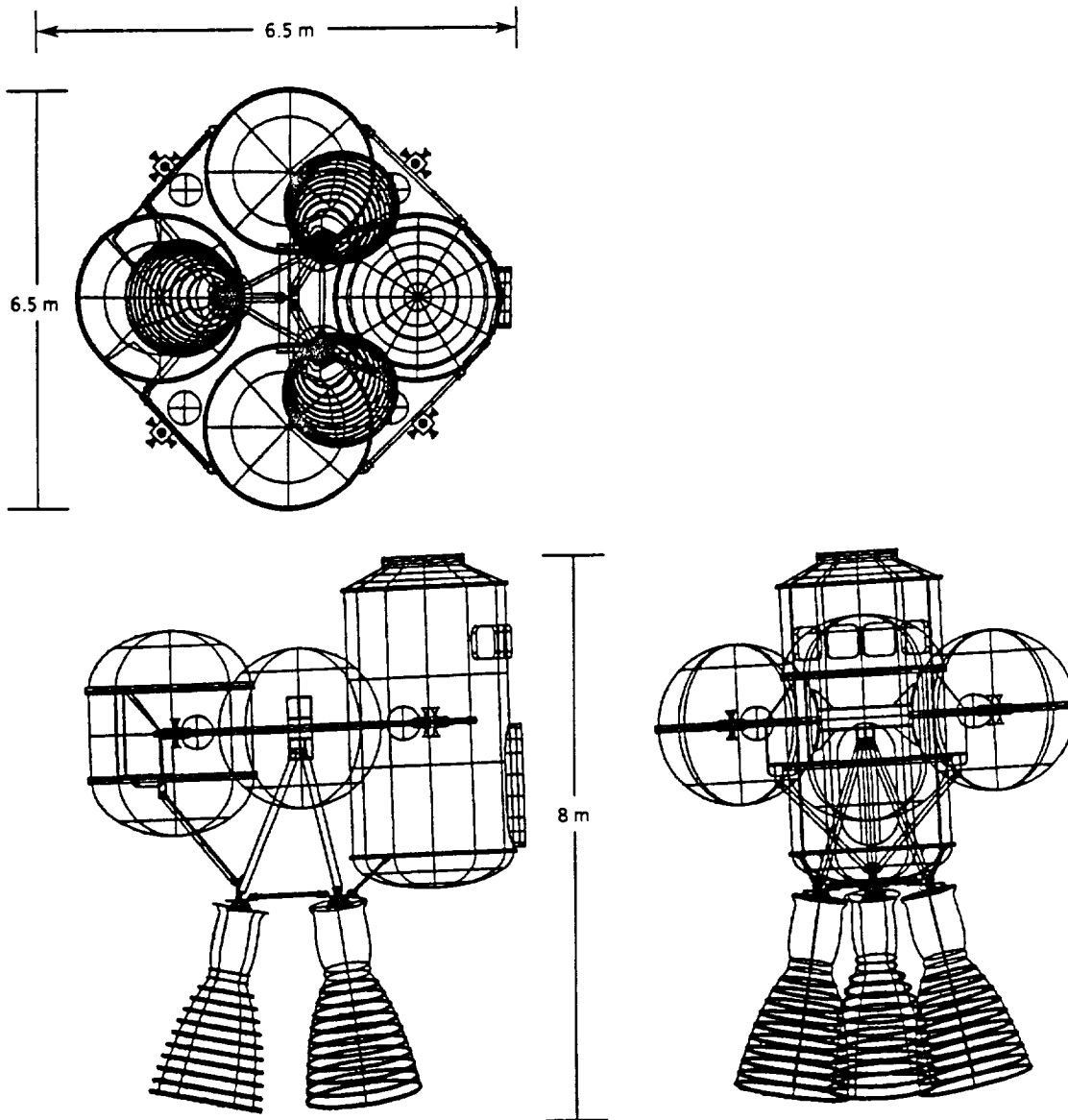


Figure 2-6. Mars Ascent Vehicle (MAV)

across the surface. However, wake-driven packaging forced the initial concept to require an extremely large aerobrake, most of whose interior was empty. In an effort to choose a narrower, more compact brake shape, a symmetrical lander was adapted. It started with four independently actuated vertical leg-columns, each with a wheel/drive assembly, to facilitate level travel over uneven terrain and straddling offloading. Finally, eliminating the straddling requirement (by having the lander frame open at one end like a gate for offloading) allowed substituting a more conventional, deployable mobility system, which resulted in a smaller vehicle, figure 2-7.

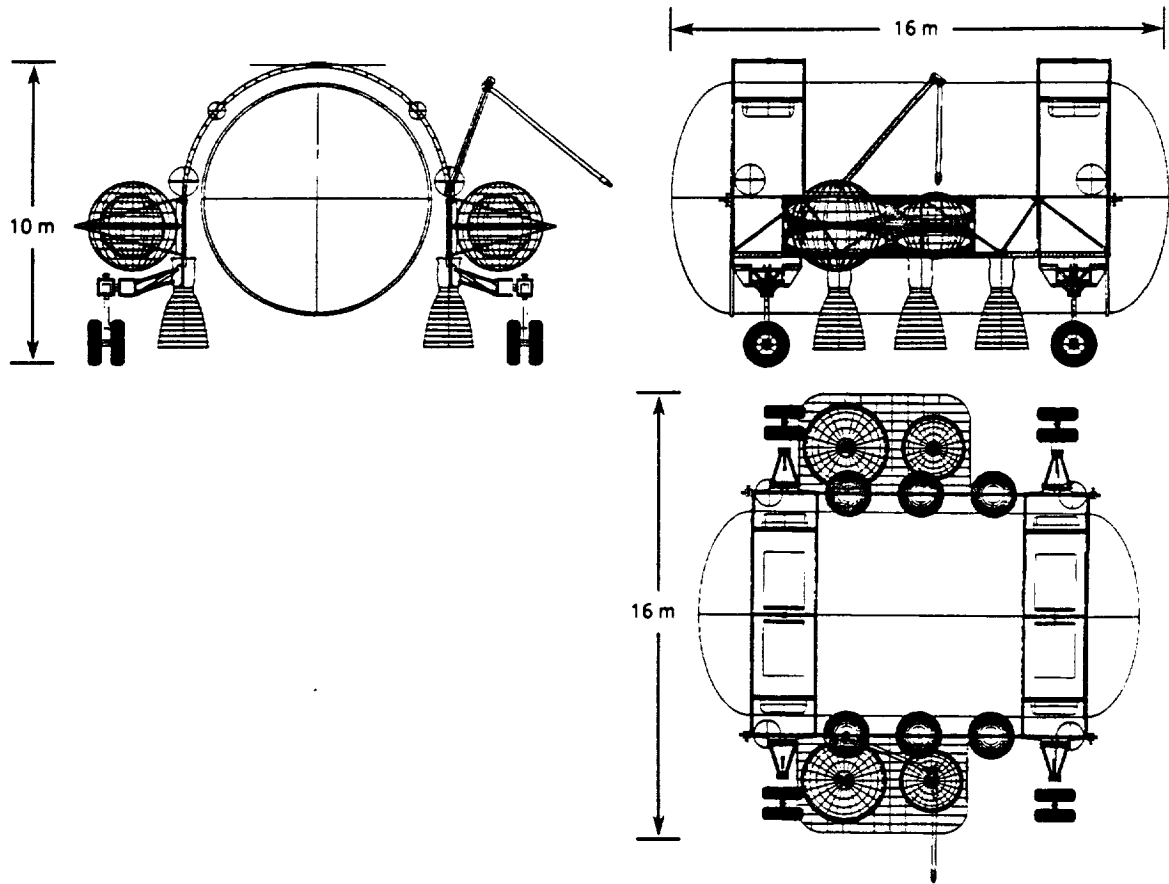


Figure 2-7a. Cargo Lander Anatomy

The bus frame is configured with two pairs of structure arches, leaving a large opening in the top for MAV integration. Attitude control, power, communications and payload hoisting subsystems are located in the spaces between each pair of arches, with propellant crossfeed, data and power lines running in the structure channels. Solar panels are stowed with their active surfaces protected during descent and deployed once on the surface. The power system is sized to collect and store a modest amount of solar power (1.5 kW) throughout most of the Martian day, allowing a higher-power, short-duration expenditure (10 kW for about 45 min) to provide "creeping mobility" (7 cm/s) to the chassis. Using this thrifty method, distances on the order of a kilometer (anticipated to be within nominal touchdown accuracy) can be covered in just a few days. A single, light-lifting manipulator system with dual end-arms, capable of reaching all vehicle subsystems and payloads, travels around a closed-loop track running down both gunwales and up across both inboard arches. The descent propulsion system is split, with three

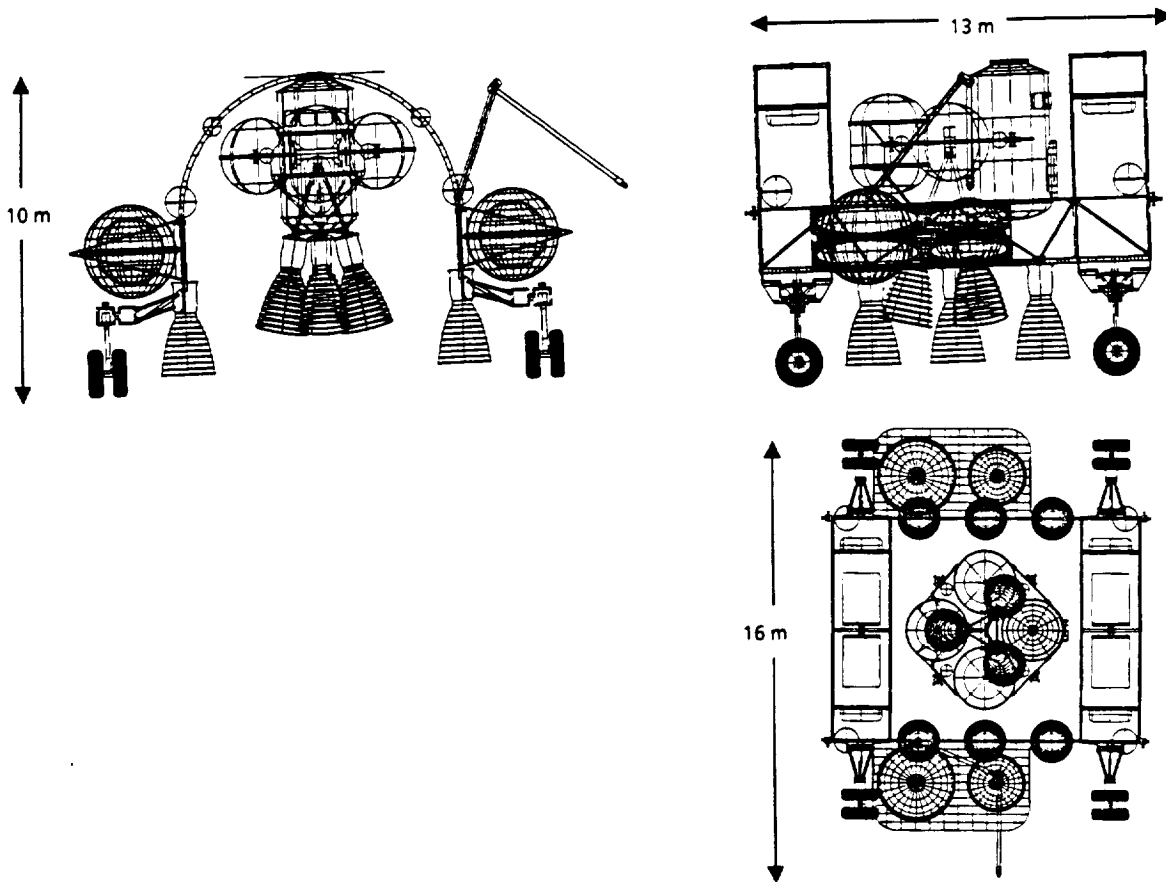


Figure 2-7b. Crew Lander Anatomy

redundant 30 kbf engines (operating nominally at 50 percent throttle) located along each gunwale. The tanks and engines are removed after touchdown by the robotic manipulator system. Frame stiffness during flight is provided by the cargo assembly: a large habitat module, a mixed-cargo carrier, or the MAV. Slow surface mobility admits the loss of stiffness after the cargo is offloaded.

An aerobrake heat shield structure concept was selected consisting of C/Mg frames and ribs (cast members due to their complex curvatures, with member-connection not yet designed) backing up a hot-structure surface of Ti/Al3 honeycomb (face sheets bonded to a superplastically formed, laser-welded "egg crate" core). The approximately 30 % of the heat shield requiring additional thermal protection would be plasma-sprayed with a zirconia thermal protection barrier. The upper shroud is a simple skin-stringer structure, also of C/Mg metal-matrix composite for high specific stiffness and high specific strength.

The aerobrake is installed in five sections around the lander, two on top and three below, figure 2-8. The preferred ETO launch scenario continues to be mounting the fully integrated HMEV on the side of a large ETO vehicle, analogous to the launch configuration for the Shuttle, figure 2-9. An ascent performance and controllability analysis was conducted for the HMEV side-mounted configuration. The required gimballed angles were found to be acceptable and are reported in section 3.6. Overall dimensions of the HMEV are not significantly different from those of the Shuttle orbiter, nor is its total mass, although the HMEV is wider at the stern and presents a larger total platform area (important for wind-loading on the launch pad and during ETO ascent). Ground integration, launch operations and flight control are well preceded for this ETO scenario. The 72 t HMEV under-utilizes the lift capacity of a 150 to 180 t launch vehicle by a substantial amount, leaving "room" in an in-line shroud for manifesting other pieces of a Mars mission vehicle.

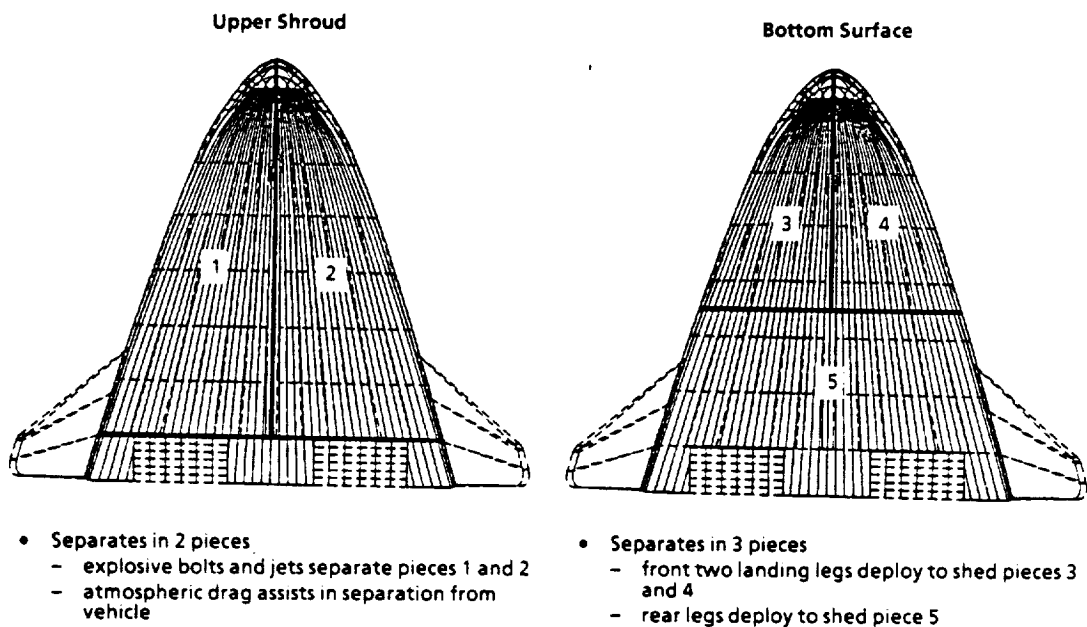
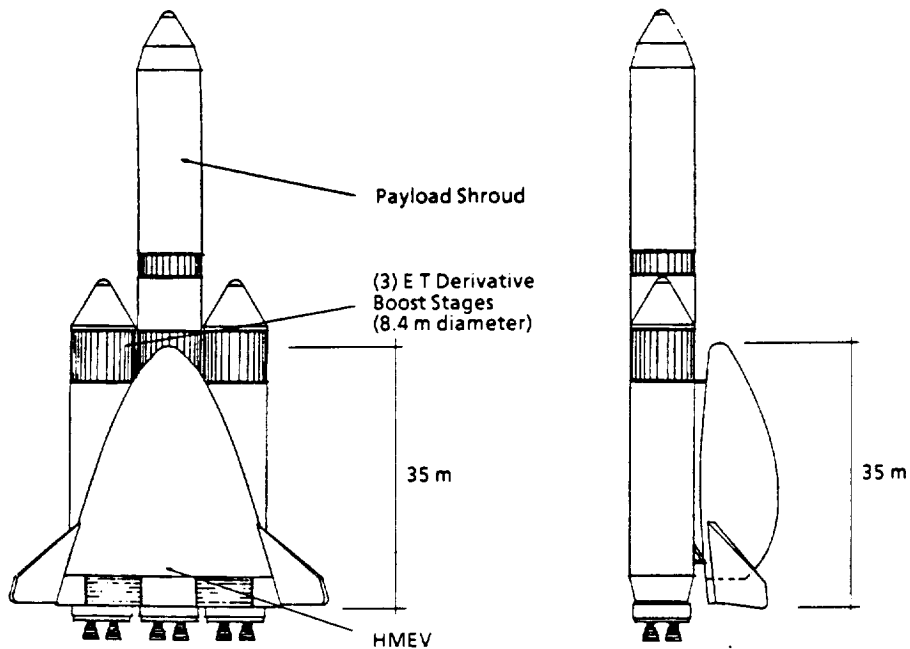


Figure 2-8. HMEV Aerobrake Jettison Scenario

At about 10 km descent altitude at Mars, the descent engine nozzles extend through ports in the brake's heat shield and start. The upper shroud splits along its length and is jettisoned in a controlled manner by small solid rockets. At the point when propulsive penalty due to the weight of the heat shield exceeds its aerodrag benefit, the lower portion of the brake is detached in three pieces, and pushed away by deployment of the lander's touchdown legs. The brake pieces fall away due to their own weight, freeing the



Launch vehicle shown represents NLS with ~115 t lift capacity to SSF orbit. Mars-class HLV baselined for STCAEM manifesting purposes would throw ~150 t.

Figure 2-9. HMEV Reference Launch Scenario

lander for touchdown. Descent abort is available at all times during descent, since the MAV (containing the crew cab) is positioned for simple separation out the top of the lander assemblage.

2.4 NUCLEAR THERMAL PROPULSION MARS TRANSFER VEHICLE (NTP MTV)

The decision to focus study effort on detailing the NTP option for Mars transfer derives from two sources. First, STCAEM Phase 1 concluded that NTP represented the most appropriate technology baseline option manned Mars transfer propulsion, based on considerations of mission flexibility, performance, crew safety, programmatic resiliency and life cycle cost for multiple missions, technology development cost, and potential for reusability. Second, the Synthesis Group (ref. 2) selected NTP as the Mars transfer propulsion option for its exploration architectures. The current effort develops an integrated spacecraft concept, incorporating results of several activities: (1) the NTP subsystem selection and sizing details; (2) the HMEV lander vehicle concept, including payloads discussed in section 2.3; (3) system sizing for mission designs to support the Synthesis architectures; (4) space assembly and checkout operations "lessons learned",

section 4.0; and (5) a smaller, microgravity-optimized transfer habitation system developed and discussed in section 5.0.

2.4.1 NTP Design Drivers and Concept Evolution

The chief design drivers for this vehicle concept were more complex than just minimum mass. Two primary drivers were: (1) practical approaches to space assembly, and (2) reduction of the required number of ETO launches of a reasonable payload capability. Three ancillary drivers were: (1) integration of the HMEV as payload, (2) optimization for microgravity flight, and (3) effective use of all available mass resources to reduce crew exposure to space radiation.

Although the basic NTP vehicle archetype remains the same as the previous study (ref. 1), several interesting and fundamental integration improvements have been introduced in response to the design drivers. Basically they involve (1) a configuration sized to support the Synthesis architectures and matched to a 150 t class ETO vehicle with a 12 x 32 m shroud; (2) a fully integrated structural spine in stackable sections; (3) a non-traditional, asymmetrical division and arrangement of main propellant tanks; (4) re-orientation of the microgravity-optimized transfer habitat module, its nestling within the forward ends of the main propellant tanks for radiation protection; and (5) engineering definition of all primary subsystems. The resulting configuration, is shown in figure 2-10.

The launch vehicle shroud volume was assumed to vary linearly with payload mass capability, with a basis of 10 m diameter and 30 m cylinder length for a 100-t vehicle. This rule yielded working dimensions of 12 x 32 m for 150 t, 13 x 35 for 200 t, and 14 x 40 m for 250 t, all having specific volume $24 \pm 1 \text{ m}^3$ per t. The NTP was sized to the 12 x 32 m dimension, assuming the shroud nose cone volume is available for reduced-diameter items that fit within the nose cone envelope. The resulting NTP hardware could also be launched efficiently on a 200 t vehicle with a 12 x 35 m shroud.

Propulsion system. The traditional way of dividing NTP Mars mission propellant splits the TMI and MOC allocations respectively into two tanks each, disposed symmetrically about the vehicle axis. Such vehicle symmetry simplifies the analysis of attitude control and main-propulsion gimbaling and is sufficient in the absence of overwhelming drivers. However, splitting the propellant loads evenly leads to significantly different gross tank sizes for TMI and MOC for the 2014 delta-V breakdown. A propellant-division trade for various tank diameters was performed, to determine the most sensible way of allocating tank sizes to different mission phases. This led to an asymmetrical configuration of three identical hydrogen storage tanks: two lateral tanks

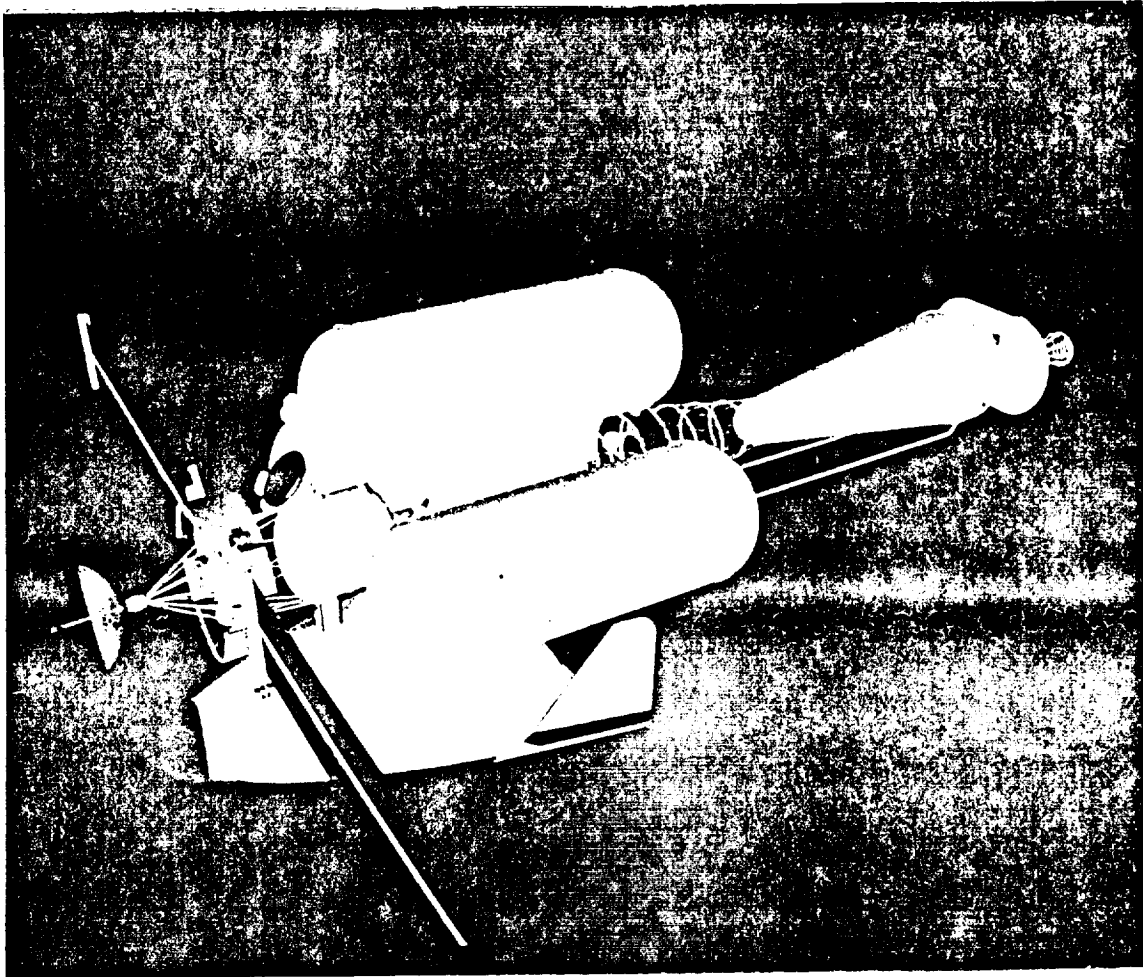


Figure 2-10a. Nuclear Thermal Mars Transfer Vehicle Concept (NTP)

(port and starboard) exclusively for TMI, and a dorsal tank for the remainder of TMI but primarily for MOC (about 90 % of the tank volume). This leaves the ventral side of the vehicle free for HMEV integration and for assembly and topoff access in LEO. It also limits the number of plumbing and other disconnects needed, and allows a shorter overall vehicle.

The tanks are 11.5 m in diameter to take maximum advantage of a 12 m launch shroud with allowances, and are sized with 5 percent ullage. The vehicle mass summary statement is shown in figure 2-11. These results indicate that for this tri-tank propellant division, an ETO launch capacity of 200 t is appropriate if the tanks are launched wet. The identical tank sizes should simplify ground and orbital operations. Insulation approaches are different, however. The lateral tanks require only short-term passive thermal control provisions, whereas the dorsal tank, which must keep hydrogen all the way to Mars, requires the same long-term storage technology (5 cm of MLI and vapor-

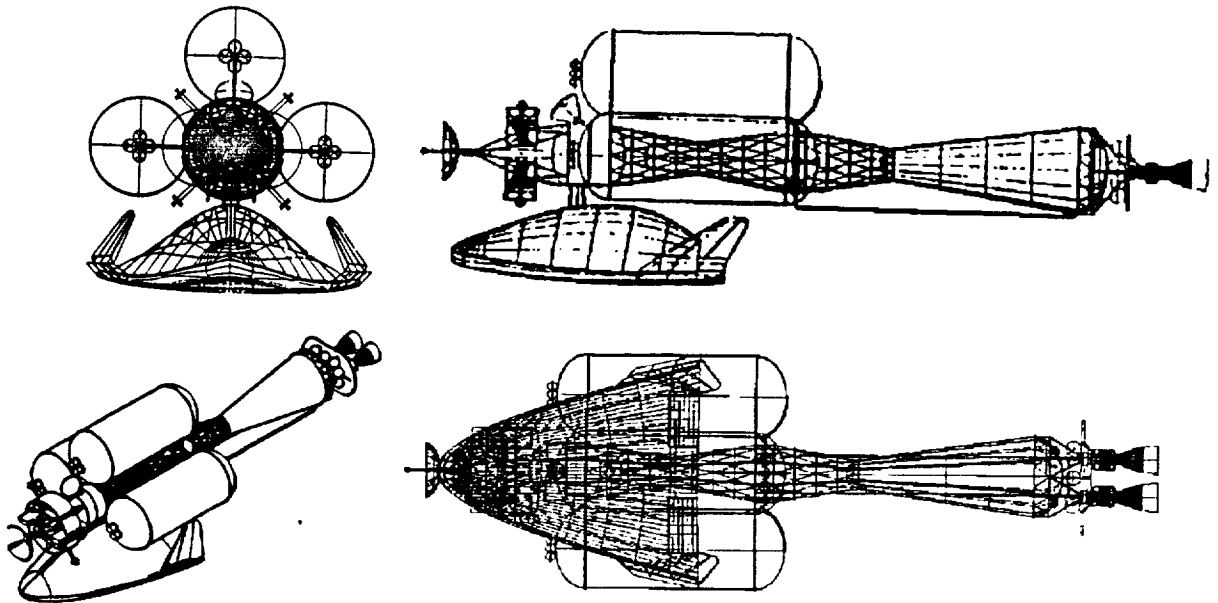


Figure 2-10b. NTP Vehicle General Arrangement

cooled shields) as the in-line aft tank (used for TEI and EOC). Each tank has a small helium initial pressurization system. Tank pressurization during the burns is provided by the introduction of hydrogen gas bled off from the engine turbopumps. Hydrogen boiloff is accumulated throughout the mission in spherical tanks located aft and forward, and used both for attitude control propellant, and for aft-tank pressurization prior to the TEI and EOC burns.

Propulsion system element schematics, showing critical interfaces, are illustrated in figure 2-12. The propellant lines, hydrogen pressurization lines and boiloff accumulation lines for the three strap-on tanks are manifolded through valved quick-disconnects in a crossfeed bay amidships. A propellant toffport is also located here, figure 2-13. Two 12-inch stainless steel main propellant lines (for redundancy in case of meteoroid strike) supply the aft manifold, bypassing the aft tank on the ventral side. Thermal contraction of these long propellant delivery lines during flowthrough is less than 15 cm, and accommodated by dual bellows near the forward disconnects. The two main lines are attached in LEO, using Marmon-type clamps. Perfect sealing of these field joints is not anticipated to be required, due to the relatively short flowthrough times involved.

Dual, advanced-NERVA-class NTP engines are baselined. The worst-case mass asymmetry during any mission phase requires only a 6° engine gimbale angle for

Crew Systems Payload		60.5		60.5
Habitat and internal subsystems	34.5		34.5	
Exterior power, TCS, communications	4.4		4.4	
Airlocks (2, 1 hyperbaric)	6.0		6.0	
Crew and consumables	14.3		14.3	
MMUs (2 + consumables)	0.8		0.8	
CRV		5.8		5.8
HMEV (cryo descent, 6 crew, 9 t cargo)		72.5		72.5
Structures		5.5		5.5
Attitude Control System		14.6		14.6
Accumulator tanks	14.3		14.3	
Plumbing	0.3		0.3	
Hydrogen Plumbing		4.6		4.6
Main lines	2.0		2.0	
Crossfeeds, valves, fittings	2.1		2.1	
Pressurization lines	0.5		0.5	
NTP Engines (2 @ T/W = 10, Isp = 925s)		6.8		6.8
Radiation Shield System		6.8		6.8
Tankage and Propellant		639.6		851.0
Aft tank dry	15.0		27.0	
Drop tanks dry (3)	77.1		96.9	
EOC propellant	0		32.7	
TEI propellant	73.2		98.6	
MOC propellant	148.4		186.0	
TMI propellant	325.9		409.8	
Total IMLEO				
		Expendable 817 t	Reusable 1028 t	

Figure 2-11. NTP Concept Baseline Mass Summary

compensation, with the engines located side-by-side. The gimbal scheme baselines slow electrohydrostatic actuators to move each entire reactor/engine/nozzle assembly. Since only one, axial, propellant feed line supplies each engine, the mechanics of NTP gimbaling should be simpler than for bipropellant engines, and $\pm 12^\circ$ is presumed feasible, although only about $\pm 8^\circ$ appears necessary for full steering with engine out. The actuators are anchored to lateral structure which also supports the shadow shield, figure 2-14. If large enough to prevent neutron scattering entirely from the dual engines, this shield cannot fit intact inside a 12 m launch shroud and requires some simple deployment. Options to reduce shield size (including lengthening the vehicle, reversing the HMEV orientation, and shaping the aft ends of the hydrogen tanks) have only a small effect, generally at great configuration cost. Since the overall fluence penalty of a small amount of neutron scattering remains uncalculated in detail (no shield

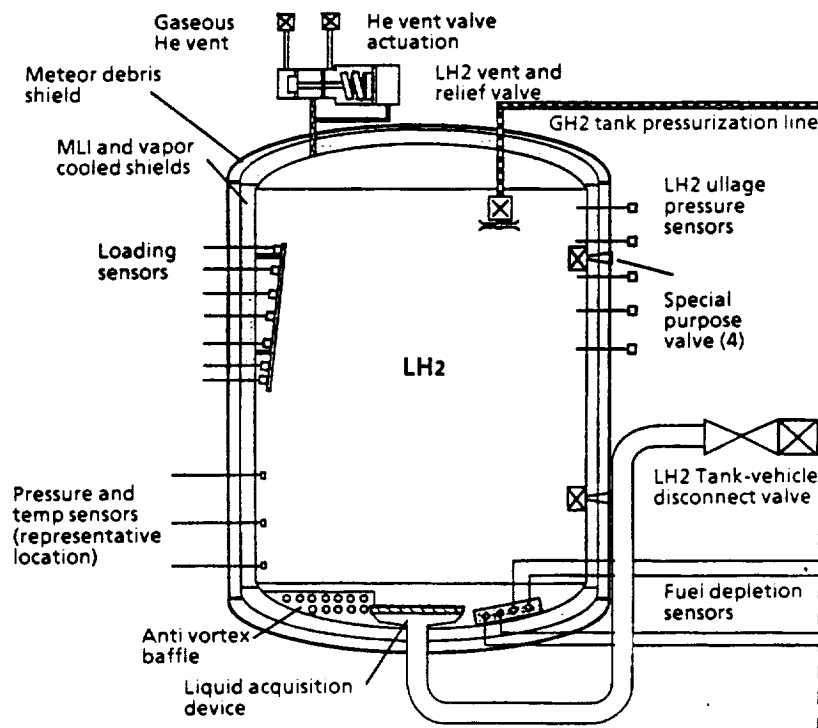


Figure 2-12a. Hydrogen Tank Schematic

thickness parametrics exist, for example), allowing the shield geometry to dominate other design drivers would be inappropriate at this time.

Structure System. The effort to simplify on-orbit assembly operations, in keeping with the recommendations of the Synthesis Report, has resulted in a highly integrated approach to the main structure. The key issues relate to interfaces between the spine and other structural components of the vehicle. Seven key structure interface areas are: (1) payload integration; (2) the hab-spine transition; (3) transition between the spine and amidships crossfeed bay; (4) crossfeed geometry and tank attachment structure; (5) transition between the spine and aft tank, and use of the aft tank as structure; (6) thrust interstructure between the engines and aft tank; and (7) shield and engine mounting.

The need for a long, stiff structure to package well for launch, be assembled easily in space, and support multiple fluid and electrical utilities, was met with a new spine concept: three conical sections of circular truss, manufactured of metal-matrix composite and analogous to the metering optical-bench used in the Hubble and AXAF telescopes. These structure segments are pre-integrated with dual, external conduits containing power, data and control lines, tank pressurization lines, and hydrogen boiloff

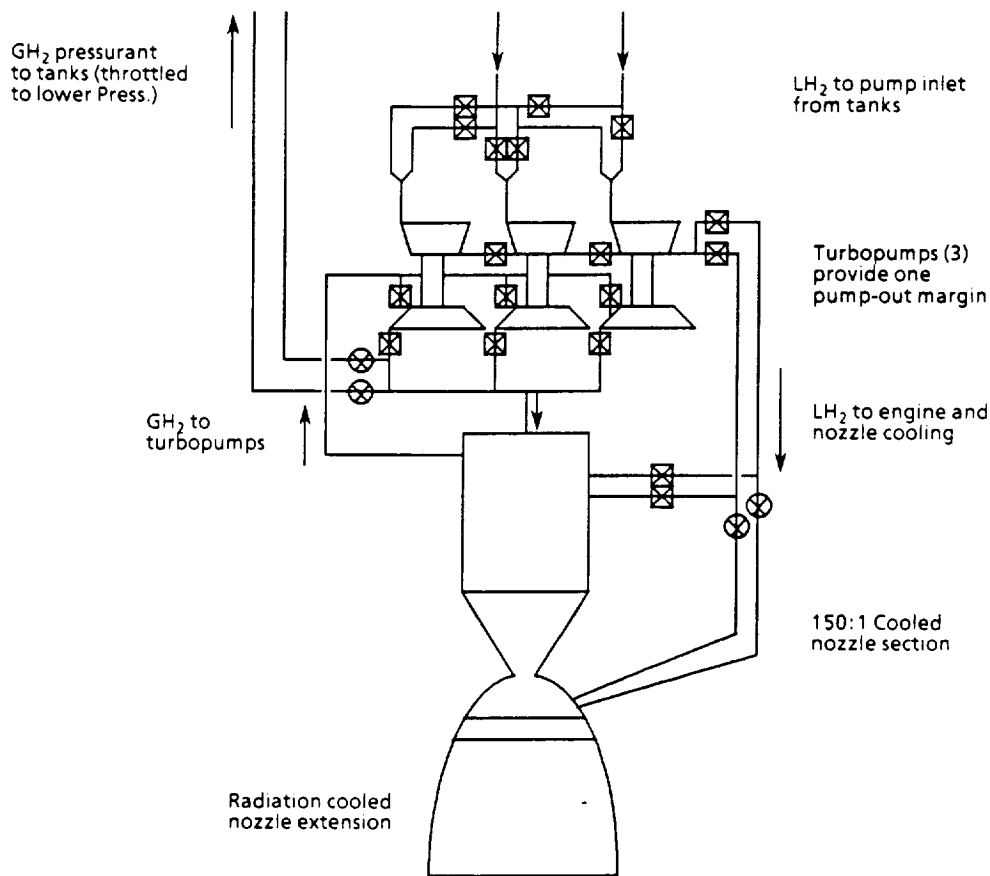


Figure 2-12b. Nuclear Thermal Engine Schematic

accumulation lines. This scheme simplifies on-orbit assembly to a set of berthing operations; the segments manifest for ETO launch by nesting together like stacked Dixie cups, then are inverted and mated robotically on-orbit. As the segments latch together, quick-disconnect mechanisms at each end make the utility conduits continuous.

The structure segments are sized to match the barrel length of the common-size propellant tanks, for simple structural attachment at the shoulder-rings of the tanks. Their diameter ranges from 8 m at one end to 4 m at the other. The cylindrical crossfeed bay between the aftmost segments is kept as short as the manifold geometry and valve maintenance access allow. Fluid disconnects between the drop tanks and the vehicle are thus located between the tanks' aft structural latches to assist QD alignment, an arrangement analogous to the Shuttle ET mounting. Various possible shapes were investigated for the aft tank. The assumed 35 m launch-shroud length limit ultimately required using the structure-segment half-angle for the aft-tank forward frustrum, so that the aftmost segment could be stacked on top of the aft tank for launch.

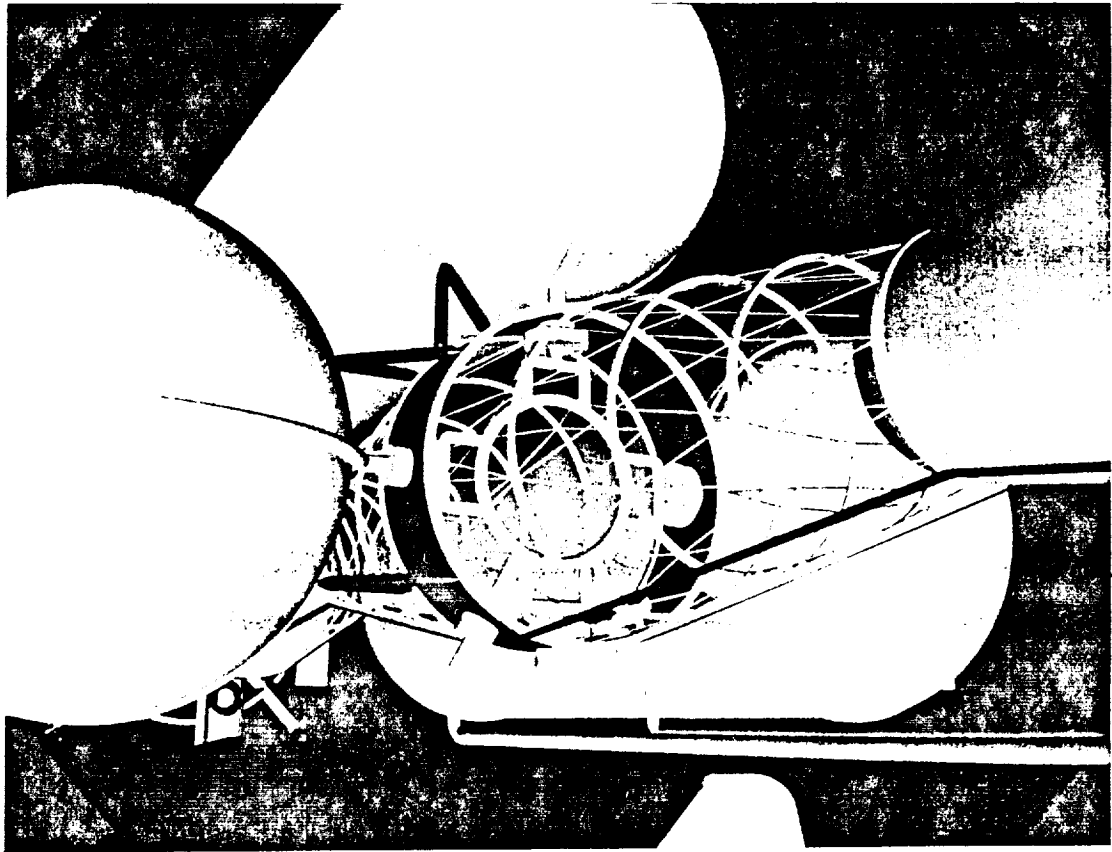


Figure 2-13. Amidships Crossfeed Bay

The short, microgravity-optimized transfer habitat module is oriented in line with the vehicle axis. This allows a simple structural interface to the forward segment of the circular-section main structure. The 8 m structure diameter at that point allows direct attachment to the aft shoulder ring of the habitat. The forward shoulder rings of the hydrogen tanks are even with the aft shoulder ring of the habitat. This nests the aft half of the module within the cluster of the forward ends of the tanks. Since the dorsal tank is virtually full of hydrogen for the outbound trip, this proximity contributes to limiting particle fluence to the crew. The lateral tanks are retained, empty, until just prior to MOC to provide additional protective mass. The in-line habitat orientation also allows simple integration through an airlock of the MAV crew cab, located just inside the top surface of the $L/D = 1.6$ HMEV aerobrake. The HMEV is oriented parallel to the vehicle axis also, with wingtips folded to reduce its visible width from the reactors' viewpoint. A second airlock, accessible from the aft pressure compartment of the transfer habitat, is located axially on the aft habitat end-dome, inside the forward structure segment. The strut spacing of the segments allows suited EVA astronaut passage to the exterior of the structure from the aft airlock.

This page was intentionally left blank.

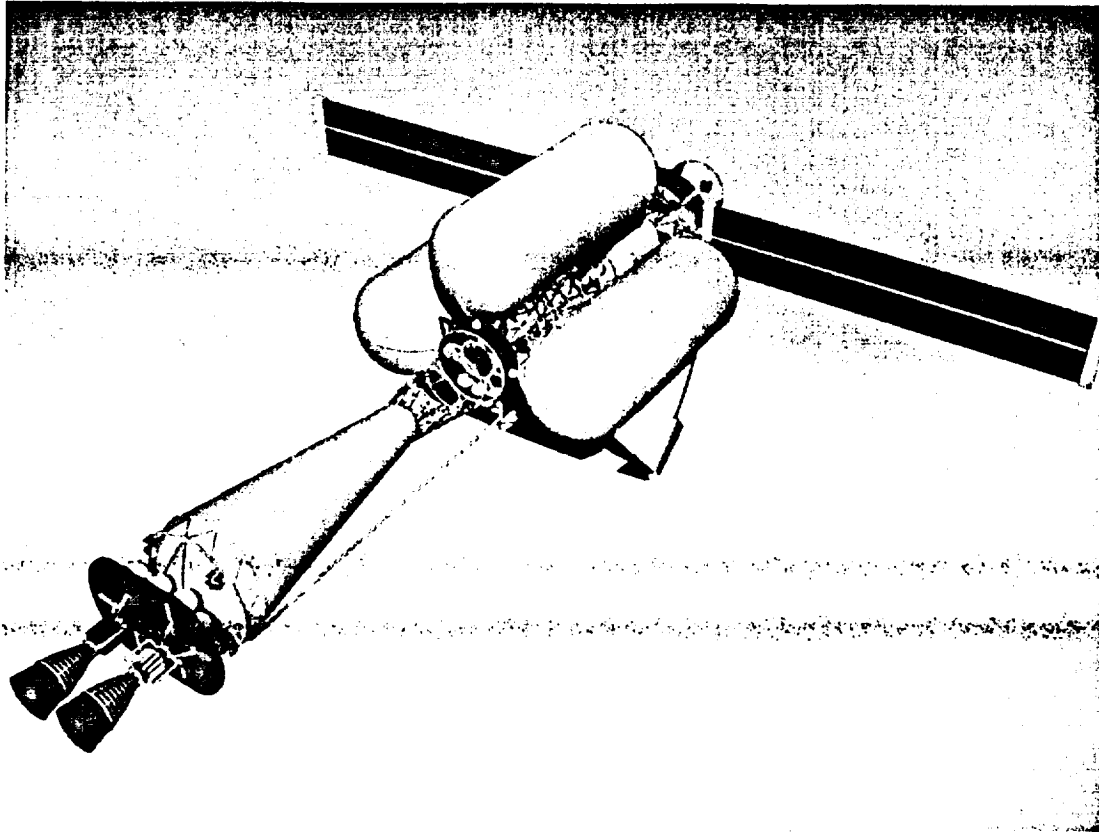


Figure 2-14. Propulsion Subsystems Configuration

Support Subsystems. A superstructure, figure 2-15, mounted to the forward shoulder-ring of the transfer habitat contains key subsystems: (1) a ring-shaped configuration of radiator heat-pipes (120 m^2) for habitat and power system thermal rejection; (2) the forward ACS boiloff accumulator tanks, and redundant thrusters on extendible booms oriented to avoid plume impingement on the HMEV; (3) two extendible photovoltaic blankets (sized to produce 64 kWe peak at Mars), storage batteries for eclipse periods and engine burns, and power conditioning equipment; and (4) navigation equipment (star trackers, inertial and horizon sensors), communication equipment (7 m tracking high-gain dish and laser telescopes), and scientific instrumentation.

Although partial solar array deployment is permissible within the shielded zone, full stowage is baselined for main propulsion maneuvers. The nominal orbital attitude in planetary space is gravity-gradient stable, with the thermal radiator ring normal to the planet nadir. The aft ACS subsystem also consists of eight accumulator tanks, attached directly to the radiation shield structure. Four, non-deploying thruster modules are aligned with the forward thruster modules, attached to the aft-tank Y-ring and tucked within the 12 m launch shroud dimension.

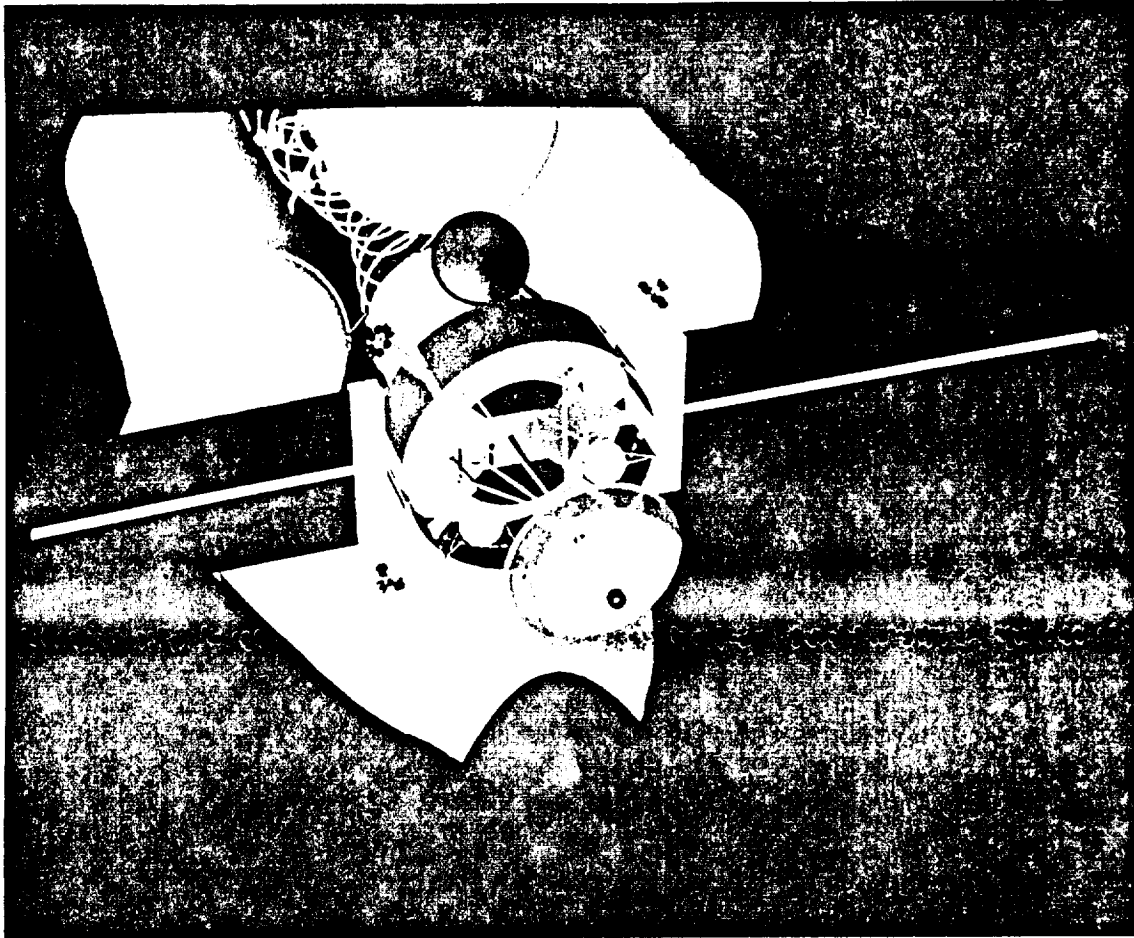


Figure 2-15. Forward Subsystems Superstructure

Launch and Assembly. The integrated NTP vehicle concept allows simple orbital berthing-integration operations. The less complex assembly requirement should in turn allow a dramatic reduction in the amount and complexity of orbital processing infrastructure required. The concept is also supported by a reduced number of ETO flights. Volumetrically, the NTR concept as shown could be packaged into just five ETO flights, one of which would also take the HMEV on the outside of the launch vehicle. The first launch would take the entire forward end: habitat, airlocks and forward superstructure fully integrated, and stacked on top of the reversed, forward main structure segment into which is nested the middle segment already attached to the crossfeed bay. This core would have available all support subsystems (except for attitude control propellant) necessary for LEO operations. The HMEV (which could be carried on the outside of this ETO launch) could provide ACS capability once berthed. The CRV could be used to board the crew prior to mission departure. The second launch would consist of the entire aft end, with the aftmost main structure segment inverted

This page was intentionally left blank.

and stacked on top. The two main propellant lines would then be robotically installed. Three more launches would bring each of the three strap-on hydrogen tanks.

This manifesting concept candidate would require, and quantitatively justifies, an ETO lift capacity -200 t, including allowances for debris shielding and flight support structure. The non-propellant launches fully utilize the available 12 x 35 m shroud volume, including a nose cone assuming 30° half-angle. Thus, the integrated NTP vehicle concept provides a datum for rigorously matching lift capacity to shroud size, and setting both at an appropriate level for Mars exploration missions. For lift capacities less than 200 t, a variety of approaches is available requiring six or more ETO flights. A complete assessment of ETO options and penalties, with the goal of recommending lift capacities and shroud sizes appropriate for Mars requirements, has not yet been performed.

2.4.2 Airlock

A precursor ingredient required for full integration design and not defined adequately earlier was an appropriate airlock concept. A new, two-crew airlock concept was designed for integration with the transfer habitat concept, but also offering potential commonality for surface applications. Mass estimates for this spartan but sufficient concept were based on flight hardware, by scrubbing the line-by-line accounting in the current SSF WP-02 mass properties report, figure 2-16. A single-chamber design, 2 m in diameter and 2.5 m long, was baselined in which "equipment lock" functions are burdened onto the parent habitat module in all cases, thus avoiding additional life support, structure and utility equipment. The small-volume, single-chamber solution is consistent with the "rackless" equipment integration of the exploration habitation systems. Berthing adapters at both ends allow modular integration and changeout, and an additional side hatch allows egress while both ends are berthed. The current mission designs call for only one of the two mission airlocks to be hyperbaric-capable.

2.4.3 Cargo MTV Concepts

Three primary options exist now for the cargo MTV required to support Synthesis-architecture Mars missions: (1) an NTP vehicle, launched integrally, which would perform a full-up flight test of the NTP system while delivering the 2014 payload to Mars; (2) a cryogenic vehicle which would provide adequate performance and perhaps less cost for cargo delivery to support subsequent missions; and (3) a small (2 to 5 MW) NEP system, launched integrally like the NTP option and simply berthed to its cargo

Airlock	<u>Category</u>	<u>Mass (kg)¹</u>
	Airlock EVA Support ²	130
	Hyperbaric hardware	210
	Structure	2340
	Airlock Controls	125
	Life Support	85
	Data Management	30
	Power	10
	Audio/Video	15
	Subtotal	2945
	Growth (~14%) ³	355
	TOTAL⁴	3300
Habitat Burden	Habitat EVA Support	
	Tools	270
	EMU	240
	Miscellaneous	145
	Airlock Controls	5
	Subtotal	660
	Growth (~14%) ³	90
	TOTAL⁴	750

- 1) Based on MDC-91H0708; *WP-02 Mass Properties Data Report*, June 1991. All values rounded to nearest 5 kg.
- 2) Includes allocation for contamination control
- 3) Actual number summed item-by-item; percentage shown represents average
- 4) Total for non-hyperbaric airlock = 2.7 t

Figure 2-16. Reference Airlock Mass Summary

MEV payload, for efficient cargo delivery. None of these options has been developed in any detail yet as an integrated vehicle concept; however, section 9.0 describes several performance runs based on presumed vehicle characteristics for the first, baseline option.

2.5 MICROGRAVITY-OPTIMIZED NUCLEAR ELECTRIC PROPULSION MARS TRANSFER VEHICLE (NEP MTV)

An initial concept for a microgravity NEP MTV, and a fully integrated vehicle concept for an artificial gravity version based on the eccentric rotator concept was developed and documented in reference 1. In the current study, key subsystems developed in detail for the artificial gravity concept (such as the power plant, radiator and engine assemblies) were adopted for the microgravity model and its design integration for the microgravity condition was subsequently optimized (figure 2-17).

The 40 MWe engine assembly is now located at the stern, with the nominal thrust vector axial with the vehicle spine. The engine subsystem shown was built up by ganging together both 20 MWe microgravity-version outrigger subassemblies end-to-end. This preserves maintenance access from each side for all engine and power processing units, as in the original design. The payload is wrapped around the spine amidships. Locating

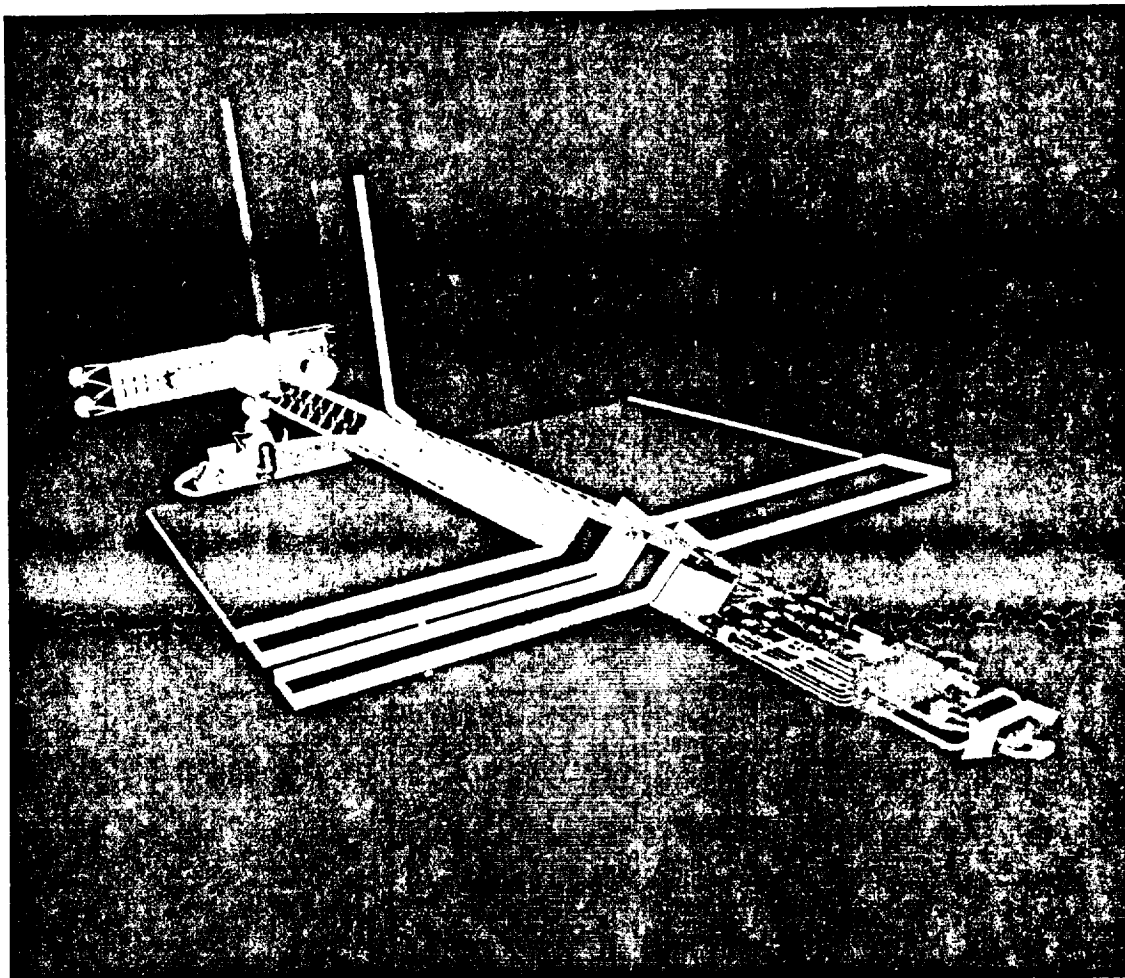


Figure 2-17a. Nuclear Electric Microgravity Mars Transfer Vehicle Concept (μ g-NEP)

the payload -- transfer habitat and MEV -- on one side of the truss avoids a connecting tunnel between them; the minor mass asymmetry is well within the gimbal capability of the engine assemblies.

The auxiliary radiator assembly and the habitat solar array are turned 90° relative to the flat arrangement of the other vehicle systems. This is allowable without radiation shield penalty because they are located so far aft that the shield width already required due to the proximity of the power plant generates a half-angle in that plane sufficient to prevent scattering by these other systems. Turning the radiator assembly "out of plane" enables a simplified, lighter plumbing connection. The simple, rectangular configuration of equal-length radiator heat pipes was retained for simplicity, and the power plant was kept close to the radiators. The increased mass of longer plumbing lines would offset the

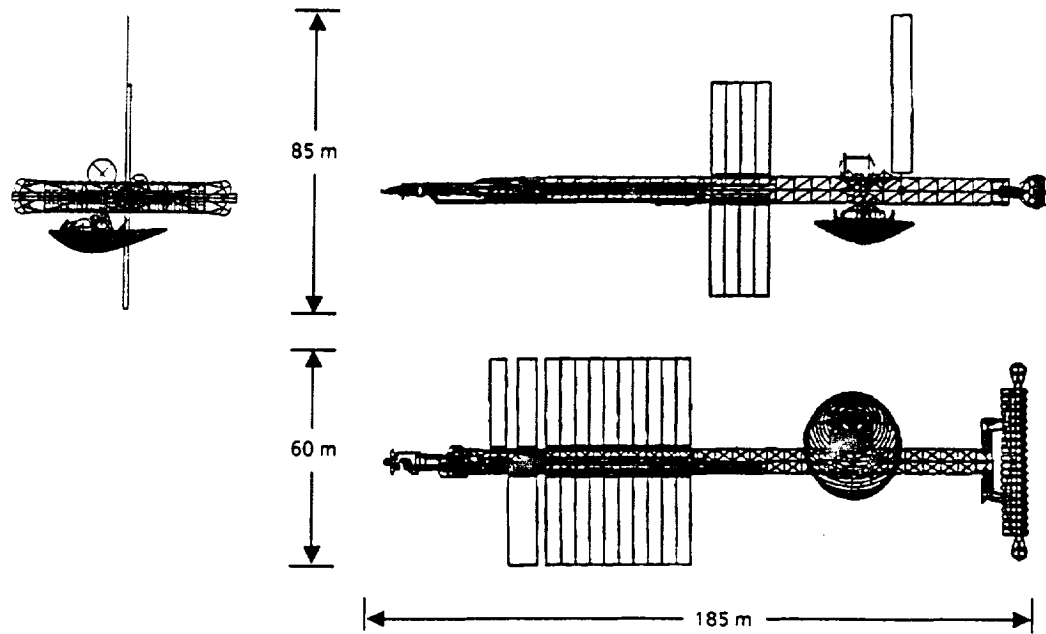


Figure 2-17b. μ g-NEP Vehicle General Arrangement

mass savings from a smaller shield; furthermore, a longer power plant would be less able to be fully integrated on the ground prior to launch.

3.0 AEROBRAKE INTEGRATION

The aerobrake integration activity involves a close coupling between the materials, structural analysis and aerothermal analysis for concept design of aerobrakes to meet mission requirements. Studies have been carried out for the work associated with the low L/D Crew Return Vehicle (CRV), the high L/D Mars excursion vehicle (HMEV), the structural analysis for the Boeing low L/D = 0.5 reference aerobrake, and a wake flow analysis for a lunar transfer vehicle aerobrake.

3.1 LUNAR CREW RETURN VEHICLE THERMAL PROTECTION SYSTEM ANALYSIS

The objective of the lunar crew return vehicle thermal protection system (TPS) analysis was to recommend a feasible TPS concept and derive a TPS mass estimate based on this analysis. The approach was to assume a trajectory and heating distribution similar to a nominal Apollo case. This study surveyed ablative materials technology and used a thermal analysis code to compare several well-known ablatives against the baseline Apollo material.

3.1.1 Trajectory

The lunar CRV configuration examined in this study was identical to the Apollo capsule except in size (see section 5). The lunar CRV has a diameter of 4.4m and a height of 3.1m. The CRV ballistic coefficient was 362 kg/m^2 with a drag coefficient of 1.24 at an angle of attack of 14 degrees. The entry conditions and final parachute deployment conditions of the Apollo capsule were used as constraints for the lunar CRV entry trajectory. The 5 g undershoot trajectory was examined as it results in the worst case heating rate for nominal lunar returns (not aborts). However, this trajectory is less severe than the Apollo Block II undershoot design (20 g abort trajectory) which was used for the Apollo TPS design. The simulated trajectory produced by the MISSION program is displayed in figure 3-1. Stagnation point heating rates were computed along this trajectory using the methods of Fay-Riddell (ref. 4) and Tauber-Sutton (ref. 5) for convective and radiative heating, respectively. The resulting heating rates are displayed in figure 3-2 where the peak heating is 560 W/cm^2 at 66 seconds at an altitude of 59.8 km. This heating rate is considerably less than the Apollo Block II 20 g undershoot design trajectory value of 800 W/cm^2 used for the Apollo TPS design. Actual Apollo lunar return peak heating rates for Apollo's 8 through 16 ranged from 308 W/cm^2 to 393 W/cm^2 .

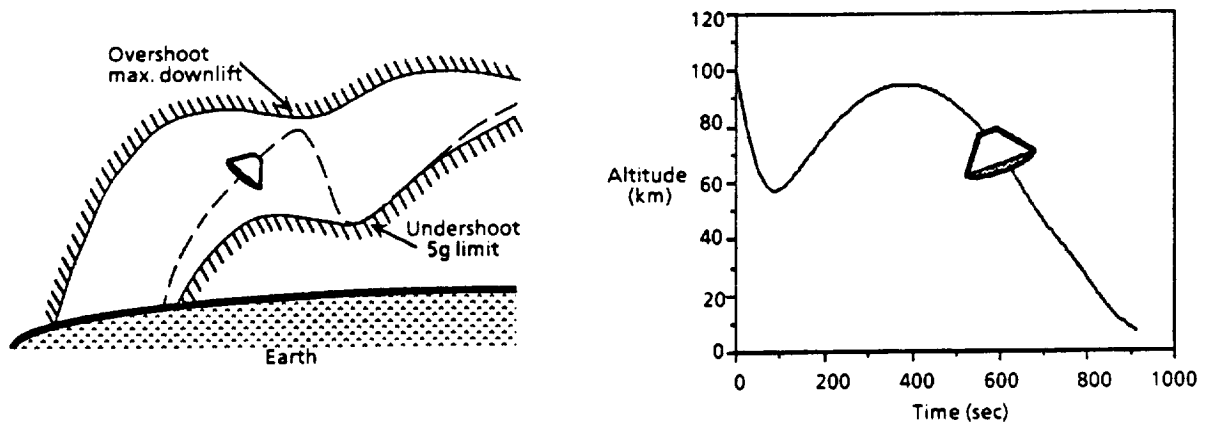


Figure 3-1. CRV Lunar Return Entry Trajectory

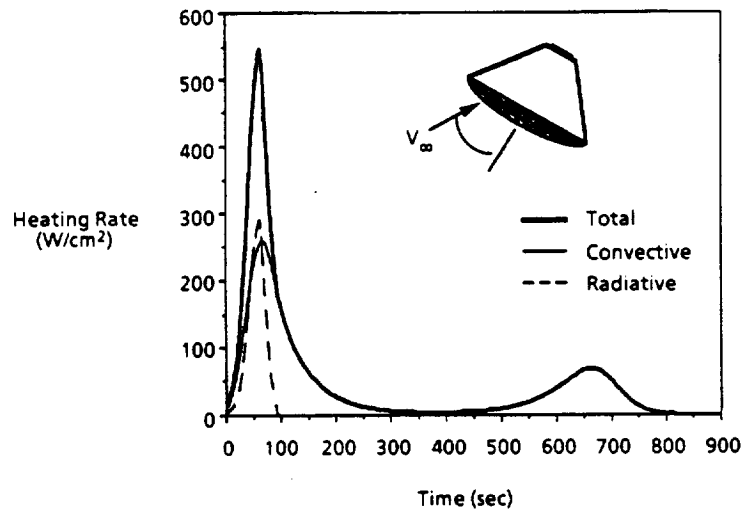


Figure 3-2. CRV Lunar Return Heating Rates

3.1.2 Apollo Configuration Baseline

The Apollo ablative thermal protection material was Avco 5026-HC/9 (496 kg/m³) phenolic novolac resin, troweled or injected into 0.95 cm (3/8 inch) phenolic honeycomb cells which were bonded to a stainless steel structure using high temperature film adhesive (ref. 6). This configuration is outlined in figure 3-3. The Apollo era phenolic novolac resin was a very efficient organic ablator due to its relatively low density, high char yield (i.e., conversion to pyrolytic graphite), toughness, and thermal shock resistance. The carbonaceous char provided a highly emissive surface which limited radiant heat flux into the Command Module and served as a thermal radiator. Ablation products diffused through the char to provide a shield of viscous gas which effectively cooled the boundary layer flow.

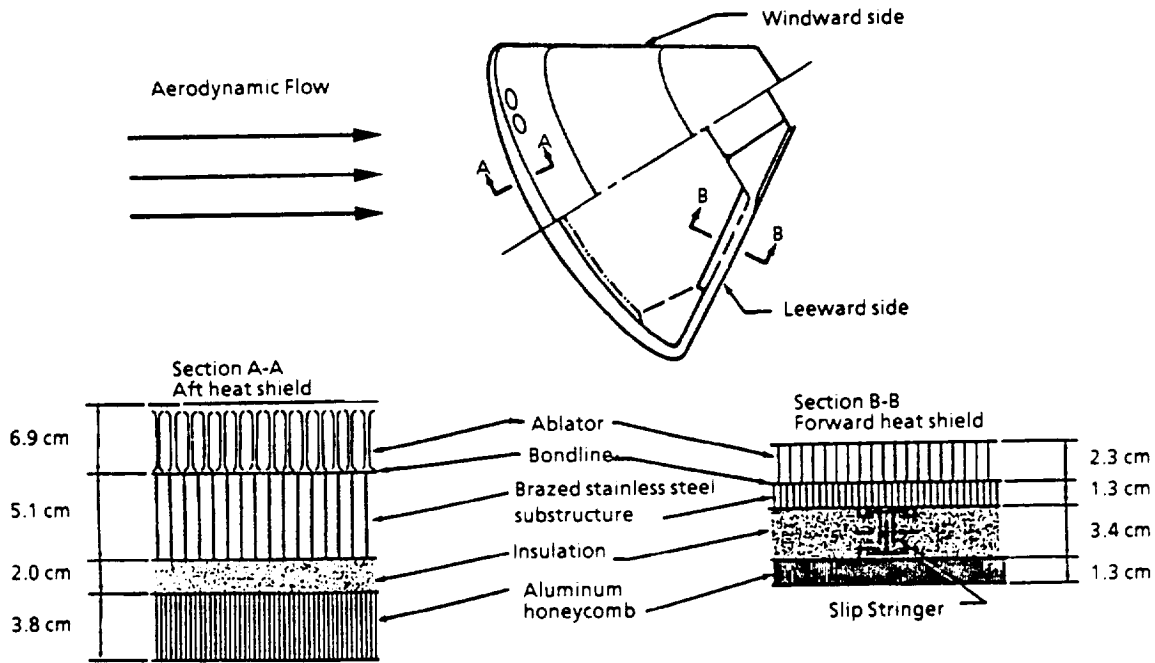


Figure 3-3. Apollo Configuration Baseline

3.1.3 CHAP Ablative Materials Comparison

Five candidate materials were selected in order to cover a wide range of physical characteristics. These materials included phenolic/silica, phenolic/carbon, Avco 5026 (Apollo ablator), and two modified silicone materials, MA-25s and SLA-561. All five candidates are current technology ablative materials having well documented usages; however, MA-25s and the SLA-561 have not been qualified for heating and aerodynamic shear conditions applicable to the lunar CRV. Data for predicting the surface recession of MA-25s were unavailable.

The Convective Heating and Ablation Program (CHAP, ref. 7) was used to analyze the performance of the five candidate materials. This program is a Boeing computer program which determines the thermal environment experienced by aerospace vehicles and the response of the materials to this environment. The calculated thermal environment includes convective heating and shock layer radiation based on the Tauber-Sutton prediction methods. The wall response considers transient temperatures, ablation, stresses, and one-dimensional conduction. The ablation analysis includes chemical reactions in the virgin material, char, surface erosion, melting, and sublimation. The CHAP program is comparable to the CMA (Charring Material Thermal Response and Ablation) program (ref. 8), and has been verified for use on NASA programs.

The performance of the five materials was evaluated for the CRV return trajectory (see fig. 3-1) using the CHAP program. The bondline temperature for the materials was constrained to below 316°C (600°F), and a minimum of 0.05 cm of virgin material was required at the end of ablation. An iterative process was used to determine the proper material thickness at four points along the forebody centerline. As an example, the data obtained at the stagnation point from the CHAP analysis is shown in figure 3-4 for the Apollo Ablator AVCO 5026, with surface temperatures, back wall temperatures, and surface recession histories. The required thicknesses at the stagnation point for the five materials are shown in figure 3-5. The thicknesses for four points along the centerline of the heat shield are graphically displayed in figure 3-6. Only four materials are shown in this figure because carbon phenolic was eliminated from further consideration due to its excessive required thickness (>8 cm). The two heat load points shown for Apollo are based on Block II design data. The actual heat loads encountered by Apollo ranged from 29,200 J/cm² to 31,700 J/cm².

Mapping the isothermal contours of the entire surface of the CRV via thermal analysis was not performed; however, the heating distribution on the CRV was believed to be similar to the Apollo case. The Apollo capsule thermal profile (ref. 6) was used to estimate the area of each temperature regime on the Command Module and extrapolate the thermal profile to the lunar CRV. The assumed heating profile in terms of equilibrium wall temperature as a percentage of total surface area is shown in figure 3-7.

3.1.4 Lunar CRV TPS Mass Estimate

On the leeward side of the vehicle in regions where the equilibrium wall temperature was less than 1273 K, reradiative materials (e.g., LI-900, AFRSI, etc.) having a density of approximately 148 kg/m³ were favored over ablatives. High performance ablative materials (nominally 435 kg/m³) were found to be required on only about 10% of the surface area. Expected equilibrium temperatures ranged from 1273-1923 K over the largest portion of the CRV surface (~63%). For this area, a more detailed trade study must be conducted to select TPS materials in the 192 to 450 kg/m³ density range. Inorganic reradiative materials offer several advantages (e.g., radiation resistance and zero outgasing), but ablative materials may prove to be more damage tolerant and weight efficient under moderately high heat loads. The TPS mass may be minimized by the use of reradiative-ablative materials. The lunar CRV TPS mass estimate is summarized in figure 3-8.

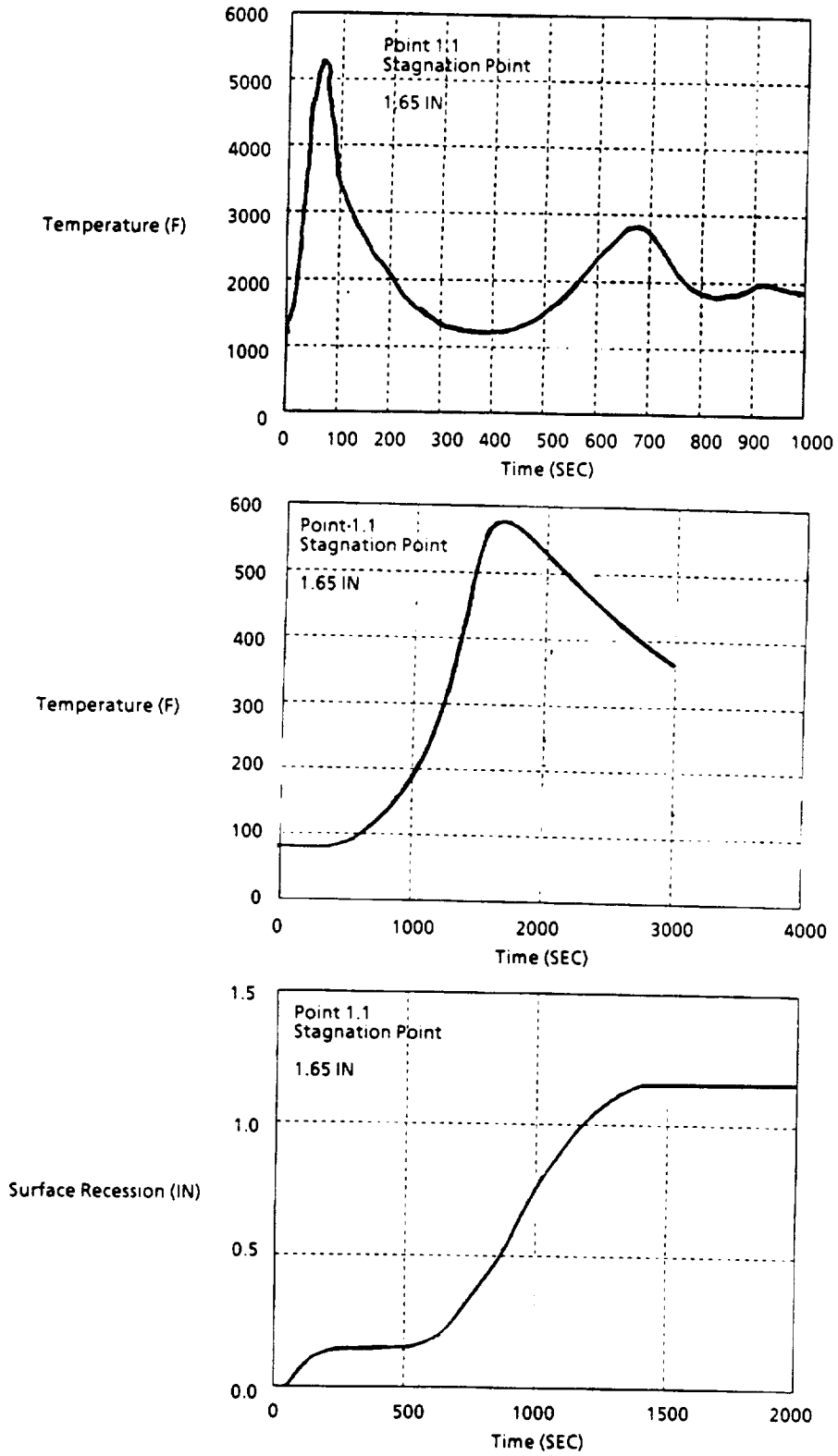


Figure 3-4. CHAP Output

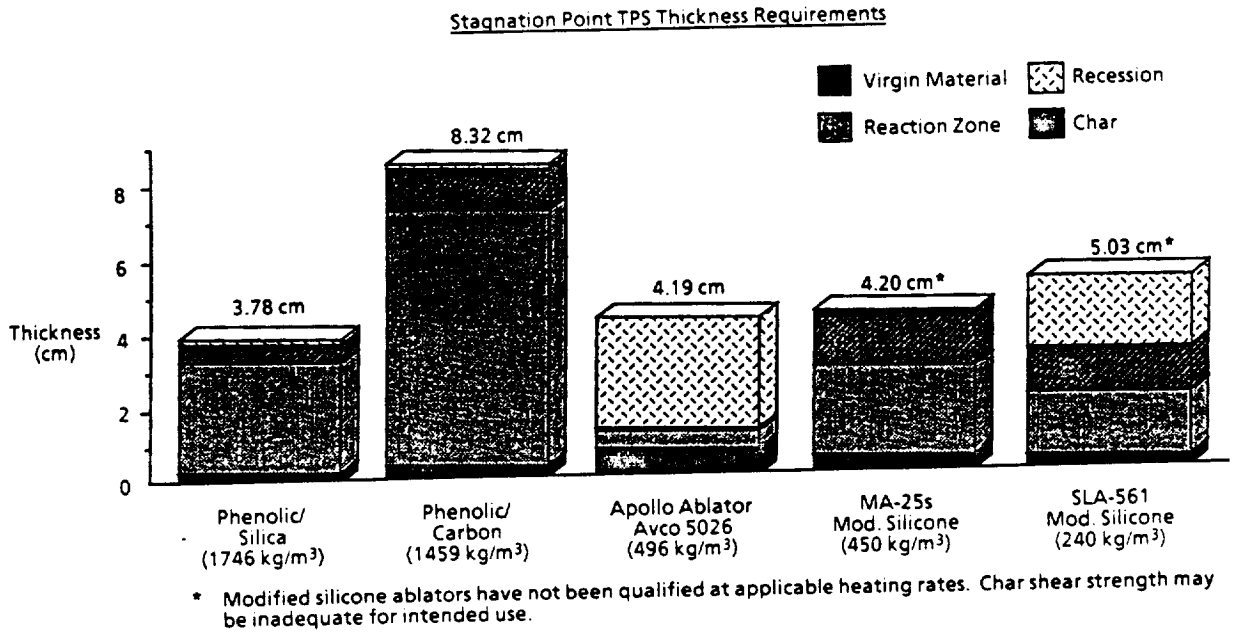


Figure 3-5. CHAP Ablative Materials Comparison.

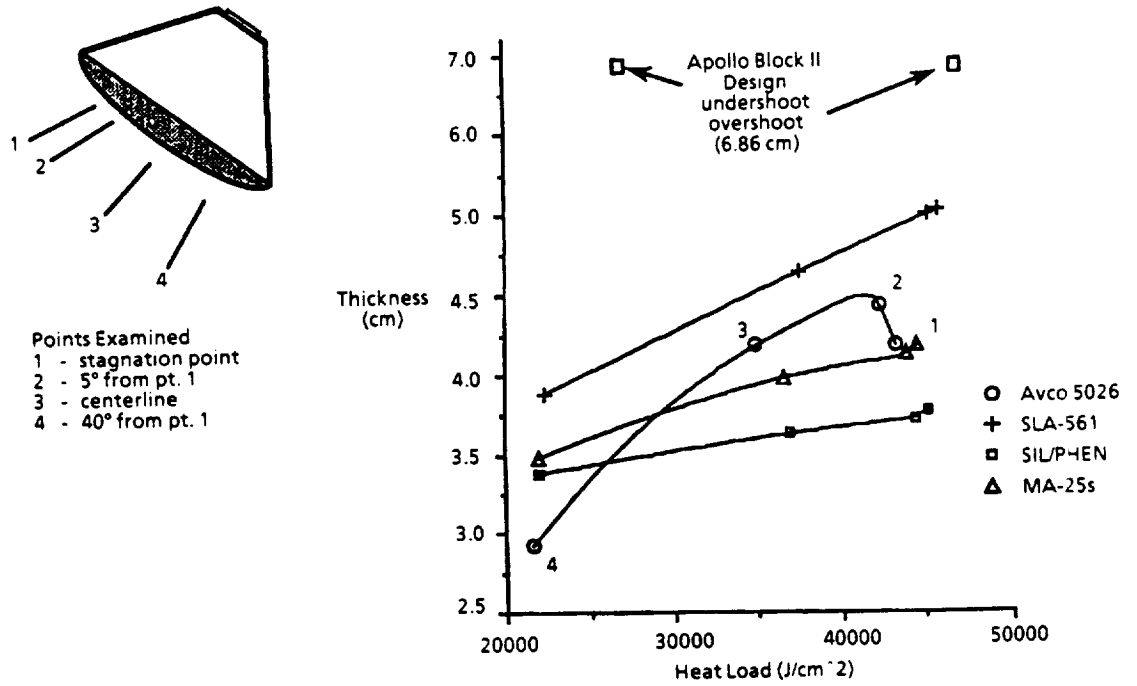


Figure 3-6. Required Thickness Along Centerline

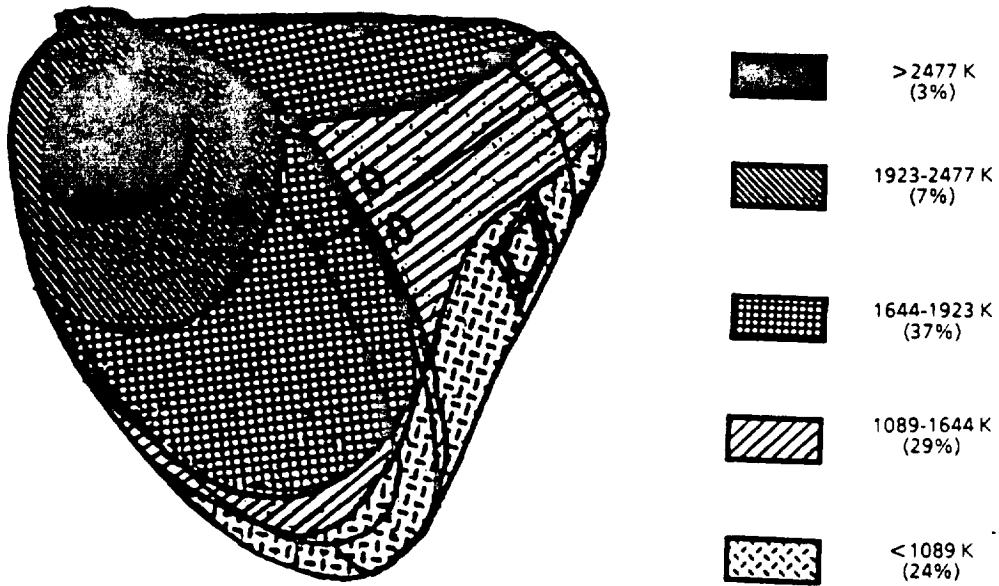


Figure 3-7. Equilibrium Wall Temperature

Equilibrium Wall Temperature (K)	<1273	1273-1923	> 1923
Candidate materials	Reradiatives	Trade study required	Ablatives
	LI-900, AFRSI, etc.	LI-2200, AETB-12, or SLA-561, MA-25s, etc.	mod. phenolic, mod. silicone, etc.
Nominal TPS density (kg/m ³)	128-160	192-450	400-544
Effective CRV surface area (m ²)	10.0 (27%)	23.4 (63%)	3.7 (10%)
Est. average thickness (cm)	2.5	5.1	4.6
Est. TPS mass (kg)	37	286	74
Total TPS Mass:		+ 15% 397 kg - 5%	

Figure 3-8. Lunar CRV TPS Mass Estimate

3.1.5 Summary

Although insufficient design definition exists to select TPS materials for the CRV, the required performance was found to correlate well with TPS material density. Improvements in thermal analysis capabilities since the Apollo era will enable CRV designers to tailor thermal protection materials to the expected heat loads with much smaller design margins than were used on Apollo. As a result of this enhanced analysis capability and improvements in thermal protection materials, the CRV was estimated to require only 397 kg in TPS mass; 40% less than the Apollo TPS, in spite of the CRV having 10% greater surface area. It was found that low density reradiative materials (128-160 kg/m³) such as LI-900, AFRSI, etc., are adequate for 27% of the surface area. Moderate density ablatives are expected to compete with moderate density reradiatives over the majority of the surface (~63%). Moderate to high density ablative materials (>400 kg/m³) are likely to be required on only about 10% of the CRV surface.

Advances in ablative materials technology are expected to produce modest improvements in ablator efficiency over the next decade. Susceptibility to aerodynamic shear erosion may limit the use of low/moderate density (<450 kg/m³) materials or require the use of reinforcing fibers. Additional cost and mass savings are expected through improved performance characterization, modeling, and through processing techniques such as resin transfer molding. High char yield phenolic-triazine, as well as fluorosilicone and polytetrafluoroethylene (PTFE) resins show promise for future ablative technology development. An optimized ablative TPS is likely to be a composite of inorganic fillers (e.g., silica microballoons) combined with an organic matrix in a ratio tailored to the expected heat load conditions.

3.2 MARS CREW RETURN VEHICLE THERMAL PROTECTION SYSTEM ANALYSIS

For the Mars CRV, an analysis was performed to determine the thermal environment and provide mass estimates based on this analysis. A nominal Mars return was examined including both radiative and convective heating. As a result of the high temperatures encountered in the shock layer, an extrapolation of existing thermodynamic and transport properties to higher temperatures was required.

3.2.1 Trajectory

For a Mars return, the CRV will perform a direct entry at Earth following a trajectory similar to the Apollo entries and the lunar CRV entry. The Mars CRV return trajectory was simulated using the MISSION program, with a return entry velocity of 13.1 km/sec ($C3 = 50 \text{ km}^2/\text{sec}^2$) at 150 km altitude. The ballistic coefficient of the

Mars CRV was 280 kg/m^2 , with an L/D of 0.3 at an angle of attack of 25° . The undershoot trajectory for the Mars CRV is displayed in figure 3-9. For this trajectory, both radiative and convective stagnation heating were computed using the aforementioned methods. The stagnation point heating history for this trajectory is presented in figure 3-10, where the peak heating rate is 790 W/cm^2 . The Apollo Block II undershoot design trajectory peak heating rate was 800 W/cm^2 , which is nearly identical to the CRV value. A comparison of stagnation point heat loads for the CRV and Apollo entries is shown in figure 3-11. Total heat loads for the Mars CRV are only slightly higher than the Apollo Block II design, but almost double the actual heat loads encountered during the Apollo entries, which were $29,200 \text{ J/cm}^2$ to $31,700 \text{ J/cm}^2$. Based on stagnation point analysis, the CRV Mars return will encounter a similar thermal environment as that imposed on the Apollo capsule design by the Block II design limits.

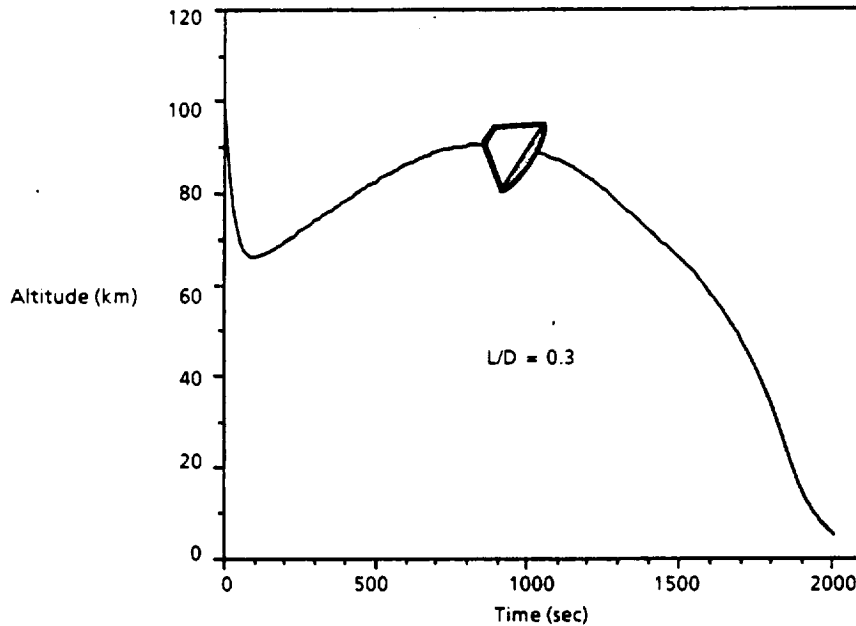


Figure 3-9. CRV Mars Return Earth Entry Trajectory

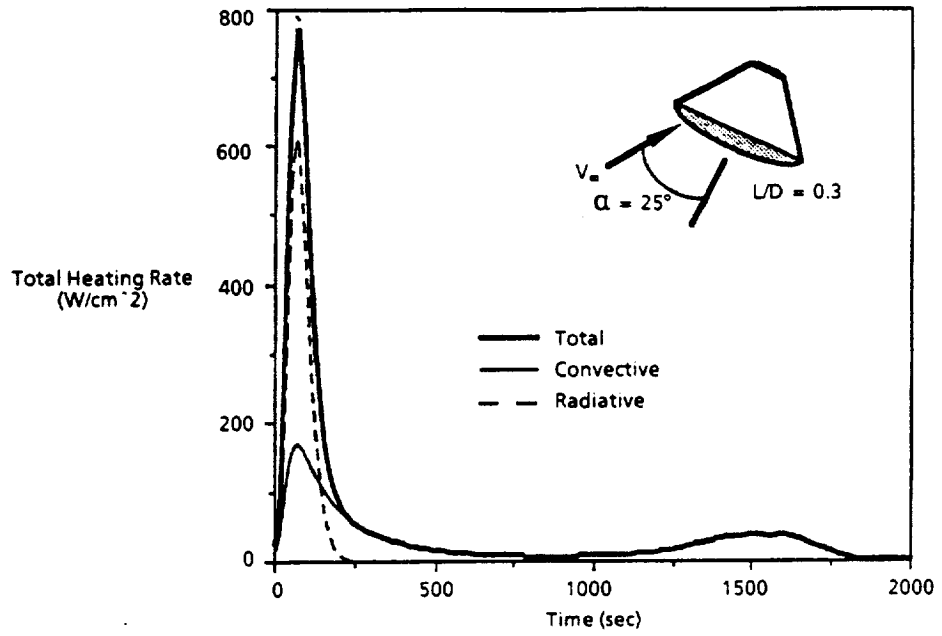


Figure 3-10. CRV Mars Return Heating Rates

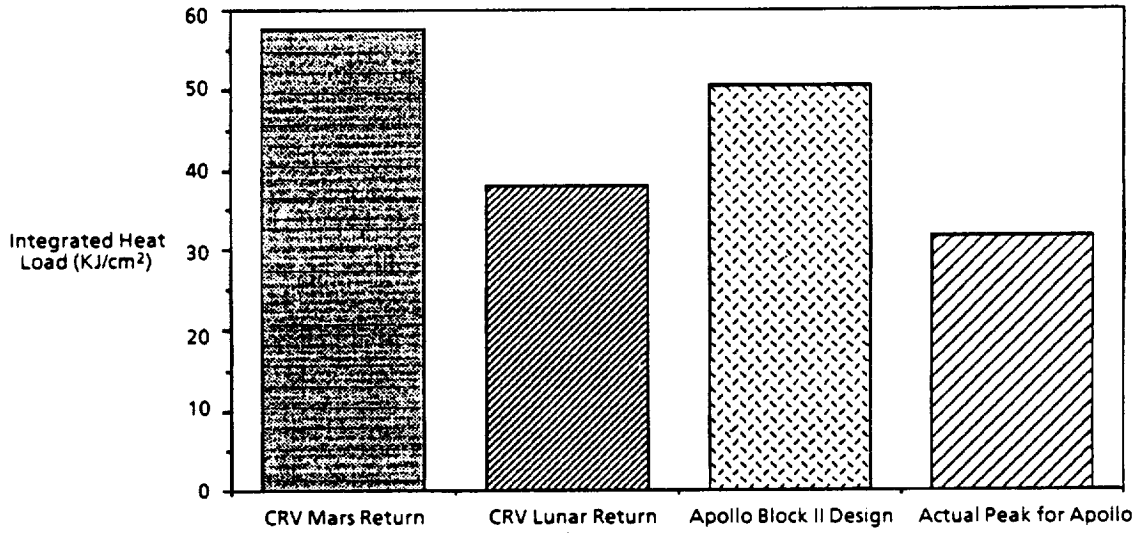


Figure 3-11. CRV Integrated Stagnation Point Heat Load

3.2.2 Temperature Profile

As the Mars CRV entry will encounter a significantly higher thermal environment than that of the lunar return, a more detailed heating distribution analysis was required in place of extrapolating the Apollo entry data. In examining the Mars return stagnation heating it was found that the current thermodynamic and transport properties for air were limited to shock layer temperatures of 15,000 K. These properties are the Peng and Pindroh values (ref. 9), which are used in the Boeing Boundary Layer Analysis Program (BLAP), ref. 10. In order to compute the CRV heating distribution these properties were extended to cover the shock layer temperatures encountered by the Mars return case (17,000 K). However, there is still uncertainty in this extended data due to transition to highly ionized flow, at which point there will be a cross over in transport properties. Further definition of the properties of highly ionized flow will be required to accurately predict the Mars return heating. Analysis of the distributive heating for the CRV was performed using the BLAP code with extended properties. No additional analysis was conducted at this time.

3.3 HIGH L/D MARS EXCURSION VEHICLE

For manned Mars landings an increase in the Mars excursion vehicle L/D was required to ensure daylight landing, provide adequate crossrange and also a larger aerocapture corridor. From descent and landing simulations the L/D identified to meet these needs was 1.5 or greater. A truncated hyperbola shaped vehicle with L/D ~1.1 was developed and analyzed previously. As this did not meet the above requirements, several new aerobrake shape concepts were derived.

3.3.1 Aerodynamic Predictions

Aerodynamic properties were calculated using the Boeing AERO program. This program uses hypersonic aerodynamics based on Modified Newtonian Impact Theory, with the lift and drag forces computed by integrating the theoretical pressures over the lifting surface of the vehicle, and resolving the net force in the lift and drag directions. Calculated reference areas are based on the plan area of the shape. The aerodynamic characteristics were computed for angles of attack ranging up to 50°.

3.3.2 HMEV Concepts

Several shape concepts were derived to provide lift to drag ratios of 1.5 or greater at an angle of attack of 35° . The angle of attack limit was imposed to decrease the chance of flow impingement on the body surface in the wake region thus reducing the thermal protection system requirements. Of the many concepts studied, three versions were reviewed for a final comparison. The concepts are displayed in figure 3-12, and the aerodynamic parameters for these concepts, numbered 1 through 3, are shown in figures 3-13 through 3-15. Concept 1 is a delta planform with a small sweep angle and has an L/D of 1.59 at 35° angle of attack. Concept 2 is a derivative of a previously reported high L/D MEV shape (ref. 1) extended to a longer hyperbola-delta type planform resulting in an increased lift capability and a narrower profile. The L/D at 35° angle of attack for concept 2 is 1.65. A similar shape was derived for concept 3, except this concept has an elliptical planform with an L/D of 1.60. The L/D as a function of angle of attack for these concepts is plotted in figure 3-16. These three concepts were analyzed for packaging volume and aerodynamic capabilities. An evaluation was performed by examining the resultant force vectors for a trim angle of attack of 35° . Internal configuration and packaging for these concepts is discussed in section 2. Based on internal configurations (lander) and aerodynamic C_p locations for trim at 35° , concept 2 was selected as the updated aerodynamic configuration for the High L/D MEV (or HMEV).

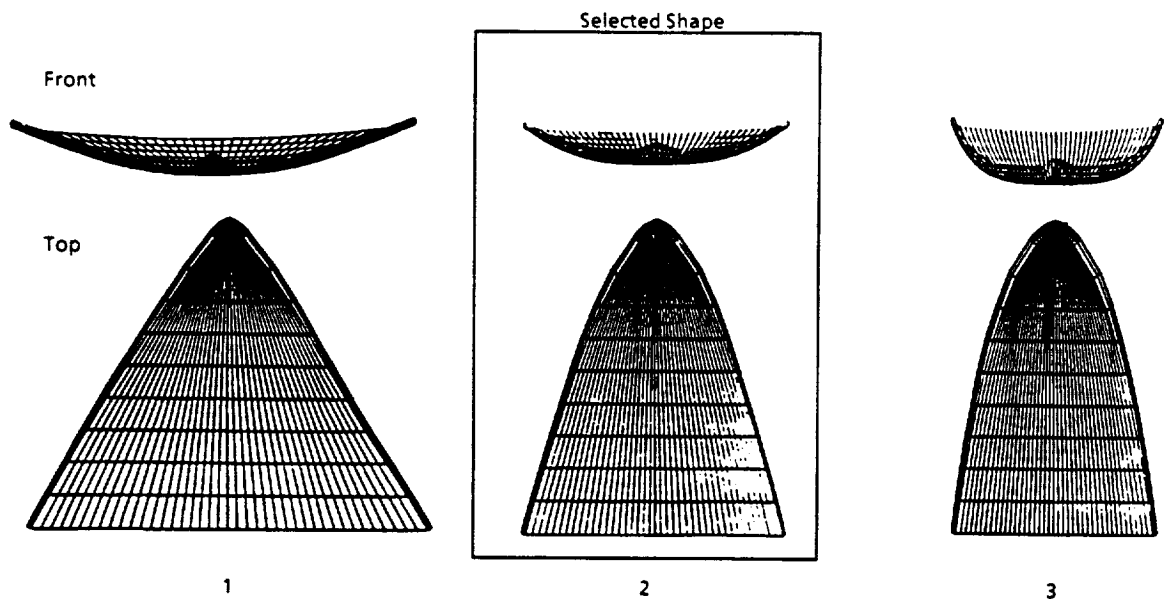


Figure 3-12. HMEV Aerobrake Shape Concepts

Values for Shape Parameters

Semimajor axis ratio	0.7000
Eccen. of body of revol.	4.0000
Eccen. of cutting cyl.	1.1550
Truncation/SMA ratio	7.0000
Lip radius/SMA	0.3000
Lip taper ratio	0.3000
Plan area	19.1605
Surface area	21.5755

Angle of attack	CL	CD	L/D	Moment arm
15	0.0345	0.0384	0.8989	-3.5767
20	0.0853	0.0536	1.5910	-2.8724
25	0.1566	0.0848	1.8455	-2.6902
30	0.2430	0.1369	1.7750	-2.6367
35	0.3378	0.2128	1.5876	-2.6230
40	0.4340	0.3139	1.3827	-2.6231
45	0.5238	0.4395	1.1917	-2.6287

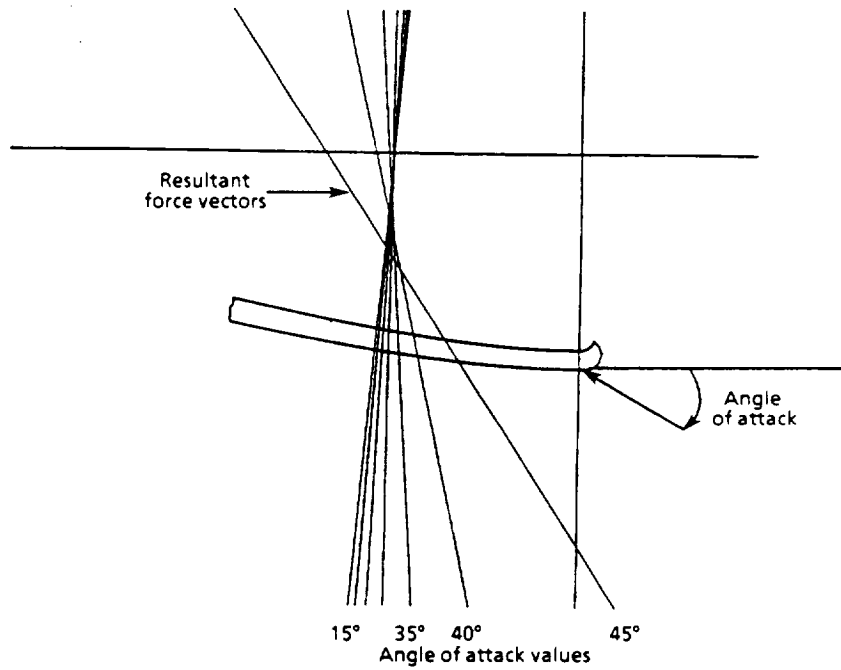


Figure 3-13. Shape Parameters and Resultant Force Vectors for Concept 1

Values for Shape Parameters

Semimajor axis ratio	2.0000
Eccen. of body of revol.	2.6000
Eccen. of cutting cyl.	1.0300
Truncation/SMA ratio	0.9500
Lip radius/SMA	0.0400
Lip taper ratio	0.3000
Plan area	2.2238
Surface area	2.5685

Angle of attack	CL	CD	L/D	Moment arm
15	0.0307	0.0329	0.9329	-1.4006
20	0.0745	0.0461	1.6162	-0.9976
25	0.1398	0.0738	1.8956	-0.8903
30	0.2217	0.1208	1.8358	-0.8584
35	0.3141	0.1908	1.6465	-0.8497
40	0.4097	0.2855	1.4348	-0.8494
45	0.5008	0.4049	1.2369	-0.8523

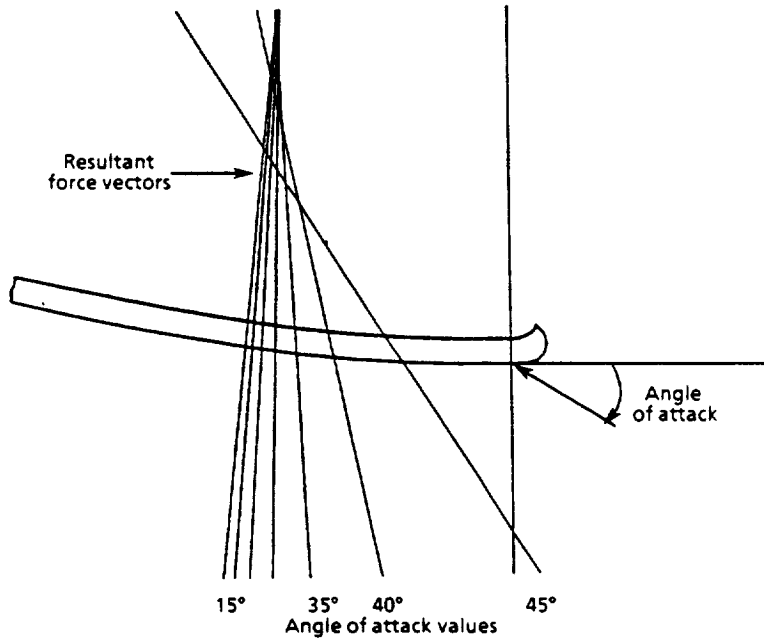


Figure 3-14. Shape Parameters and Force Vectors for Concept 2

Values for Shape Parameters

Semimajor axis ratio	2.0000
Eccen. of body of revol.	2.6000
Eccen. of cutting cyl.	1.0300
Truncation/SMA ratio	0.9500
Lip radius/SMA	0.0400
Lip taper ratio	0.3000
Plan area	2.2238
Surface area	2.5685

Angle of attack	CL	CD	L/D	Moment arm
15	0.0307	0.0329	0.9329	-1.4006
20	0.0745	0.0461	1.6162	-0.9976
25	0.1398	0.0738	1.8956	-0.8903
30	0.2217	0.1208	1.8358	-0.8584
35	0.3141	0.1908	1.6465	-0.8497
40	0.4097	0.2855	1.4348	-0.8494
45	0.5008	0.4049	1.2369	-0.8523

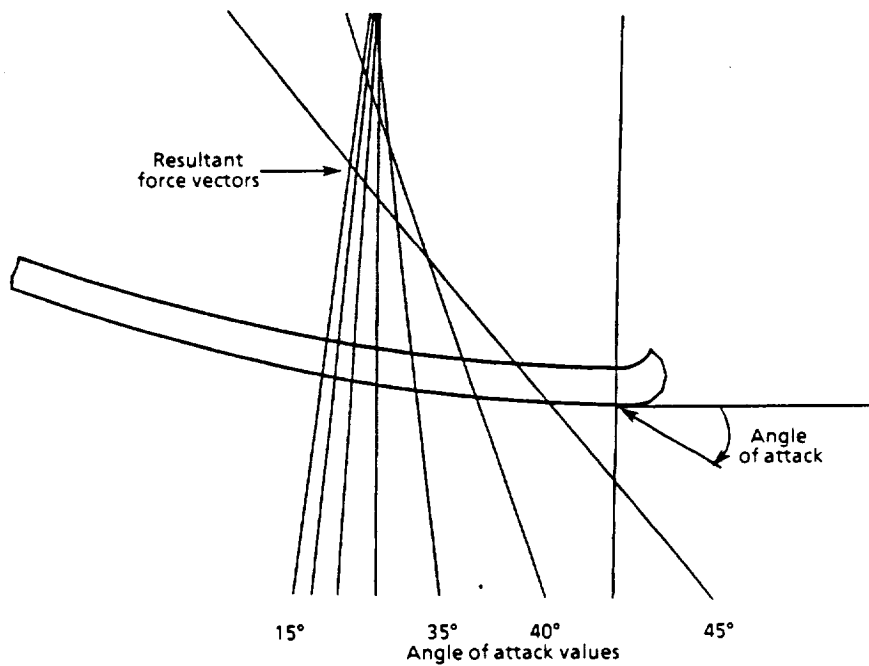


Figure 3-15. Shape Parameters and Force Vectors for Concept 3

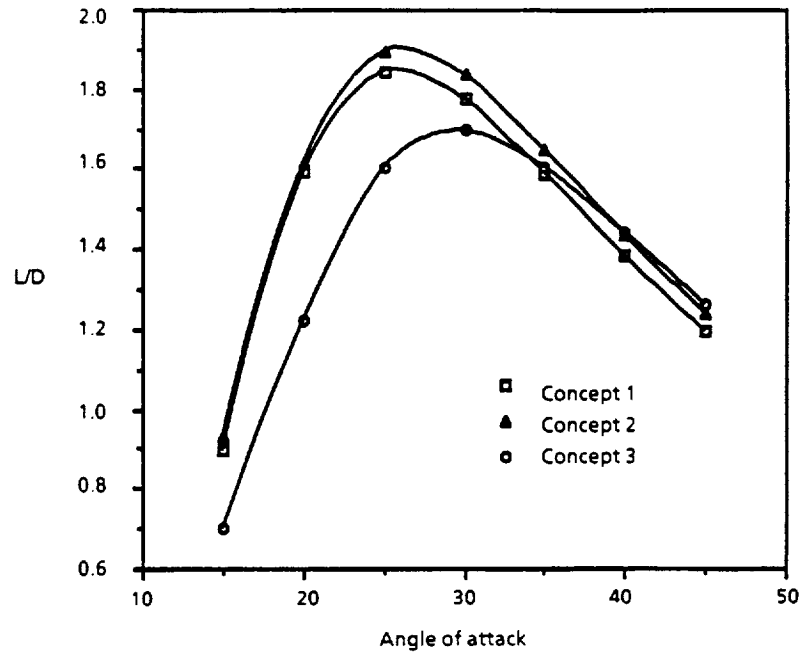


Figure 3-16. Concepts Lift to Drag Parameter

Concept 2 was selected as it was capable of providing the most aft center of gravity location thus reducing the required planform area of the aerobrake. An aftbody shroud was blended with the base aerodynamic configuration. The configuration was shaped to provide a favorable pressure gradient, which will give the HMEV better aerodynamic characteristics when launched in the integral launch configuration (e.g., STS shuttle). The aerobrake configuration is displayed in figure 3-17.

3.4 AEROBRAKE STRUCTURES

Two tools were compared for applicability for the structural analysis. Since some configurations were anticipated to include advanced composite materials, the features of ANSYS and NASTRAN finite element analysis programs were reviewed to evaluate their suitability for performing stress analysis of aerobrake structures.

Both ANSYS and NASTRAN have the capabilities to perform basic structural analysis. The differences arise when advanced or specialized problems are encountered such as layered composite structures, geometric nonlinearities, and cyclic symmetries. ANSYS provides a wider choice of elements whereas NASTRAN provides more advanced techniques to achieve the same results. While both programs have capabilities to analyze layered composite materials, ANSYS promises a somewhat easier approach by providing specialized composite elements. NASTRAN, on the other hand, uses standard

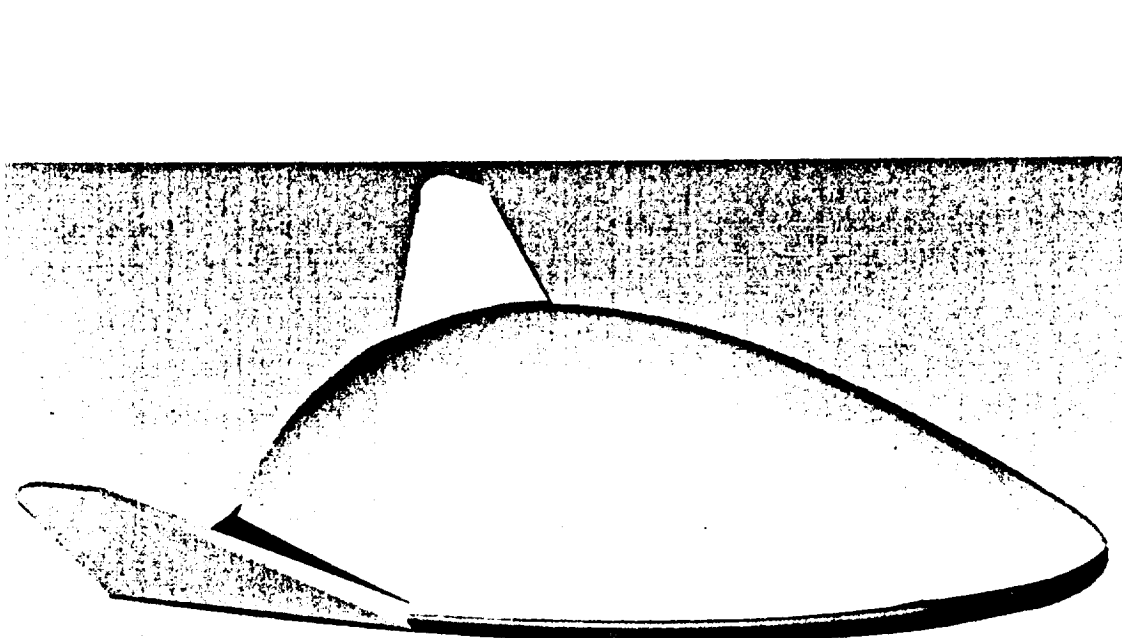


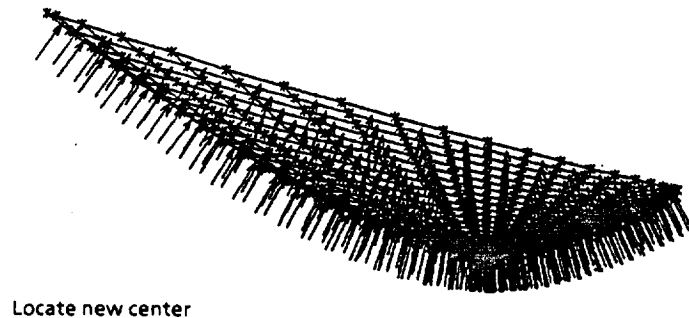
Figure 3-17. High L/D Mars Excursion Vehicle

plate elements with specialized property cards to specify the composite layers. Geometric nonlinearities in ANSYS are accounted for by special elements whereas in NASTRAN these are accounted for by using a nonlinear solution. NASTRAN also includes superelement analysis capabilities using DMAP routines. ANSYS simplifies the modeling and results evaluation process with a built-in pre- and post-processor interface and a simpler execution format. Each code has merits associated with it. ANSYS and NASTRAN were available for use. The current analysis was conducted with ANSYS.

The first concept chosen for analysis consisted of a semi-monocoque shell of sandwich construction with advanced composite/laminate materials. A simple configuration was modeled initially to provide a "skeleton" mesh and to verify the final model's geometry and expected accuracy. For purposes of preliminary sizing for inclusion in the initial finite element model, the shell was assumed to be monolithic of spherical section fabricated of titanium. A preliminary sizing exercise yielded a minimum required thickness of 2 cm (0.8 in) for the shell, resulting in a mass of approximately 36 metric tonnes.

Due to its immediate availability, IDEAS Supertab was used for pre-processing and preparation of the initial aerobrake model. This model was then converted to ANSYS for analysis and subsequent iterations and/or modifications.

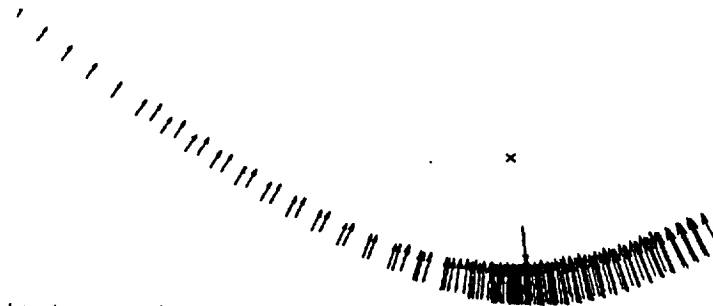
The preliminary model consists of thin shell elements which define the aerobrake geometry. These elements are loaded by element face pressures as calculated in a separate aerodynamics analysis. The pressure loading is variable and ranges from 0 at the aft lip section to 13,675 Pascals (≈ 2 psi) at the stagnation point. The loaded model is shown in figure 3-18. Note that the pressure vectors do not represent magnitudes and are not scaled. A scaled left-side view of the pressure distribution is shown in figure 3-19.



Locate new center

Figure 3-18. Finite Element Model with Loads

K - Key_in_fraction
V - Visible
I - Backup
\$ - Abort



Locate new center

Figure 3-19. Scaled Load Vectors, Left Side View

An analysis of the initial model was performed. While the resultant principal stresses were low (margin of safety ≈ 4), displacements were extremely high (≈ 38 cm at the edges of the shell), indicating a stiffness-critical design problem. A principal stress contour plot of the analysis results is shown in figure 3-20. A second, analogous load case (6 g loading, constrained at edges) was analyzed to verify the analysis approach. Results showed a deviation of less than 10% from the first analysis.

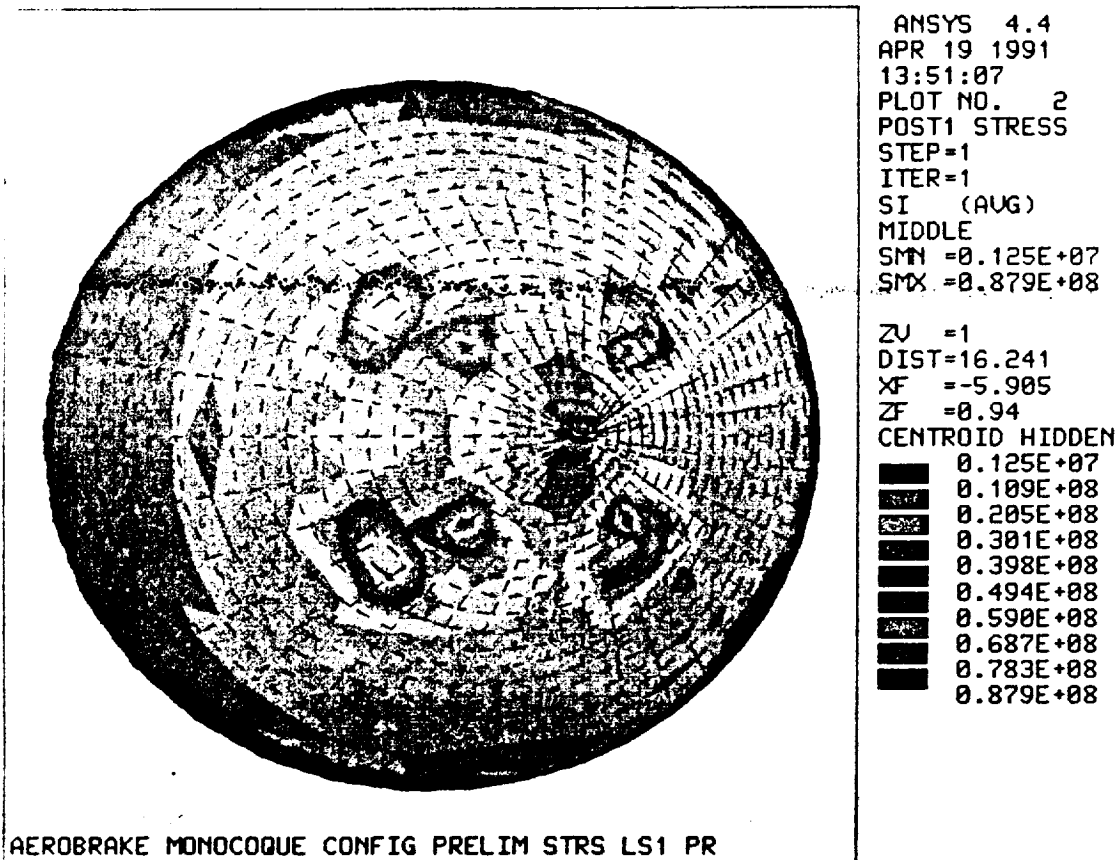


Figure 3-20. Aerobrake Structural Integration

A composite honeycomb sandwich panel configuration was then defined and sized which provides stiffness much greater than the monolithic shell at a reduced weight (23 metric tonnes). This configuration is shown in figure 3-21. Materials were then selected for the composite laminate shell. A silicon carbide-reinforced titanium aluminide composite (40% SiC/Ti₃Al) was chosen for the face sheets of the sandwich. This advanced composite material was chosen on the basis of its exceptional stiffness-to-weight ratio and the retention of structural properties up to 700°C. Avoidance of the expense and technical complications associated with beryllium and consideration of the progress in silicon-carbide technology also favor this selection.

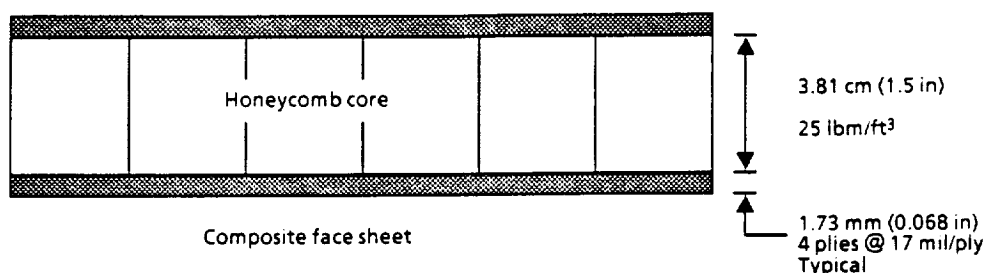


Figure 3-21. Sandwich Configuration Cross-Section (Constant)

The plies of the composite are estimated to be 0.043 cm (17 mil) thick. A minimum of four plies for each face sheet is assumed to be minimum gage. Titanium aluminide (Ti₃Al) was chosen to be the honeycomb core material. The material properties for the composite sandwich configuration are shown in figures 3-22 and 3-23. Additional structural analysis design studies are planned in order to evaluate the structural and mass characteristics of the aerobrake.

Property	Value (room temp)	Value (700 C)
Matrix volume fraction	60%	60%
Fiber volume fraction	40%	40%
Ply thickness	0.432 mm (17 mil)	0.432 mm (17 mil)
Matrix moisture content	0.0	0.0
Fiber moisture content	0.0	0.0
Reinforcing factor for E. parallel to fibers	1.8	1.8
Factor for E. perpendicular to fibers	0.67	0.67
Reinforcing factor for Poisson's ratio	1.0	1.0
Reinforcing factor for shear modulus	1.0	1.0
Mass density (face sheets)	4041 kg/m ³ (.15 lb/in ³)	4041 kg/m ³ (.15 lb/in ³)
Mass density (honeycomb core)	400 kg/m ³ (25 lb/ft ³)	400 kg/m ³ (25 lb/ft ³)
F _{si} . shear str. core (longitudinal)	TBD	TBD
F _{sw} . shear str. core (transverse)	TBD	TBD
G _{si} . shear mod. core (longitudinal)	TBD	TBD
G _{sw} . shear mod. core (transverse)	TBD	TBD

Figure 3-22. Composite Properties

3.5 LUNAR TRANSFER VEHICLE (LTV) WAKE ANALYSIS

An investigation was performed to assess the wake characteristics of the Lunar Transfer Vehicle. The specific study is to determine the volume of the wake for payload components and to develop an engineering method of predicting the heating environments on payloads within the wake during aerobraking. Three specific potential aerobrake geometries were examined, although the heating method and wake volume estimates are applicable to a broader range of aerobrake configurations. The three

Property	Silicon-Carbide (Si-C)		Titanium alum (TiAl3)	
	700 C	Room temp	700 C	Room temp
Young's modulus, E	372 GPa	410 GPa	133 GPa	140 GPa
Poisson's ratio	0.10	0.10	0.28	0.27
Mass density	3.05 g/cc	3.05 g/cc	4.65 g/cc	4.65 g/cc
Shear modulus	169 GPa	186 GPa	52 GPa	55 GPa
Allowable - tension	3723 MPa	4137 MPa	827 MPa	896 MPa
Allowable - compression	3447 MPa	4000 MPa	641 MPa	641 MPa
Allowable - shear	1227 MPa	1379 MPa	538 MPa	579 MPa

Figure 3-23. Material Properties, 700°C and Room Temperature

shapes analyzed are shown in figure 3-24, and belong to the low L/D family of aerobrakes. The option 1 configuration is a 50 foot (15.24 m) diameter sphere-cone-torus with a 10 foot (3.05 m) nose radius, a 70° half cone angle, and a 1 foot (0.30 m) radius skirt. Option 2 is a 50 foot (15.24 m) diameter raked cone, which is proportional to the AFE but with a 1 foot (0.30 m) radius skirt. Option 3 is a 50 foot (15.24 m) diameter sphere-torus with a nose radius of 54 feet (16.46 m) and a 1 foot (0.30 m) radius skirt. This study was conducted by REMTECH, Incorporated (ref. 11).

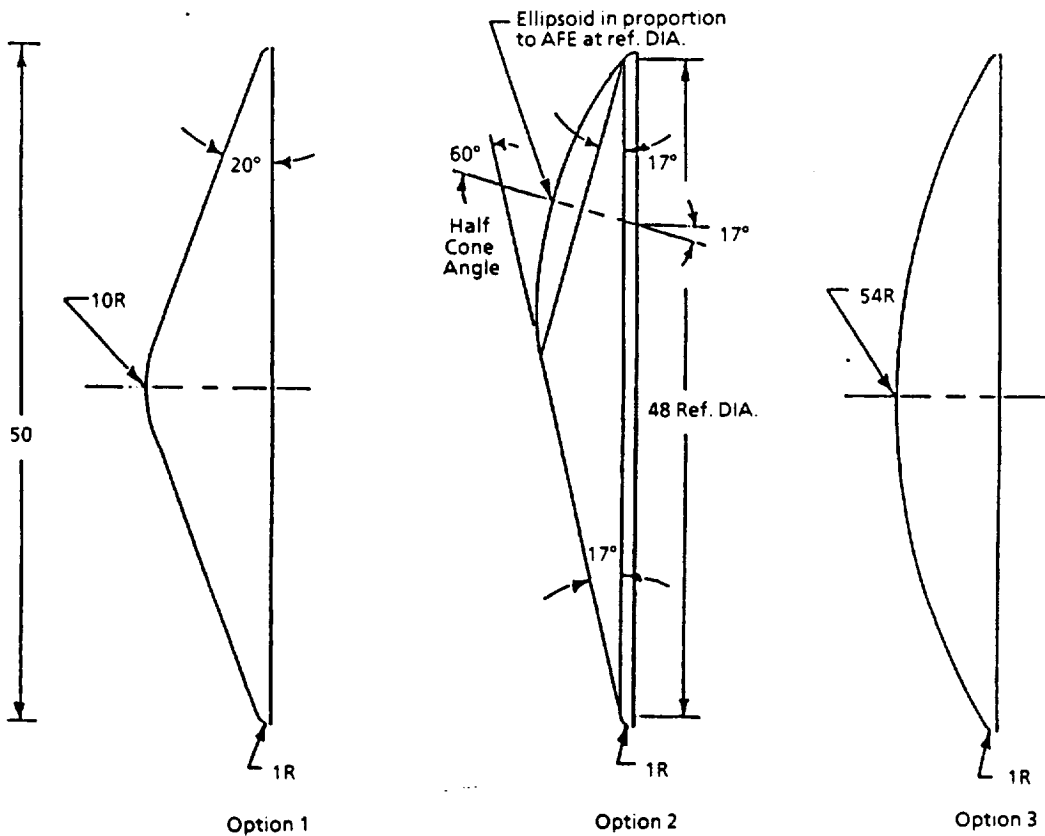


Figure 3-24. Lunar Return Aerobrake Shapes

3.5.1 Flight Conditions

The peak heating conditions were calculated for nine specific lunar return trajectories with vehicle L/D values of 0.15, 0.20 and 0.30 and ballistic coefficients of 10, 20 and 30 lb/ft² (49, 98, 146 kg/m²). The peak heating stagnation values were calculated using Fay and Riddell's method (ref. 4). The flight conditions at peak heating for the nine trajectories are shown in figures 3-25 and 3-26. For the range of L/D and W/C_DA studied, the velocity was about 32.5 K ft/sec (9.9 km/sec), altitude about 242 K ft (74km), with unit Reynolds numbers from 8000 to 16000 per foot, (26,000 to 52,000 per meter). The maximum peak heating rate occurred at 235 K ft (72 km) for W/C_DA = 20 lb/ft² (98 kg/m²) and L/D = 0.15.

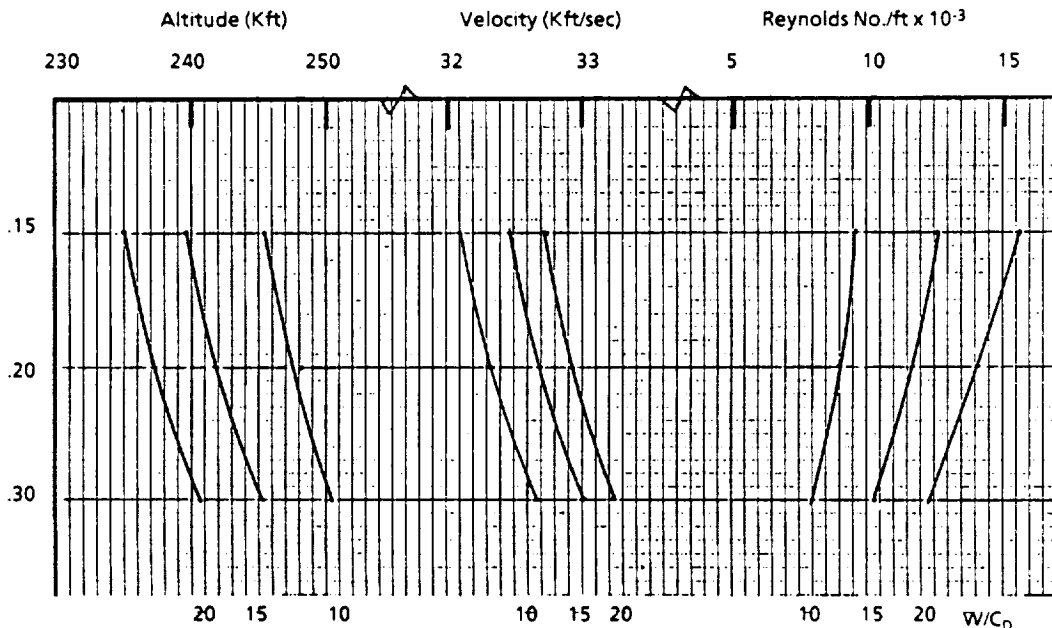


Figure 3-25. Flight Conditions at Peak Heating as a Function of Lift to Drag Ratio

3.5.2 Shear Layer Edge

For the blunt aerobrake shapes considered, several definitions have been employed in describing the near wake and the wake closure or expansion angle. The wake expansion angle has been defined in many ways, usually referred to the initial flow direction (flight path).

- a. Outer edge of the shear layer where the flow is basically inviscid and no total enthalpy has been lost, (ref. 12).
- b. Shadowgraph of the wake flowfield.

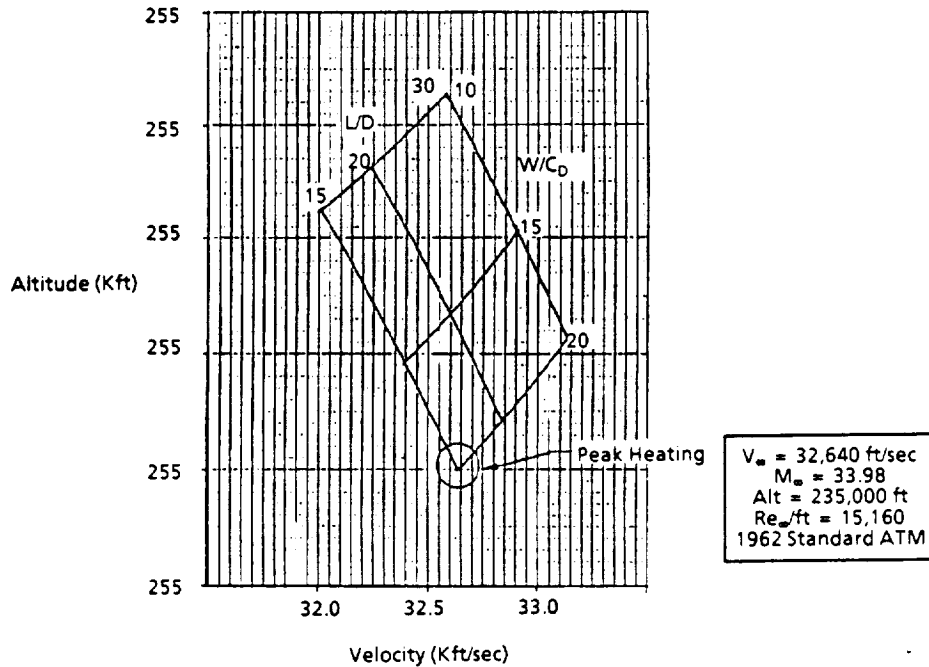


Figure 3-26. Peak Heating Condition Carpet Plot

- c. CFD results where Mach 1.0 lines can be identified from contour plots, (ref. 13).
- d. Shear layer dividing streamline in a Korst base flow model.
- e. CFD results where the total enthalpy line of $H_T/H_{T_\infty} = 0.6$ is chosen, (ref. 13).
- f. Peak heating location on a cylindrical payload where the cylinder is perpendicular to the base, (ref. 14).

For the current work, definition (a) is used for theoretical work and (b) and (f) are used for experimental work. Definition (a) also corresponds to the angle produced by CFD results where H_T/H_{T_∞} approach 1.0 from the inside of the wake (i.e., shear layer edge).

The wake expansion angle is calculated theoretically using a slightly modified method (ref. 12). In this model the wake expansion angle is defined as the angle computed by a Prandtl-Meyer expansion from the front face sonic point to the base pressure. The base pressure is determined by one of the three empirical relations below.

Sambamurthi and Warmbrod (ref. 12) give

$$\log_{10} \frac{P_B}{P_t} = 0.06873 (\log_{10} Re_{2D})^3 - 0.85 (\log_{10} Re_{2D})^2 + 3.556 (\log_{10} Re_{2D}) - 6.718 \quad (1)$$

$$\text{Where } \frac{P_B}{P_t} = 0.02 \text{ for } Re_{2D} = 10^4$$

P_B = Base pressure, P_t = Total pressure behind normal shock and Re_{2D} is the Reynolds number based on conditions behind the normal shock and body diameter.

Brant and Nestler (ref. 15) give

$$\frac{P_B}{P_t} = 0.008 \quad (2)$$

for high Reynolds numbers

Engle et al. (ref. 16) give a relationship for ($M_\infty > 8$)

$$\frac{P_B}{P_\infty} = 10^{[.18708 + 0.10806(M_\infty - 8)^.8]}$$

Parametric results from this method are shown in figure 3-27 where the expansion angle, θ_s , is shown as a function of post shock specific heat ratio, γ , at specific Mach numbers ranging from 10 to 30. Results are presented for the base pressure method of Engel. The expansion angle is shown to be a strong function of post shock specific heat ratio and a weak function of freestream Mach number. The effect of specific heat ratio is addressed in the next section. The Mach number effect is shown in figure 3-28 for a constant specific heat ratio of 1.4.

The range of ground test data is shown on figure 3-27 for ideal gas air conditions. Usually the angle which is measured is the wake turning angle plus the angle of attack (i.e., angle from the horizon down from the shoulder). The theoretical data for $(\theta_s + \alpha)$ are plotted versus the measured data in figure 3-29. The total set of data is in general agreement with the theory; however, there is significant scatter. These data are for six different aerobrake shapes and show no shape or shoulder geometry effect. The theory indicates that the wake expansion angle is independent of angle of attack. The ratio of the experimental to the theoretical expansion angle is shown in figure 3-30 for the range of angle of attack. Some observations may be drawn. First, the peak impingement point derived data from Hair (ref. 14) and Wells (ref. 17) are in general lower than the AMES

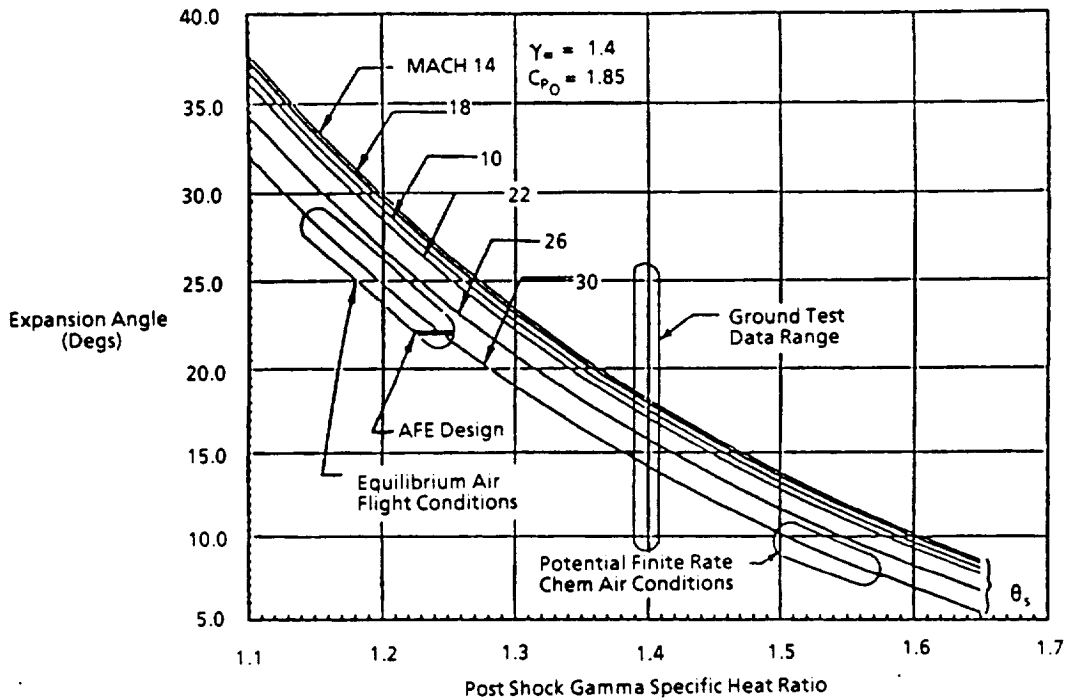


Figure 3-27. Theoretical Expansion Angle Range

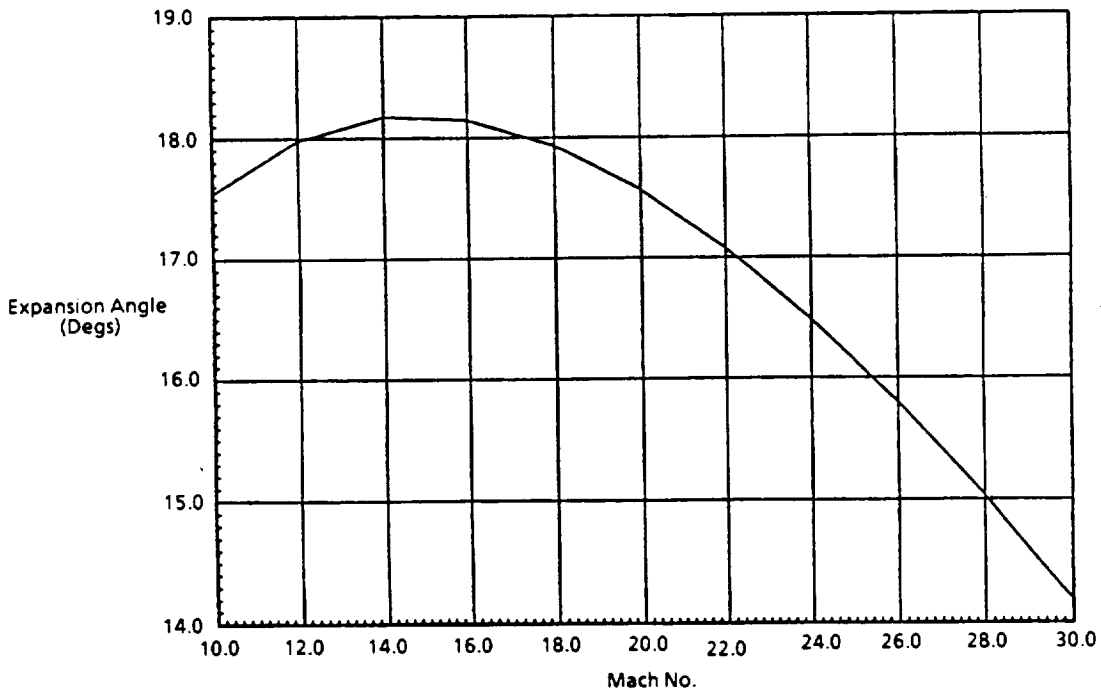


Figure 3-28. Expansion Angle Versus Mach Number for Gamma of 1.4

ballistic range shadowgraph data. This shift may be due to the difference in the process being measured. Secondly, the impingement data do have a trend with angle of attack. At lower angles of attack the wake base pressure is increased by the sting. This increase in base pressure lowers the wake angle. The sting to brake diameter ratio was 0.30 for the Hair et al. data and 0.275 for the Wells data. The effect of the sting on base pressure and thus wake angle is shown in figure 3-31. The theory and data are in much better agreement when this base pressure effect is included in the comparison calculations. In fact the three data points in the figure for $\alpha = 10^\circ$ would shift from near the $-\sigma$ line on figure 3-30 to the $+\sigma$ line (i.e., near equal agreement with theory). Consequently, the current data suggest that the method of Sambamurthi et al. provides an acceptable estimate of the wake expansion angle on the windward side of the aerobrake if the base pressure and effective specific heat ratio are known.

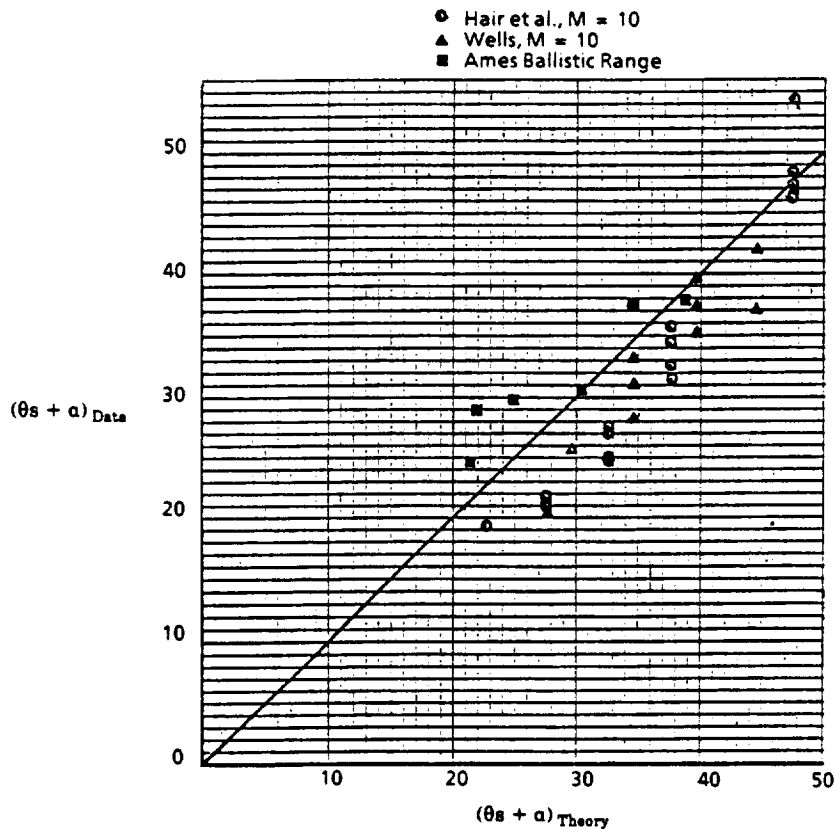


Figure 3-29. Measured Shear Layer Turning Angle Versus Theoretical Value

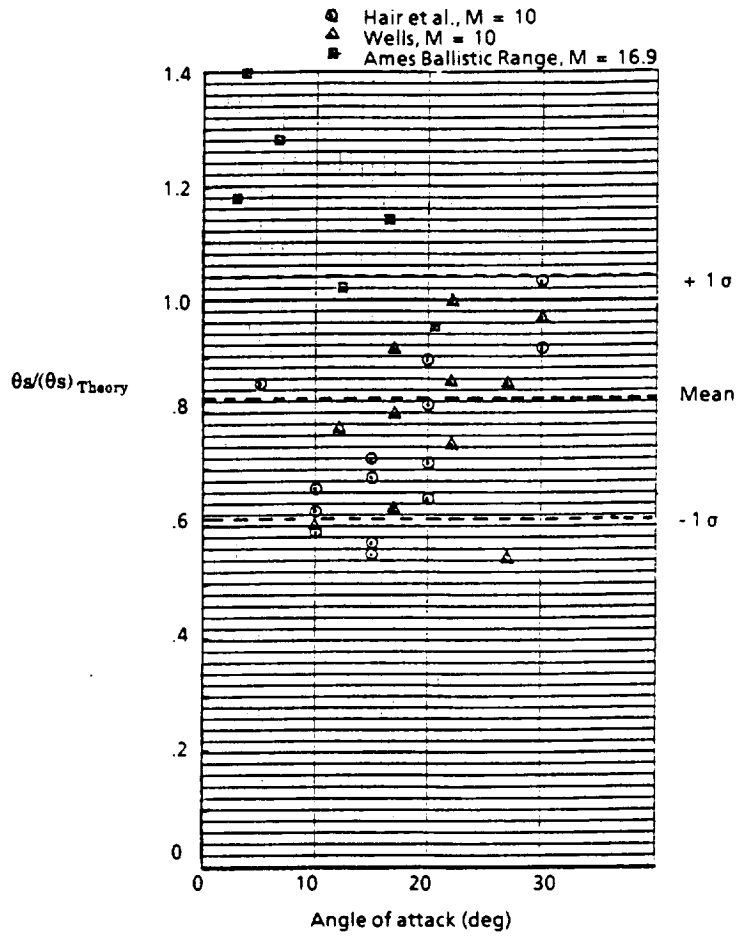


Figure 3-30. Measured Shear Layer Edge Angle Data to Theory Ratio

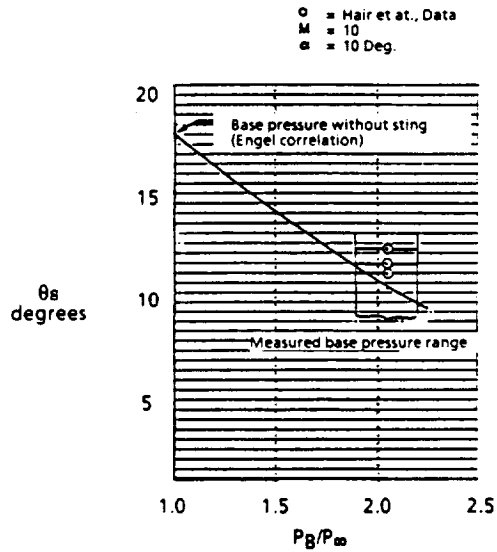


Figure 3-31. Base Pressure Effect on Wake Expansion Angle

3.5.3 Inviscid Flowfield Analysis

The expansion process from the sonic point on the front side of the aerobrake around the shoulder controls in large part the wake expansion angle. Although the viscous boundary layer effects are known to have an influence on the expansion process and the wake shear layer, its effects are secondary to the inviscid Prandtl-Meyer expansion process. The Prandtl-Meyer expansion process is controlled by the initial to final pressure ratio and the specific heat ratio of the gas throughout the process.

Equilibrium real gas air calculations were made using the BLIMPK computer code for the current geometries. The specific heat ratio at the edge of the boundary layer as a function of body angle at the peak heating condition is shown in figure 3-32a. At these flight conditions, γ increases through the expansion process and then decreases until the base pressure is matched at $\theta_s = 24.4^\circ$ on the rear side of the body. This wake expansion angle agrees with previous AFE calculations of the expected equilibrium air γ and expansion angle shown in figure 3-27.

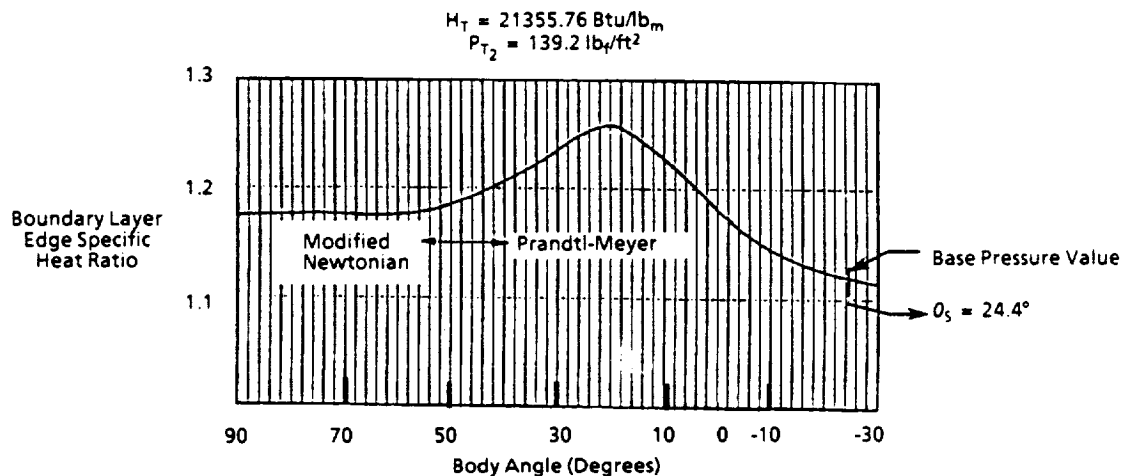


Figure 3-32a. Boundary Layer Edge Equilibrium Air Specific Heat Ratio at Lunar Return Peak Heating Conditions

At these velocities and altitudes, equilibrium conditions may not be valid. Finite rate chemistry air calculations made by Gnoffo (ref. 13) for lunar return and AFE conditions provide contours suggesting the wake expansion angle is lower than equilibrium air conditions would permit. In fact these results suggest that the effective γ is somewhat larger than 1.5 as shown in figure 3-27.

The effects of finite rate chemistry on the specific heat ratio in an inviscid stream tube starting at the stagnation point and extending to the wake shear edge were

explored. Calculations were made for the sphere-torus (option 3) configuration with the GASP code (ref. 18). A finite rate air chemistry model (ref. 19) which accounts for 11 species and 47 reactions was used. Calculations were carried out for the peak heating trajectory point. The mixture specific heat ratio was determined and is shown in figure 3-32b. The base pressure matches the Engel (ref. 16) correlation value at -4 degrees and the Brant and Nestler (ref. 15) base pressure at -9 degrees (i.e., $\theta_s = 4$ or 9°). The edge of the shear layer as determined by the total enthalpy lines given by Gnoffo is approximately $\theta_s = 8.5^\circ$. The limited finite rate chemistry results from the present study and from that of Gnoffo tends to indicate that the real gas air condition for lunar return is dissociated and nearly frozen through the shoulder expansion process. As a result, the effective specific heat ratio is high resulting in rather low wake expansion angles. Accordingly, the current rather limited information indicates that a low wake turning angle of $\theta_s = 9^\circ$ could be used for preliminary design work at near peak heating conditions.

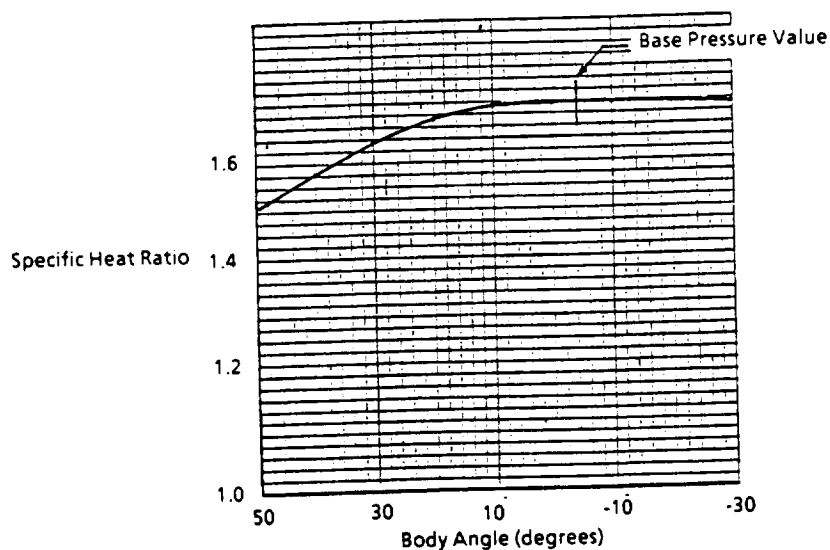


Figure 3-32b. Finite Rate Air Specific Heat Ratio at Lunar Return Peak Heating Conditions

3.5.4 Wake Volumes

The wake volume where payloads could potentially be placed consists of two components. First, the volume inside the aeroshell and forward of the back plane can be used. Second, the volume inside the shear layer and in front of the wake neck may be used. Equations describing each of these components were derived for the three configurations under consideration and are presented in reference 11.

Volumes for the three aeroshells under consideration were calculated for diameters ranging from 40 to 60 feet (12.19 to 18.29 m). These results are given in figure 3-33. Options 1 and 2 give nearly the same volume over the range of diameters examined and all three options provide about 7,200 cubic feet (204 m³) for 50 foot (15.24 m) diameter vehicles. The internal aeroshell volume is small compared with the potential volume within the shear layer edge limits. The free wake volume is shown in figure 3-34 as a function of wake angle for three diameters and three angles of attack. The wake volume is a weak function of angle of attack, somewhat stronger function of brake diameter and much stronger function of wake expansion angle. For the wake expansion angle, an estimate of the free wake volume potential can be obtained.

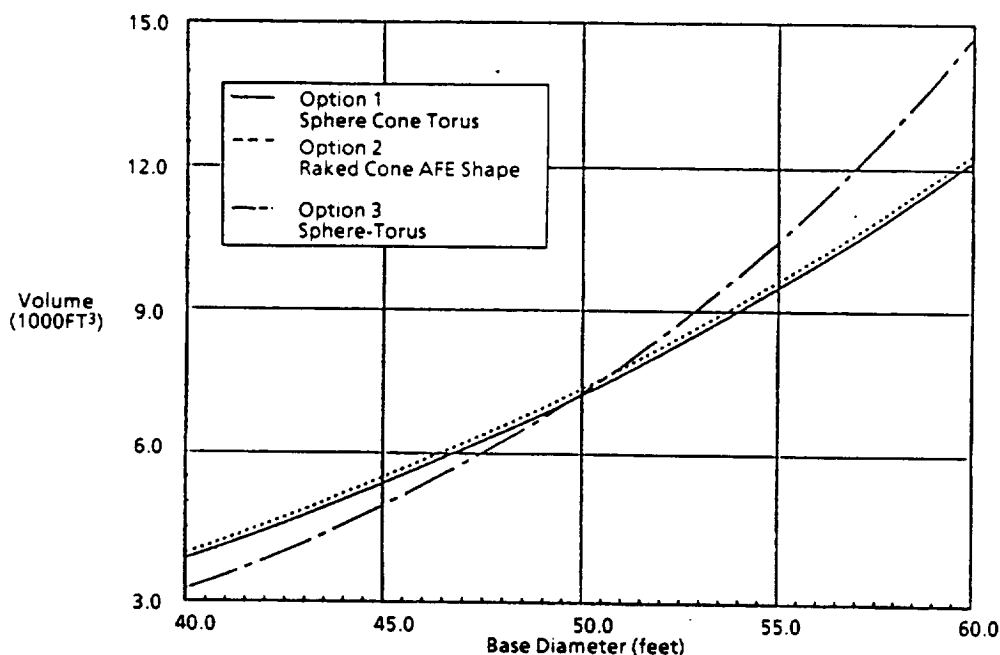


Figure 3-33. Volumes of the Three Aerobrake Configurations

3.5.5 Wake Heating

An engineering method for calculating heating for different wake payload geometries has been developed. The method is based on available laminar heating relations, AOTV data correlations developed by Hair et al. (ref. 14), and correlation of theoretical enthalpy profiles from Gnoffo et al. (ref. 13). The wake is divided into four regions from the wake exterior, where no total enthalpy has been lost, to the interior where subsonic lower enthalpy gasses exist. The heat transfer coefficient and heating rate to a payload component can be calculated with this model knowing the stagnation

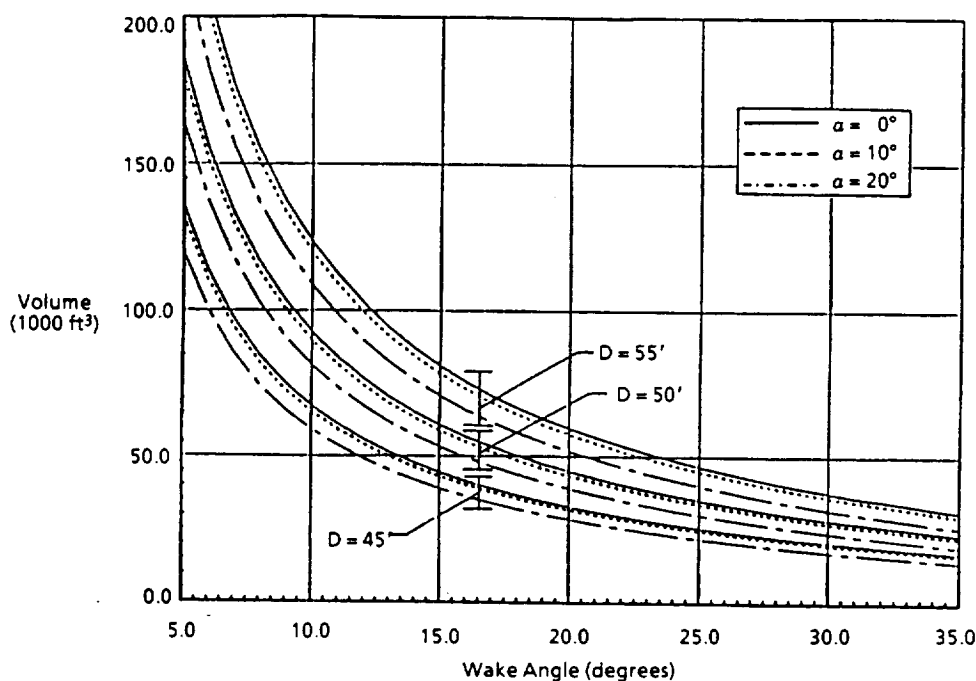


Figure 3-34. Wake Volumes of a Circular Body

heat transfer coefficient, total enthalpy, brake radius as well as the wake impingement angle, and wake payload component geometry and orientation within the wake.

The engineering method may be used to provide first estimates of the wake heating on aerobrake payload components. The method is primarily applicable to peak heating conditions where continuum laminar flow exist. The method may be used throughout the aerobraking flight although future improvements to account for wake closure and rarefied flow heating should be made to improve the heating load prediction.

A sample case was calculated to illustrate the type of heating rate distributions which may be expected on payloads in the brake wake. The following assumptions were made:

Angle of attack = 10°

Wake impingement angle = 8°

Geometry: Cylinder

Cylinder radius = 5 feet (1.32 m)

Brake radius = 25 feet (7.62 m)

Stagnation heat transfer coefficient, $h_s = 0.00221 \text{ lbm/ft}^2\text{sec}$

for $R_B = 25 \text{ feet (7.62 m)}$

Stagnation enthalpy, $H_s = 21360 \text{ Btu/lbm}$

Wall temperature $T_w = 1000^\circ\text{R}$ (556 K)

Orientation: The payload cylinder centerline is parallel to the aerobrake centerline. The payload is placed at the centerline and at 5, 10, and 15 feet (1.5, 3.05, and 4.5 m) radially away from the aerobrake centerline and toward the windward side.

The results of this sample problem are shown in figure 3-35 where the payload stagnation line heating rate is plotted as a function of axial distance for four locations of the payload.

$h_s = 0.00221 \text{ lbm/ft}^2 \text{ sec}$
 $H_s = 21360 \text{ Btu/lbm}$
 PAYLOAD: Cylinder, $R = 5 \text{ ft}$, Axis parallel to centerline
 Cylinder stagnation line located 5, 10, and 20 feet from brake centerline

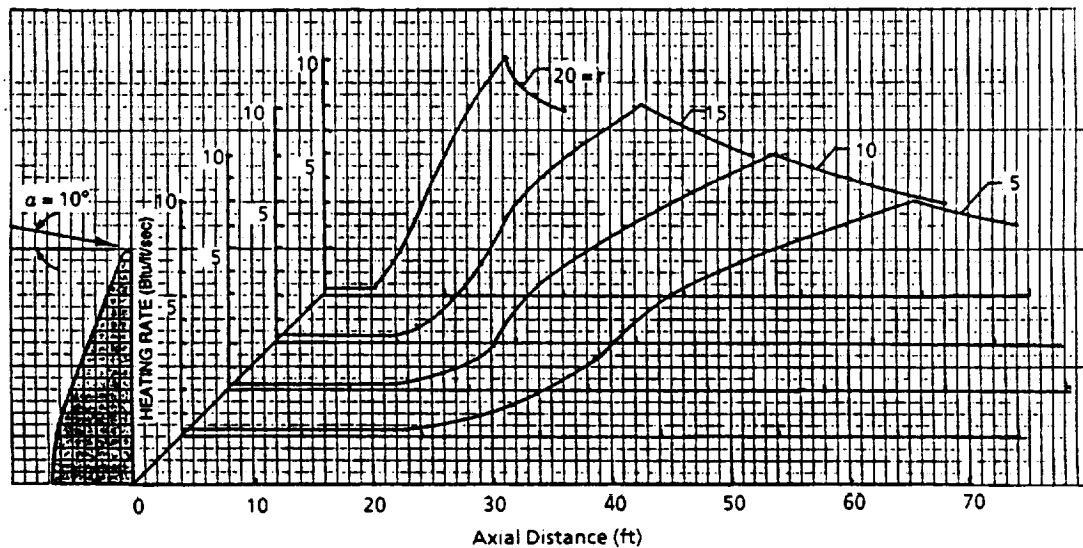


Figure 3-35. Heating Sample Case

3.6 MAIN ENGINE GIMBAL ANGLES

The HMEV configuration of the HLLV has generated concerns as to whether there exists sufficient thrust vectoring capabilities of the STME nozzle gimbals. The requirements are driven by primarily two factors: First, the dynamic center of gravity (CG) of the vehicle and secondly, the required thrust compensation for aerodynamic pitching moments.

As the center of gravity of the launch vehicle moves with propellant expenditure and staging, the nozzle must vector the thrust through the CG. As the launch vehicle is very similar in weight and configuration to the shuttle, there should be no problem. CG analysis indicates a required gimbal angle of $\sim 1^\circ$ (nozzle - center of gravity line with

reference to the longitudinal axis of the vehicle) at launch to $\sim 12^\circ$ at main engine cut off.

Aerodynamic data have been extrapolated from shuttle data by adjusting them for differences between the HMEV and shuttle configurations. These data indicate an HMEV pitching moment roughly double that of the shuttle and increase severely with angle of attack. However, flight simulation shows that this condition is ameliorated by maintaining an angle of attack near zero during the portion of the flight when aerodynamic forces are most severe (maximum dynamic pressure). Thus aerodynamic moment compensation amounts to a maximum of approximately 5° early in the flight when CG compensation is small. The total nozzle angle is plotted as a function of flight time in figure 3-36 and can be seen to stay within design limits ($\pm 10^\circ$). It should be noted that the nozzle may be biased with reference to the vehicle longitudinal axis.

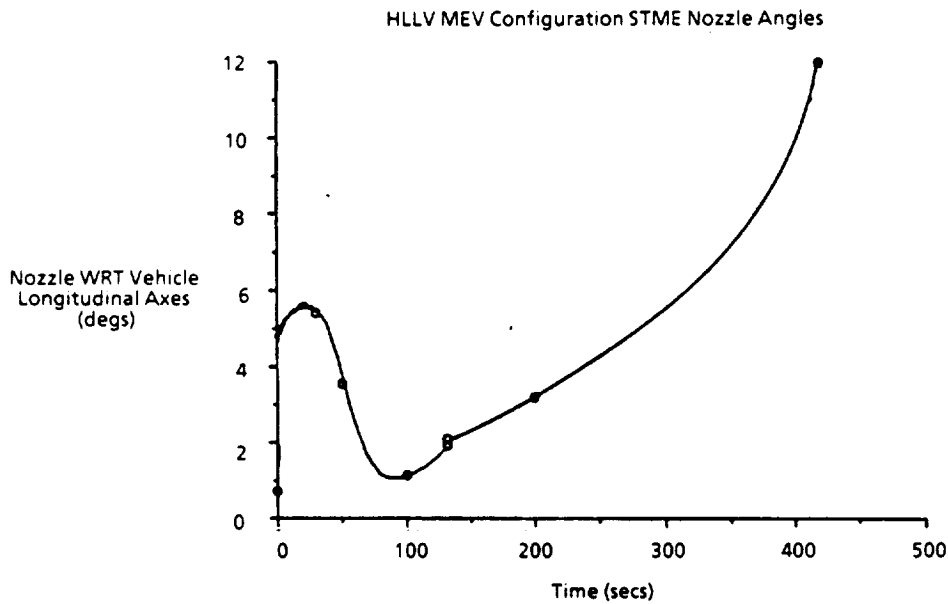


Figure 3-36. HLLMEV Configuration STME Nozzle Angles

4.0 ASSEMBLY OPERATIONS

4.1 ON-ORBIT ASSEMBLY OPERATIONS

In previous studies, a series of platform designs were conceived and evaluated for use and operations with the four vehicle types for Mars missions, Cryogenic/Aerobrake, Nuclear Thermal Propulsion, Nuclear Electric Propulsion and Solar Electric Propulsion, reference 1.

The current study is an assessment of multiple NTP support designs. From the concepts considered, only three were considered acceptable, figure 4-1. The elimination of Space Station Freedom based assembly resulted from the Augustine Commission Report recommendations. This report stated that the Space Station should be used primarily for research in life sciences and microgravity experiments and should lend "operational support" to the SEI missions. This was interpreted to mean that the Space Station could not be directly used for an assembly node (due to disturbances of the microgravity envelope that the addition of the SEI vehicle element weight would entail), but would allow an interior IVA work station and habitation for the SEI support crew, the exterior housing and servicing of the CTV and exterior storage of small item assembly materials. In addition, the recent (April 1991) NASA version of the Space Station is of such a compact design that utilizing it for SEI vehicle support would impose major changes. Other schemes were eliminated based on the ability of the proposed elements to do the task. Some were upgraded with additional vehicle definition. Some were eliminated by launch requirements, complexity or operational demands. This resulted in three candidate concept systems: I Beam, Vehicle as the Platform, and Gantry on Rail.

These three candidate system elements were modified into one platform system with independent auxiliary support hardware, figure 4-2. The platform node consists of an I-beam platform with the required support services, robotic arms capable of long reach and "strongback" supported element movement, two robotic walkers with additional manipulator arms having several interchangeable end effectors, a small element carrying capacity and a small connector inventory. The walker robots are able to traverse the length of the vehicle between the forward tanks and over the aft tank to attach, replace or repair any element. The I-beam platform attaches to the vehicle truss and carries the support services systems on the side away from the vehicle. Originally the platform-to-vehicle attach point was by a mobile, rotating "lazy susan" apparatus that swings forward (without the tanks emplaced) to reach the MTV-Lander area. It was later replaced by a rail puller and set of rails that spans the length of the NTP truss. This was done to accommodate changes in the updated versions of the NTP. The rail

<u>Concepts</u>	<u>Accept</u>	<u>TBD</u>	<u>Reject</u>	<u>Reject</u>
Free-flying concepts: Dedicated platform			X	Requires too many launches, too high a level of support, and will be too time consuming to construct on orbit
I-Beam plain modified "lazy susan"	X			This class of platforms appears to fulfill the buildup requirements
Smart HLLV	Will not be used alone, but will be evaluated for use with other platforms			
Vehicle as the platform	X			Requires a better definition of the vehicle configuration
Assembly flyer	Will not be used alone, but will be evaluated for use with other platforms			
Tethered robotic assembly			X	Length of central beam prohibitively long for the robots to clear the tanks
Gantry on rail	X			This class of platforms appears to fulfill the buildup requirements
Common hab and assembly/servicer			X	Functions can be carried out by the CTV
Assembly ball platform			X	Possible interference with major components
H-O assembly platform			X	Same as the dedicated platform
Hinged truss			X	This configuration has too many complications for use with this type of vehicle
Attached to SSF: SSF-FEL assembly			X	(1) Current design of SSF may not allow extended truss structures or tethered platforms to be attached to the basic structure
Attached to SSF: SSF-FEL assembly				(2) the impact to SSF schedules, buildup and function are estimated to be unacceptable

Figure 4-1. 2nd NTP Platform Assessment

Accept: Will be given first consideration in the analysis
TBD: Requires more information to evaluate
Reject: Eliminated from consideration

system is easily adapted to other truss systems. Its movement is dependent only on its own set of translational gear (anywhere the rails can be placed the system can be used). One of the platform impacts of this change was the moving of the mobile remote manipulator systems from the exterior side of the platform to the top of each end piece. This allows the arms to work more to the center of the U enclosures and relegates storage to the external surfaces. No problems were observed on clearances and reach capabilities with this configuration.

The platform would be launched in two HLLV flights (one basic deployment and one for on-platform support systems and auxiliary hardware) and be flown gravity gradient stabilized with the arrival of the first vehicle element. The remote manipulators could

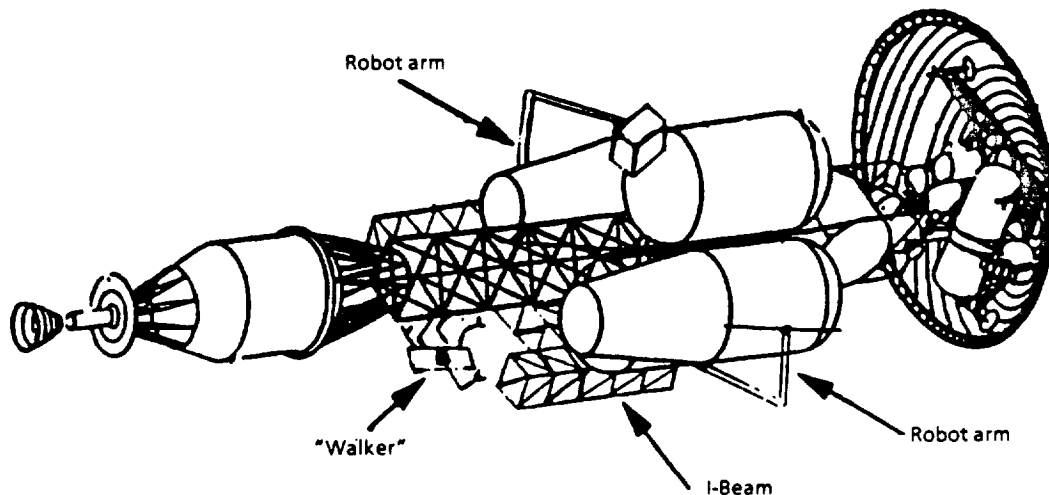


Figure 4-2. I-Beam on typical NTP Configuration

fly with the first element launch, which uses a "smart" HLLV and be transferred to the platform or arrive with the support launch.

For the I-beam NTP platform, a 5-meter square truss section was chosen with deployable end pieces. When fully extended the central section (without solar arrays) is 35 m by 30 m and will have an access section of 20 m wide by 15 m in depth to reach around the habitat and access the lander-habitat area with two 15 m robotic arms for initial connections. In the launched configuration, the central section contains services that are fixed before launch into the truss system with temporary solar arrays folded, and launched extended with the deployable sections folded, figures 4-3 and 4-4. This

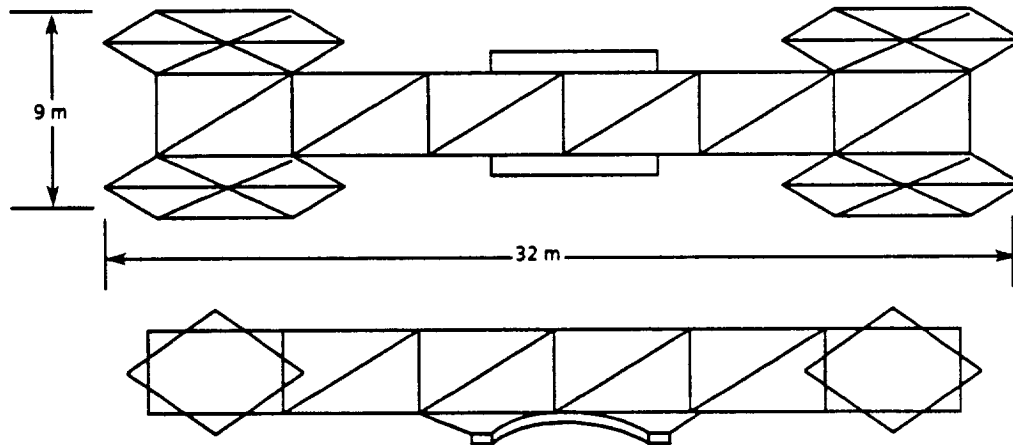


Figure 4-3. Basic Truss Stowed Configuration

permits the main platform to be launched in the the smallest candidate launch vehicle shroud with a 4-m extended nosecone. The rail system serves several purposes: (1) adapts the 5-m truss of the platform to the 7-m or other truss of the NTP vehicle, (2) allows the platform to use the 15-m robotic arms to grapple the aft tank and allow the main NTP truss to be built up to and including the NTP truss manifold box while the rails are attached to truss structure for translation, figure 4-5, and (3) traverses the platform truss after it is attached to the NTP truss, allowing the access section to emplace the habitat and lander sections on the forward portion of the vehicle.

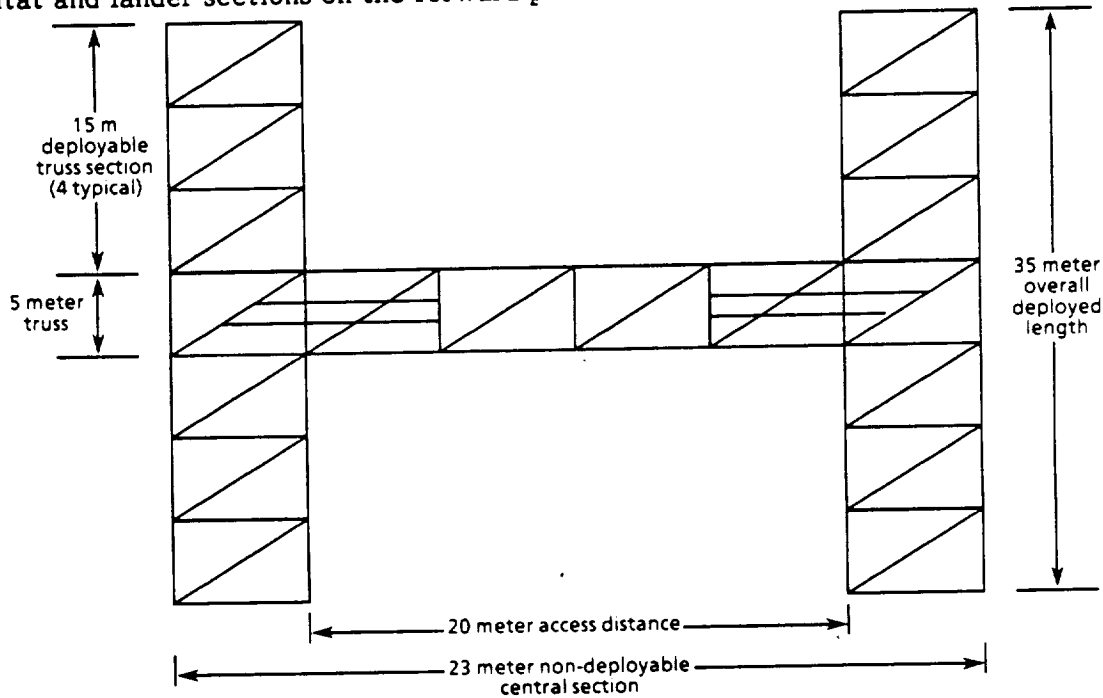


Figure 4-4. Basic NTP Platform Structure

The services provided in the deployed sections are launched in a second flight and assembled by a CTV (manned) operations. The services provided by the platform are listed in figure 4-6. A block diagram of the position of the services on the NTP platform is shown in figure 4-7. All the electronics systems that demand cooling are located on the central truss where deployed cooling radiators can be attached to the solar array strut. A corridor for the robot walker is left between the communications area and the avionics systems. The area above the rail puller has a standoff, rotatable berthing post with a docking collar. Two 12-m fixed robotic arms remove the payload from the delivery shroud, hand it off to the mobile arms and push off the expendable shroud. They may also be used in the manipulation of element portions in addition to the strong arms. The interior of the inboard trusses on the central sections is allocated for the RCS

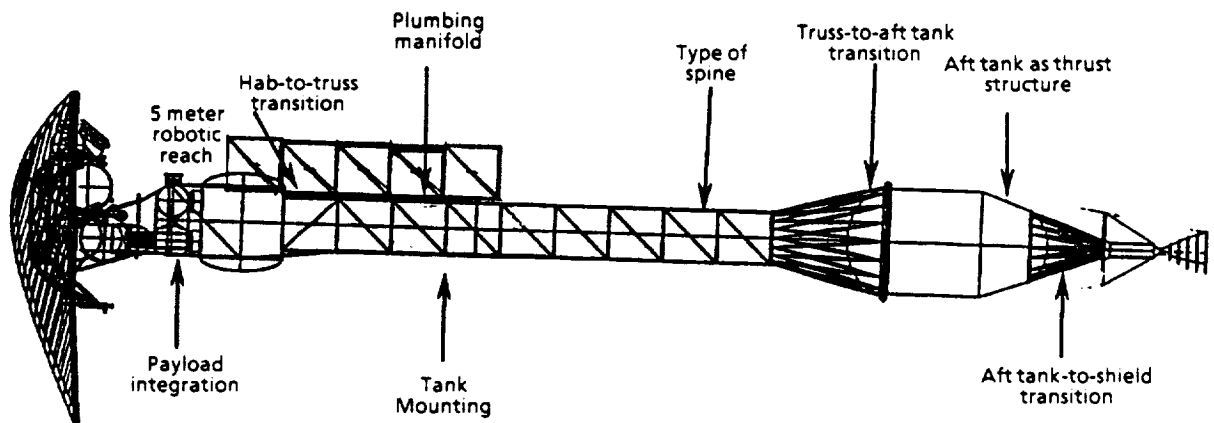


Figure 4-5. Platform Translated Forward

Services the platform must provide:

- Assembly support structure (on-orbit strongback, guide fixture, alignment, sensor reference net, etc.)
- Power for itself, operations and vehicle (as required) plus a distribution system
- GN&C
- Communications link (platform-SSF-ground)
- Visual systems data (consistent lighting, camera and visual data)
- RCS control
- Parts storage space for vehicle temporary hardware, assembly parts, test and special assembly equipment
- Thermal control loop
- EVA housing (at least temporary)
- Robotics control and support
- EVA tether, tie and reference points
- Berthing spaces/attachments for major vehicle assembly sections, CTV and ETO
- Debris shielding not provided by the vehicle

Figure 4-6. General Platform Service System

propellant. The propellant tanks are sent up with the platform in the first launch and are replenished by a manned operation. They may be either fillable or removed and replaced as the platform use demands. The outer side of the deployable members have the mobile heavy duty robotic arms that travel the 15-m length of the deployed section maneuver the large elements into place and hold them there until they are assembled into the vehicle. These also come up on the second platform support launch. A CTV manned operation is needed to connect the truss interior cables and take up reel for the MRMS systems. All the parts for the platform are listed in figure 4-8. The third launch is the first vehicle element launch, the aft tank with fuel, that begins vehicle assembly.

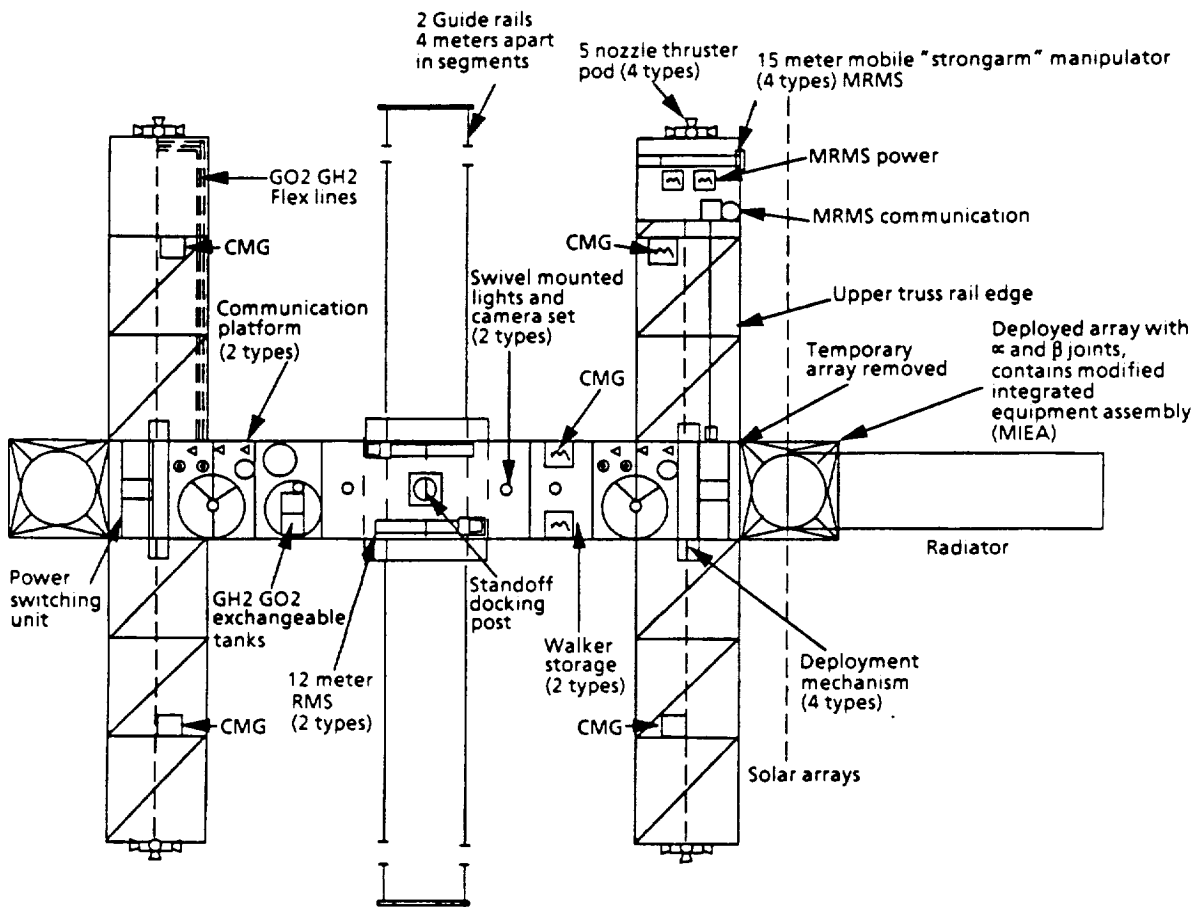


Figure 4-7. Assembly Platform -A, Top View

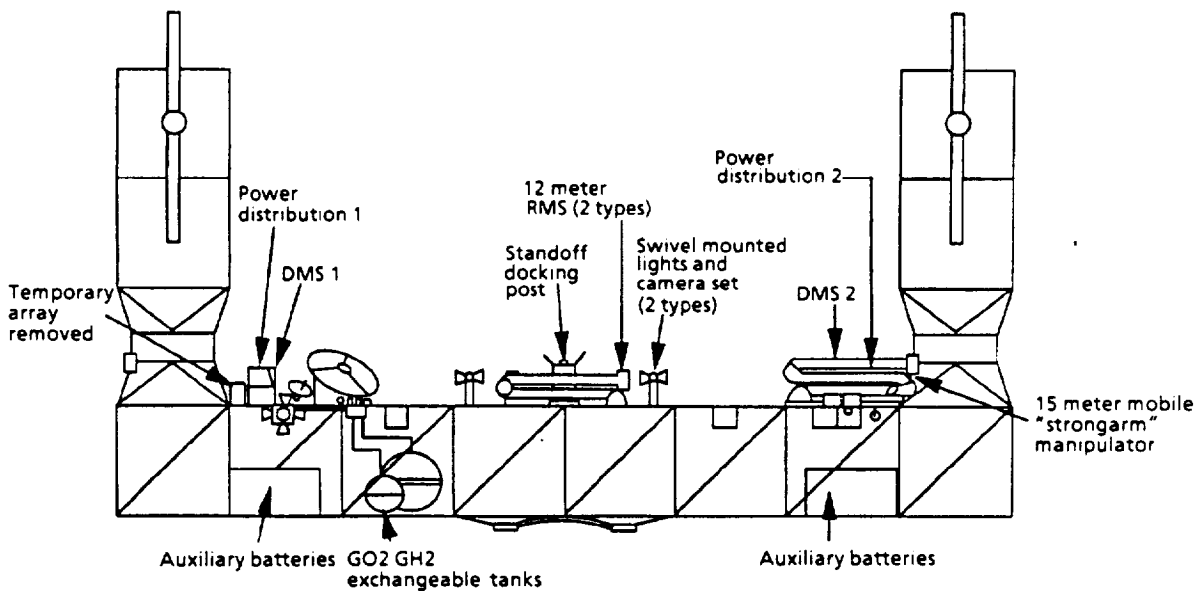


Figure 4-7. Assembly Platform -B, Side View

Item	Item Description	Quantity	Mass	Source	Manufacturers
Solar array system	Photovoltaic arrays with radiators, modified integrated equipment assembly (MIEA), alpha joint, one beta joint, one set of PV arrays (SSF configuration from alpha joint to station 3), 5m cubic truss	2	23 mt estimated	Old Space Station design	Prime: Rockwell Alternate: TBD
Truss structure	5m by 5m by 5m truss cube pattern of 10 cm diameter composite members with conductive wire embedded in the surface for charging control. Entire structure is seven bay end pieces on a 4 bay cross piece	1 set	17 mt estimated	Old Space Station design	Prime: McDonnell-Douglas Alternate: TBD
Thruster pod	5 thruster grouping of 25 pound thrust GO_2/H_2 thrusters, initially built for the Space Station, manifolded together	4	16 kg	Old Space Station design	Prime: Rockwell International Alternate:
Propellant	Combination of fixed and flex lines of TBD length, that will deploy with the end pieces (flex) and be hardlined to the propellant tanks and thruster pod manifold 1 H_2 line and 1 O_2 line	4 sets	TBD	Current terrestrial design	Prime: Alternate:

Figure 4-8. Assembly Platform Parts List-A

Item	Item Description	Quantity	Mass	Source	Manufacturers
GO_2 tank	Insulated tank, 2 meter diameter that can be removed and replaced	2	TBD		
GH_2 tank	Insulated tank, 2.7 meter diameter that can be removed and replaced	2	TBD		
Propellant manifold	Manifold that allows one tank set to feed two thruster pods	2	TBD		
Control Moment Gyros (CMG)	Station keeping and position sensing	8	50 kg	Current available	Prime: Ithaco Alternate: TBD
Antennae:					
High Gain	- Ground, SSF, and CTV communications 2.7 m diameter	2	TBD	- Similar Pioneer upgraded electronics	
Omnidirectional	- Backup communications, 1 meter	4	TBD	- TDRS/communications, sats.	
Robot/data	- Visual, digital 1 meter dia.	2	TBD	- Com. sats.	
RF	- Proximity operations, robot control 46cm by 23 cm cone	6	TBD	- Com. sats., exploration vehicles	

Figure 4-8. Assembly Platform Parts List-B

Item	Item Description	Quantity	Mass	Source	Manufacturers
(MRMS) Mobile Remote Manipulator	15 meter "strongarm" used for maneuvering into place large assembly elements. It is on a mobile base that translates the length of the end piece but does not translate the central crosspiece. The base is on a rail system that will be part of the deployed truss.	4	TBD	From Space Station designs	
(FRMS) Fixed Remote Manipulator System	12 meter arms fixed to the central crosspiece that will be used to guide in the HLLV cargo to the docking port, help remove the cargo and hand it off to the MRMS for assembly or storage	2	TBD	From Space Station/Space Shuttle designs	
Robot Walker	A TBD sized, self contained system with dexterous manipulators that can "inchworm" itself along the platform vehicle and HLLV to assist in actual assembly, component removal/storage and fine manipulation work	2 to 4	TBD	Various current walker designs (MacDonnell-Douglas, Carnegie-Mellon, etc.)	

Figure 4-8. Assembly Platform Parts List-C

Item	Item Description	Quantity	Mass	Source	Manufacturers
Power distribution net	Power distribution system that will handle the power demands from the temporary arrays for initial deployment, and any other functions not covered by the MIEAs in the permanent array package	2	TBD	Standard requirement	
Data management system (DMS)	Handles communication linkage, robot control, data linkage, sensor system identifications	2	TBD	Standard requirement	
Power switching unit (PSU)	Handles power switching during occultation that is not handled by the MIEAs in the permanent array package, and all switching with the temporary arrays	2	TBD	Standard requirement	
Berthing port	Standard berthing port on a 2 meter standoff for docking the HLLV to the platform	1	TBD		
Lighting/camera post	Swivel mounted camera and lighting assembly on a 1 meter post for wide angle observations	2	TBD		
Temporary arrays	Small deployable/retractable arrays that will power the initial platform deployment. Each array has 2 panels 2 meters by 25 meters	2	TBD		

Figure 4-8. Assembly Platform Parts List-D

Item	Item Description	Quantity	Mass	Source	Manufacturers
(IDM) initial deployment mechanism	Jackscrew/telescoping mechanism that pushes out the folded end pieces to deploy them on the initial flight	4	TBD	Extendible exit cones, SSF deployment strategies	
Rail crawler	Supporting undercarriage that will extend a pulling mechanism that will work in both directions along the rails (forward and back)	1	TBD	SSF RMS translation strategies	
Rails	44.5 meter segmented rails that will be fitted along the truss of the vehicle (makes the platform independent of truss configuration), which will allow the platform to translate the vehicle for assembly. The rails are segmented to allow the removal of several sections to clear the tank installation area.	2 (one set)	TBD		
Outside panels	Lightweight paneling (A1/composite?) that will be set up with attachment points for part storage	14 (5m by 5m)	TBD		

Figure 4-8. Assembly Platform Parts List-E

Modeling of the platform is shown in figures 4-9 and 4-10. Elements and major parts have been taken from known sources either from past Space Station design, or from other previously flown satellite hardware. Using "off-the-shelf" and tested technology items will leave new development to those items that are truly new and different, reducing risk to design and development.

The level of detail on the walker has been refined, figure 4-11. This design was taken from the Flight Telerobotic Servicer (FTS) and modified to "inchworm crawl" over both the platform structure and the vehicle. It makes the fine connections (small electrical cabling, small to medium structural connections and fluid lines, etc.) and is capable of repair and inspection activities where the large arms cannot conveniently reach.

The concept design for the NTP assembly has been scanned for obvious interference problems and incompatibilities. No problems were observed in the current design. The steps of the sequence are as follows:

- a. The platform is launched on an HLLV. After shroud release the end pieces deploy, then the temporary solar arrays and radiators are deployed. The communication system deploys and contacts both the ground and Space Station Freedom for co-orbit instructions.

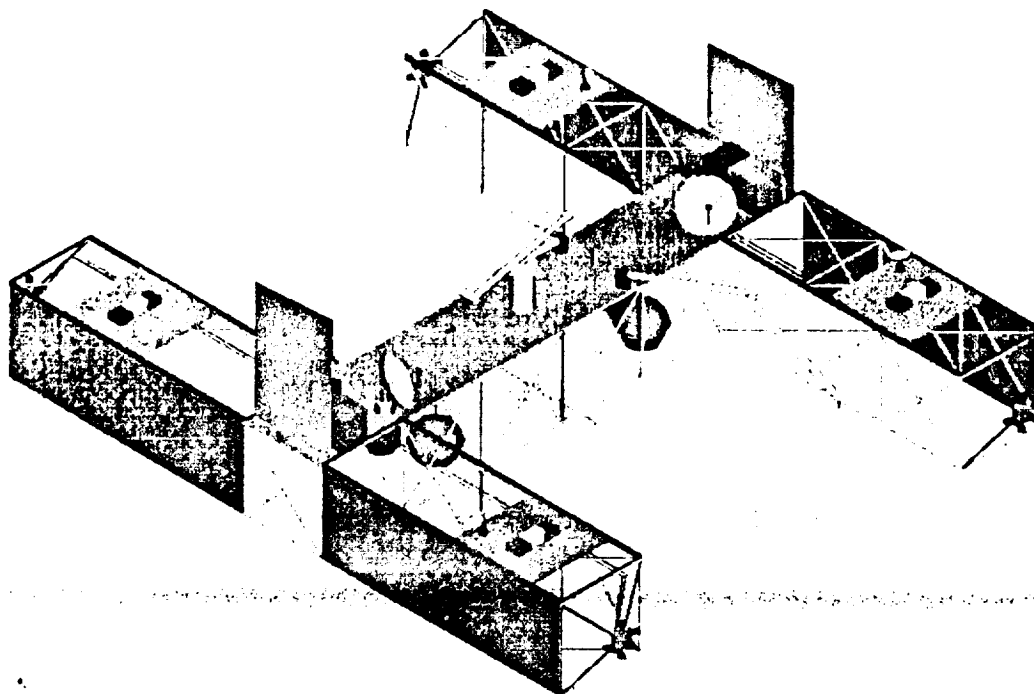


Figure 4-9. NTP Platform Initial Deployment

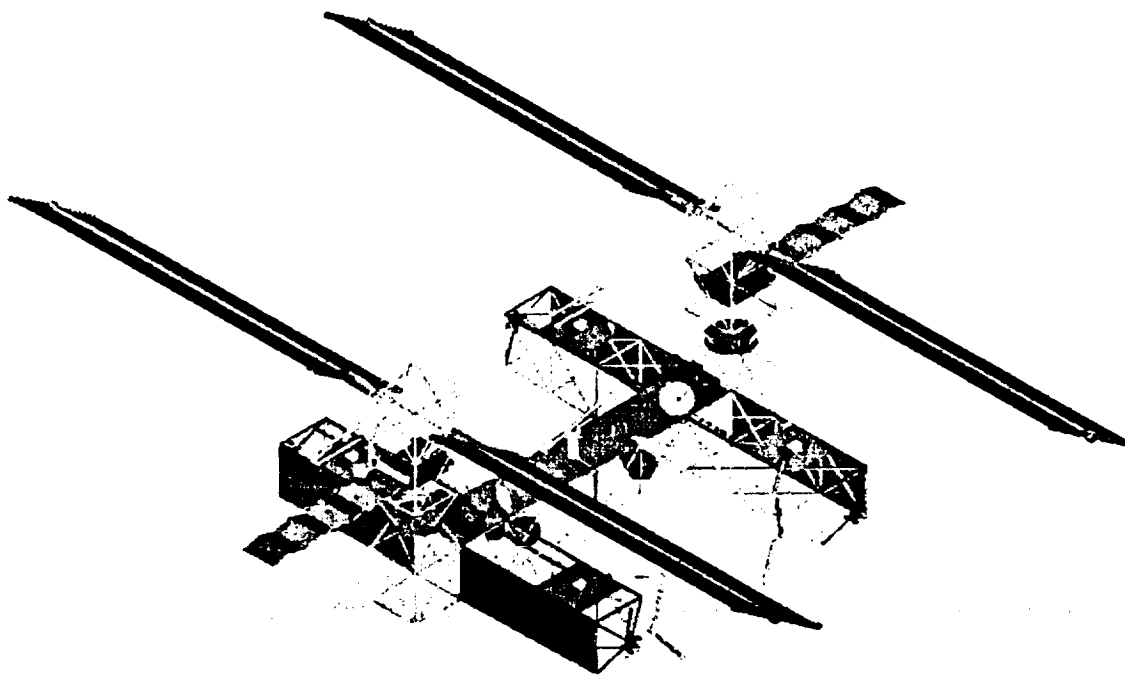


Figure 4-10. NTP Platform Full-Up Configuration

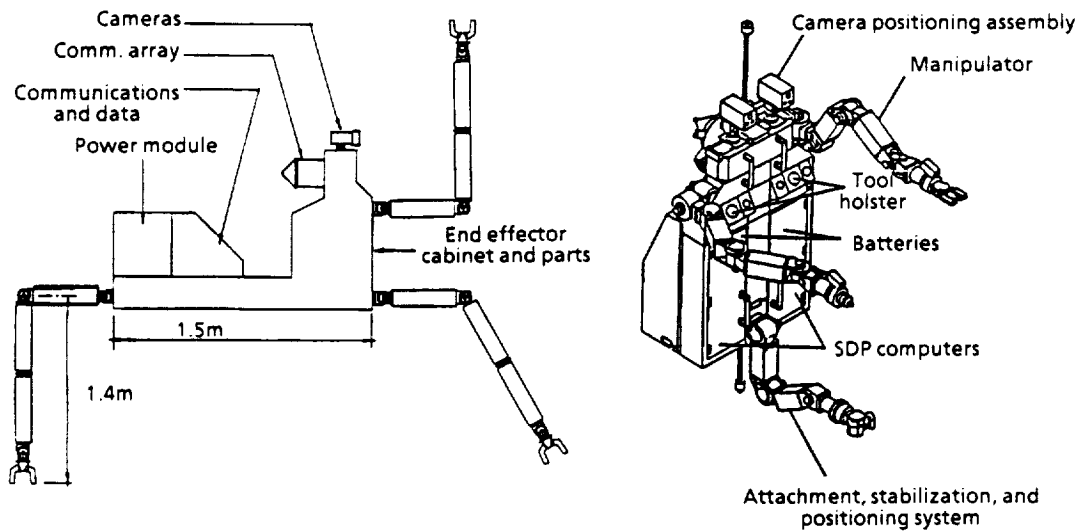


Figure 4-11. Preliminary On Orbit Assembly "Walker"

- b. The platform support systems are launched on an HLLV in conjunction with a manned CTV flight. The items transported are: (1) two to four walker robots which are transferred to the platform, (2) four 15-m "strongback" arms and the mobile platforms for installation on each end piece, (3) the two large permanent solar arrays with radiators, modified IEA and truss segments, (4) rail system to be placed in storage and miscellaneous parts for installation. The manned CTV flight will install the mobile platforms and strong arms with any threading of parts in the truss as necessary and emplace the permanent solar arrays. The CTV crew will stand by for deployment of the arrays and operational checkout of the major systems.
- c. The first element launch is the loaded aft tank, radiation shield engines and nozzles delivered by HLLV launch. The shroud is released and an unmanned CTV assists in delivering the cargo to the reach of the strongarms which grapple the aft tank and bring it toward the platform.
- d. The main truss elements are launched in an HLLV with the MTV habitat. This may require a manned CTV flight to build the truss or not, as may be most efficient. At this point, the truss is built from the back forward while the habitat is held off by the front pair of strongarms. The aft tank is held by the back strongarms. The rails are attached to the truss and the platform engages the rails, releasing the aft tank, then travels forward bringing the habitat into place for connection by the walker and then the forward arms release. The habitat and MEV must be processed in line (done at the same time) and the MEV delayed to the next flight or an identical

- habitat module on the ground with a frozen configuration used to process the MEV in order to maintain checkout and configuration integrity.
- e. The central truss and the MEV are launched by an HLLV. It is supported by an unmanned CTV flight at the beginning of the operations. The central truss is assembled by the walker and transported to the platform by an unmanned CTV. The two forward arms grapple the MEV below the platform and bring it into position for structural attachments. It is then released by the forward strongarms. All connections, pass-throughs and tunnels from the lander to the habitat are done by the walker.
 - f. There are four main tank launches using HLLVs for the configuration shown in figure 4-2. Beginning with the bottom tank, the platform is in the forward position, and the forward arms reach below the assembly and bring the tank into position for connection. The two side tanks are brought into position after the platform is moved aft on the rails to clear the area where they will be placed (using one forward arm for positioning). For the final tank emplacement, the platform is drawn fully aft and the rail system (which was installed in segments) removed to clear the area where the tank will be installed. The platform position for tank installation clearance is checked and the tank grappled above the assembly and maneuvered into place. The walker does the final connections on each tank as they are emplaced.

The vehicle is then checked out and refurbished, if necessary, with the platform attached. Prior to release, all additional materials that do not make the Mars transit, such as vehicle debris shielding, are removed and stored at the platform on the perimeter. After the final checkout and inventory have been performed, the vehicle is released and the platform and vehicle move apart. The sequence of buildup is shown in figure 4-12.

As a result of the redesign of the NTP into the "dixie cup" truss design and a change in launch sequence, a smaller platform that can be launched with the lighter habitat and Mars Return Crew Capsule (MRCC) was conceived that could give minimal, but critical services to the Mars vehicle assembly. The platform is a semicradle system completely assembled on the ground and is launched with all systems hardlined. It deploys a set of rails that allows the platform to traverse the vehicle. The top is recessed fore and aft to clear the MRCC on launch and the forward and aft tanks during construction. It principally supplies a Reaction Control System (RCS), platform-vehicle-Space Station, ground communications, mobile walker robots and robot control and data interchange, figure 4-13. Minimal power is provided to the platform (RCS, data management, position

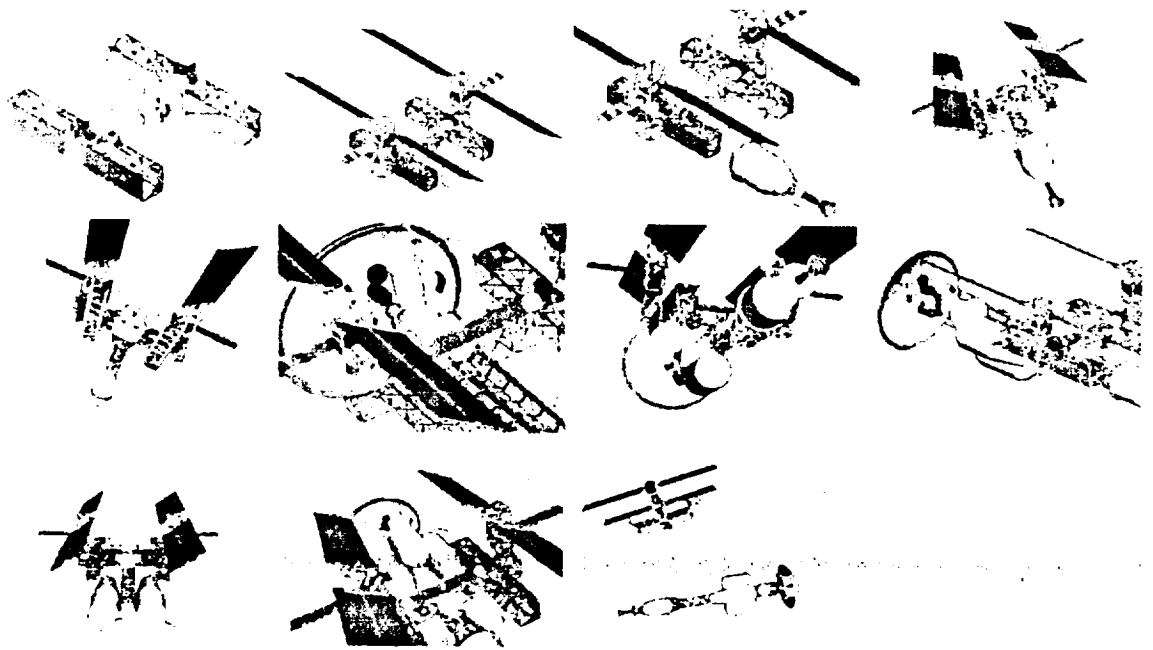


Figure 4-12. NTP Assembly Sequence with Assembly Platform Deployment

identification, robotic battery storage, lights and video cameras) by the platform solar arrays. Any additional power will be provided by the vehicle through the vehicle - platform communications network. This is possible with the first launch being the habitat, MRCC and forward structure and the first two "dixie cup" truss sections. Changes to the vehicle design are the addition of several support and data passthrough rings in the vehicle truss. These will not interfere with the launch stowage configuration of the "dixie cup" truss sections. The launch sequence is as follows:

- a. The first element launch includes the forward structure, the MRCC, the MTV habitat; attached to the MTV habitat is the "saddle" platform, the first "dixie cup" truss section and the second "dixie cup" truss section stored reversed over the first section, figure 4-14. After the payload is deployed, the manipulators on the platform pull off the second truss section, reverse it and connect it to the first section. The rails are then extended to move the platform aft to await the next element launch. At this point the habitat can be manned as noted above; a flight qualified "dummy habitat" must be available on the ground to test and checkout operations.
- b. The second launch consists of the aft tank and third truss section stowed in the reverse position. Support of the CTV is needed to maneuver the payload element

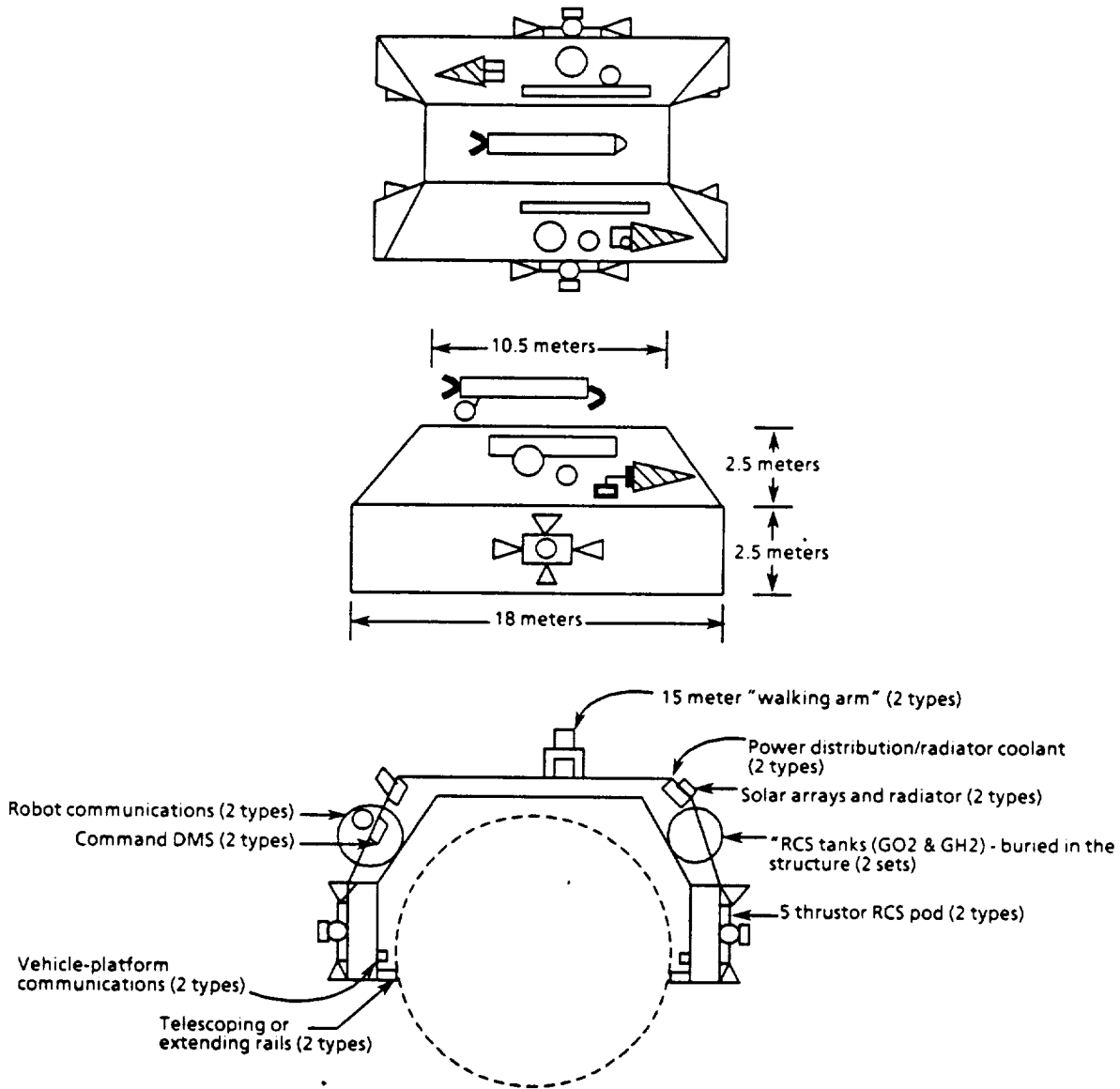


Figure 4-13. NTP "Saddle" Assembly Platform

within the reach of the platform manipulators. The platform manipulators remove the truss section and connect it to the other sections, then move aft. With the aft tank brought into manipulator reach, the aft tank is engaged, maneuvered into position and connected to the rest of the structure.

- c. The HMEV is brought up next and maneuvered into position (CTV) below the truss. The platform is moved forward and the manipulators engage it from the top to maneuver it into position for connection.

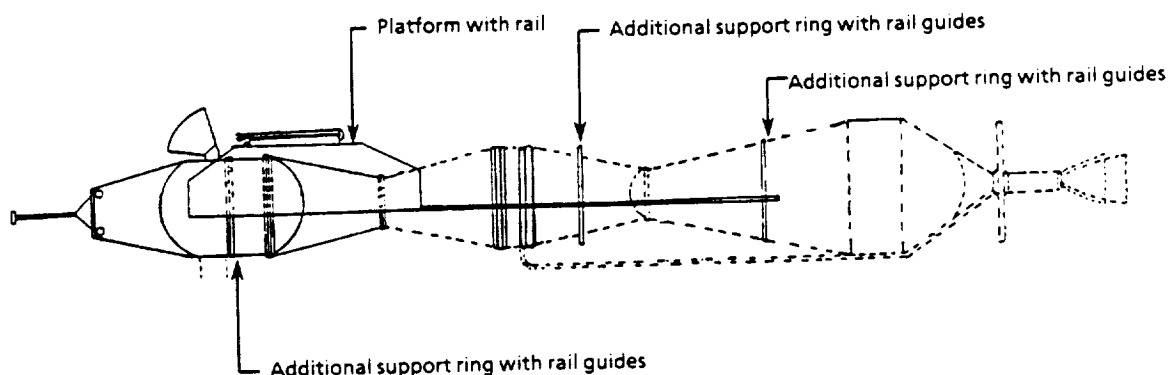


Figure 4-14. "Saddle" Platform on the New NTP Central Truss

- d. The following flights are the three tank flights. The platform is moved aft and the rails over the forward section retracted to clear the tank area. The tanks are engaged by the manipulators and emplaced for connection.
- e. The final flight, which will be of a yet to be determined vehicle, will refurbish the MTV habitat and complete the final checkouts and tests. After this, the vehicle and platform separate, with the platform maneuvered to the vicinity of the Space Station for refurbishment and modification as required.

4.2 MADISON RESEARCH DATABASE

A preliminary database catalog that contains the top-level elements and element descriptions for the platform has been developed as a subcontracted study, reference 20. The database contains design information on the platform systems and investigates the availability of existing or similar systems. The database catalog is a 4th Dimension version 2.1:1 formatted program for use with a Macintosh II computer.

The data stored in the catalog include the component name (item), the detailed description of the item (item description), the number of that item used in the platform design (quantity), the mass of the individual item, the source of the design (source), possible manufacturer (both a prime and an alternate), a graphic illustration of the item that can be built on the computer or scanned into the system (item picture), and a dictionary that defines the terms used in the item description (terms of reference). The database has a customized menu and may be searched on any one of the subjects in the catalog with reports made in several formats. Information records may be added, deleted or modified by those with access clearance as the design of the platform or the

equipment characteristics change. Examples of these reports are shown in figures 4-15 through 4-17.

Item	Item Description	Quantity	Mass	Source	Manufacturers
Propellant lines	Combination of fixed and flex lines of TBD length, that will deploy with the end pieces (flex) and be hardlined to the propellant tanks and thruster pod manifold 1 H2 line and 1 O2 line	4 sets	TBD	Current terrestrial design	<u>Prime</u> <u>Alternate</u>
Thruster pod	5 thruster grouping of 25 pound thrust GO/H2 thrusters, initially built for the Space Station, manifolded together	4	16 kg	Old Space Station	<u>Prime</u> Rockwell International <u>Alternate</u>
Solar array system	Photovoltaic arrays with radiators, modified integrated equipment assembly (MIEA), alpha joint, one beta joint, one set of PV arrays (SSF configuration from alpha joint to station 3), 5m cubic truss	2	23 mt estimated	Old Space Station design	<u>Prime</u> Rockwell International <u>Alternate</u> TBD
Truss structure	5m by 5m by 5m truss cube pattern of 10 cm dia. composite members with conductive wire embedded in the surface for charging control. Entire structure is seven bay end pieces on a 4 bay cross piece	1 set	17 mt estimated	Old Space Station design	<u>Prime</u> MacDonnell-Douglas <u>Alternate</u> TBD

Figure 4-15. Data Needs Catalog, Report Format 1

Information on sizes and masses of applicable off-the-shelf items that are space qualified can be obtained. Applicable items that are not space qualified can provide a real number for point-of-departure estimates of size and mass for a space qualified analog.

Item	Item Description	Quantity	Mass	Source	Manufacturers Prime	Manufacturers Alternate
Propellant lines	Combination of fixed and flex lines of TBD length, that will deploy with the end pieces (flex) and be hardlined to the propellant tanks and thruster pod manifold 1 H2 line and 1 O2 line	4 sets	TBD	Current Terrestrial Design		
Item Picture			Terms of Reference (Dictionary)			

Figure 4-16. Data Needs Catalog, Report Format 2

Item	Item Description	Quantity	Mass	Source	Manufacturers Prime	Manufacturers Alternate
Propellant lines	Combination of fixed and flex lines of TBD length, that will deploy with the end pieces (flex) and be hardlined to the propellant tanks and thruster pod manifold 1 H2 line and 1 O2 line	4 sets	TBD	Current Terrestrial Design		
Item Picture						
Terms of Reference (Dictionary)						

Figure 4-17. Data Needs Catalog, Report Format 2

5.0 TRANSPORTATION CREW MODULES AND HABITAT

5.1 INTRODUCTION

The crew module and habitat update has focused primarily on three vehicle types; transfer habitats, crew return modules, and excursion crew modules. The specific vehicles studied include the Mars transfer habitat for six crew, with configuration options for induced gravity and microgravity transfer vehicles, a lunar excursion crew module for four crew, and lunar and Mars crew return vehicles.

5.2 MARS TRANSFER HABITAT

The induced gravity habitat configuration was analyzed in the earlier study (ref. 1). Further analysis has been conducted on the structural elements and some subsystems. The structure of the habitat was designed to resist launch loads primarily, but was also designed to resist internal equipment loads while attached to a transfer vehicle, spinning at four revolutions per minute, in order to provide simulated Earth normal gravity, figure 5-1. To reduce loads on the pressure vessel, the floor structure within the module was cantilevered from the central bulkhead. Two floor levels on either side of the bulkhead were connected with columns and shear panels in order to form a unified deep structure. The point loads imparted to the bulkhead, caused it to become much heavier than would normally be required for a uniform pressure load. An evaluation was done to see if the overall mass of the structural system could be reduced by eliminating the cantilever and attaching the floor joists to strong points located along the length of the pressure vessel wall. The analysis revealed a 7% savings in mass by eliminating the cantilevered floors.

At the beginning of the MTV habitat design process, induced gravity was deemed necessary for crew conditioning and health during the 1000 day overall mission duration time associated with a variety of different vehicle types. Subsequent to the release of the Stafford Commission report, a decision was made to reevaluate the Mars transfer habitat assumptions and look at an optional configuration based on the report's recommendations. The primary changes made to the design were a result of the Commission's recommendation that nuclear thermal propulsion be used for Mars transfer vehicles. For this propulsion system, the total transfer times are relatively short, approximately 400 days, and therefore induced gravity is not being considered as a requirement for early manned Mars exploration.

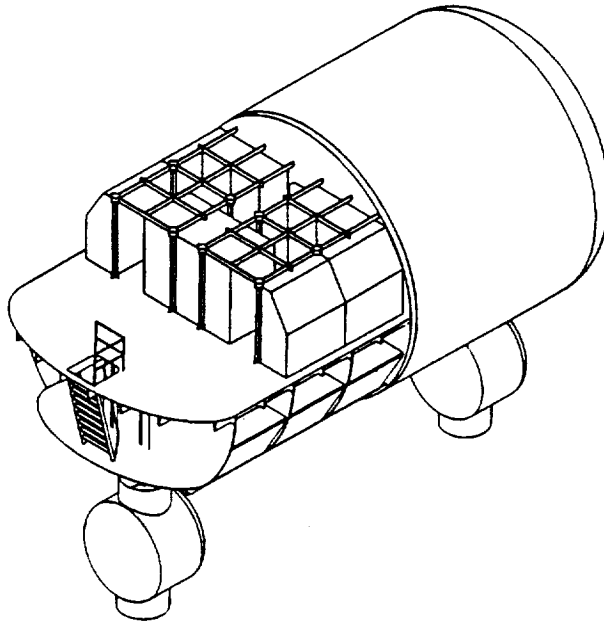


Figure 5-1. Induced Gravity Transfer Habitat, 6 Crew

A new approach was taken in configuring the transit habitat. The microgravity environment allows the internal structure to support equipment loads primarily during launch, without having to account for internal live loads on "floors". The structure is for equipment support only, and the equipment defines the internal arrangement of the habitat, much like Space Station Freedom, figure 5-2. Crew operations in microgravity also allowed the habitat to become smaller. Crew circulation in microgravity requires less volume and allows easier access to equipment, controls, and storage areas. The habitat module length was reduced from 16.2 meters to 9.2 meters overall, with volume reduction from 660 cubic meters to 360 cubic meters. Volume requirements were based on equipment sizes, minimal crew circulation needs, and personal space requirements for group or social activities.

Derived requirements (ref. 1) identified 20m^3 as a minimum circulation volume per crew for missions greater than 2 months in duration. However, this does not account for privacy needs, or for personal space required during group activities. The two group activity areas, recreation/exercise and wardroom/galley, located in the domed ends of the vehicle, were allotted an additional 3m^3 each per crewmember for these needs. Total minimum free volume aboard the transfer habitat is 153m^3 , and overall minimum volume including equipment requirements is 345m^3 . Due to equipment and outfitting geometry, the length of the vehicle was set at 9.2 m, resulting in an overall volume of 360m^3 .

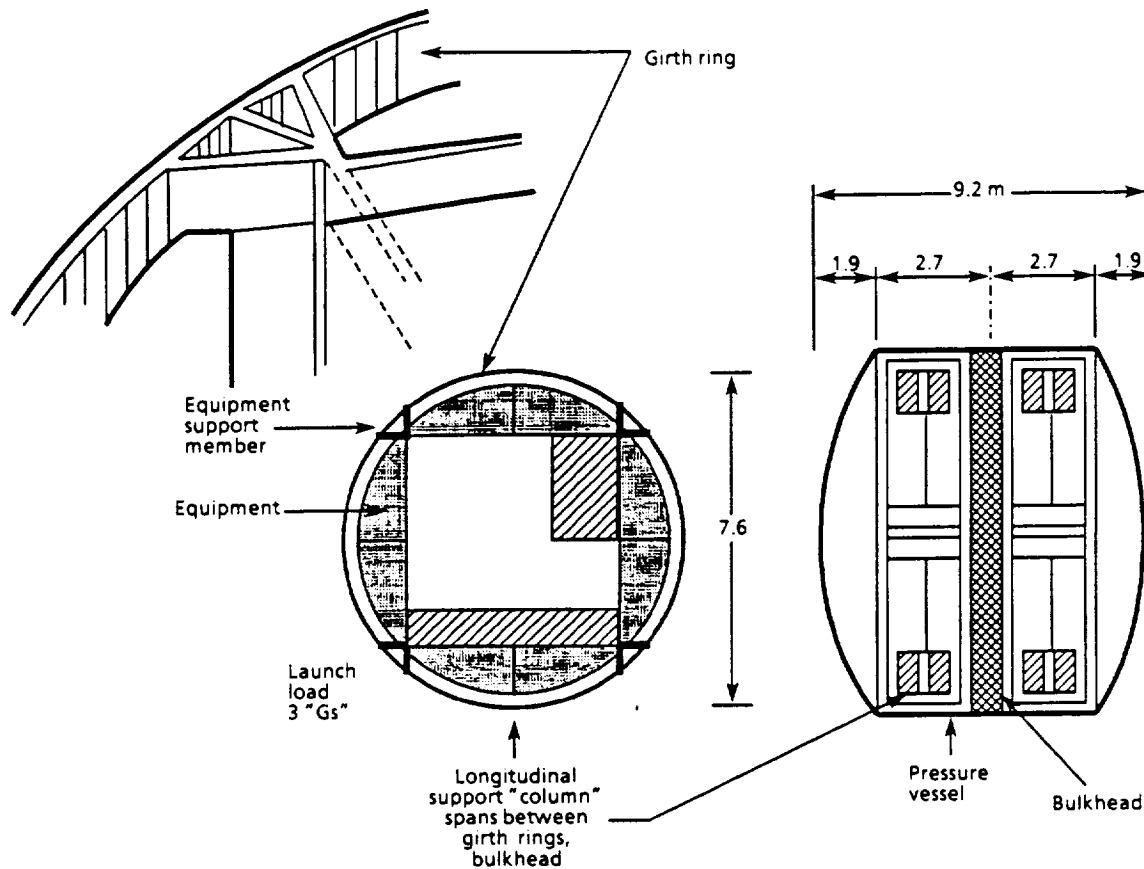


Figure 5-2. Microgravity Hab Structural Concept

Functional arrangement of the habitat is similar in some ways to that of the induced gravity option. Common crew areas for exercise and entertainment were left as open, domed spaces at each end of the module. Private and work areas make up the central, cylindrical portion, figure 5-3. A radiation protection strategy was developed that locates the crew quarters, a high use volume aboard the transit habitat, internal to the bulk structure, equipment and consumables. This scheme allows the vehicle itself to provide some radiation shielding, reducing the size and mass of any "storm" shelter that might be required, figure 5-4.

Other areas of the habitat that were updated include the thermal control system, data management and avionics. External systems that had not previously been included in mass estimates were included and preliminary designs based on updated space station equipment were done in order to refine mass estimates for these systems. DMS/Comm/Avionics system mass was reduced from 4680 kg to 3520 kg, and a 120 m² radiator was added to the thermal controls estimate. The entire habitat system is estimated to weigh approximately 58 tonnes, figure 5-5.

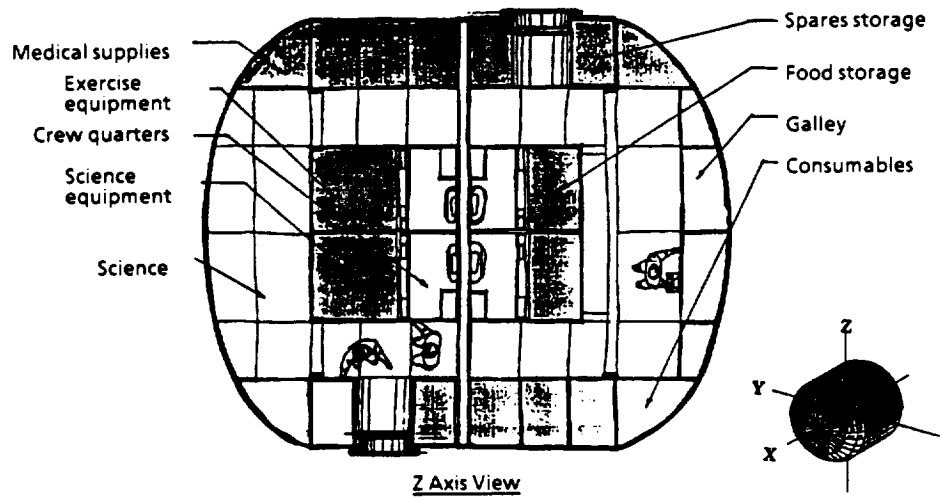
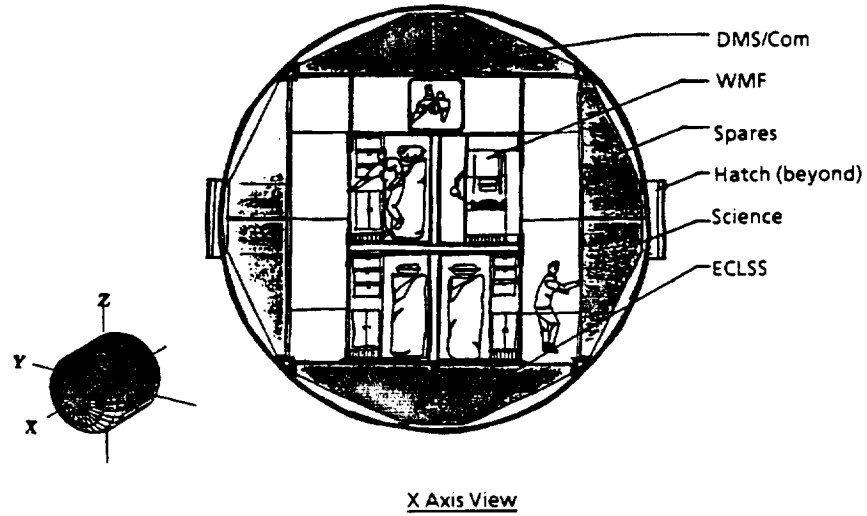


Figure 5-3. Microgravity Transit Hab

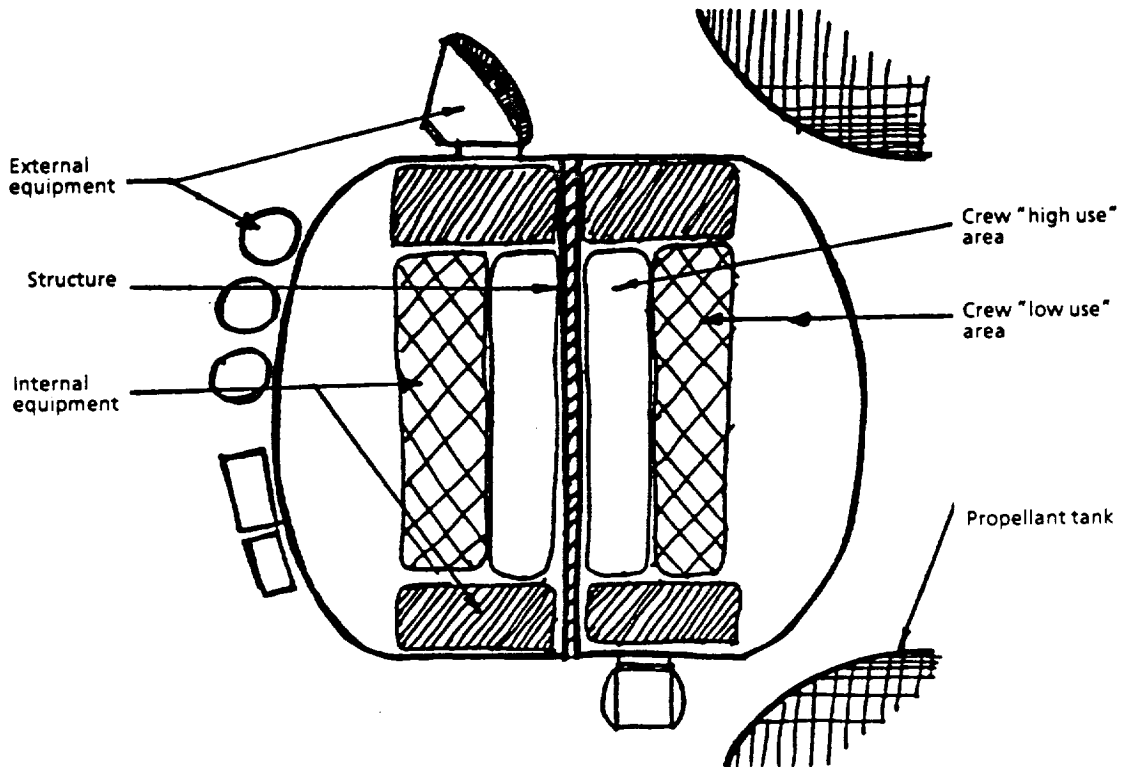


Figure 5-4. Shielding Strategy

	Volume	Mass	Notes
Structures		9535 kg	designed for launch loads, microgravity operations
Crew Systems	57.7 m ³	6956 kg	
Life Support	18.3 m ³	13,075 kg	closed loop ECLSS, EVA suits
DMS/Comm./Avionics	8.0 m ³	4044 kg	
Power Systems	21.5 m ³	2623 kg	20 m ³ is exterior equip.
* Cruise Science	6.2 m ³	1650 kg	
* Consumables	21.7 m ³	13,809 kg	Sized for 2014, opp., 552 day mission
* Crew		463 kg	
Total	133.4 m³	52,155 kg	

15% Growth	5435 kg	Spares included in system mass estimate
Total Estimated Mass	57,590 kg	*Not included in growth

Figure 5-5. Transit Hab Mass Analysis 6 Crew

5.3 CREW RETURN VEHICLES

Configurations for Mars and lunar crew return vehicles were studied, including bionics, winged reentry vehicles, and ballistic reentry vehicles, figure 5-6. It was assumed that the CRV did not need to have great cross range capability, a water landing was acceptable, and a reusable vehicle was not necessary. An evaluation of the mass for each of the different vehicle types related to the surface area and volume revealed that the ballistic shape would be lighter for the six crew vehicle. The ballistic shape's relative simplicity also allows easier manufacturing, and therefore a lower probable cost. Based on its simplicity, reliability and lower relative mass, the Apollo type ballistic capsule was selected. To accommodate a crew of six for direct entry at the end of the Mars mission and a crew of four for lunar missions, the vehicle's size is slightly larger than its predecessor, the Apollo command module. Vehicles for both mission types are virtually the same, with the exception of an added service module, which provides life support and power consumables for the longer lunar missions. The vehicles and their mass estimates are shown in figures 5-7 to 5-10.

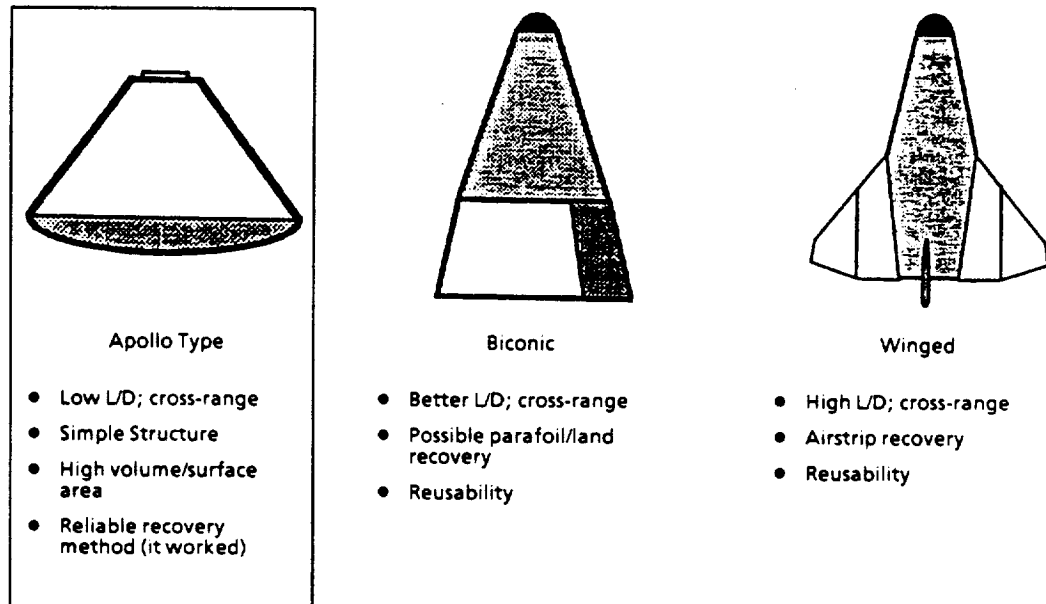


Figure 5-6. CRV Shape Options

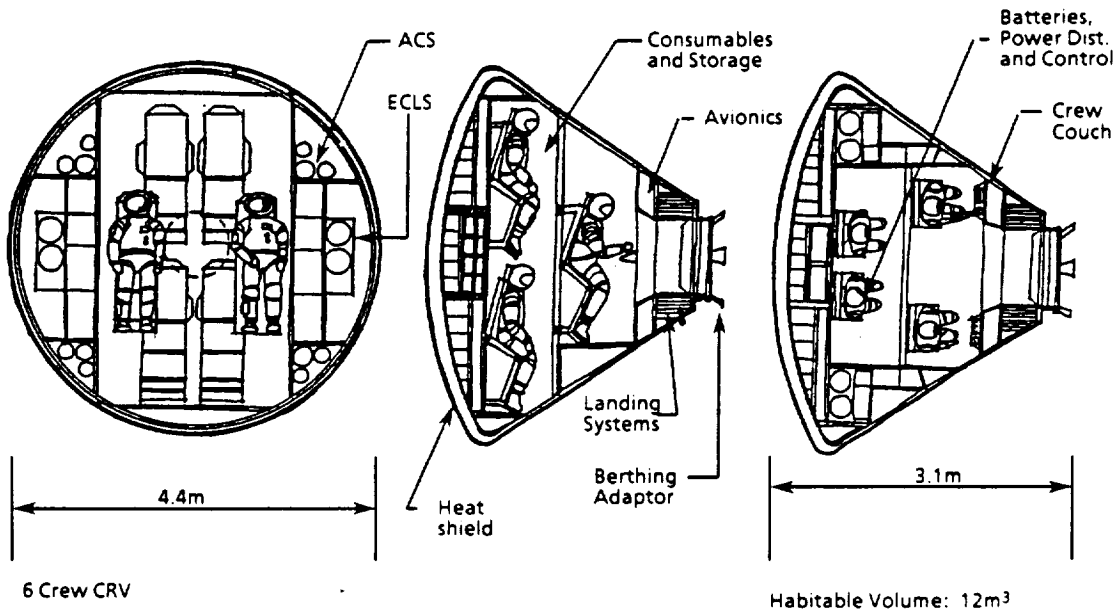


Figure 5-7. Mars CRV Configuration

System	Mass kg
Structure	● 1700
Ablator and insulation	* 800
Landing Systems	* 445
GN&C	● 503
Power, Dist. and Control	244
Stabilization and Control	* 370
ECLS, Thermal Control	* 470
Crew Systems	* 84
Flight Suits	180
15% Growth	692 kg
Vehicle Mass	5488 kg
Crew	463 kg
Entry Mass	5951 kg

* scaled from Apollo CM
 ● scaled from Boeing PLS

Figure 5-8. Mars CRV Mass Estimate

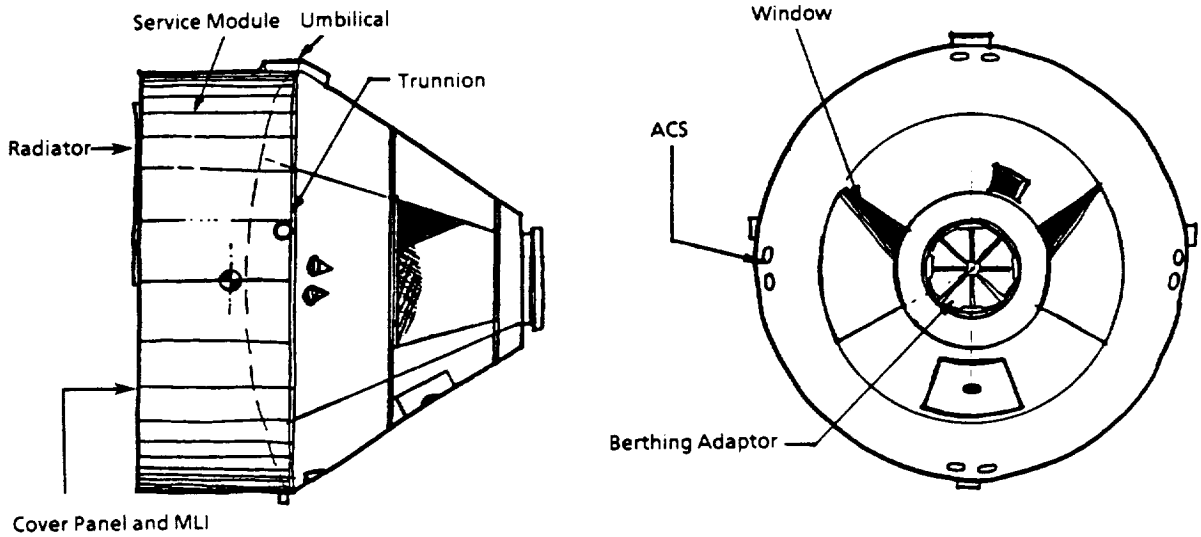


Figure 5-9. Lunar CRV Configuration

System	Mass kg
Structure	● 1550
Ablator and insulation	* 400
Landing Systems	* 428
GN&C	● 503
Power, dist. and control	200
Stabilization and control	* 250
ECLS, thermal control	* 450
Crew systems	* 60
4 crew and EVA suits	750
CRV Service Module	
Structure	1050
Fuel Cells	184
Reactants and Tanks (cryo)	1144
Life Support O ₂ /N ₂ (cryo)	374
Potable Water	141
15% Growth	752 kg
Total Mass	8236 kg

* scaled from Apollo CM
 ● scaled from Boeing PLS

Figure 5-10. Lunar CRV Mass Estimate

5.4 LUNAR EXCURSION MODULE

A preliminary sketch for a four crew lunar excursion crew cab was developed as part of a Lunar Transfer System (LTS) family of vehicles. The vehicle design is similar to that of the Apollo LEM, in that the crew flies in a standing position, operating the vehicle from dual control stations located adjacent to forward-down looking windows. Surface access is through a hatch at the front of the cab with a docking access hatch located in the module "roof", figure 5-11. Interior vehicle systems include life support, guidance, navigation and control, and crew systems. These weights are reflected in the mass estimate, figure 5-12. Life support consumables, reaction control and power subsystems are located on an attached ascent stage, not shown on the drawing above. Outfitted mass of the crew cab is estimated to be 2481 kg.

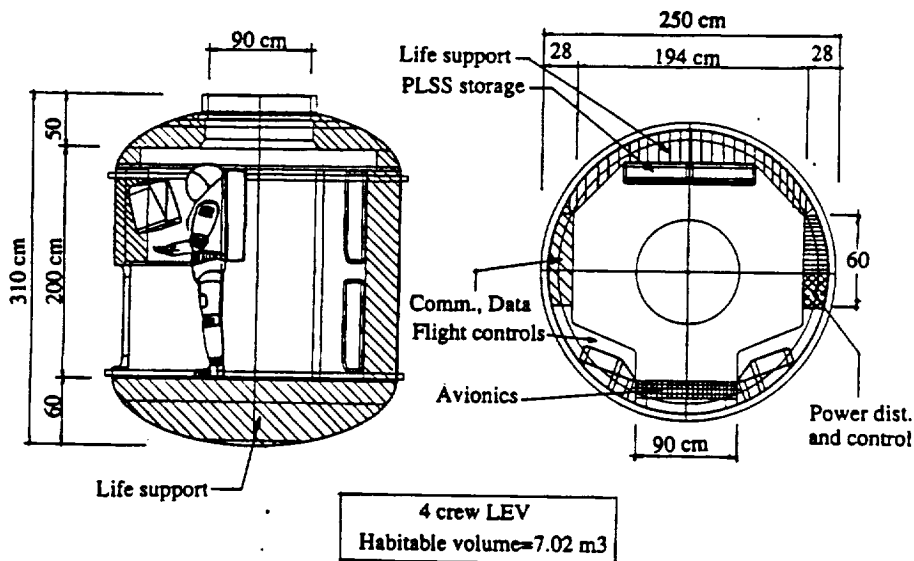


Figure 5-11. Lunar Excursion Crew Module

	Mass		Volume		Notes
	internal	external	internal	external	
Structures	90 kg	529 kg	0.03 m ³	0.19 m ³	
Protection	49 kg	129 kg	0.13 m ³	0.12 m ³	
Life Support	238 kg	34 kg	1.27 m ³	0.06 m ³	
DMS/Comm./Avionics	452 kg	221 kg	0.24 m ³	0.12 m ³	
Displays and controls	108 kg	0 kg	0.06 m ³	0.0 m ³	
Power Systems	131 kg	38 kg	0.04 m ³	0.01 m ³	
Crew Systems	55 kg	0 kg	0.03 m ³	0.0 m ³	
*Consumables	49 kg	47 kg	0.55 m ³	0.13 m ³	
Total	1172 kg	998 kg	2.31 m ³	0.63 m ³	
15% Growth		311 kg			
Total Estimated Mass	2481 kg		* Not included in growth		

Figure 5-12. Lunar Excursion Crew Module Mass Estimate

6.0 RADIATION ANALYSIS

6.1 INTRODUCTION

For early orbital flights, the spacecraft's inherent mass has provided sufficient protection from ionizing radiation, due in large part to the short mission durations and just good fortune. Future programs on the other hand, must address radiation shielding to insure crew safety. Astronaut exposure to the natural radiation environment of space is unavoidable. At best, vehicle designers will be able to reduce but not completely eliminate this exposure. Early development of innovative solutions effectively and efficiently limiting crew dose is critical. With the Boeing radiation exposure model (*Brem*), radiation assessment has been brought forward into preliminary design programs where major design changes will have the least effect on complexity, mass, and ultimately program cost.

6.2 MODELS AND METHODS

6.2.1 Background and Description of the Analysis

Evaluating the radiation environment within a spacecraft involves determining the incident radiation flux at the surface of the spacecraft and "transporting" the radiation through the vehicles structure to derive the attenuated internal radiation environment. To determine the exposure and resulting risk to the crew, the internal radiation environment is then transported through a simulated astronaut to determine the radiation field at specified critical organs. Accurate radiation assessment requires precise measurements and models of the natural space radiation environment and of the non-uniform distribution of shielding provided by the spacecraft's inherent mass and anatomy of the astronaut. In addition, attenuation of the incident radiation field by the shielding, and biophysical models used to convert the radiation field at critical organs to a measure of medical risk consequences resulting from the exposure must also be determined.

6.2.2 Natural Radiation Environment Models

Analysis was completed using two of the three dominant natural particle radiation sources; (1) Galactic Cosmic Radiation (GCR) and, (2) Solar Proton Event (SPE) emissions, figure 6-1.

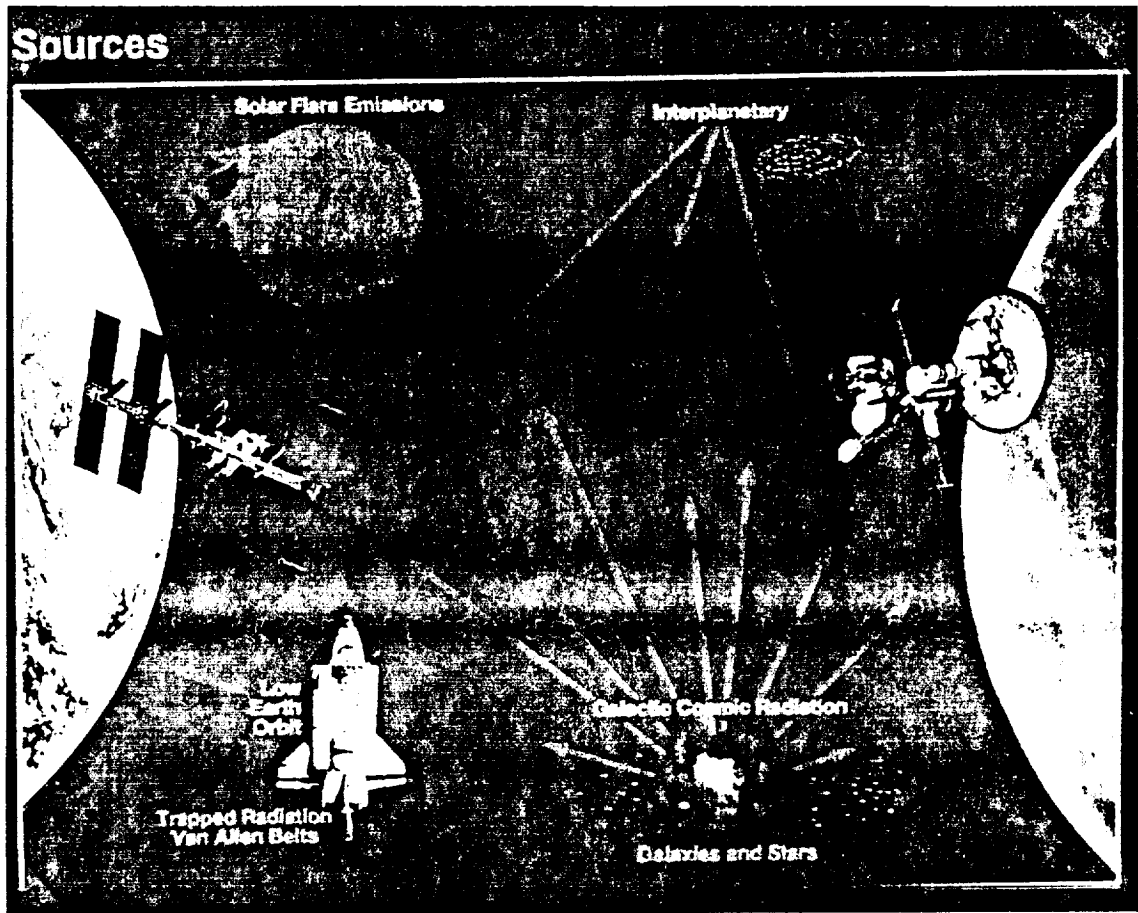


Figure 6-1. Radiation Sources

When astronauts leave the relative protection of the geomagnetic field, they are exposed to unpredictable solar proton events. The level of solar activity and modulation of radiation sources is tied directly to the strength of the sun's pervasive magnetic field. During the course of the roughly 11-year solar cycle, several tens of solar flares, as illustrated in figure 6-2, will produce sufficient energy to release elevated charged particle fluxes, primarily protons. Typical events are classified as "ordinary" and would have little effect on crew or spacecraft. Detailed radiation analysis should evaluate probable exposure from ordinary flares as part of the total mission exposure. Historically, an average of two to four flares per cycle release tremendous energy and particle fluxes and are classified as Anomously Large Solar Proton Events (ALSPE). The cumulative fluence resulting from proton events during the solar cycle are dominated by the few occurrences of ALSPE. Large solar proton events can deliver debilitating or lethal doses to unprotected astronauts.

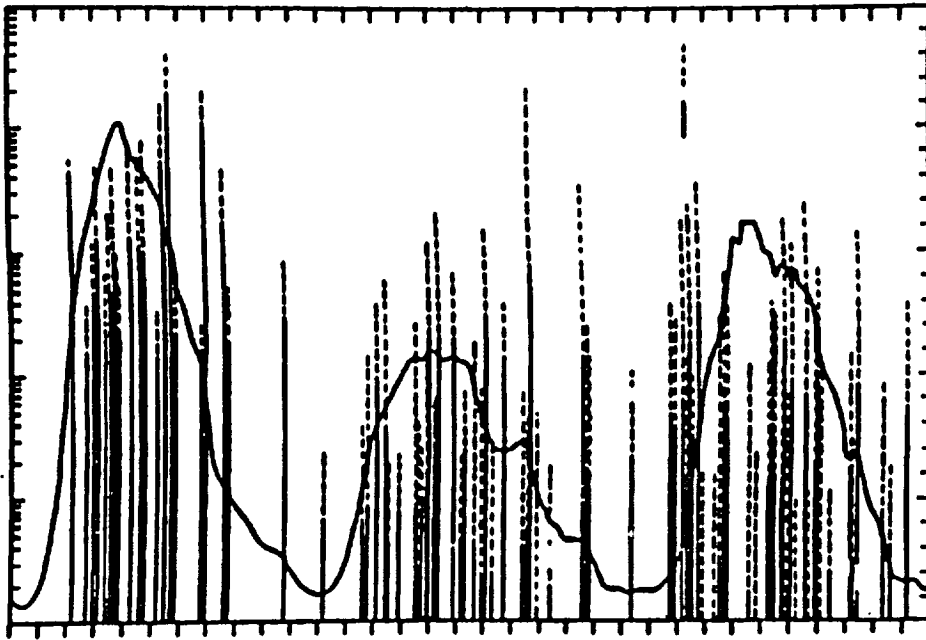


Figure 6-2. Zurich Smoothed Sunspot Number and Proton Fluence for Solar Cycles 19, 20, & 21

Two such ALSPE were used in the investigation of the Mars Transfer Habitat (MTH) and Crew Return Vehicle (CRV); the August 8, 1972 and October 19, 1989 events. Both are considered reference events but each has characteristic spectral qualities. Spectra differences show the August '72 event to have had a very large flux and the October '89 event with a much harder energy spectra, a lower flux relative to the August '72 event. A comparison between the cumulative differential proton spectra for these events is shown in figure 6-3. The determination of the differential fluence spectra used in the transport analysis was the result of direct measurements made by geostationary platforms monitoring the free-space radiation environment such as GOES -7.

The second source used in the analysis was that of GCR which originates from sources far outside our solar system. GCR is understood in part to be the result of super-novae. Composed primarily of protons, high atomic number (Z) and energy (E) particles comprise roughly one percent of the total component but constitute the largest dose equivalent contribution. Our understanding of these high energy particles and their effects on living systems is limited. Because of the exceedingly high energies (with the greatest flux occurring between 100 MeV/nucleon and 10 GeV/nucleon), GCR is far more penetrating than other forms of radiation. The GCR environment is modeled using the

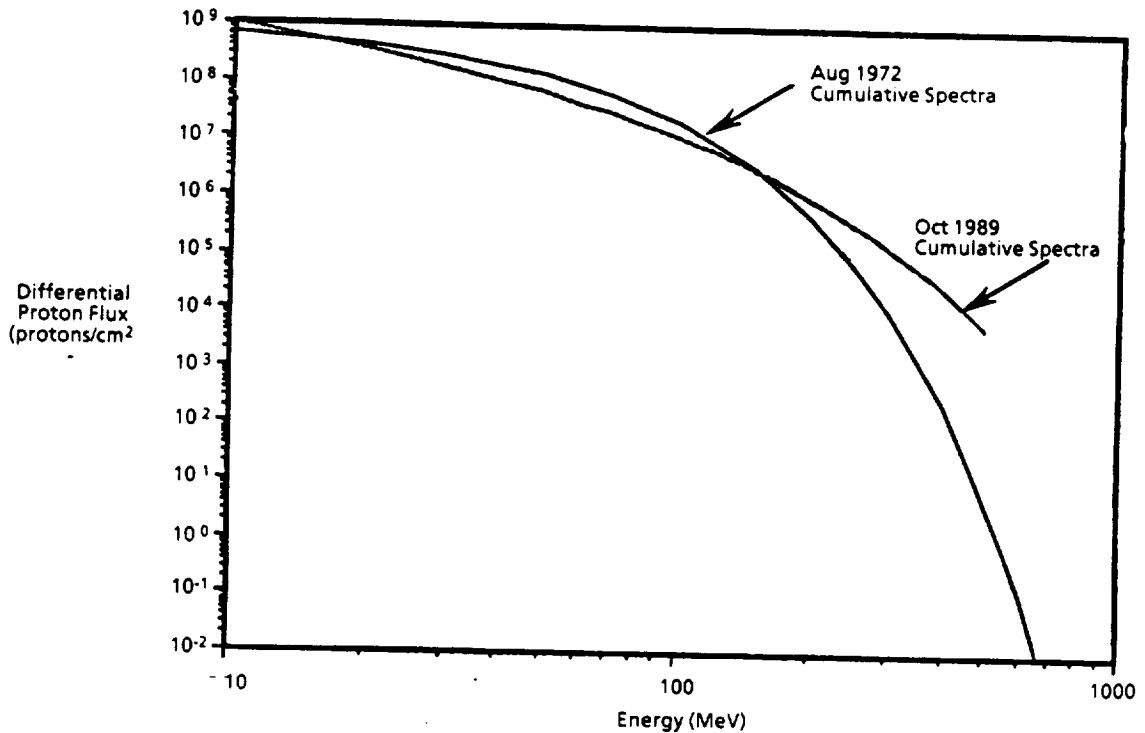


Figure 6-3. Flux/Energy Distributions for August '72 and October '89 Solar Proton Events

flux-energy distributions from various ions predicted by the Naval Research Laboratory (NRL) Cosmic Ray Effects on Micro-Electronics (CREME) model, reference 21. A comparison of the time-integrated differential energy spectra of protons from the August 1972 flare and GCR are shown in figure 6-4. CREME, accounts for modulation of the GCR spectra as a result of variations in strength of the solar activity which appears to reduce the GCR flux by a factor of 2 during the periods of solar maximum. It is during this period that the sun's magnetic field has maximum strength and particle energy cutoff.

6.2.3 The Boeing Radiation Exposure Model

A new analytical modeling system, *Brem*, was employed to perform the radiation analysis task. *Brem* combines Computer Aided Design (CAD) capabilities with established NASA transport codes permitting fast, accurate and consistent radiation analysis. A functional flow of the *Brem* system is shown in figure 6-5. *Brem* uses an Intergraph workstation to create the solid models of the vehicles. VECTRACE (VECTOR TRACE), a custom ray-tracing subroutine contained within *Brem* was used to establish the shield-distribution about the desired analysis points within the MTH and CRV,

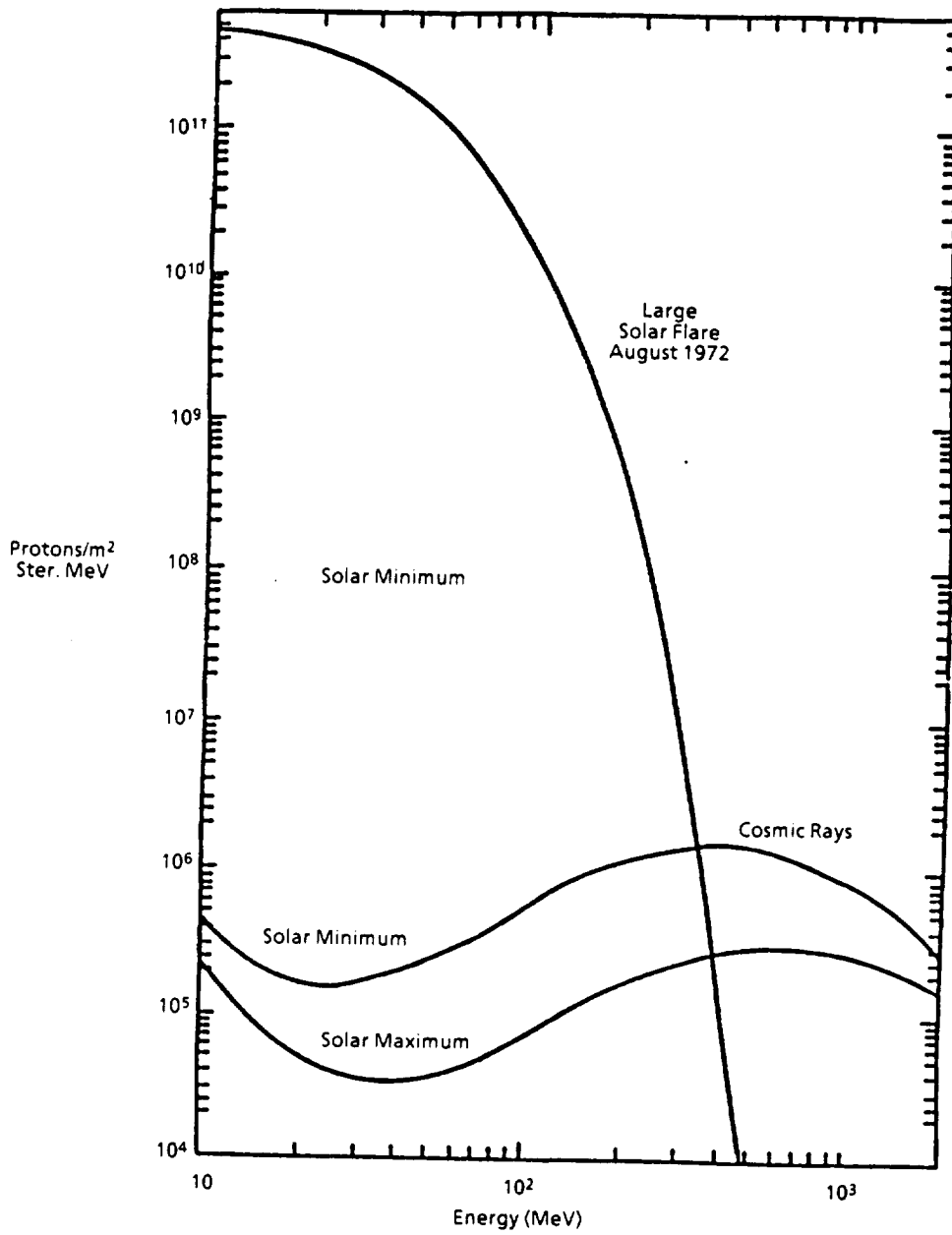


Figure 6-4. GCR Spectra and August '72 Solar Proton Event

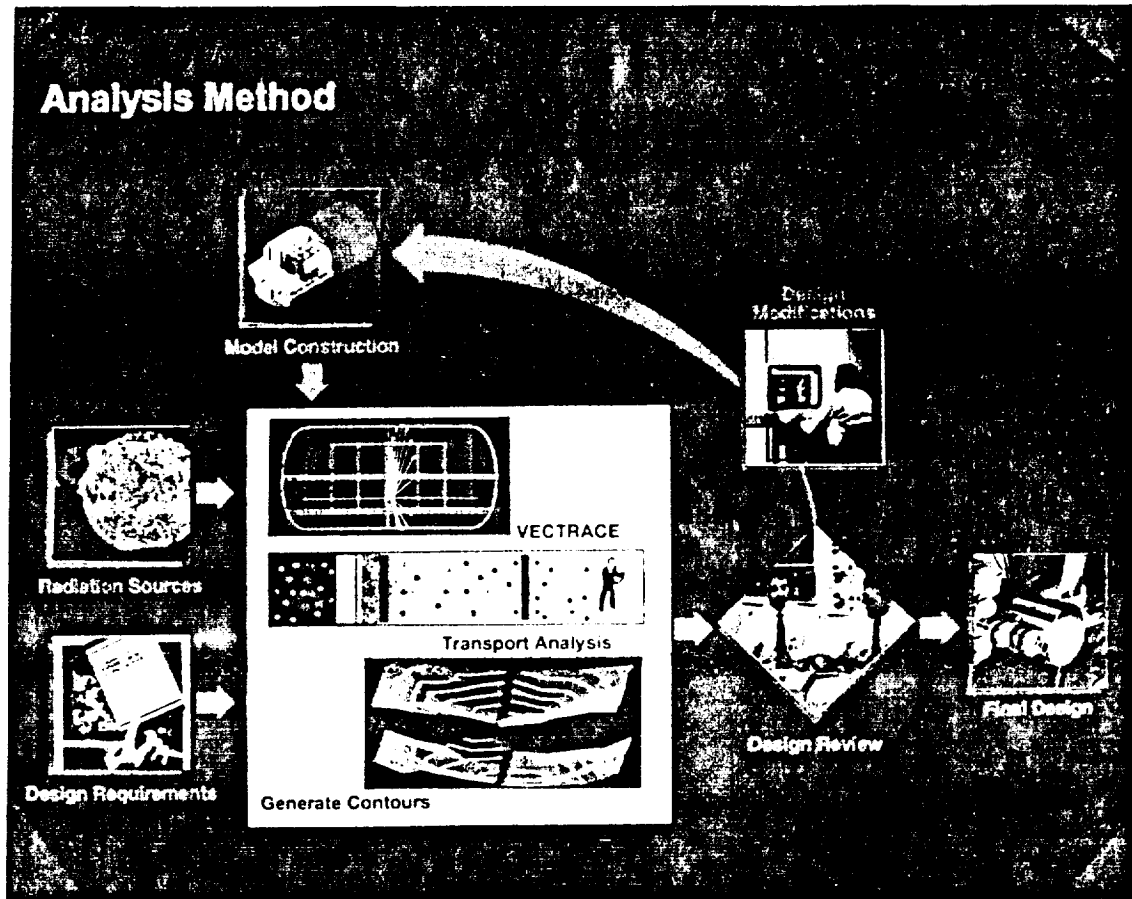


Figure 6-5. The Boeing Radiation Exposure Model Analysis Method

figure 6-6. VECTRACE divides the 4π solid angle surrounding a "detector" into a number of equal solid angles as specified by the analyst. Vectors originating at the detector point and co-aligned with the centers of solid angles traverse the spacecraft shielding to determine the shield thickness and composition. Previous techniques to determine the shielding provided by very complex and inhomogeneous spacecraft structures either relied on over simplifications such as average shield thickness or on modeling the spacecraft structure through a process known as combinatorial geometry. The latter method is extremely slow, labor intensive, tedious and complex, significantly increasing the potential for errors. Current design programs rely heavily on the use of CAD based systems which allow advantages in understanding the integration and compatibility of large complex systems. The logical step to development of *Brem* was to make use of these systems for radiation protection studies.

Modified versions of the NASA Langley Research Center nucleon and heavy-ion transport codes BRYNTRN (Baryon Transport Code) and HZETRN (Heavy-Ion Transport Code) were used to model the propagation and interaction of nucleons (protons and neutrons) and heavy-ions through several shield layers, reference 22. Both methods

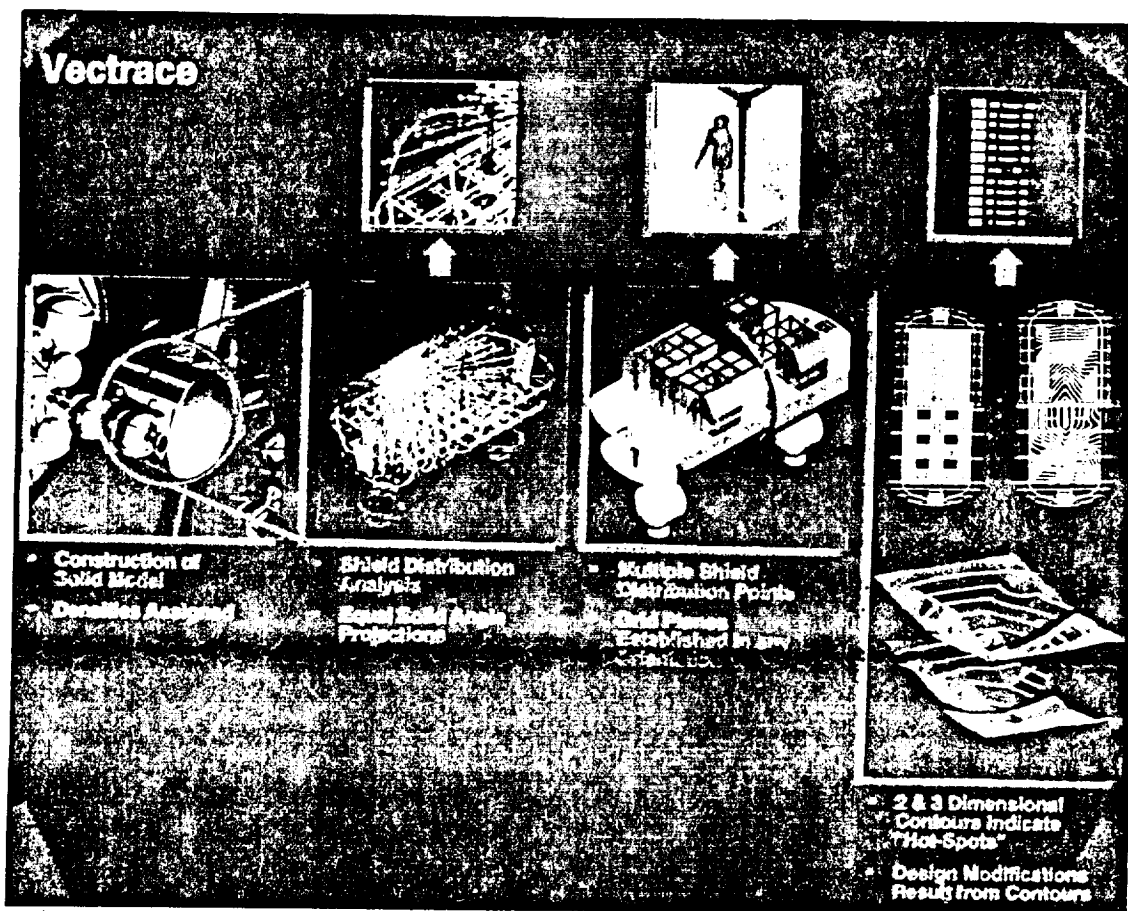


Figure 6-6. VECTRACE Shield Distribution Analysis System

provide rigorous solutions to the Boltzmann transport equation. A third transport code, PDOSE (Proton Dose Code), was used to determine crew exposure. PDOSE has adopted a continuous slowing down approximation to calculate the attenuation and propagation of particles in various shield materials. Secondary particles generated by nuclear interactions are not included in PDOSE as they are in BRYNTRN and HZETRN. Results from PDOSE have been extensively compared against Shuttle measurements by NASA's Radiation Analysis Branch, Johnson Space Center, and has been found to be fairly accurate, reference 23. Organ dose calculations, necessary for risk assessment, were performed using a detailed mathematical anthropomorphic phantom. The phantom model known as the Computer Anatomical Man (CAM) represents the anatomical structure of a fiftieth percentile Air Force male. The shield distribution for critical organs are generated using a method similar to that employed by the VECTRACE routine. The CAM model provides a more realistic shield distribution for the blood forming organs (BFO), ocular lens and skin than simple water sphere geometries. In the assessment, the

BFO and skin represent the average distribution of 33 points distributed throughout the BFO and skin organs.

Brem's graphical display allows for on-screen viewing of the spacecraft model, analysis points, and topological contour maps of exposure levels. By proper selection of graphical attributes it is easy to rapidly spot areas which may exhibit higher general exposure rates (undesirable for crew quarters) and "hot-spots", which may require avoidance or additional shielding. Through the interactive shield alteration provided by CAD, attempts to improve dose rate topology or the elimination of "hot spots" can be rapidly evaluated on-screen.

6.2.4 Solid Modeling

One of *Brem's* attributes is its use of CAD technology to produce the spacecraft shield distribution at points or areas of interest. This approach provides great savings in time, accuracy, and functionality. Three dimensional solid CAD models not only portray hardware geometry but serve as the data base for structural, thermal, and human factors analysis.

The system relies on the use of engineering databases created in the spacecraft design program. By using CAD databases, the radiation analyst taps into the many man-hours of careful work invested in their construction, rather than duplicating the effort. CAD based systems produce shield models with fewer errors (i.e., undesirable voids or overlapping regions) and greater accuracy compared to combinatorial geometry models. This reduces overhead in model error checking and verification, and improves confidence in results which rely on the shield model distribution. Finally CAD solid models allow for easy removal, addition, or rearrangement of spacecraft components and quick analysis of resulting changes in dose patterns. Changes in spacecraft configuration as the vehicle design matures, or changes in vehicle configuration as the mission progresses can be evaluated interactively for its impact on dose rates inside the structure. This flexibility also lends itself to parametric analyses to determine optimal vehicle designs in terms of radiation exposure.

Solid elements are assigned densities relating their mass properties (i.e., equipment racks) material composition (i.e., metal matrix composite used in construction of the pressure vessel). The densities serve three roles: (1) the product of the density and the measured slant path length of the projected vector gives the areal density (g/cm^2), a standard parameter used in transport analysis; (2) densities serve as flags to access nuclear and atomic cross section data files; and (3) finally densities allow access to data

files used to convert the defined materials to an equivalent aluminum form based either on mass properties or the ratio of stopping powers, figure 6-7.

Material	Density (g/cm ³)	Major Elements
40% V ₂ O ₅ /SiC/6061-T6 Matrix	2.850	Al, Si, C, Mg
Multi-Layer Insulation (MLI)	0.192	C, O, Si, H, Al
6061 Aluminum Alloy	2.710	Al, Mg, Si, Cr, Cu
Graphite/Epoxy Composite	1.600	C, O, H, Br, N
Food (61% Water)	0.700	C, H, O, N
Water	1.000	H, O
Phenolic Ablator	0.541	C, H, O, Si
Regolith	1.52	O, Si, Al, Fe, Mg

Figure 6-7. Listing of Materials Defined in Analysis

6.3 ANALYSIS RESULTS

Crew doses and dose equivalent quantities have been determined as a result of simulated exposure to two large solar proton events and galactic cosmic radiation for the initial and redesigned Mars transfer habitat and Mars direct entry CRV. Solid models used in this analysis were developed as illustrated in section 5.0 of this report.

The purpose of this study was to characterize potential exposure to astronauts on exploration missions to Mars. The National Council on Radiation Protection and Measurements (NCRP) has recommended both career and annual exposure limits for NASA to use in planning manned missions, figure 6-8. Career limits vary with gender and the age at the start of the astronaut's career and are based on a three percent risk of cancer mortality. Current limits have been recommended for missions taking place in Low-Earth-Orbit (LEO). For discussion purposes only, these limits are typically applied to exploration studies. Currently astronauts are given an annual exposure limit that is ten times greater than Earth-bound high risk counterparts. The higher doses given to astronauts are based in part on risk versus gain and a relative comparison to other potential mission risks such as vehicle system failures.

6.3.1 Mars Transfer Habitat, Artificial gravity

The artificial gravity transfer habitat was baselined for the STCAEM Phase 1 NTP. Results of radiation analysis are presented here since these results strongly affected the Phase 2 zero-g habitat, for which radiation analysis results are presented below in section 6.3.3.

To perform the analysis four grid planes were established; two on the lower deck and two on the upper. The grid planes at each level were separated by the pressure bulkhead. The shield distributions at 110 dosimeter locations were established, figure 6-9. The

All values presented in cSv			
Time Period	BFO*	Lens of Eye	Skin
30 day	25	100	150
Annual	50	200	300
Career	See table below	400	600

Blood forming organs. This term has been used to denote the dose at a depth of 5cm

Career whole body dose equivalent limits based on a lifetime excess risk of cancer mortality of 3%

Age (years)	Female	Male
25	100	150
35	175	250
45	200	320
55	300	400

Data from Guidance on Radiation Received in Space Activities, NCRP Report No. 98

Figure 6-8. Current NCRP Recommended Exposure Limits

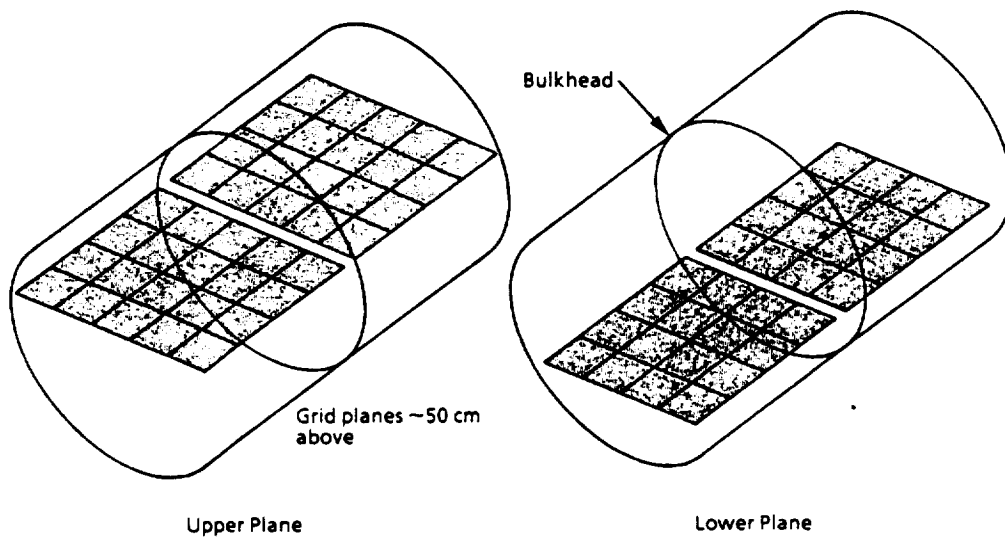


Figure 6-9. Analysis Grid Layout for Mars Transfer Habitat

determined shield distributions for each dosimeter location will differ due to geometric variabilities. As the dosimeter "view point" changes, the measured slant path length of each projected vector passing through solid elements varies. For example, analysis points close to walls or racks have greater shielding effectiveness due to the increased slant path lengths resulting from the walls. It is important to point out that the method uses straight-ahead or one-dimensional transport calculations. The same effect would not be expected with a more rigorous three-dimensional or Monte Carlo analysis.

GCR analysis of the habitat revealed that annual blood forming organ dose equivalent values ranged from approximately 13 to 44 rem/yr. As was expected, the lowest exposures were encountered at the lightly shielded end cones. The annual exposure distribution is shown in figure 6-10. The annual exposure rates are simply reduced to hourly rates assuming the exposure source to be constant over time; this is indicated in figure 6-11. By developing hourly crew proximity schedule diagrams, figure

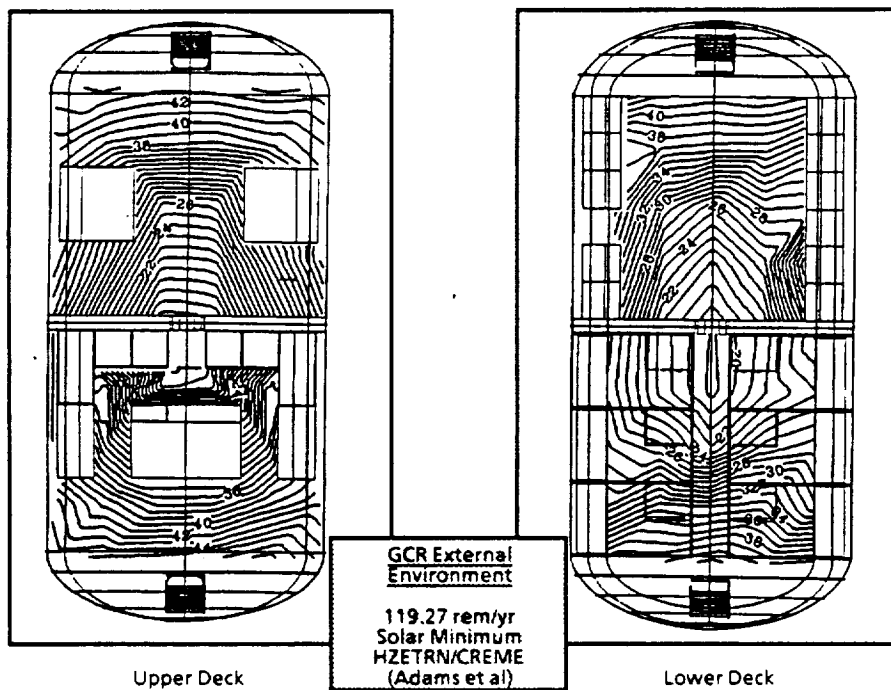


Figure 6-10. Rem/Year to Blood Forming Organs

6-12, and relating them to the hourly iso-dose rate contours, daily astronaut exposures based on the habitat dose equivalent distribution were determined. Potential mission exposure was determined parametrically, as shown in figure 6-13, by using this method. Incident spectra used were based on the solar minimum activity model. This represents

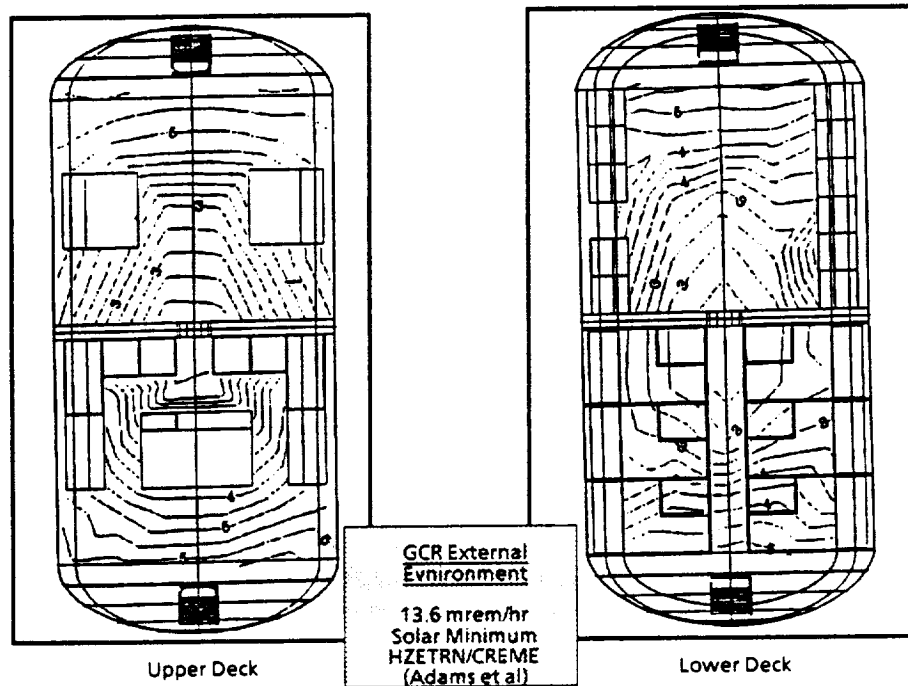


Figure 6-11. Rem/Hour to Blood Forming Organs

the worst case environment for GCR as the interplanetary magnetic field is weakest and particle attenuation below 100 MeV/nucleon is minimal.

An important result of the GCR analysis was the identification of the habitable region having the greatest shielding capabilities. Note in figures 6-10 and 6-11 that the lowest exposures can be observed in and around the galley (refer to fig. 6-12 for location). This area would serve as a "storm shelter" which would provide protection in the event of a large solar proton event. Studies indicate that for a crew of six, 8.2 metric tonnes of food, which includes provisions for contingency operations, is required for the range of design missions. Higher concentrations of lighter elements associated with food makes it valuable in providing radiation protection. Operational concerns are out of scope of this analysis but would have to be addressed to determine nominal solutions to maintaining shielding integrity. During the course of the mission, food is consumed and the protection scheme breaks down. One such method involves replacing consumable shielding with stabilized and stored waste. No attempts were made to obtain complete closure of the shelter, develop a complete shielding plan or establish operational procedures that would minimize ionizing radiation exposure. At the very least the analysis indicates that consumables should be considered as part of the concentration of shielding needed for protection against the solar proton events.

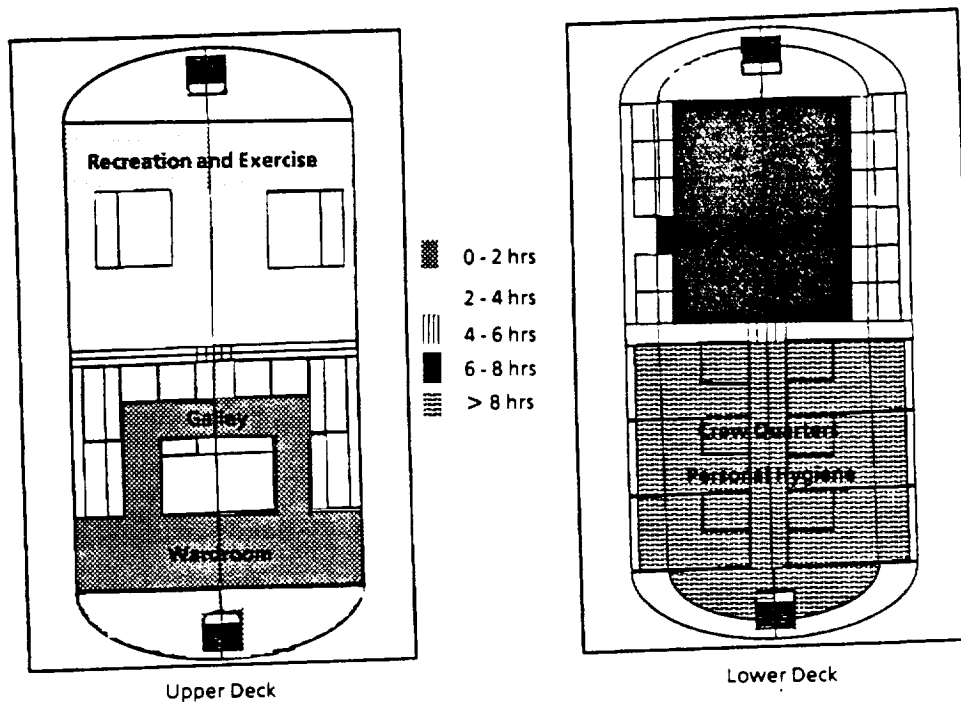


Figure 6-12. Habitat Proximity and Work Schedule

The dosimeter grid established to perform the SPE analysis for the galley/storm shelter region is shown in figure 6-14. The shaded regions indicate both thermally stabilized and "wet" (~65% water) food storage racks. No distinctions were made between the two in the transport analysis. Protection in this region was provided under floor by ECLSS equipment and water storage and overhead by food and equipment. Equivalent doses to the blood forming organs ranged from 1 to 8 and 1 to 10 rem/event to the blood forming organs for the August 1972 and October 1989 SPEs respectively. Iso-dose equivalent contours are presented in figures 6-15 and 6-16. The results indicate that stowed consumables and in particular food can provide significant radiation shielding.

Another lesson learned in this investigation and one carried on to the transfer habitat redesign effort, was the need to move high use crew regions into the heavily shielded central portion of the habitat. Crew quarters for example, where astronauts spend at least one third of their day, should be moved from lightly shielded peripheral regions to more centrally located positions. Referring to figure 6-12, the crew quarters experience increasing GCR exposure as one moves away from the bulkhead. It is important to note that many of the habitat design decisions were based on functional relationships, such as user needs, accessibility, and volumetric requirements. The intent of the study was to evaluate a design without presupposing radiation shielding solutions.

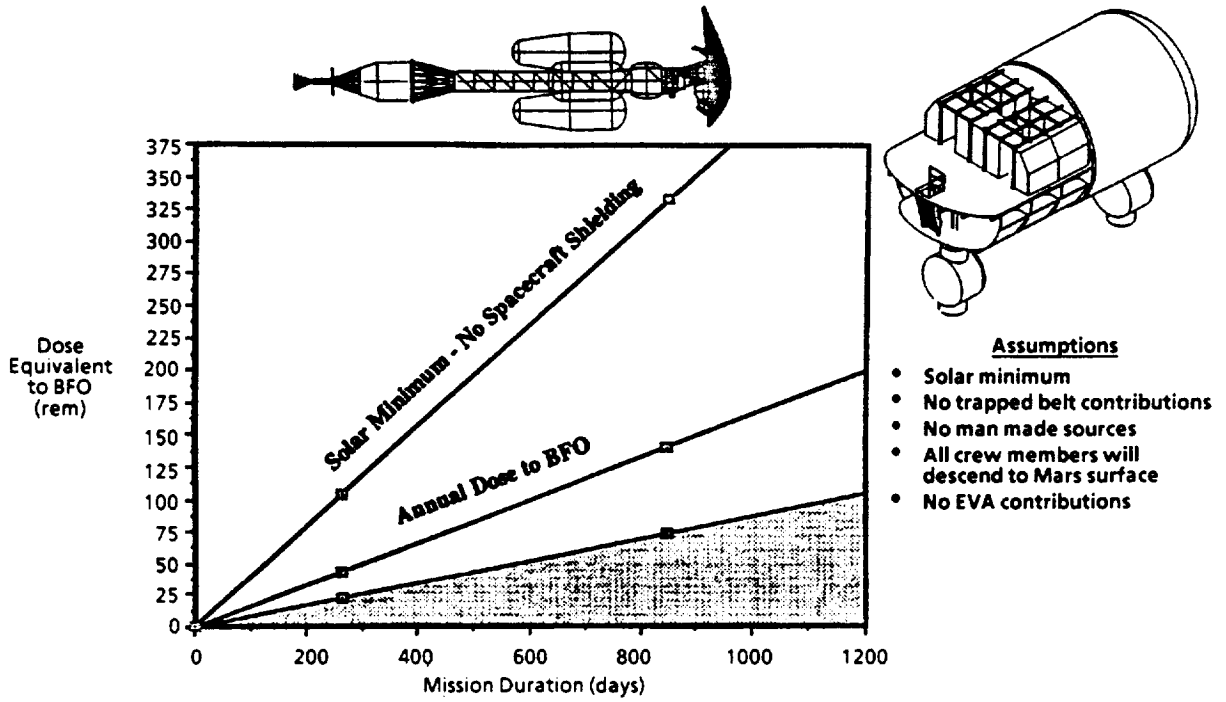


Figure 6-13. Mission Exposure from Galactic Cosmic Radiation

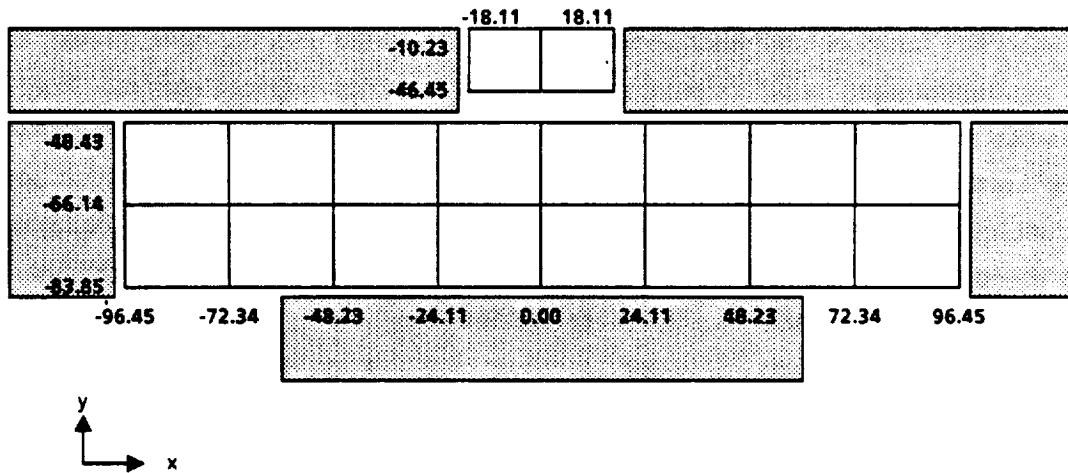


Figure 6-14. Galley Grid Layout

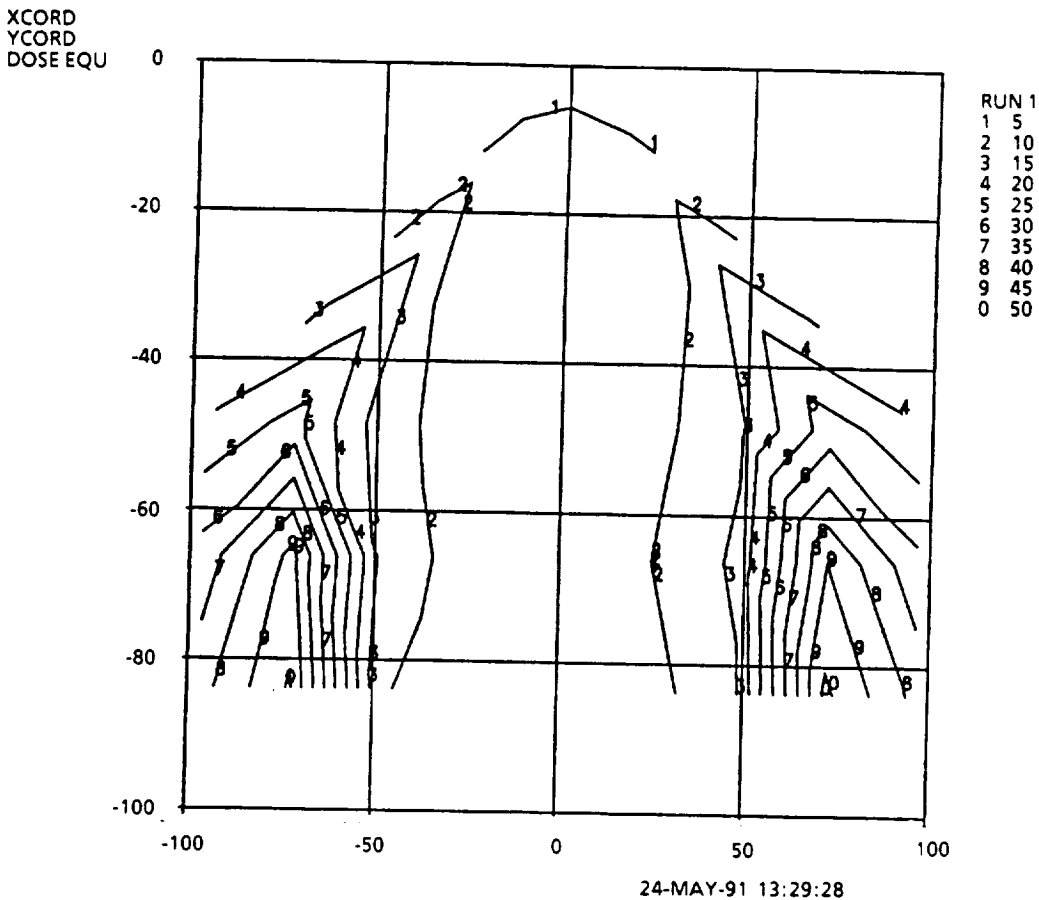


Figure 6-15. ISO-Dose Contours of Dose Equivalent (REM) to BFO for August 1972 SPE

6.3.2 Mars Crew Return Vehicle

A radiation evaluation of the Mars Crew Return Vehicle has been conducted. Current mission design operations call for astronauts to enter the Apollo style capsule, separate from the Mars Transfer Vehicle for a direct Earth entry. This study investigated acute crew exposure resulting from the October 19, 1989 SPE. The NOAA five minute data set for the initial thirty-six hours of the event is shown in figure 6-17. This data was recorded directly by the Geostationary Operational Environmental Satellite (GOES-7). GOES-7 monitors the temporal development and energy characteristics of the emitted protons. The arrival of the the shock-front is seen at roughly 25 hours. The start of the event is declared as the $\geq 10\text{MeV}$ protons reach a flux greater than 10 protons / cm^2 - sec-sr. The initial and third twelve hours of the event were used in the investigation to simply characterize the potential impact to the crew from a large SPE. The period from 24 to 36 hours was included in the analysis because of the arrival of the shock front.

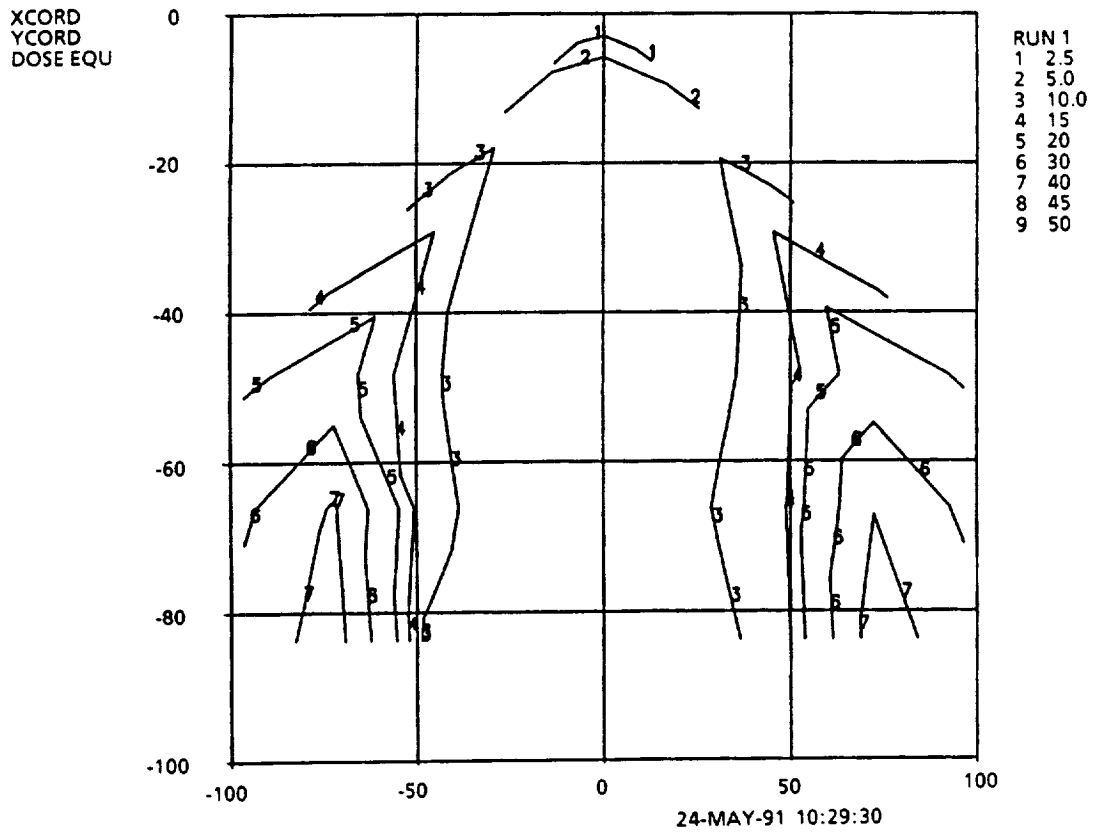


Figure 6-16. ISO-Dose Contours of Dose Equivalent (REM) to BFO for October 1989 SPE

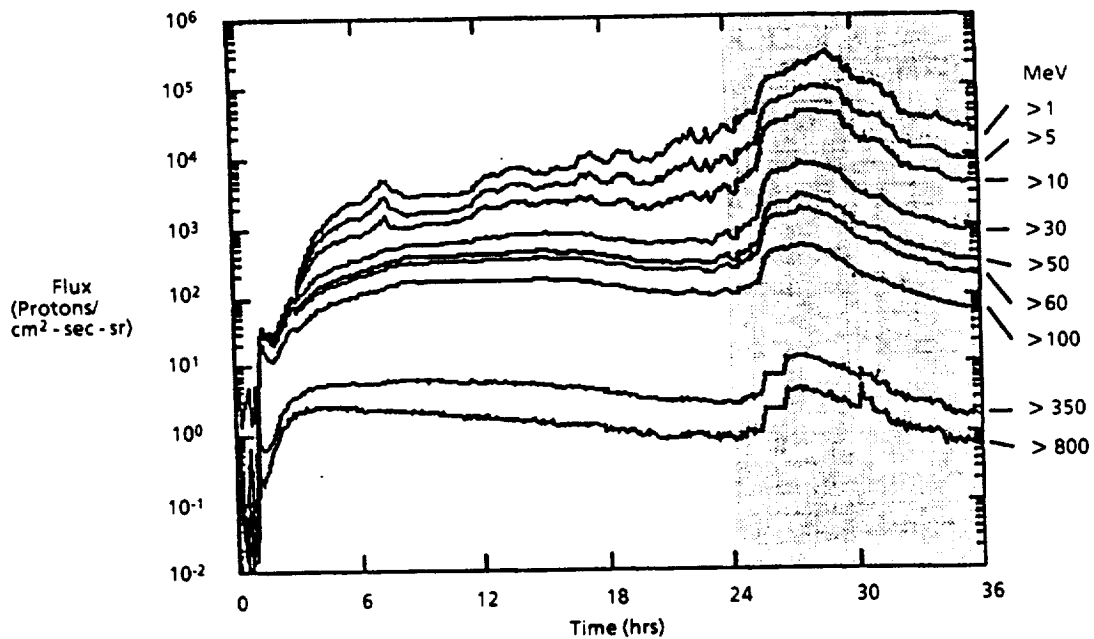


Figure 6-17. NOAA 5 Minute Data Set for Initial 36 hours of October 19, 1989 SPE

The differential flux energy distributions for each of these time intervals were determined using the NASA code SPESPEC (Solar Proton Event Spectrum). SPESPEC is used to determine $P(o)$ and $N(o)$ values which are then used to determine the needed flux/energy distribution. $P(o)$ is the characteristic rigidity of the particle spectrum in MV and $N(o)$ is a constant related to the size of the SPE. It is determined from $P(o)$ and $J(>P)$, which is the fluence of particles with a rigidity greater than P , the particle rigidity (momentum/charge). A comparison between the flux/energy distributions is shown in figure 6-18. Also indicated on this graph are the respective $P(o)$ and $N(o)$ values. No transmittance function was used to adjust the incident spectra during the period in which the CRV has entered the Earth's magnetic field.

Dosimeter locations were established at each of the six crew couch positions. It was assumed that crew members would stay positioned in their couches during the full twelve hours of the return. It was necessary, as seen in the cut-away image of figure 6-19, to construct solid anatomical figures that would provide some degree of radiation protection. The anatomical figures are constructed of water which simulates the bodies' self shielding capabilities. Five of these figures were "turned-on" while the shield distribution for the sixth was being established. The Computerized Anatomical Man model provided the shield distribution analytically for the sixth crew member. A typical dosimeter location was established, located roughly at a mid chest position.

Exposure results for each of the time intervals are provided in figures 6-20 and 6-21. An increase in exposure for all couch positions is observed during the period from 24 to 36 hours due to the arrival of the shock front. Contrary to what one would expect and due once again to geometry and one-dimensional transport calculations, the exposure to positions 3 and 4 were not consistent with 5 and 6 and greater than 1 and 2. A comparison of positions 4 and 5 are presented in figure 6-22. The figure compares the differential shield distributions of the two positions. The upper figure provides a difference of the differential distributions. One can see by the difference the greater number of "heavy" shield entries for position 5. This directly translates into a lower exposure to the position.

It is important to note that SPE doses were the result of only limited exposure time. In the case of the lunar CRV the analysis would change considerably. Lunar transfer times could take as long as 5 days, exposure to GCR and total event duration SPEs would be investigated. Exposures would be expected to be in line with the Apollo/Lunar missions if we assume minimal impact from solar proton events. One advantage of the Lunar CRV as compared to the Mars CRV would be the presence of the service module, again like that of the Apollo Service Module. Lunar CRV analysis completion would entail further definition of the integrated vehicle.

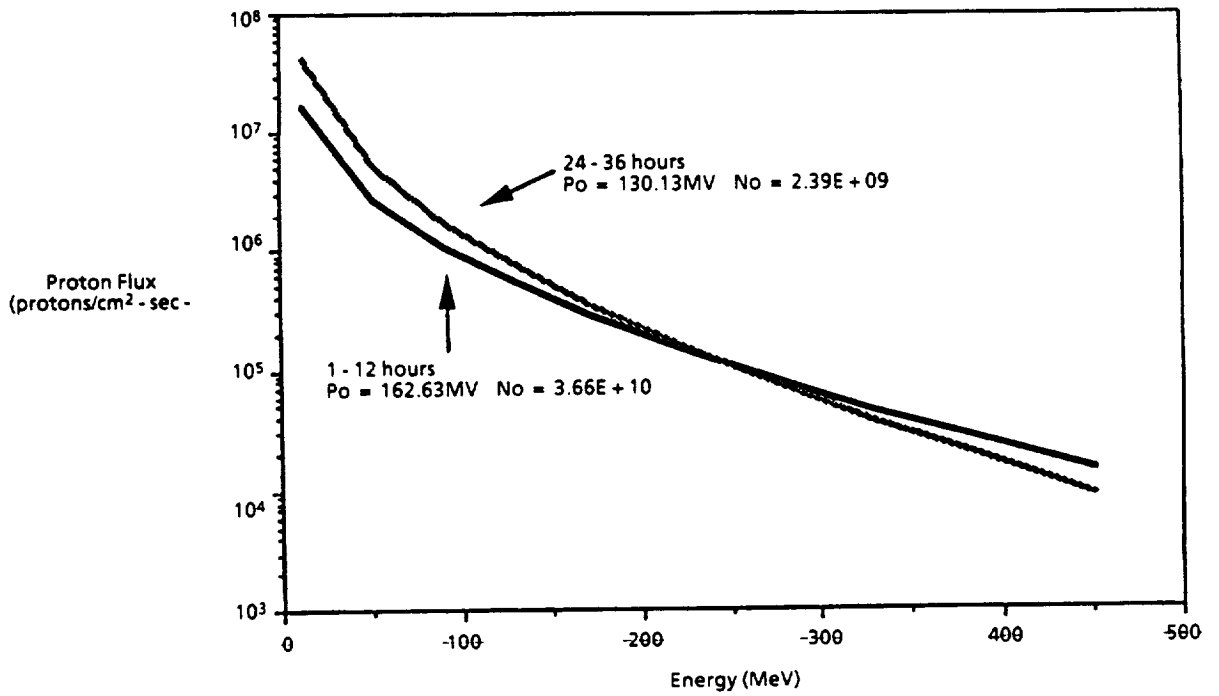


Figure 6-18. $P(o)$ and $N(o)$ and Generated 12 Hour Flux Energy Distributions

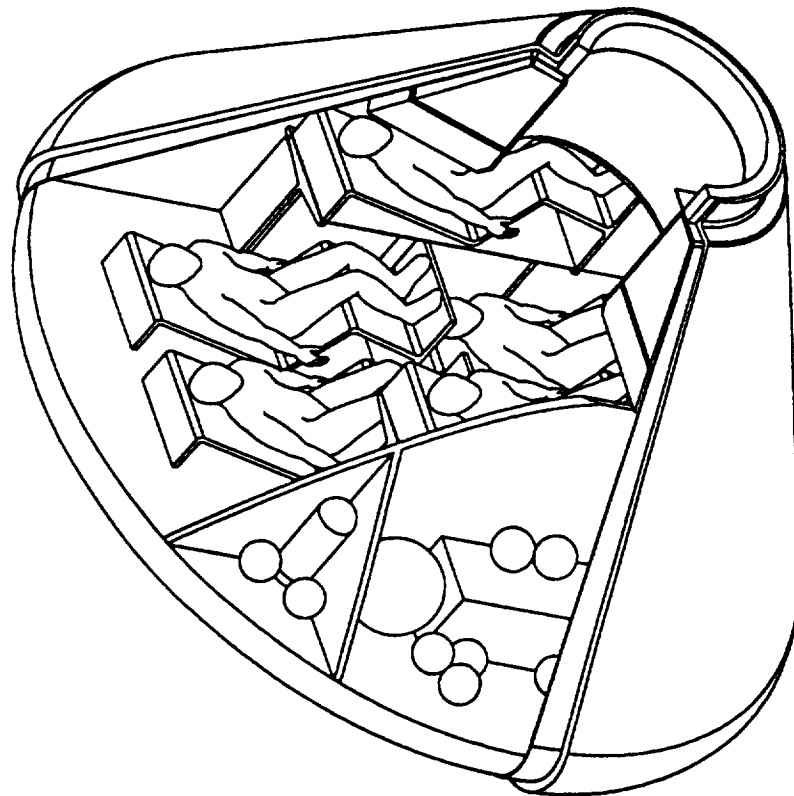


Figure 6-19. Cut-away Image of CRV and Crew Positions

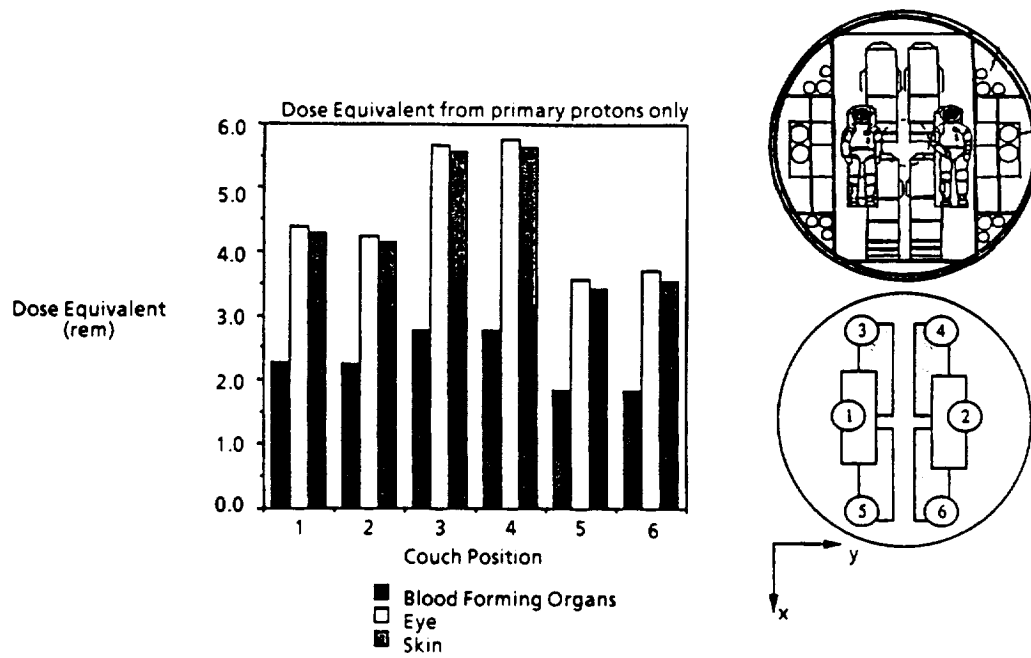


Figure 6-20. Dose Equivalent Resulting from Initial 12 Hours of 19 Oct. '89 SPE

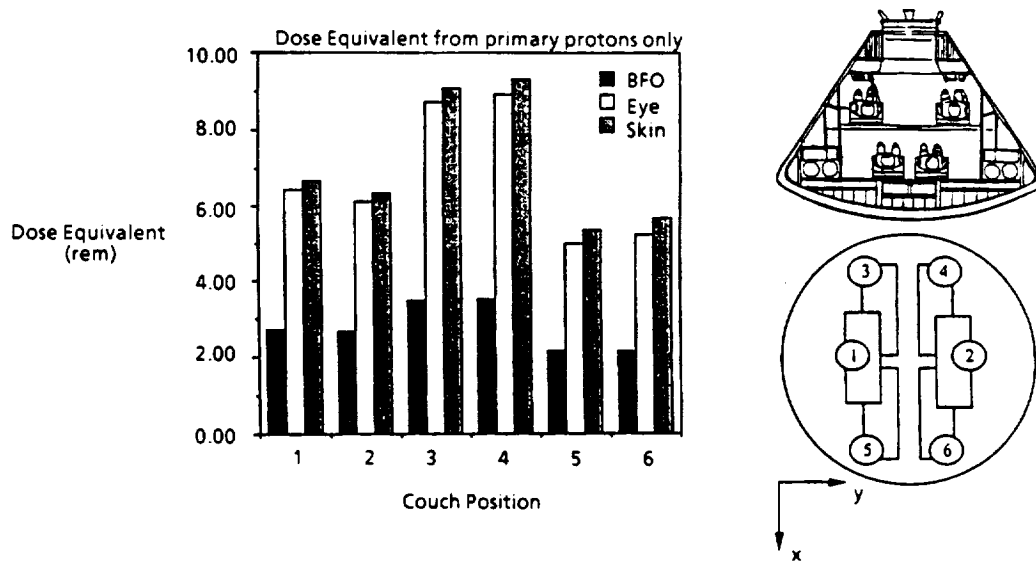


Figure 6-21. Dose Equivalent Resulting from Third 12 Hours of 19 Oct. '89 SPE

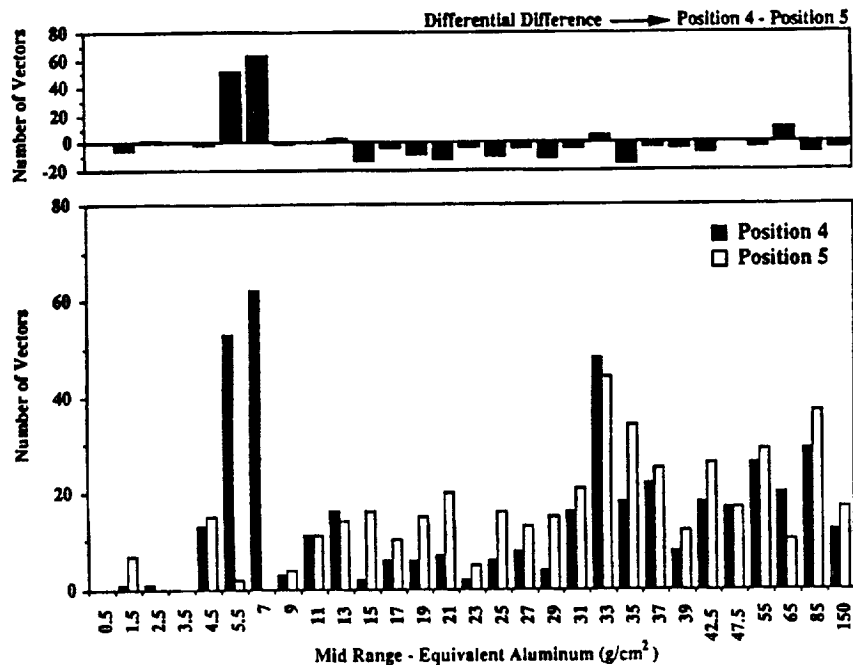


Figure 6-22. Differential Shield Distribution for Couch Positions 4 and 5

6.3.3 Mars Transfer Habitat, Zero-g

Design mission changes and shorter mission durations associated with the Synthesis mission profiles, and re-evaluation of payload, contributed to the redesign of the Mars transfer habitat module for STCAEM Phase 2. These re-evaluations also resulted in a reduction of potential inherent shielding material such as food and equipment. The design effort dealt with deficiencies in radiation protection provided in the initial habitat study.

A major difference in the habitat designs was the removal of the artificial gravity constraint. Crew quarters were moved from exterior walls to the center of the vehicle and were in close proximity to food storage, the bulkhead, and other massive equipment. These changes were made to provide added protection to the high use habitable regions. Additionally, analysis incorporated external elements such as propellant tanks. The design integration of the vehicle calls for the habitat to be partially enveloped by the Mars Orbit Capture and Trans-Mars Injection tanks. The relative positions of the tanks and habitat module are indicated in figures 6-23 and 6-24. During the course of the mission, tanks will contain varying levels of propellant. Liquid hydrogen provides effective shielding due to its low atomic number and large nuclear cross section. Nearby liquid hydrogen tanks can produce "cold" radiation regions in the habitat. On the

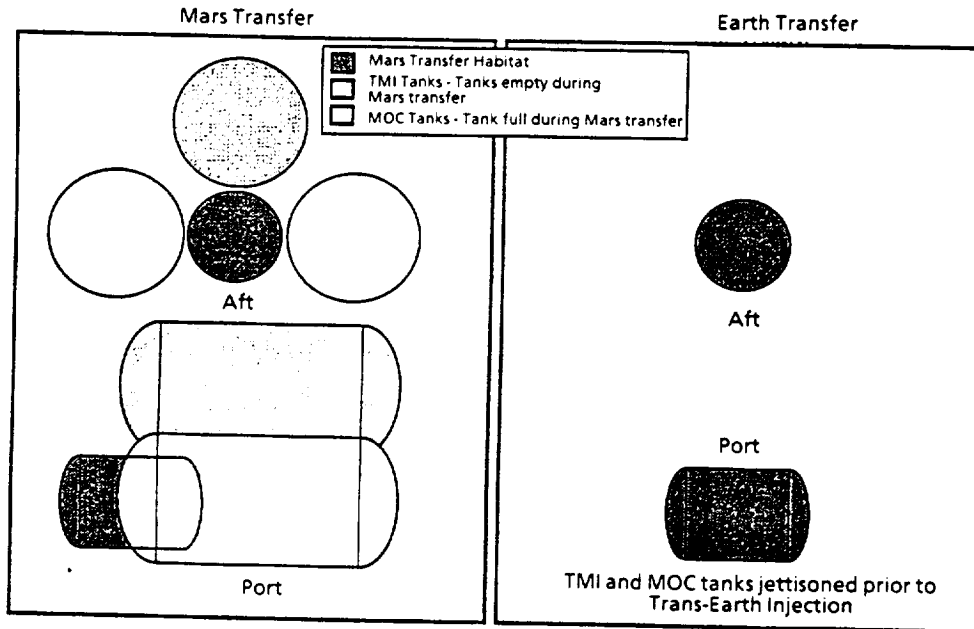


Figure 6-23. MTV Habitat Radiation Analysis Scope

out-bound portion of the mission the MOC tank is nearly full while the TMI tanks are empty. For the in-bound portion of the mission the habitat is exposed as both the MOC and TMI tanks have been jettisoned after Mars arrival. These two mission phases set the scope of the radiation analysis.

Since the vehicle was configured for zero-g, two axially intersecting and perpendicular grid planes were established, each of which provided locations for 60 dose points. The analysis was completed in the same fashion as the earlier habitat. Five-hundred and twelve vectors were projected over equal solid angles and provided input for the transport analysis. Exposure from GCR and SPEs was evaluated.

GCR equivalent doses to the blood forming organs ranged from 19 to 39 rem/yr and 23 to 45 rem/yr for the out-bound and in-bound mission phases respectively. As with the earlier habitat analysis, the minimum solar activity model was used. Low exposures were seen again in and around the galley region. Annual GCR exposures to the blood forming organs fall below 50 rem/yr. Three dimensional contours describing the exposure on the locally horizontal plane are shown for each of the mission phases in figures 6-25 and 6-26. Analysis of the planes perpendicular to the horizontal plane showed the same trends with minimal exposure occurring at the galley and maximum exposure at the lightly shielded end domes. Crew quarters benefit from added protection provided by approximately 5.5 metric tonnes of food and other equipment. We assumed that protection provided by the food was held constant through a replacement scheme in which the wall of protection provided by the food was being

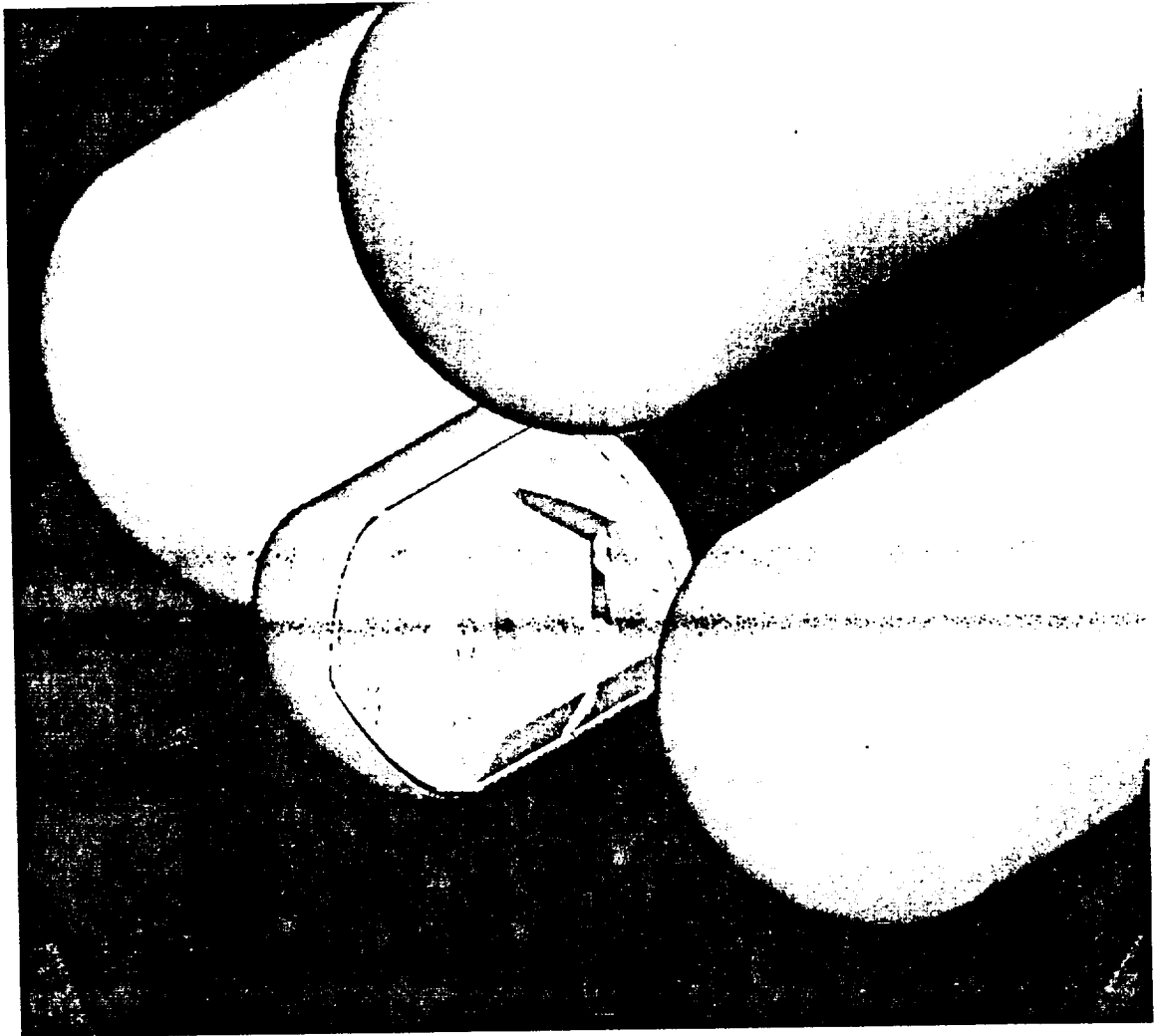


Figure 6-24. Proximity of MOC and TMI Tanks to Habitat

replaced. Additional shielding was provided by the presence of propellant in the MOC tank during the trans-Mars portion of the mission. This is evidenced by the variation in exposure range between the mission phases.

The cumulative spectra for the October '89, and August '72 SPEs were used to evaluate the shielding characteristics of the habitat to such events. A dedicated shelter scheme was not integrated into the design. The direction of the study was to identify effective shielding regions of the vehicle and determine if lessons learned from the previous habitat study were effective. Further work would then benefit from these results to maximize shield effectiveness for the crew. Exposure for the out-bound portion of the mission ranged from approximately 5 to 46 rem/event and 4 to 35 rem/event for the August '72 and October '89 SPEs respectively. The in-bound portion of mission finds the exposure range rising slightly. Exposure to the blood forming organs ranged from 14 to 77 rem/event and 8 to 55 rem/event for the August '72 and October '89 SPEs. Three-dimensional contours of equivalent dose distributions to the blood

ORIGINAL PAGE IS
OF POOR QUALITY

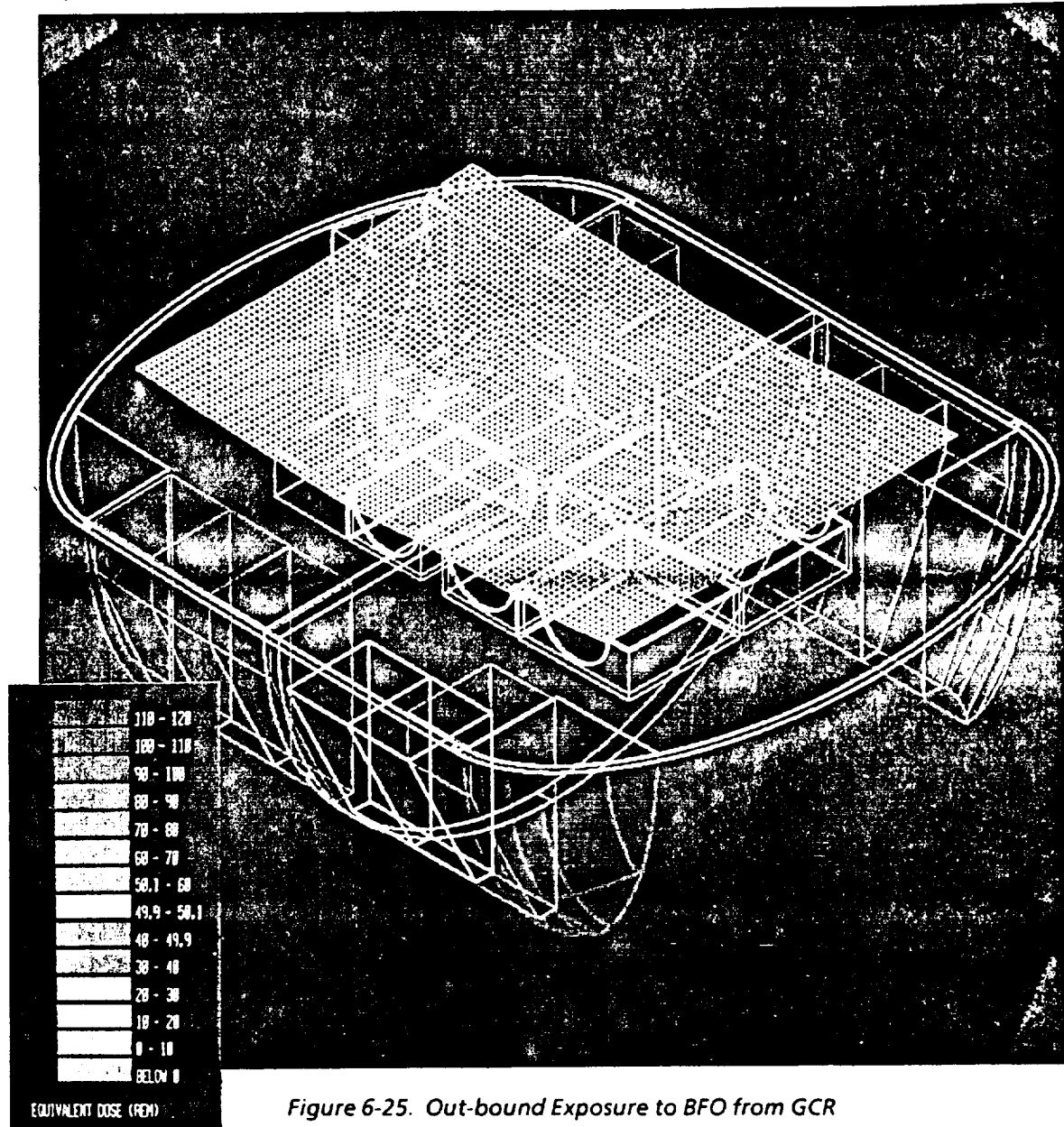


Figure 6-25. Out-bound Exposure to BFO from GCR

forming organs during Mars and Earth transfer for the August '72 SPE are shown in figures 6-27 and 6-28. Additional analysis is required to obtain better definition of the safe haven area.

6.4 CONCLUSIONS AND RECOMMENDATIONS

By using *Brem*, radiation analysis was brought into the preliminary design phase where major design modifications could be easily made. With these initial studies, the results provide insight of ionizing radiation protection methods. The technique employed centers around using inherent mass and structure to provide the base for radiation protection and then diverging from this scheme to obtain protection closure. Far more

This page was intentionally left blank.

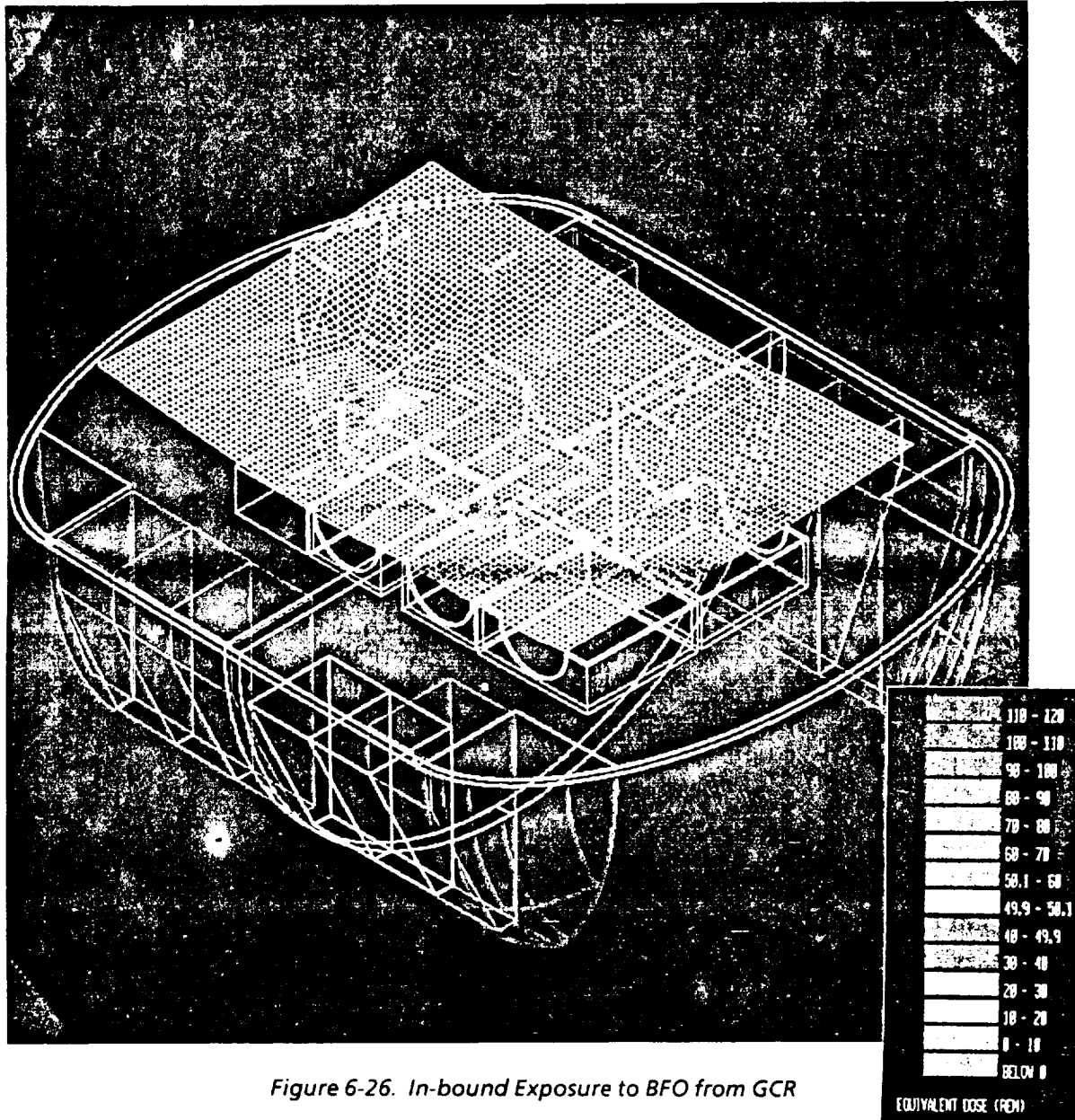


Figure 6-26. In-bound Exposure to BFO from GCR

indepth studies of shielding concepts, materials and impacts must be undertaken to get a better handle of this critical area. At minimum, early designs must evaluate protection capabilities of the concept and determine where their deficiencies arise if any, and if necessary, modify the shielding, possibly with dedicated materials.

Radiation analysis of the early Mars transfer habitat concept revealed both strengths and weaknesses in providing ionizing radiation protection. Initial habitat designs were based on considerations and constraints other than protection requirements. From the analysis, it was found that substantial protection is provided by the stored food and other massive equipment. Further studies are needed to capitalize on shielding schemes which, at minimum, utilize existing or inherent spacecraft mass. The radiation

This page was intentionally left blank.

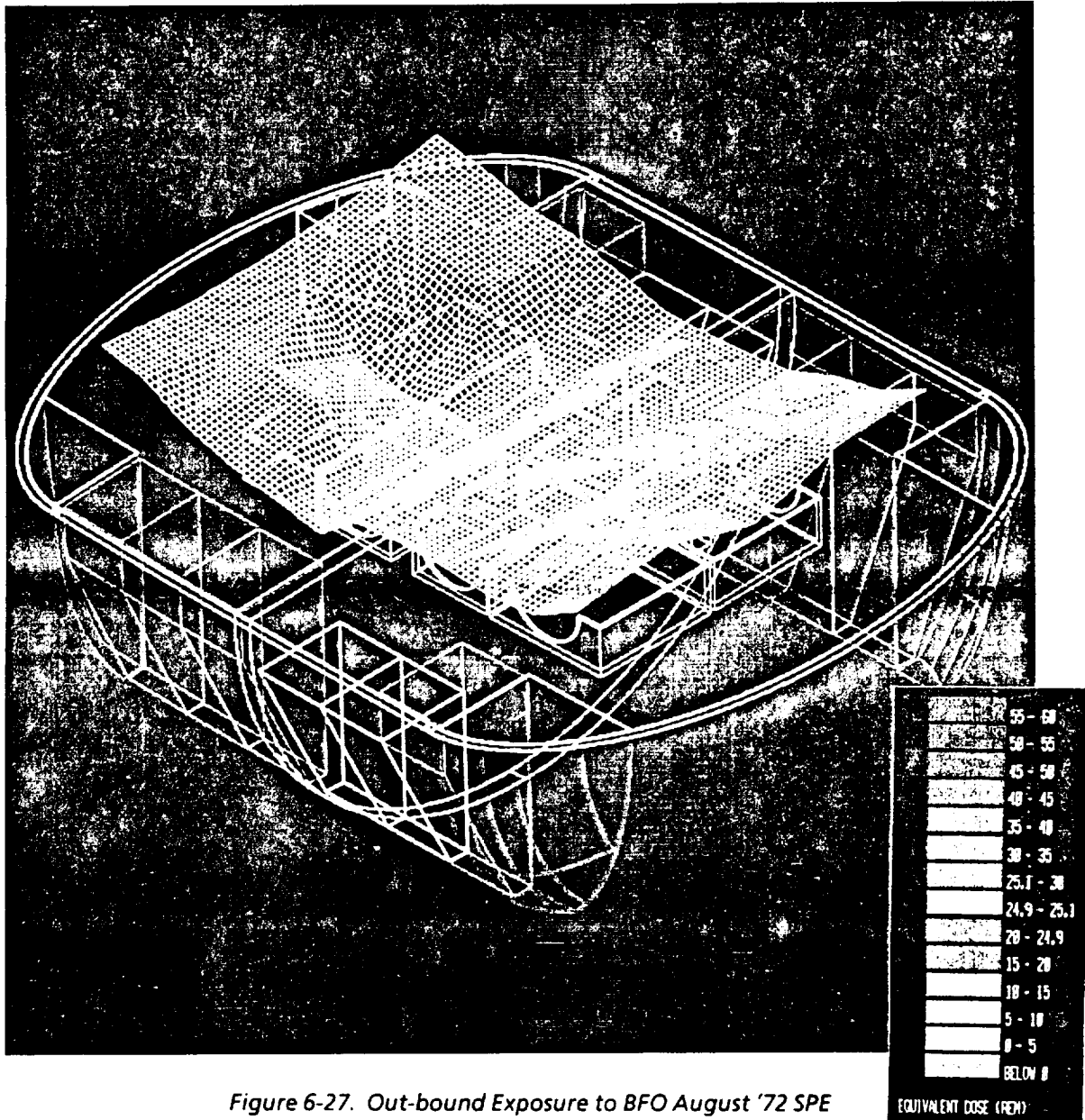


Figure 6-27. Out-bound Exposure to BFO August '72 SPE

environment that will be encountered by astronauts traveling to Mars represents a worst case. The only protection available is that which is carried by the vehicle. In other words, the crew does not benefit from natural shielding enhancements such as geomagnetic shielding, planetary mass or an atmosphere. Some protection concepts must also address a number of operational questions such as the aspect of maintaining a constant wall of protection, and the configuration and distribution of mass to provide maximum shielding effectiveness. The results also indicate that high use crew areas need to be enveloped by an extended protection method. Through proper distribution of inherent mass (consumables, equipment, structure, etc.) it may be possible to obtain

This page was intentionally left blank.

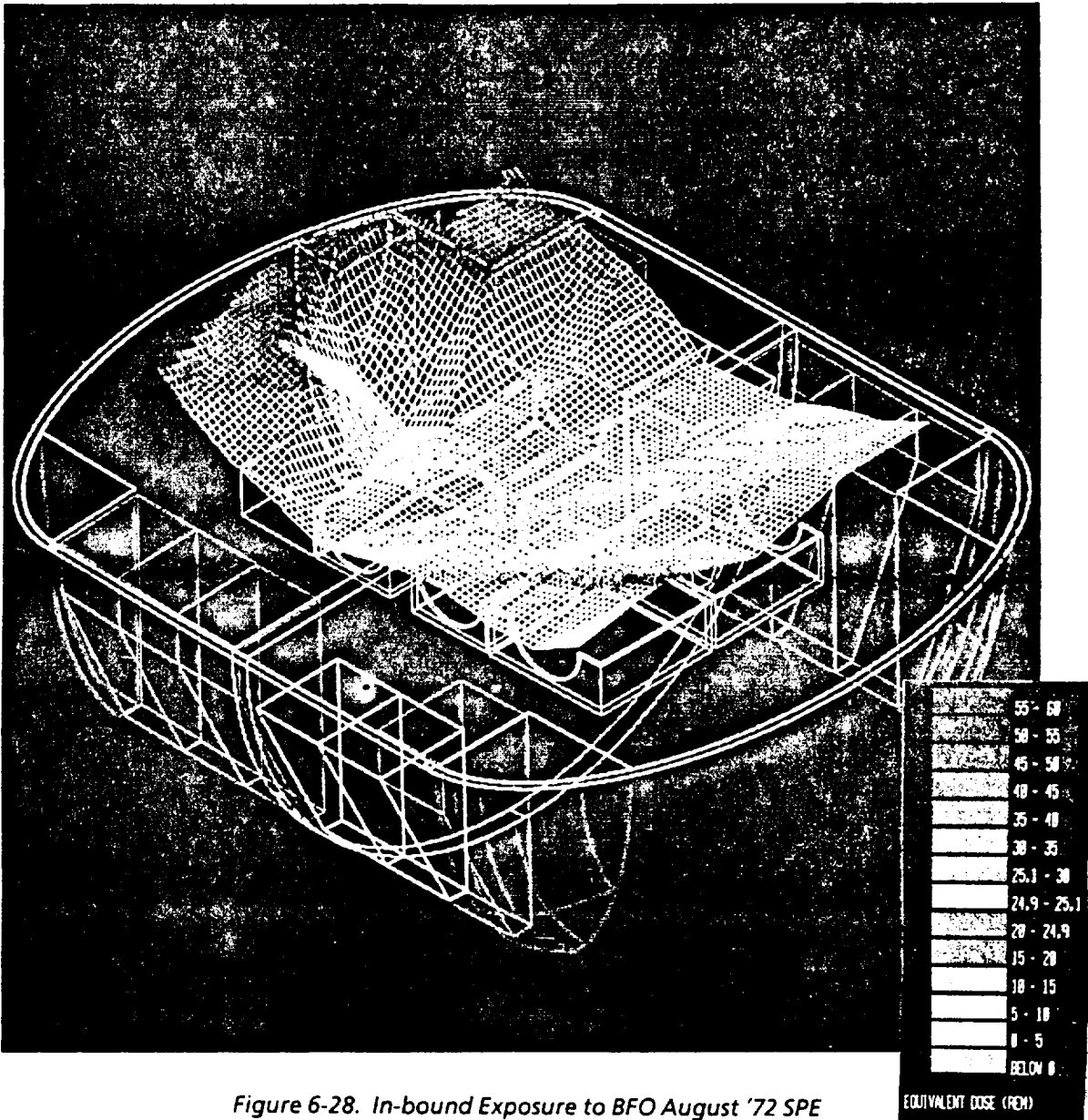


Figure 6-28. In-bound Exposure to BFO August '72 SPE

closure for these high use regions. The intent in enclosing the larger area is to both provide protection from acute as well as constant sources.

The redesign effort of the habitat module moved to correct the protection deficiencies of the earlier concept. Crew quarters were moved into an area where more of the inherent mass could provided added protection. The *Brem* analysis shows that we have taken a step forward in providing astronaut protection. The results would not be classified as having met NASA's method of ALARA (As Low As Reasonably Achievable), but did show promise. The corrective measures did indicate that high use regions could be enveloped by stored mass. Shielding was limited to simply positioning mass and did

This page was intentionally left blank.

not evaluate safe-haven or storm shelter regions. Through analysis and redesign it is possible to define the area and the material desired for the core of the shielding concept.

Analysis of the CRV served to characterize the radiation environment within the vehicle. The probability of SPEs of such magnitude (October 19, '89 class) occurring during this phase of the mission are exceedingly remote. However, this is a mission phase when crew will have no option but to leave the protection of the habitat. The exposure would be effected by a dynamic transmission function as the crew proceeds through the Earth's magnetic field. As the crew approaches LEO, geomagnetic shielding capabilities will increase. This natural shielding was not taken into account in this analysis. When missions one day fly, it will be necessary to evaluate all potential risks to the crew, this being one of them. Exposures are expected to be much the same as those experienced by the Apollo astronauts as returning crews pass directly through the trapped radiation of the Van Allen belts.

It is evident from this study that radiation analysis must start during the design phase. At the very least, stowed consumables and equipment can and should support the protection strategy. High use areas such as the crew quarters and galley should provide added protection that can be utilized in case of a solar proton event and from the constant GCR flux.

The questions and concerns regarding crew risks to ionizing radiation and methods to reduce these potential risks abound. The current state of understanding is far from acceptable. Significant work is being performed at NASA, DoD, DOE and universities to close the gaps. However, fundamental uncertainties remain; uncertainties which some estimates predict could have analysis results in question by as much as a factor of two. Unless research into such areas as radiobiological effects, transport theory, nuclear cross-section determination and environment modeling increase and become more precise, we must be willing to address the way exploration missions are to be flown or accept greater biological risk to the crew. Potential "grass-root" solutions regarding each of these issues include: (1) an acceptance of potentially higher cancer rates; (2) increasing dedicated space craft shielding to compensate for various uncertainties; this solution has a direct impact on total vehicle mass and hence, IMLEO; and (3) reduce crew exposures by considerably reducing trip times. All of these solutions will have major implications to the program such as complexity, mass, and cost. Our investigations have focused on a single avenue of providing astronaut protection. Although significant in method and result, there is a tremendous amount of work to be accomplished. Our goal has been to provide the best possible protection using existing mass to reduce the potential shielding burden.

7.0 ELECTRIC PROPULSION PERFORMANCE PARAMETRICS

A software tool is being developed that will make the analysis of low thrust interplanetary spaceflight easier, faster, and more accessible than is possible with present-day, state-of-the-art technology. This simplification is to be accomplished through the design of a software system (PROMULGATE) that uses a database of precalculated one-way, minimum-propellant trajectories to produce a complete multileg trajectory that is optimized with respect to a performance index specified by the user. This technique will eliminate the more serious difficulties inherent in typical low thrust mission analysis programs, such as the requirement to find sufficiently accurate starting values for the solution search, and a host of convergence problems that invariably arise which are case-dependent. The accuracy of the solutions, although less than that of solutions optimized using calculus of variations, is adequate for a wide range of applications. This work is being performed under a contract to AdaSoft, Inc.

The current work is to produce a proof of concept. The range of data for the demo is restricted to a single opportunity and is appropriate for the optimization of an Earth-Mars-Earth trajectory. The details of the design of PROMULGATE itself and of the database that houses the data are dealt with in the specifications document, reference 24. The layout of PROMULGATE is shown in figure 7-1.

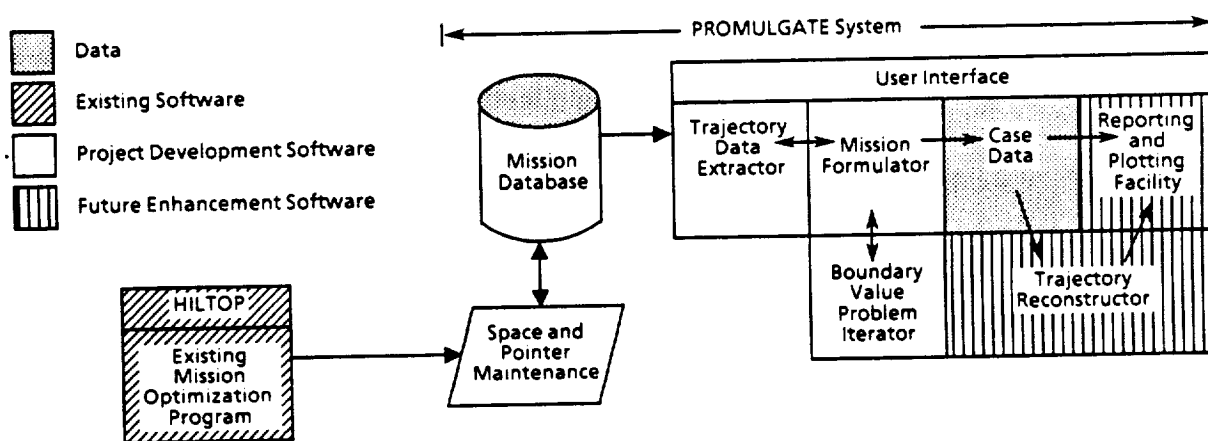


Figure 7-1. Low Thrust Mars Mission Mapping Project Software Systems

7.1 INTERPOLATION SCHEME

The database houses data for one-way trajectory legs between specified solar system bodies. Each record in the database corresponds to a point in a six-dimensional grid of independent parameter values where the independent parameters are —

- a. Launch date.
- b. Flight time.
- c. Specific impulse.
- d. Excess speed at departure.
- e. Excess speed at arrival.
- f. Initial thrust acceleration.

In order to perform the required trajectory optimization, the software must be able to interpolate the values of the dependent parameters on the grid of independent parameters. From the list of independent parameters, the first five produce a grid that is "regular", which means that the set of values in the database for any one of the five parameters is the same for every fixed value of the four. For instance, examination of the points in the five-dimensional space of parameters that corresponds to a launch date 50 days prior to opposition, a flight time of 150 days, and departure and arrival excess speeds of zero, shows that values of the specific impulse for that choice are the same as the values for any other set of those first four parameters. It is not possible to do the same for all six of the independent parameters, because for a given set of the first five parameters, there is a minimum initial thrust acceleration, and that minimum value differs from point to point. The interpolation scheme chosen has to take into account the nature of the six-dimensional grid of independent parameter points and has to return sufficiently accurate results for the dependent parameters.

The result of linear interpolation on values of the effective delta-V for the range of specific impulse of probable interest in the analysis of near-term Mars missions is shown in figure 7-2a. The symbols show the values of actual data points, and the lines represent the least-squares, best-fit lines through the data points. Four flight times were used, and for each a value of the thrust acceleration near the minimum for that time was chosen. The launch date is the same for each case and only trajectories with zero excess speed at departure and arrival were considered. The equation of the best-fit line for each case, correlation coefficient (r^2), flight time, (F.T.), and thrust acceleration, (a_0), are indicated on the figure. (A correlation coefficient of one corresponds to a perfect fit of the data.) The linear fit was not sufficiently accurate (i.e., the correlation coefficients were not close enough to unity), and after attempting

several different polynomial fits, it was concluded that a cubic fit was adequate for current purposes. The results of using a cubic fit on one of the curves of figure 7-2a is shown in figure 7-2b. Two cubic fits were calculated using two sets of the independent variable (Isp) from the data corresponding to a flight time of 260 days. The equations for the two cubic fits are shown in figure 7-2b. The first cubic fit was calculated using data corresponding to specific impulse values (in seconds) of 4,000, 6,000, 8,000, and 10,000. The second cubic fit was calculated with data corresponding to specific impulse values (in seconds) of 3,000, 6,000, 9,000, and 12,000. The cubic fits were calculated using a Lagrange interpolate so the correlation at the four specific impulse values used for each cubic fit is unity.

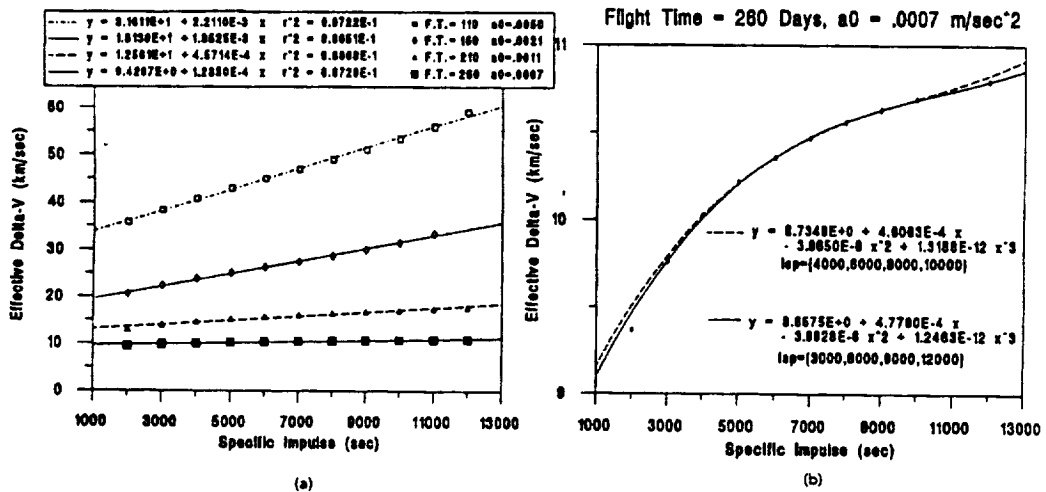


Figure 7-2. Comparison of (a) Linear and (b) Cubic Interpolations

Cubic interpolations for a range of flight times and thrust accelerations are shown in figure 7-3. The curves represent flight times ranging from 110 days to 260 days. The thrust accelerations represented are the minimum thrust acceleration for each flight time and a thrust acceleration approximately twice the minimum for each flight time. The equations for the cubic interpolates are stated at the top of the figure and the specific impulse values (in seconds) used to compute the cubic fits are 4,000, 6,000, 8,000, and 10,000.

The variation of the costate variables as a function of specific impulse is shown in figure 7-4. The curves shown are not the result of cubic interpolation, but are included to show that the other dependent variables, being well behaved, do not pose any new problems for interpolation with cubic polynomials.

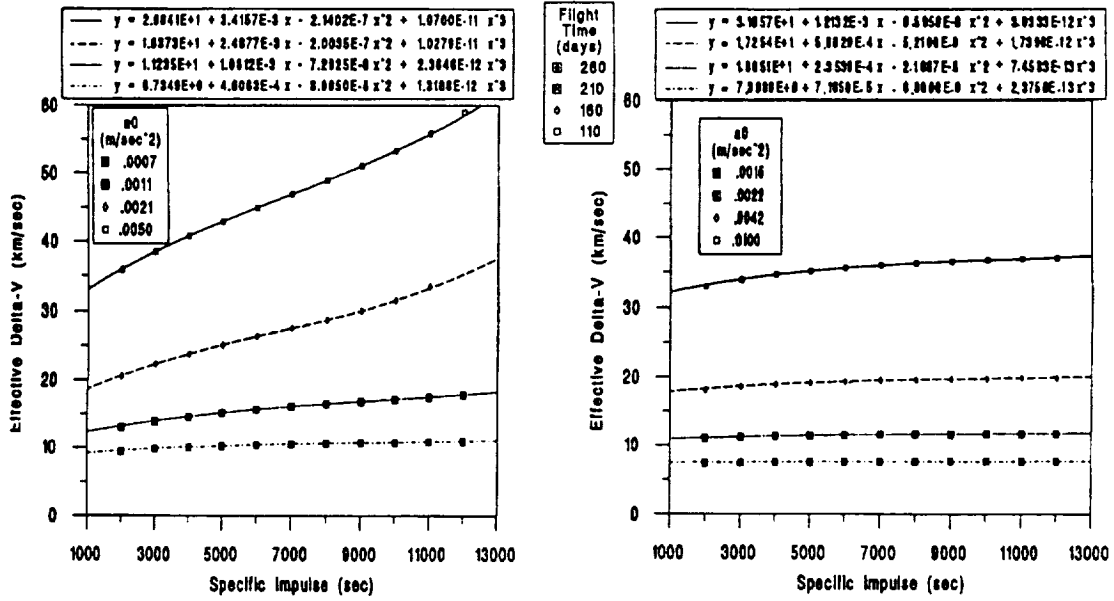


Figure 7-3. Cubic Interpolations for Several Values of Flight Time and Trust Acceleration

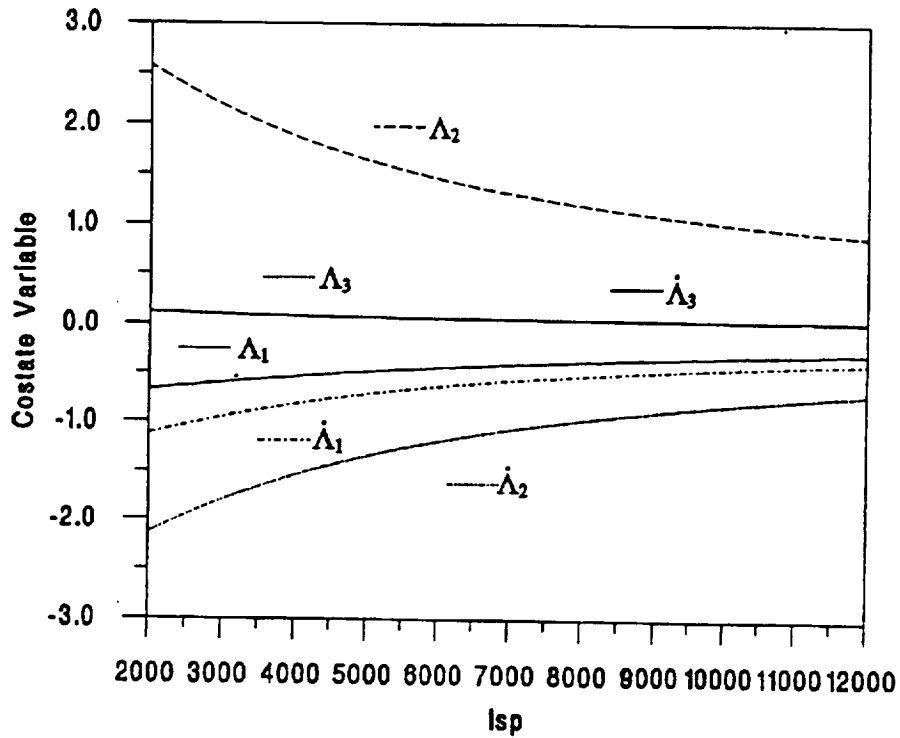


Figure 7-4. Variation of Costate Variables with Isp

While a single cubic interpolate seemed to work for the entire range of interest of specific impulse, the variation of effective delta-V with thrust acceleration was much more sensitive and required several cubic interpolates to fit the range needed. The reciprocal of the effective delta-V was better fit by a cubic interpolate than the effective delta-V itself. The result of fitting five separate cubic interpolates to the range of thrust accelerations of 0.7 to 3 mm/sec², for a specific impulse of 12,000 seconds and a flight time of 260 days is shown in figure 7-5. Each of the five interpolates is represented by a different kind of line. The variation of the other dependent parameters with respect to both specific impulse and thrust acceleration follows that of the effective delta-V. The variation of the dependent parameters with respect to flight time and launch date does not appear to present any special problems that would make cubic interpolation inappropriate to fit it.

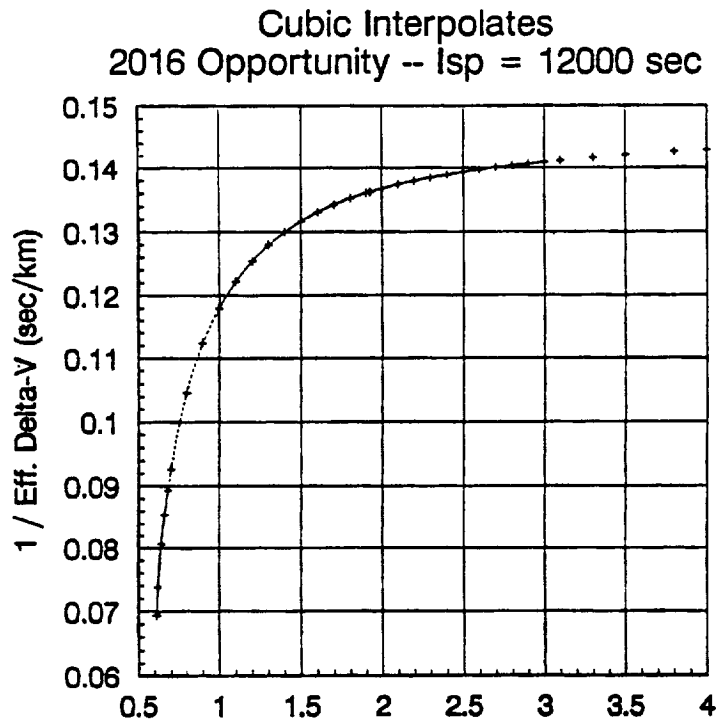


Figure 7-5. Thrust Acceleration (mm/sec²)

The result of the investigation into different interpolation methods gave way to the conclusion that a sliding cubic interpolate works for each of the independent parameters and will return sufficiently accurate values of the dependent parameters. The fineness of the grid will be different for each of the independent parameters. It is the fineness of the grid that will determine the number of one-way trajectories that must be calculated initially for the code to be able to perform the optimization.

7.2 SPECIFICATIONS DOCUMENT

The design and structure of the software package PROMULGATE and the database that stores the trajectory information used by PROMULGATE are given in reference 24. The document states the overall purpose of the system, provides the mathematics needed to take the optimum one-way trajectory legs, constructs a complete optimized trajectory, and describes the design and structure of the database that houses the information required by PROMULGATE.

7.3 DATA GENERATION

Work proceeded on the calculation of one-way trajectories for a four dimensional grid of points that will be used in the proof of concept. A 2026 launch opportunity is being used to generate the data and the independent parameters such as specific impulse, thrust acceleration, launch date, and flight time are being varied. For the purposes of the demo, only cases with escape and arrival hyperbolic excess speeds of zero are considered. The final product will have a six-dimensional grid of independent parameters as variable excess speeds are allowed at both ends of the trajectory.

7.4 INTERPOLATION SUBROUTINE

The subroutine used for the six-dimensional interpolation was constructed by adapting several routines from reference 25. The interpolation routine was tested on several different analytical functions and worked properly. The accuracy of the interpolation itself will depend on the spacing of the data points. Because of the requirements on the allowed values of the initial thrust acceleration, the six-dimensional grid of independent parameter points is not regular in that variable. Although the interpolation routine was designed to be used on a regular grid because only one parameter has values that are irregularly spaced, it is possible to perform the six-dimensional interpolation by interpolating on the irregular variable first. This provides the values of the dependent parameters that are needed to complete the interpolation on the five-dimensional, regular grid of the remaining variables.

In order to perform the interpolation, it is first necessary to locate the six-dimensional hypercube that encompasses the given point in independent parameter space. As explained in the specifications document, a database record contains the address of the record that has the next higher and next lower value of each of the independent parameters. By always entering the database at the point that has the minimum value for each parameter, a forward step can be taken in one parameter direction until the first data point that has a value of that parameter greater than the given value is found. The same procedure is followed for each of the other parameter directions, making sure that the thrust acceleration is done last. It is then an easy matter to move to the adjacent grid points that are needed to perform the interpolation. If all six parameters are being varied in the optimization, each interpolation will require 4,096 data points. The code will check to see if certain of the parameters are being held fixed at exact grid points. In that case, they don't need to be interpolated. Because PROMULGATE solves the optimization problem by calculating partial derivatives of the dependent parameters with respect to the independent parameters, it may be worthwhile to calculate the coefficients of the cubic interpolates in each of the six parameter directions as this will make the calculation of the partial derivatives much faster. These coefficients can be calculated at the same time that the interpolation itself is being performed.

8.0 FLIGHT MECHANICS SUPPORT

8.1 INTRODUCTION

Trajectory analyses have been performed consistent with the recommendations of the Synthesis Report, reference 2. The analyses primarily reflects an investigation of Mars missions of Architecture I and IV of the Synthesis Report. The following guidelines were held throughout the analyses:

- a. The initial cargo mission leaves in the preceding opportunity to support the first piloted mission (2014 or 2016).
- b. The first piloted mission will be an opposition type (stay times from 30 to 100 days) with a return Venus swingby.
- c. The subsequent cargo missions will arrive at Mars while the astronauts are on the surface.
- d. Subsequent piloted missions (after the first) will be fast transfer conjunction missions (Mars stay times approximately 600 days).
- e. The propulsion system will be nuclear thermal.

There are several options and issues that are addressed in the following sections. Options to the Mars missions that were investigated included abort modes/profiles, transfer trip times, landing site accessibility, and circular versus elliptic parking orbits. In addition, several related issues were addressed on a mission-by-mission basis: outbound/return launch windows, fast transfer conjunction delta-V, mission abort delta-V, L/D needed for daylight landing, and losses such as g-loss, plane changes, and apsidal misalignment.

8.2 THREE-BURN EARTH LAUNCH WINDOW ANALYSIS

Human exploration mission launches to Mars occur from a particular parking orbit, i.e., the assembly orbit, unless a very large vehicle can launch the entire Mars space vehicle in a single launch. Present concepts for SEI piloted Mars missions do not anticipate such large launchers.

The problem with launch from the assembly orbit is that the orbit line of nodes regresses rapidly, about 7 degrees per day, and the departure S -vector becomes rapidly far enough out of plane to cause large plane change delta-V penalties. This large penalty can be ameliorated by three-burn departures from Earth parking orbit. The first burn places the Mars vehicle in a highly elliptic orbit; the second burn makes a plane change at apogee so that the elliptic orbit contains the S -vector; the third burn at perigee of the elliptic orbit achieves trans-Mars injection energy. The geometry is shown in figure 8-1, where all orbits are drawn as ground tracks for simplification.

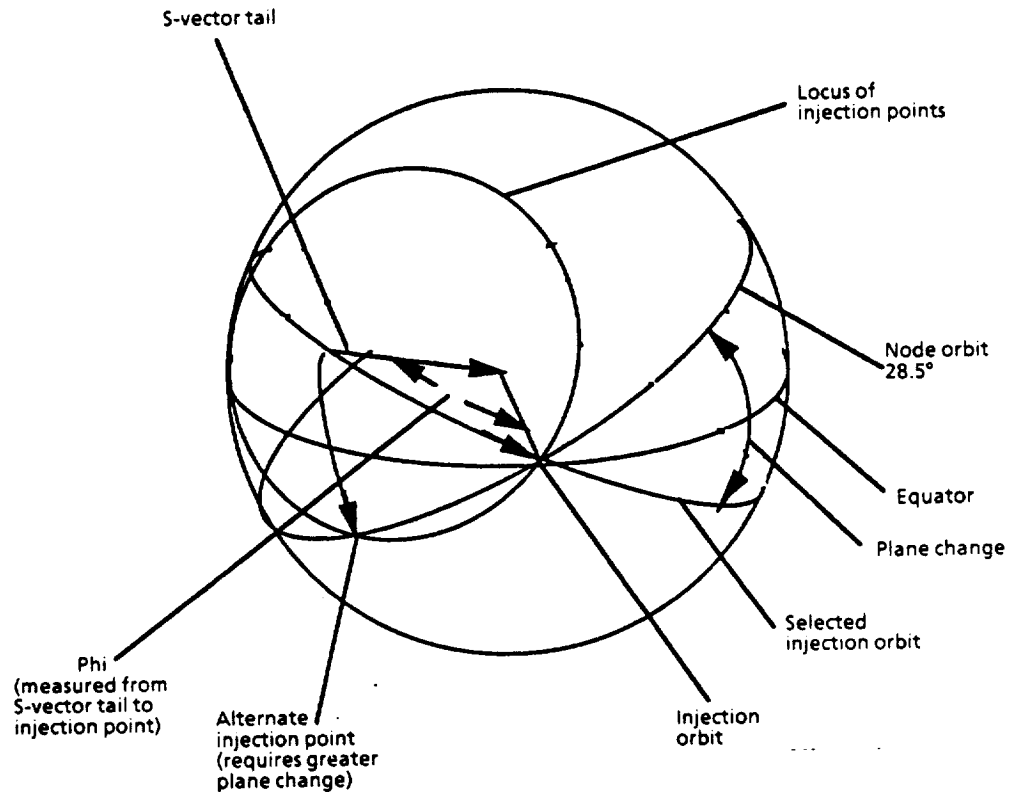


Figure 8-1. Three-Burn Departure launch Window Diagram

8.2.1 Analysis Approach and Discussion

The following steps were taken in performing the analysis:

- a. The trans-Mars injection trajectory is hyperbolic at Earth; thus, the injection point (periapsis of the Earth departure hyperbola) occurs after passing the S -vector tail. In this analysis the angle is designated as ϕ , and its variation with injection energy is shown in figure 8-2. The vehicle can fly in any direction from the S -vector tail through the angle ϕ and make a TMI impulse, attaining the desired S -vector. Therefore, there is a circular locus of injection points.
- b. The actual trans-Mars injection is a finite burn, lasting 15 to 30 minutes for a typical NTP thrust-to-weight ratio. However, the periapsis vector is quite "stiff" during this maneuver, and moves less than 5 degrees. (The burn starts approximately 35 degrees before periapsis of the elliptic orbit and ends 30 to 60 degrees past periapsis of the now hyperbolic path.) These results were obtained using non-optimal finite-burn simulations. The location of periapse relative to cutoff condition was determined from the following equation:

$$\text{True Anomaly} = \text{Cos}^{-1}\{[a(e^2 - 1) - r]e/r\}$$

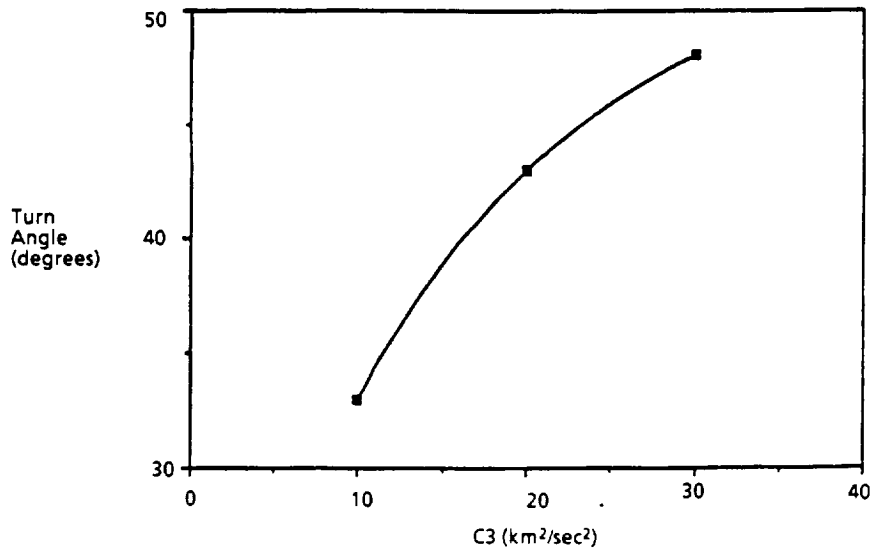


Figure 8-2. Turn Angle Versus TMI C3

- c. Where the locus of injection points crosses the node orbit ground track, an impulsive insertion into the initial elliptic orbit can be made, placing the apoapse on the dihedral line between the initial elliptic orbit and a feasible insertion orbit. There are two such points; one will exhibit greater plane change than the other. The apoapses of these two points are the ones desired for plane change into the insertion orbit. That point yielding the least plane change is the one chosen.

The actual insertion into the initial elliptic orbit is also a finite burn. At an initial thrust-to-weight of 0.1, a typical nuclear rocket Isp of 925, and an arbitrarily-chosen C3 of 20 km²/sec², the burn covers about 125 degrees and drags periapsis about 60 degrees in the process. Thus, the burn must be initiated at a point that places the line of apsides correctly.

- d. The "V" vectors that point to the injection points are specified by three conditions:
1. The angle between the **S**-vector tail and the injection point is ϕ , hence $\mathbf{V} \cdot \mathbf{S} = \text{Cos}(\phi)$,
 2. The angle between the orbit vector, **O**, and the injection point is 90 degrees, hence $\mathbf{V} \cdot \mathbf{O} = 0$,
 3. The vector **V** is a unit vector, hence $\text{magnitude}(\mathbf{V}) = 1$.

These three equations in the three unknowns of the **V** components are solved in a classical quadratic equation.

8.2.2 Earth Launch Window Analysis Results

Results for the 2014 reference trajectory (200-day Mars transfer) are shown in figure 8-3. This opportunity has a declination of launch asymptote (DLA) of about 4 degrees. The value of C_3 is about $10 \text{ km}^2/\text{s}^2$, and ϕ is about 30 degrees. Large plane changes (70 degrees) are required for a 2014 worst case scenario.

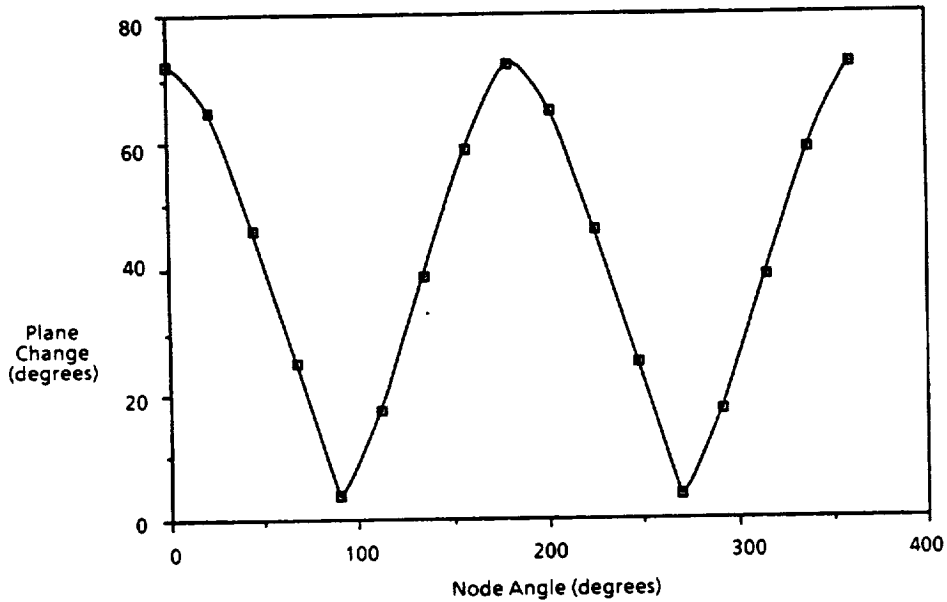


Figure 8-3. Plane Change Requirements for 2014 Mars Opportunity, 200-Day Transfer

Results for the 2014 reference trajectory with 150-day transfer are shown in figure 8-4. The shorter trip time (reduced by 50 days) means going to a higher C_3 . DLA remains about 4 degrees, and ϕ is about 50 degrees, yielding a larger injection locus circle. Given the larger injection locus circle, the worst case plane changes are less (approximately 45 degrees). When launch window considerations are included, the penalty of going to higher C_3 is somewhat compensated for by reduced plane change requirements. The apogee plane change delta-V for orbit periods from 24 to 96 hours is shown in figure 8-5. In view of the significant reduction in delta-V for greater periods, a 72-hour intermediate orbit is recommended.

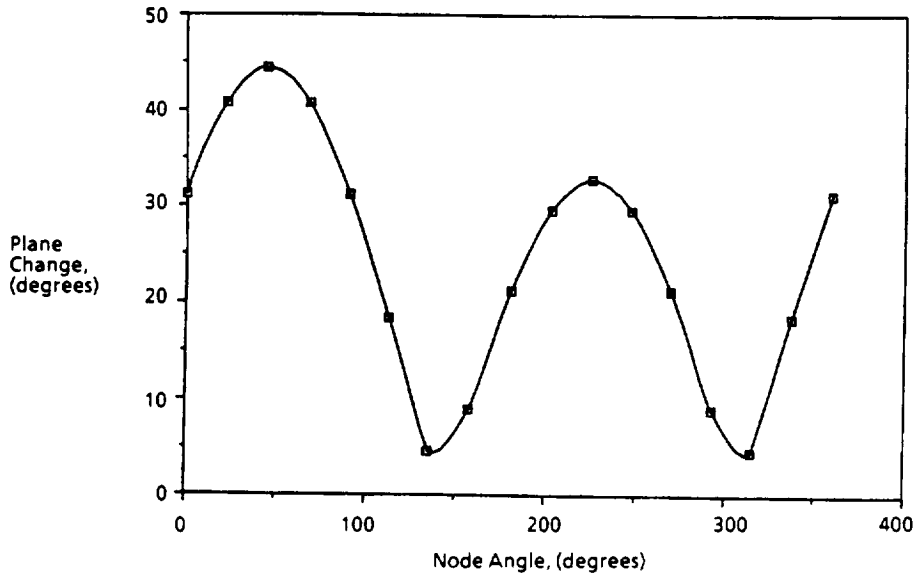


Figure 8-4. Plane Change Requirements for 2014 Mars Opportunity, 150-day Transfer

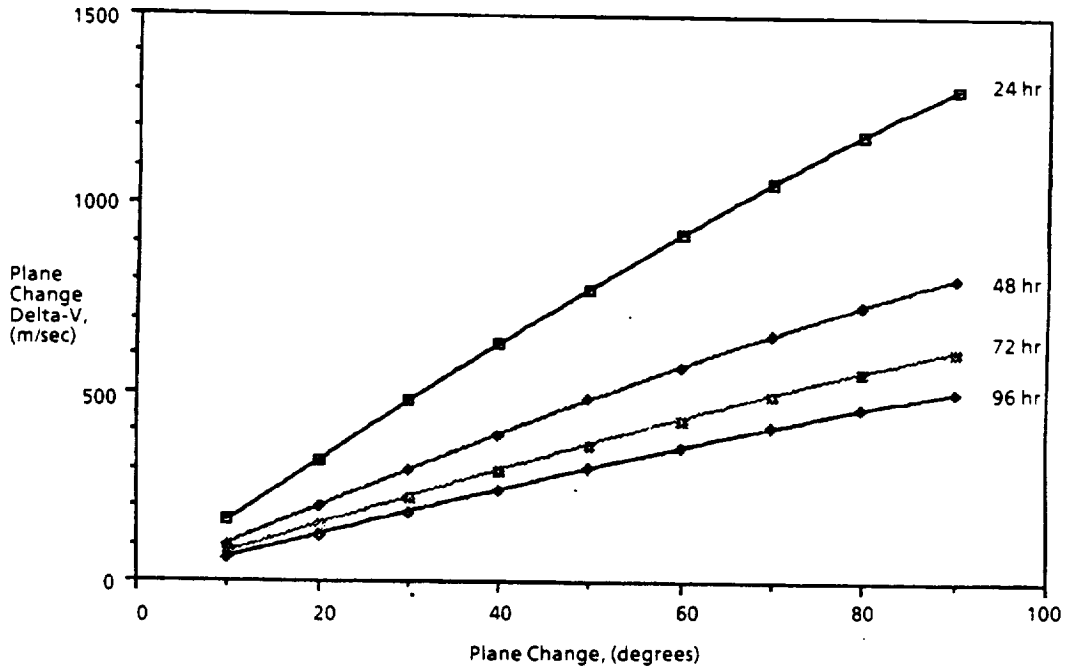


Figure 8-5. Plane Change Delta-Vs for Range of Elliptic Orbit Periods

In the 2014 opportunity, the 150-day Mars transfer represents the latest reasonable date to depart; Earth launch C3 for this 150-day transfer is approximately $35 \text{ km}^2/\text{sec}^2$, the largest Earth departure C3 considered for this analysis. Longer transfers leave earlier with essentially the same Mars arrival date. Therefore, the 150-day transfer is considered "window closed". For a 25-day launch window, "window open" occurs 25 days earlier with C3 about $14 \text{ km}^2/\text{s}^2$. A detailed description of launch windows and their associated contours providing C3 values is given in section 8.4. Adjustment of the node orbit altitude over a range of about $\pm 60 \text{ km}$ for 2 years prior to the launch can strategically place the node line at window closed, yielding the minimum plane change of 10 degrees. The worst case plane change will then occur about 5 to 10 days after window opens with C3 about $20 \text{ km}^2/\text{s}^2$. The following approximate delta-Vs are provided over the range of C3 corresponding to the aforementioned windows:

	Window Open	Worst Plane Change	Window Close
C3 (km^2/sec^2)	14	20	35
Impulsive (m/s)	3785	4045	4700
Finite Burn (m/s)	200	250	320
Plane Change (m/s)	300	350	100
Total Delta-v (m/s)	4285	4645	5120

These finite-burn and plane change losses assume all plane changes occur at apogee. A full optimization of the 3-burn trajectory would reduce the delta-V slightly.

8.3 CARGO MISSIONS DELTA-V ANALYSIS

A bar chart indicating delta-V sets for Mars cargo missions, with Level-II and Boeing data juxtaposed for comparison, is shown in figure 8-6. The bars designated as "Level-II Impulse" do not include losses and represent Level-II data from NASA Johnson Space Flight Center. Level-II data "with losses" have losses included as indicated in the footnote. The parking orbits defined by Level II for piloted missions are for a 500 km circular orbit. Boeing missions include losses of similar nature as those added for Level-II, but the piloted missions have elliptical parking orbits chosen to yield a reasonably large periapsis lighting angle (to ensure daylight landing) and a low departure delta-V.

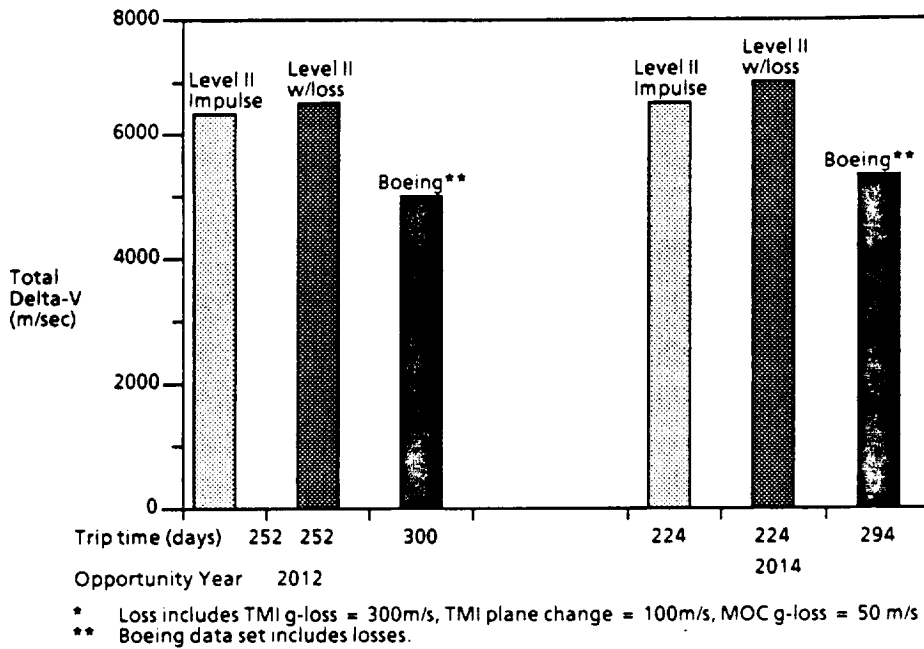
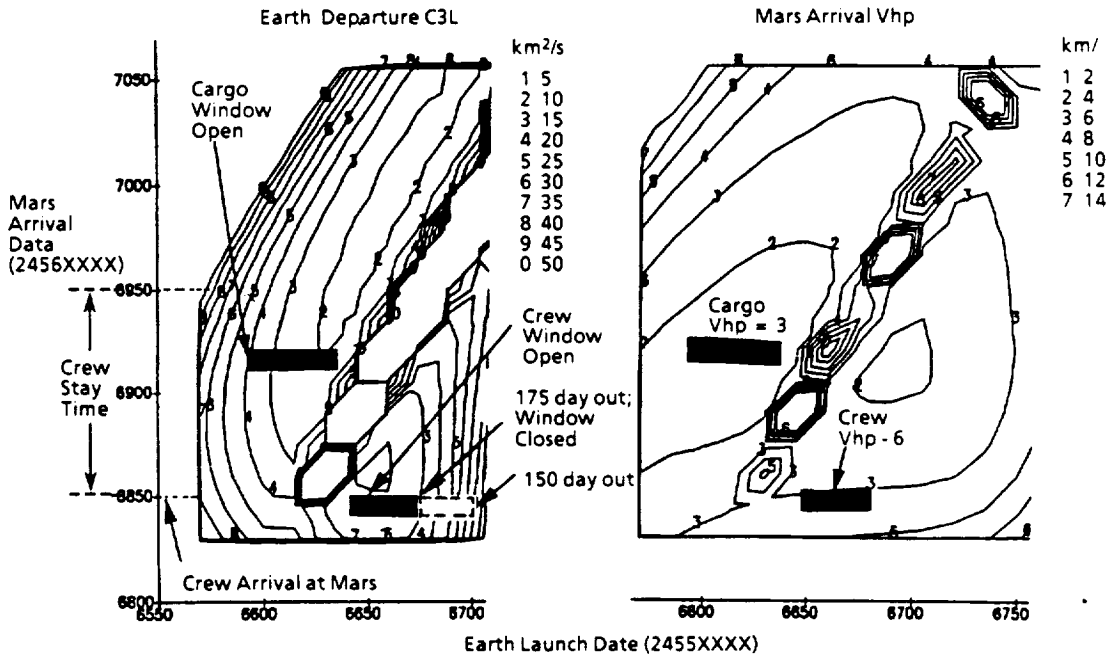


Figure 8-6. Mars Cargo Missions Delta-V



* 2014 Cargo arrives 30-50 days before crew departure from Mars

Figure 8-7. 2014 Cargo and Crew TMI Window

Observations concerning the cargo mission delta-V set are as follows:

- a. Boeing's shorter transfer times, as compared to Level-II transfer times, and elliptical parking orbits yield a lower total mission delta-V.
- b. TMI and MOC losses are a significant component of the overall delta-V budget.

8.4 EARTH/MARS LAUNCH WINDOWS

An Earth departure C3 contour and a Mars arrival Vhp contour for the mission opportunity year 2014 are shown in figure 8-7. The dark bars on the contours indicate the possible launch window extent for the 2014 opportunities. The Earth launch window, as shown by the lower dark bar, for the 2014 piloted opportunity is greater than 30 days (175 days out = window closed) and the cargo Earth departure window, indicated by the upper dark bar, is about 40 days long. The cargo window is earlier than the piloted mission and in the longer transfer part of the C3 contour; thus, the cargo and piloted launch operations are more independent, and yet the cargo mission can arrive while the piloted mission is on the Martian surface.

The return C3 contour for the 2014 piloted mission opportunity is shown in figure 8-8. The large upper lobe defines the Venus swingby mission space for 2014 and the lower part of the contour depicts the direct return opportunity. This contour indicates that the Mars launch window for a return Venus swingby is approximately 50 days. The concomitant Earth return Vhp for this same swingby opportunity is shown in figure 8-9. A window closed maximum Vhp is approximately 5.5 km/s, yielding a CRV Earth atmosphere entry of 12.1 km/s. This Earth entry velocity is within the limits for TPS requirements.

Concerning the 2014 window analysis, figure 8-10 shows curves relating Mars departure delta-V to days from nominal return (return window closed). The bottom curve, periapsis-to-periapsis transfer, represents departure delta-V for elliptical orbits, but the losses for plane change and apsidal rotation are not included. The top curves indicate departure delta-V curves as those relate to arrival over the north and south hemispheres of Mars. Lastly, the star on the nominal return line shows the delta-V required for departure from a circular orbit of 500 km altitude. The north approach is chosen as our nominal mission due to its relatively lower departure delta-V. The window for this nominal mission is greater than 50 days where the reference maximum delta-V is chosen at the nominal return date of 2456950 (10/19/14).

Deep space maneuver contours of Mars departure C3 and its concomitant Earth arrival Vhp are shown in figures 8-11 and 8-12. For the nominal departure date of 2456950 (10/19/14) the C3 value is significantly higher than the C3 for the Venus swingby

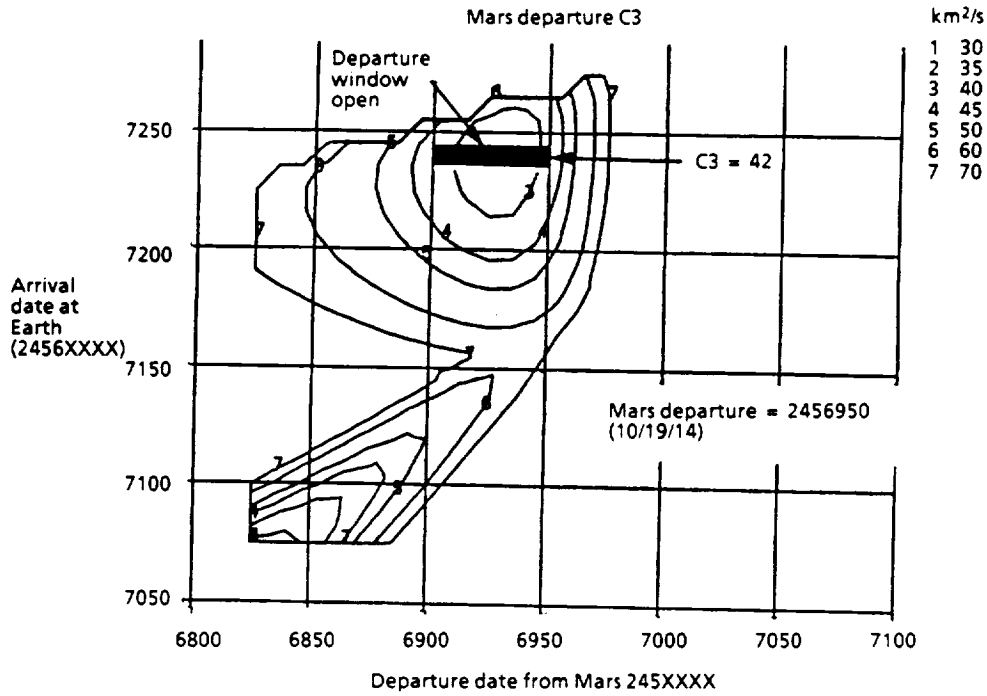


Figure 8-8. 2014 Crew Return Window

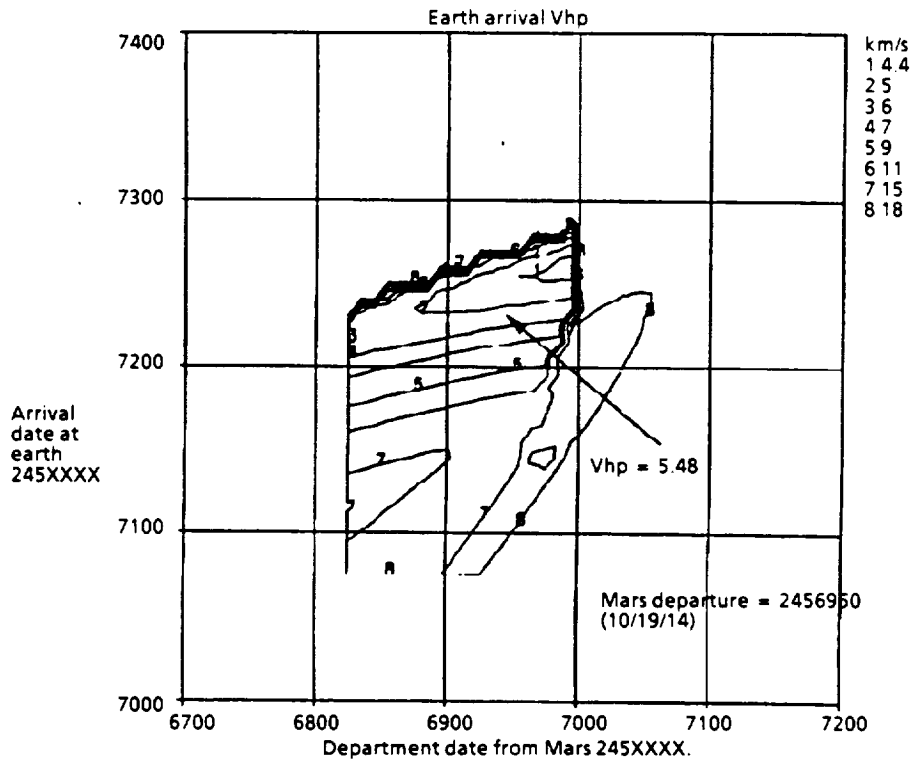


Figure 8-9. 2014 Crew Return Vhp at Earth

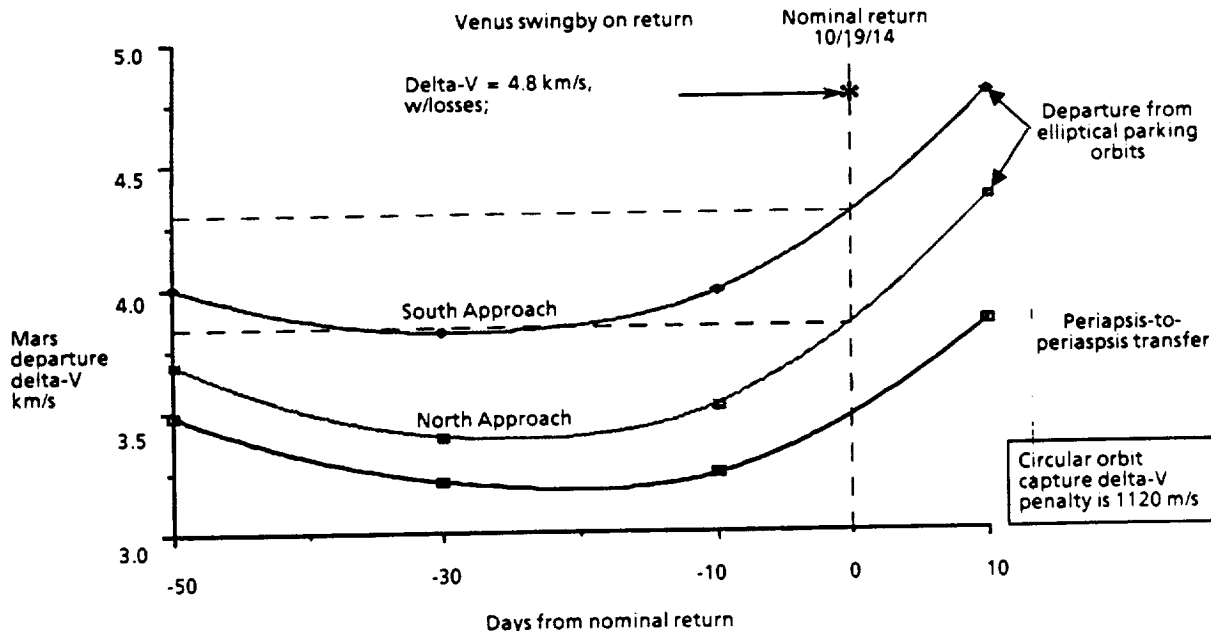


Figure 8-10. 2014 Abort From Surface Window Analysis

scenario. It should be noted that the Earth return V_{hp} (see figure 8-12) is close to the Venus swingby V_{hp} (see figure 8-9). The trip time, however, may be reduced significantly but at a greater cost in overall delta-V from Mars departure and deep space maneuver contributions. Other information that may be derived from the contours include the following:

- Direct Mars return has high $C3 \approx 70 \text{ km}^2/\text{s}^2$ for nominal departure of 2456950; also this direct return has high Earth return $V_{hp} = 16 \text{ km/s}$, but the direct return is 75 days shorter than the Venus swingby case.
- For short stay (TEI at 2456880) the $C3$ for direct transfer is reduced to $45 \text{ km}^2/\text{s}^2$, with an Earth return V_{hp} of 14 km/s .
- Deep space burn on return for the nominal departure date yields a $C3$ at Mars departure of $65 \text{ km}^2/\text{s}^2$ and a V_{hp} at Earth of 6 km/s . This deep space burn is optimized to keep V_{hp} within a limit of 7 km/s .

Included for comparison is a set of calculations representing a 2016 Mars return window analysis performed identically to that discussed for the 2014 opportunity, figures 8-13 through 8-17. These figures are included to yield some insight into the 2016 abort from surface scenario or, in the case of 2016 being the first piloted mission, (as is provided for by the Synthesis Report) the actual return conditions. The following observations are made:

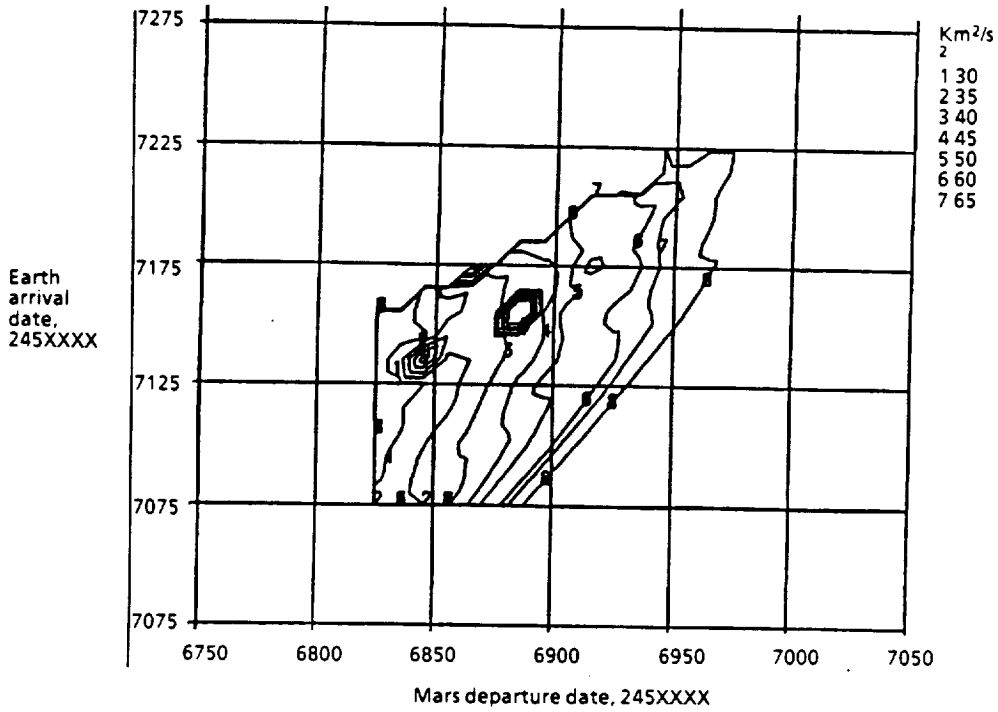


Figure 8-11. 2014 C3 Mars Departure Contour, Deep Space Maneuver

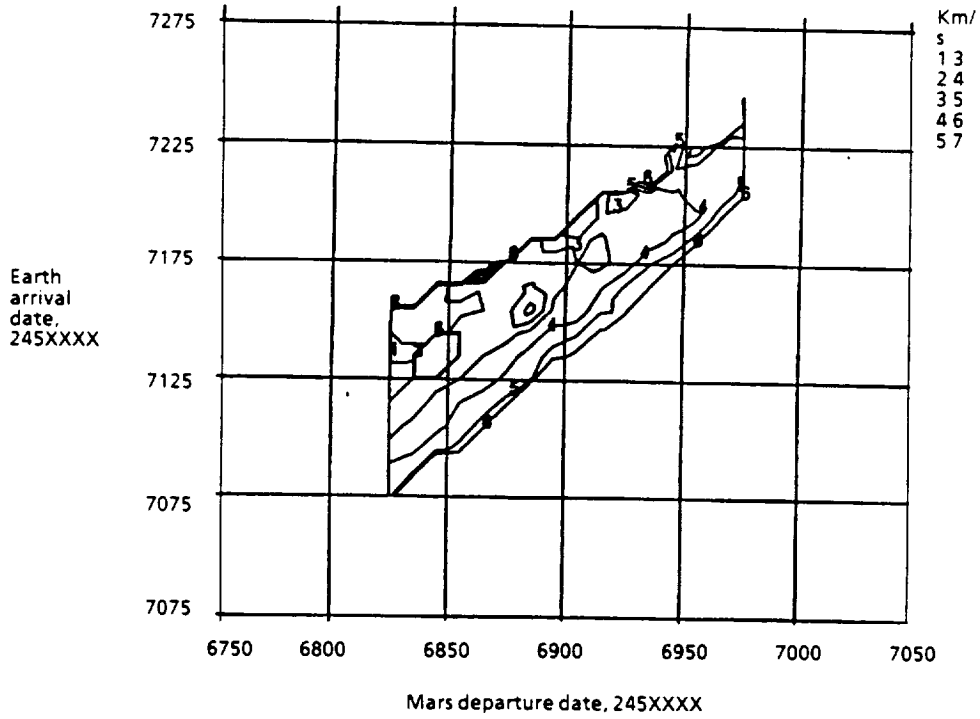


Figure 8-12. 2014 Vhp Mars Departure Contour, Deep Space Maneuver

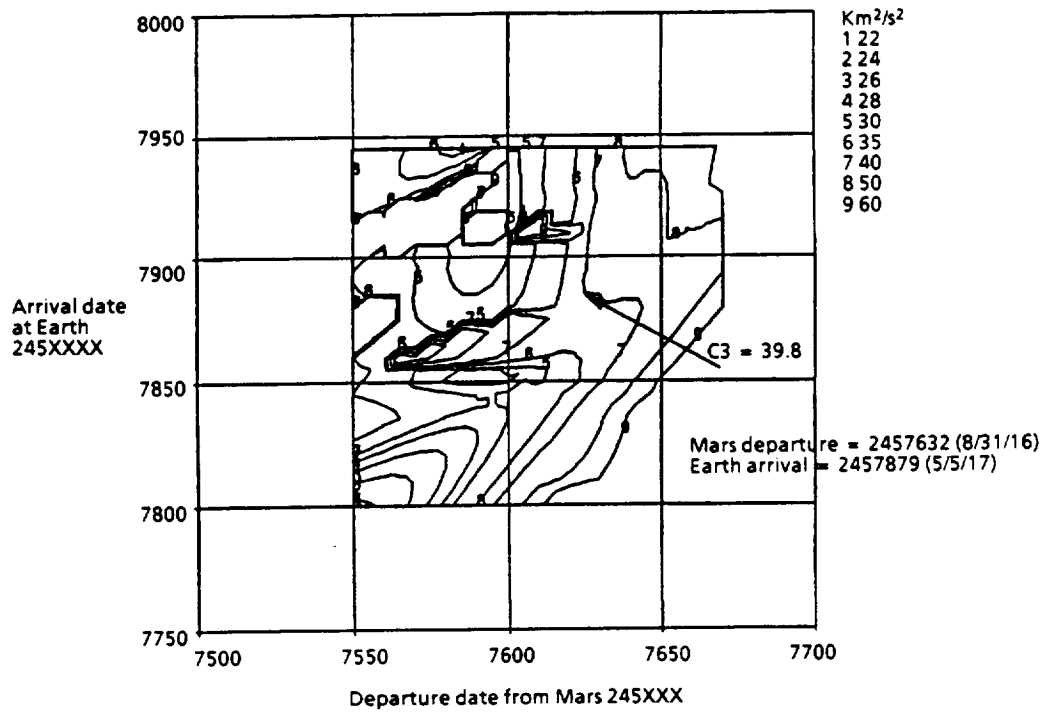


Figure 8-13. 2016 Crew Return Window

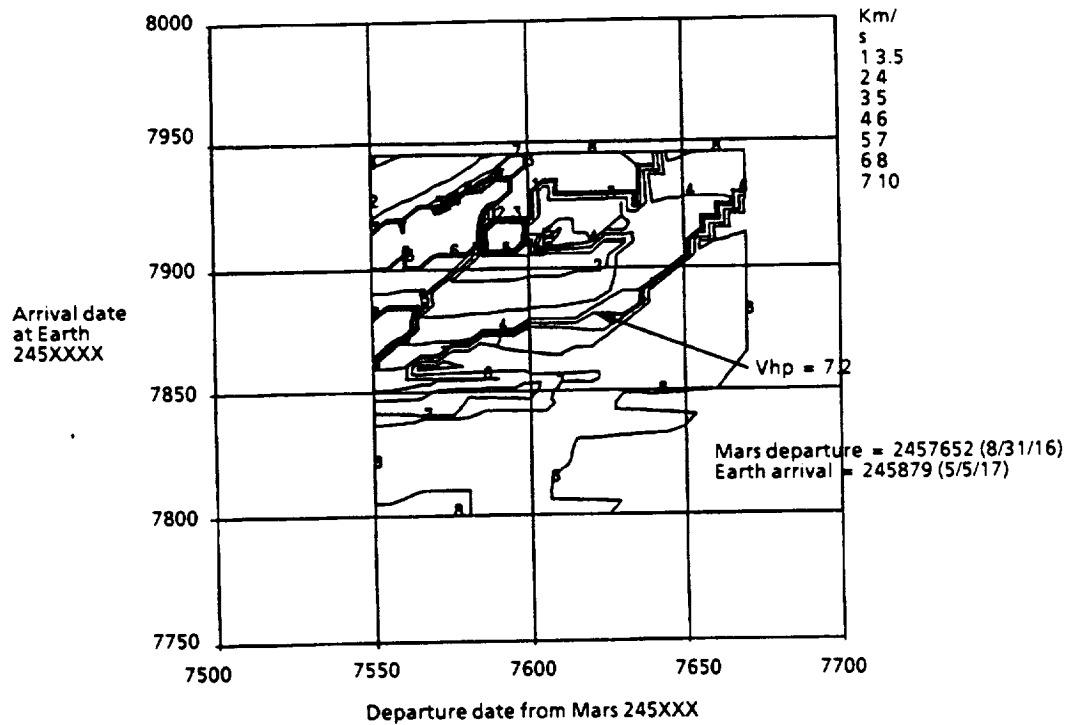


Figure 8-14. 2016 Crew Return Vhp at Earth

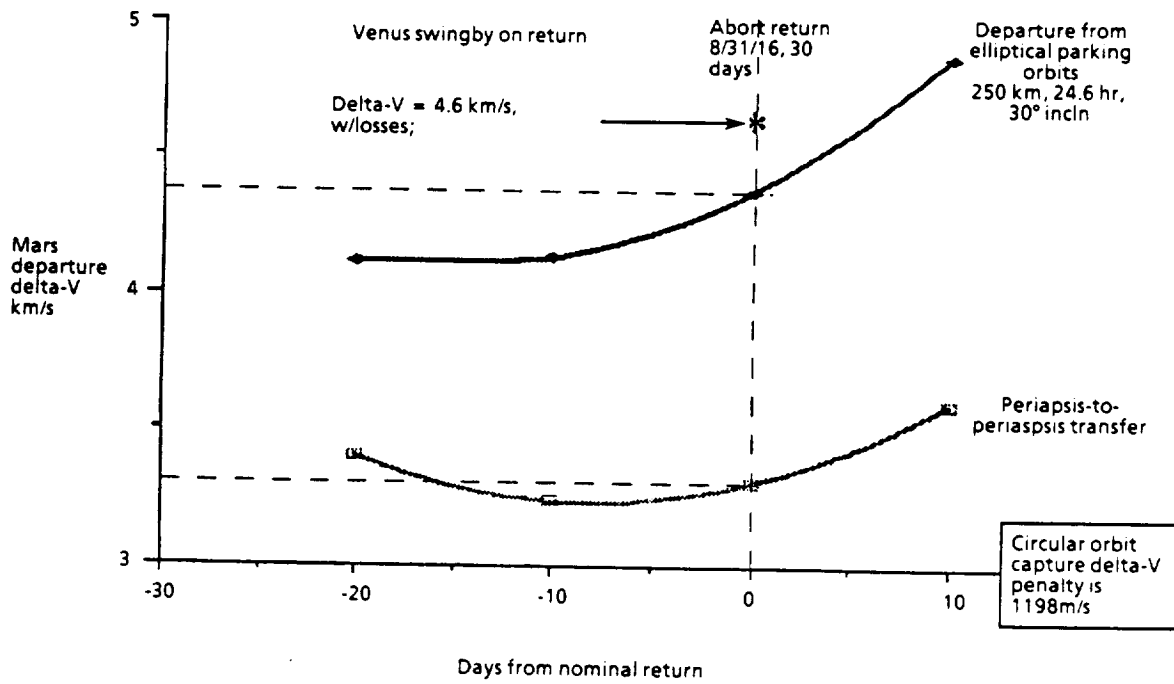


Figure 8-15. 2016 Abort From Surface Window Analysis

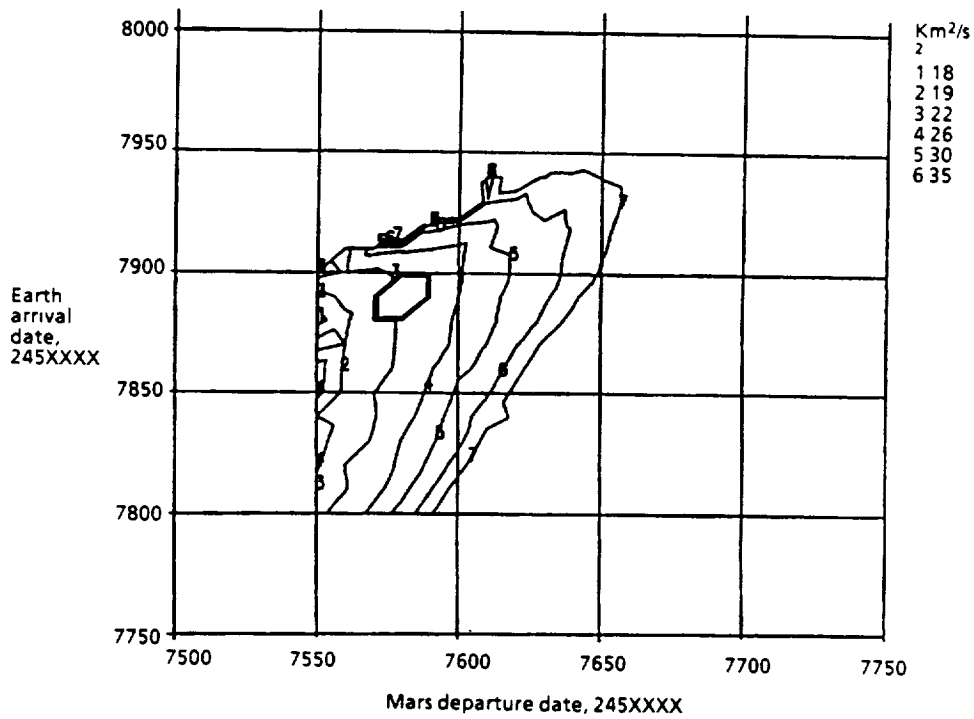


Figure 8-16. C3 Mars Departure Contour, Deep Space Maneuver

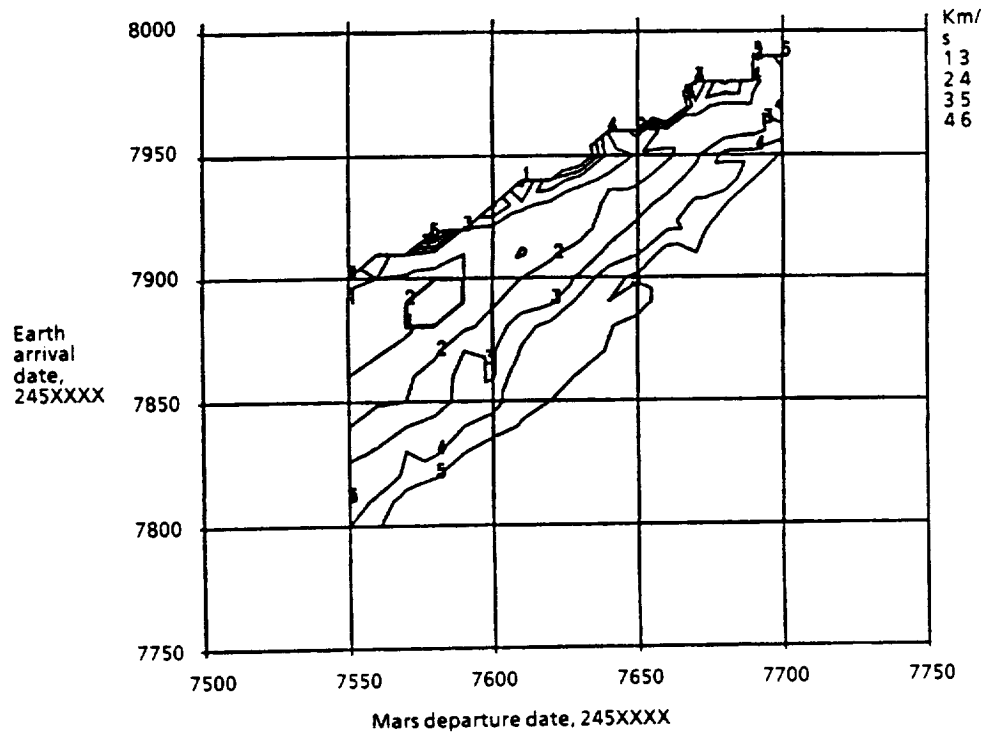


Figure 8-17. Vhp Mars Departure Contour, Deep Space Maneuver

- a. Given a nominal departure date of 2457600 (8/31/16) and a window closed C3 of $40 \text{ km}^2/\text{sec}^2$, a departure window of some 30 days is possible, figure 8-13.
- b. An Earth return Vhp of 7 km/s or less is possible over the above mentioned launch window, figure 8-14. A Vhp of 7 km/s corresponds to an atmospheric entry velocity of 12.8 km/s, within the limits set by TPS requirements for the CRV.
- c. A departure window of greater than 20 days for elliptical parking orbits is shown in figure 8-15. This departure window provides adequate abort from surface time for an early termination of the 2016 long stay mission.
- d. Delta-V savings of approximately 1400 m/s may be realized for elliptical over circular parking orbits.
- e. Deep space maneuver C3 and Vhp contours for Mars departure and Earth arrival respectively are shown in figures 8-16 and 8-17. These figures show that, for the 2016 nominal departure window, comparable Mars departure C3 and Earth arrival Vhp exist, as referenced to the Venus swingby scenario. This deep space maneuver case, however, is not highly attractive because the Mars departure C3 is about the same as the C3 for the Venus swingby case. Thus the overall delta-V for this deep space maneuver scenario is higher than the Venus swingby case because of the additive deep space maneuver.

8.5 PARKING ORBIT ANALYSIS

A 2014 interplanetary trajectory trace and parking orbit are depicted in figure 8-18 (see also section 1.4.2.2). The Mars arrival conditions (and therefore the range of possible parking orbits) are dictated by the Earth launch and Mars arrival times. For this 2014 opportunity, figure 8-19 shows the Mars departure delta-V and the Mars arrival periapsis lighting angle as a function of the arrival inclination (minimum inclination 10.7 is dictated by the latitude-of-vertical-impact, LVI, of the V-infinity vector). An optimal period and inclination was chosen to yield the smallest Mars departure delta-V, assuming periapsis-to-periapsis transfer at arrival, and to provide adequate periapsis lighting conditions for a daylight landing. A borderline acceptable lighting angle of 7.2 degrees is associated with a departure delta-V of 3.8 km/s. This choice of lighting angle allows a daylight landing within 20 degrees north or south of the equator (see landing analysis section for details). This small lighting angle of 7° places L/D requirements on the MEV as described in the landing section.

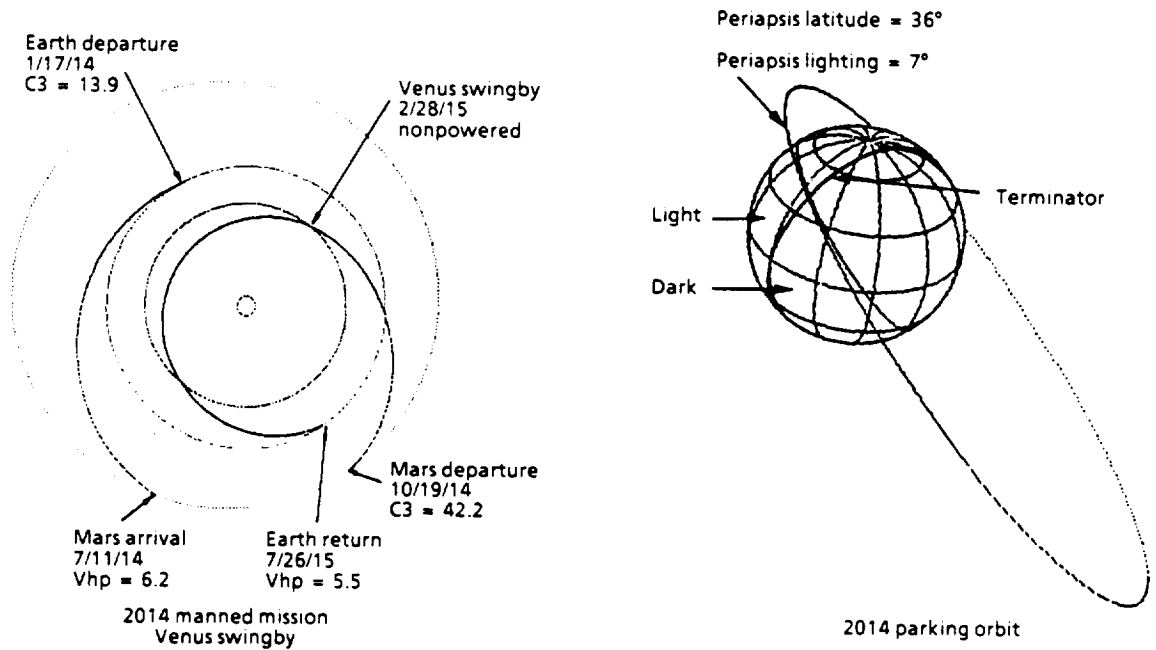


Figure 8-18. Trajectory Trace and Parking Orbit

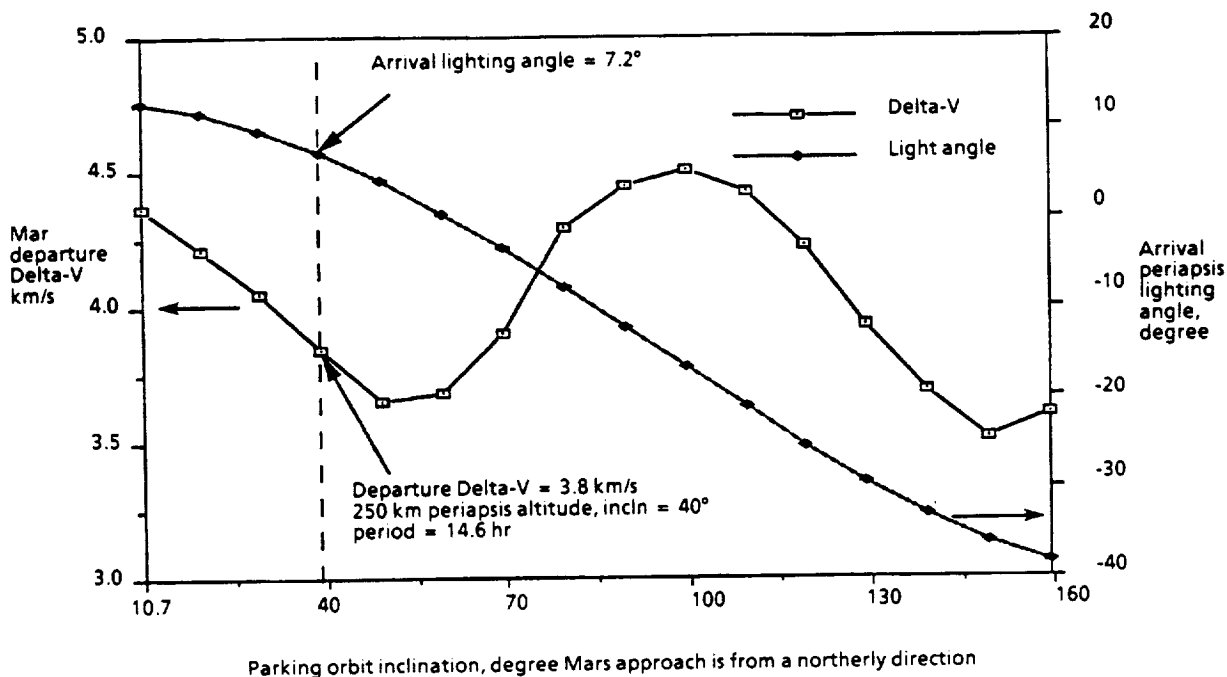


Figure 8-19. 2014 Parking Orbit Periapsis Lighting and Departure Delta-V

8.6 MARS MISSIONS DELTA-V AND TIMELINE

8.6.1 2014 and 2016 Piloted Delta-V Comparison

A comparison between Level II data and Boeing data for Mars piloted mission delta-V is given in figure 8-20. The primary differences between the Level II data and the Boeing data are Level II circular versus Boeing elliptical parking orbits and Level II faster transfer times as compared to Boeing's intermediate transfer times. The tradeoff between transit time and delta-V is a judgment question. Somewhat longer transit times were selected in view of the sensitivity of IMLEO to delta-V. Elliptic parking orbits also reduce delta-V typically by 1.5 km/sec and were selected for that reason. The Level II delta-V without TMI and MOC losses have been included for comparison. There is a significant delta-V penalty for losses. The 2016 flyby abort and abort from surface delta-V are also included for comparison purposes.

Several observations may be drawn. First, elliptical parking orbits and longer transfer times can significantly reduce the overall delta-V. Second, the 2016 mission optimized for a flyby abort has significantly less delta-V penalty than the mission designed for abort from surface capability. The last bar on the right of the graph is the delta-V requirements for a 2016 abort from surface within 31 days of Mars arrival. The immediately preceding bar reflects the actual delta-V required to perform the 2016 long

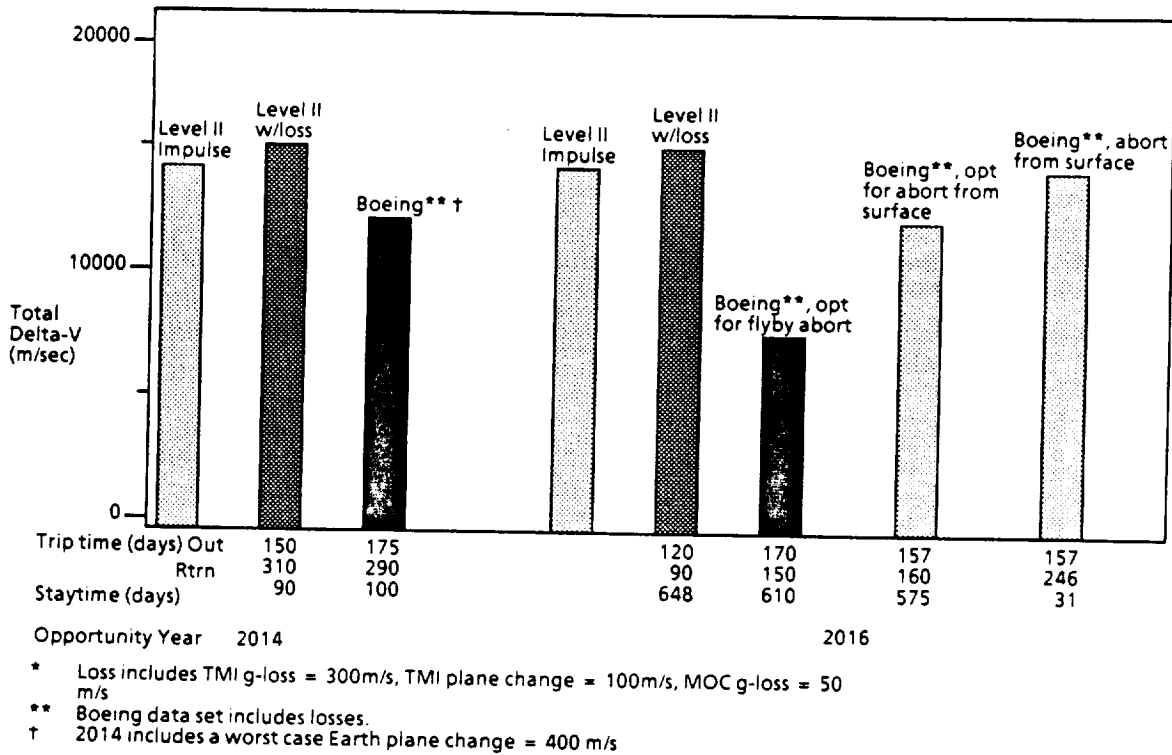


Figure 8-20. Mars Piloted Mission Delta-V

stay mission. The mission should be designed for the abort from surface delta-V contingency, thus allowing for abort from surface and ample delta-V to reduce the actual return transfer time in the event of a successful mission (a non-abortive mission).

8.6.2 Level II and Boeing Delta-V, Optimal Elliptical Parking Orbits

Relevant delta-V data such as TMI, MOC, and TEI are presented in figures 8-21 and 8-22. The highlighted data of figure 8-21 is the 2014 reference mission. A comparison of these figures shows a significant difference between the sets for total delta-V. Basically, the difference arises from the shorter transfer times for the Level II missions as opposed to the longer transfer times associated with the Boeing data.

8.6.3 Mission Time Line

A Mars mission time line for cargo and piloted missions for the 2012 to 2018 mission opportunities is shown in figure 8-23. The overall continuity of the Level II missions has been preserved in the Boeing missions; i.e., the Boeing missions were optimized for longer transfer times, yet maintaining the overall mission profiles.

Mission Type	Launch Date		Outbound (days)	MOI* ΔV	Mars Stay-Time (days)	TEI* ΔV	Return (days)	Return V inf*	Mission Duration (days)	Total ΔV*	Abort Type
Cargo 1	11/9/11	3960	300	982	---	---	---	---	300	4942	---
Cargo 2	12/4/13	3988	294	1184	---	---	---	---	294	5172	---
Piloted 1	1/17/14	4490	175	3407	100	3840	290	5482	555	11737	---
Abort Option 1	1/17/14	4490	175	---	flyby	1224	376.6	5166	552	5714	flyby surface
Abort Option 2	Piloted 1 has sufficient delta-V budget for abort from surface of more than 50 days before nominal departure										
Piloted 2**	3/14/16	4152	170	2200	610	1720	150	8072	930	8072	---
Abort Option 1	3/14/16	4152	170	---	flyby	1776	275	5484	445	5922	flyby
Piloted 2***	2/25/16	4022	157	3790	575	3680	160	8997	907	11492	---
Abort Option 2	2/25/16	4022	157	4060	31	3740	246	7200	434	11822	surface
Piloted 3	5/26/18	4403	170	1340	610	2000	150	3585	930	7374	---
Abort Option	5/26/18	4034	170	1340	flyby	2551 1549 +	312	7066	482	8134	flyby
Piloted 4	7/13/20	4205	170	1620	600	2434	150	6539	920	8259	---
Abort Option	7/13/20	4205	170	---	flyby	1599	346	7033	516	5624	flyby

Note - TMI g-loss = 300 m/s, MOI g-loss = 50m/s, TMI plane change loss = 400 m/s for 2014 and 100 m/s for 2016-2020.

- * Delta-V and V-inf are in the units of m/s.
- ** Optimized to provide abort from surface capability.
- *** Optimized for an abort from surface within 31 days of arrival.
- + Deep space maneuver of 1549 m/s on 5/5/19.

Figure 8-21. Mission Delta-V Data

Architecture Ref.	Opportunity Year/Type	Maneuver/ Dates	Level 2 Ideal Delta V	Finite Burn Loss	Plane Change Loss	Elliptic Orbit Savings*	Elliptic Orbits Delta V
1	2012 cargo conjunction	TMI 11/28/11 MOC 8/6/12	3653 2538	300 50	100 N/A	N/A 1198	4053 1340
1	2014 crew opposition	TMI 2/1/14 MOC 7/1/14 TEI 9/29/14-12/4/14	4127 5299 4370	300 50 30	100 N/A 72	N/A 1259 1042	627 4090 34304
1	2014 cargo (for 2016)	TMI 1/17/14 MOC 8/29/14	3808 2802	300 50	100 N/A	N/A 1192	4208 1660
1	2016 crew conjunction	TMI 4/11/16 MOC 8/8/16 TEI 5/19/18-8/17/18	4958 4700 4212	300 50 50	100 N/A 37	N/A 1120 989	5358 3630 3290
4	2016 crew opposition	TMI 3/12/16 MOC 8/4/16 TEI 9/23/18-5/11/17	3789 4685 5454	300 50 30	100 N/A 54	N/A 1175 -32	4189 3560 5570
1 & 4	2018 crew conjunction	TMI 6/18/18 MOC 10/1/18 TEI 8/8/20-11/1/20	4615 3916 5309	300 50 30	100 N/A 46	N/A 976 703	5015 2990 4606

Figure 8-22. Reference Delta-V Set, Level II

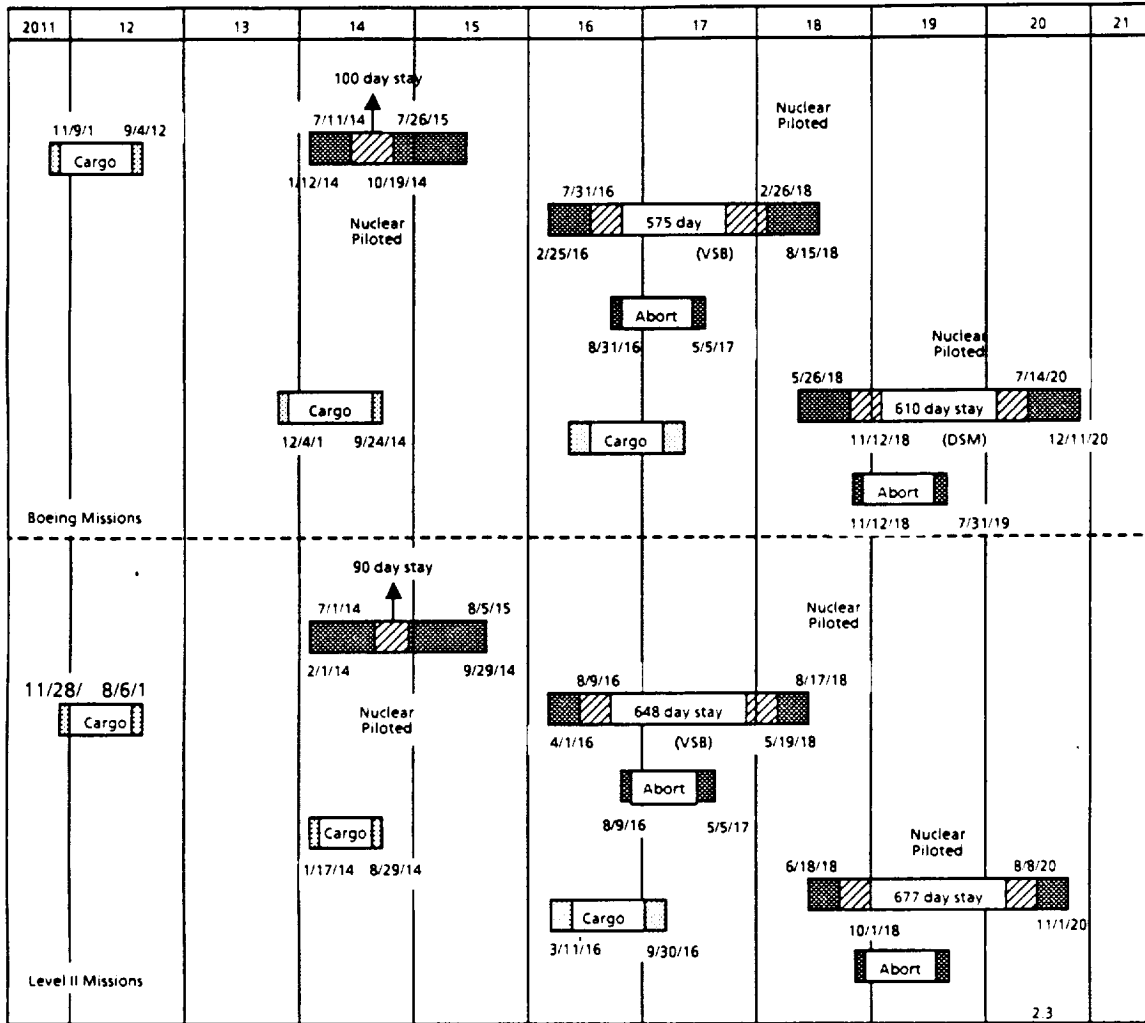


Figure 8-23. Mars Missions Timeline, 2012-2018

8.7 LANDING ANALYSIS FOR 2014 MISSION

An analysis has been conducted to determine whether landing may be achieved between $\pm 20^\circ$ latitude on the day side of either the morning or evening Mars terminator for the mission opportunity 2014. A question that this analysis addresses is whether there is enough lift generated by a High L/D Mars Excursion Vehicle (HMEV), maximum L/D of 1.6 at an angle of attack of 35 degrees, to successfully land within the aforementioned landing range. The 2014 opportunity was chosen for this analysis because the point at which the descent begins is approximately 8 degrees from the terminator. The entry geometry of this problem at the time of atmospheric encounter is illustrated in figure 8-24. Given that the descent originates so near to the evening

terminator, the vehicle must have adequate maneuvering abilities for landing to occur on the day side of the terminator.

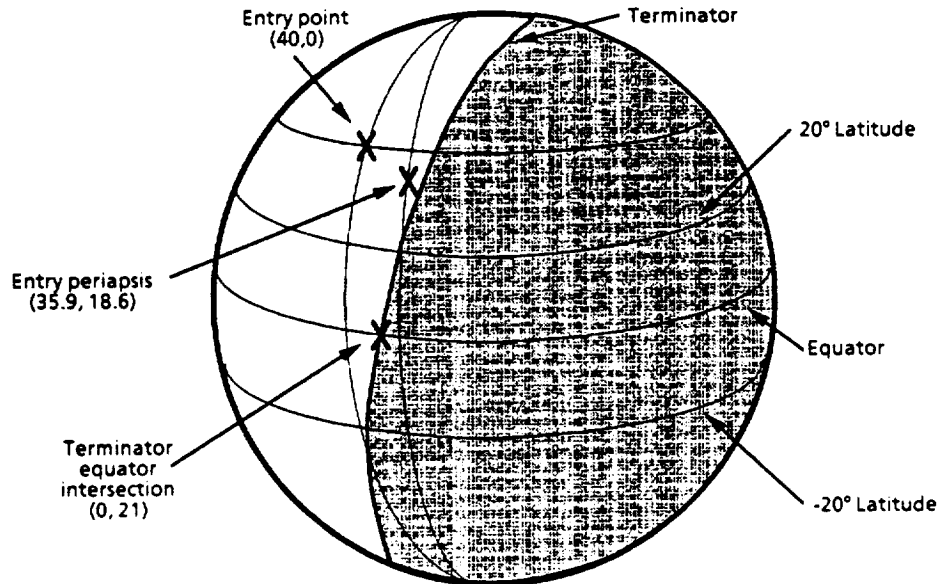


Figure 8-24. 2014 Descent Diagram

The two types of maneuvers simulated were a turn with partial skip-out and a skip-out with a long coast to the other side of the planet. Four descent trajectories were examined with identical initial conditions. The end point and end constraint of each trajectory are as follows: (1) end at -20 degrees latitude and minimize longitude, (2) end at -20 degrees latitude and maximize longitude, (3) end at +20 degrees latitude and maximize longitude, and (4) end at +20 degrees latitude and minimize longitude. The parking orbit from which the trajectories began is characterized by an apoapsis altitude of 21,800 kilometers, a periapsis altitude of 40 kilometers, an inclination of 41.5 degrees, and an argument of periapsis of 120.29 degrees. All trajectories began at an altitude of 100 kilometers (corresponding to a latitude of 40 degrees) and a velocity of 4.5 kilometers/second. The various descent trajectories were optimized for either maximum or minimum longitude and were generated using OTIS (Optimal Trajectories by Implicit Simulation). The final conditions for each of the descent trajectories ended at an altitude between 10 kilometers and 15 kilometers and with the latitude and longitude as previously stated. Two control variables, bank angle and relative wind angle, were used in the analysis. The relative wind angle is defined in figure 8-25. The bank angle was allowed to vary between -360 degrees and +360 degrees and the relative wind angle was allowed to vary between 0 degrees and 70 degrees.

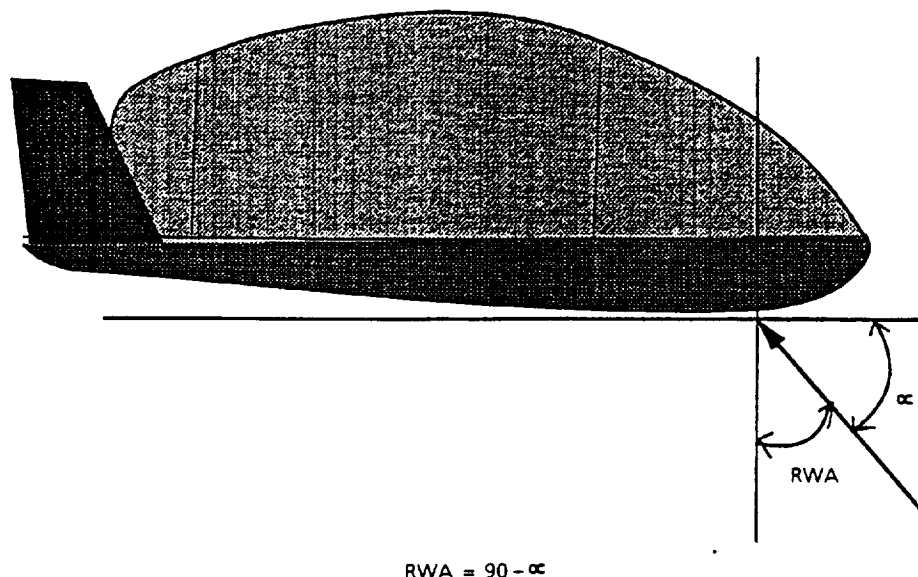


Figure 8-25. Relative Wind Angle Definition

The results of this descent analysis are shown in figure 8-26.

Case	Final Latitude (Constraint)	Final Longitude	Comments
1	-20°	+ 24° minimized	Insufficient L/D to achieve daylight landing
2	-20°	270° maximized	Achieved daylight landing on morning side of terminator
3	+ 20°	67° maximized	Insufficient L/D to achieve daylight landing
4	+ 20°	12° minimized	Achieved daylight landing on evening side of terminator

Figure 8-26. Landing Analysis Results

Cases 1 and 3 could not land in the daylight. Case 2 (final latitude of -20 degrees and maximized longitude) and Case 4 (final latitude of +20 degrees and minimized longitude) have sufficient maneuverability to land on the day side of the terminator. The ground trace for each of the trajectories of case 1 through 4 is shown in figure 8-27. From these ground traces, it can be seen that the simulated descents meet the final latitude conditions of either ± 20 degrees, depending on the Case. For Case 2, the optimal maneuver to meet the final condition of -20 degrees latitude required the vehicle to travel to nearly -40 degrees in latitude and then back to -20 degrees. In the process of reaching the latitude end condition, the vehicle traversed over 250 degrees in longitude. The ground traces for Cases 1, 3, and 4 show a fairly straight forward traversal to the final conditions and Case 2 demonstrates a more extreme latitude/longitude traversal indicative of a skipout trajectory to the relative far side of Mars.

The altitude time history and velocity time history for each descent trajectory are shown in figure 8-28 and figure 8-29, respectively. All four of the trajectories ended with a final altitude of 10 kilometers and, with the exception of Case 3, a final velocity

of less than 1 kilometer/second. In Case 3 the vehicle constraints and final conditions dictate the end velocity of approximately 1600 m/s.

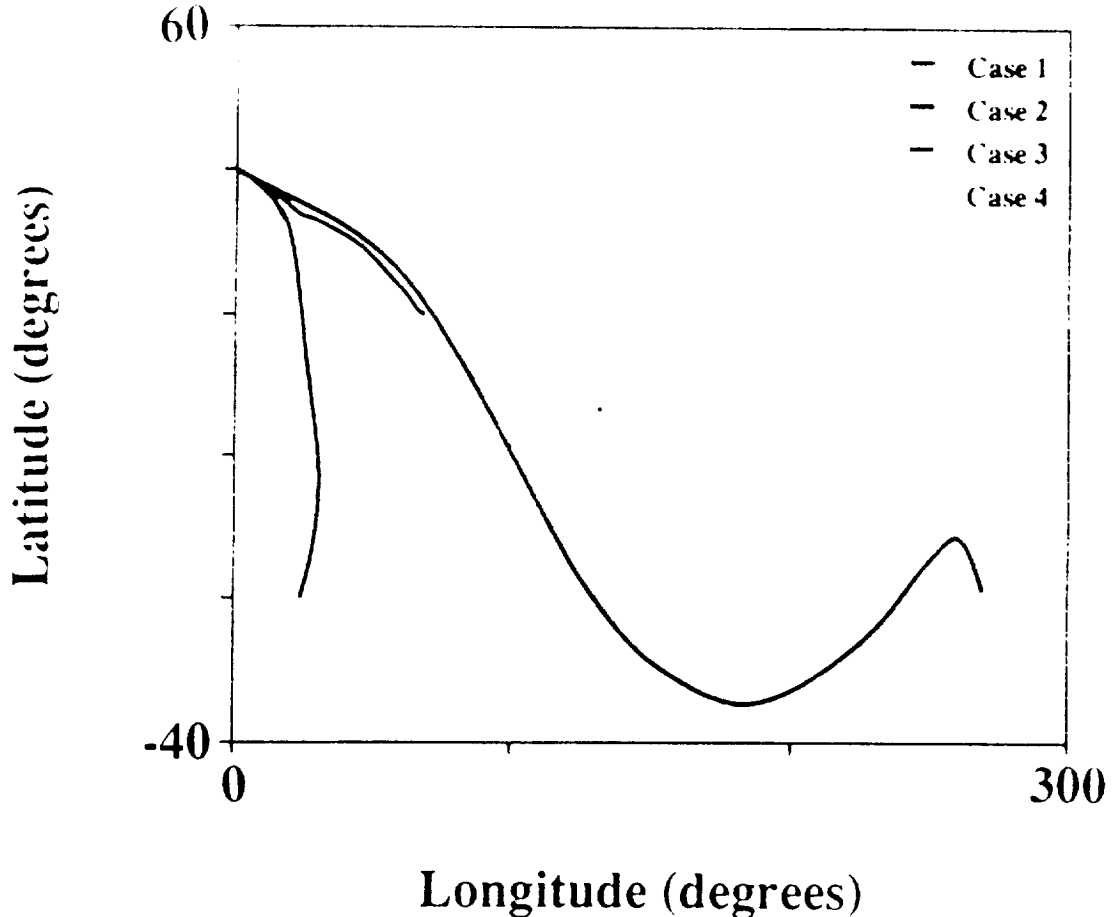


Figure 8-27. Ground Trace

The time histories for the control variables bank angle and relative wind angle are shown in figures 8-30 and 8-31. All four cases demonstrate extensive banking maneuvers, but the bank angle limits discussed earlier are never reached. As with the bank angle, there is extensive modulation of the relative wind angle throughout the trajectories. The modulations in the bank angle and the relative wind angle are expected for optimal trajectories where large variations in altitude are permitted. If constraints were incorporated in the simulation forcing the descent to glide to final conditions (constant altitude change), a smoothing effect would likely be seen in the control variable time histories. Further simulations must be performed to determine the effect that glide type descent trajectory constraints would have on meeting the daylight landing requirements for the 2014 piloted mission.

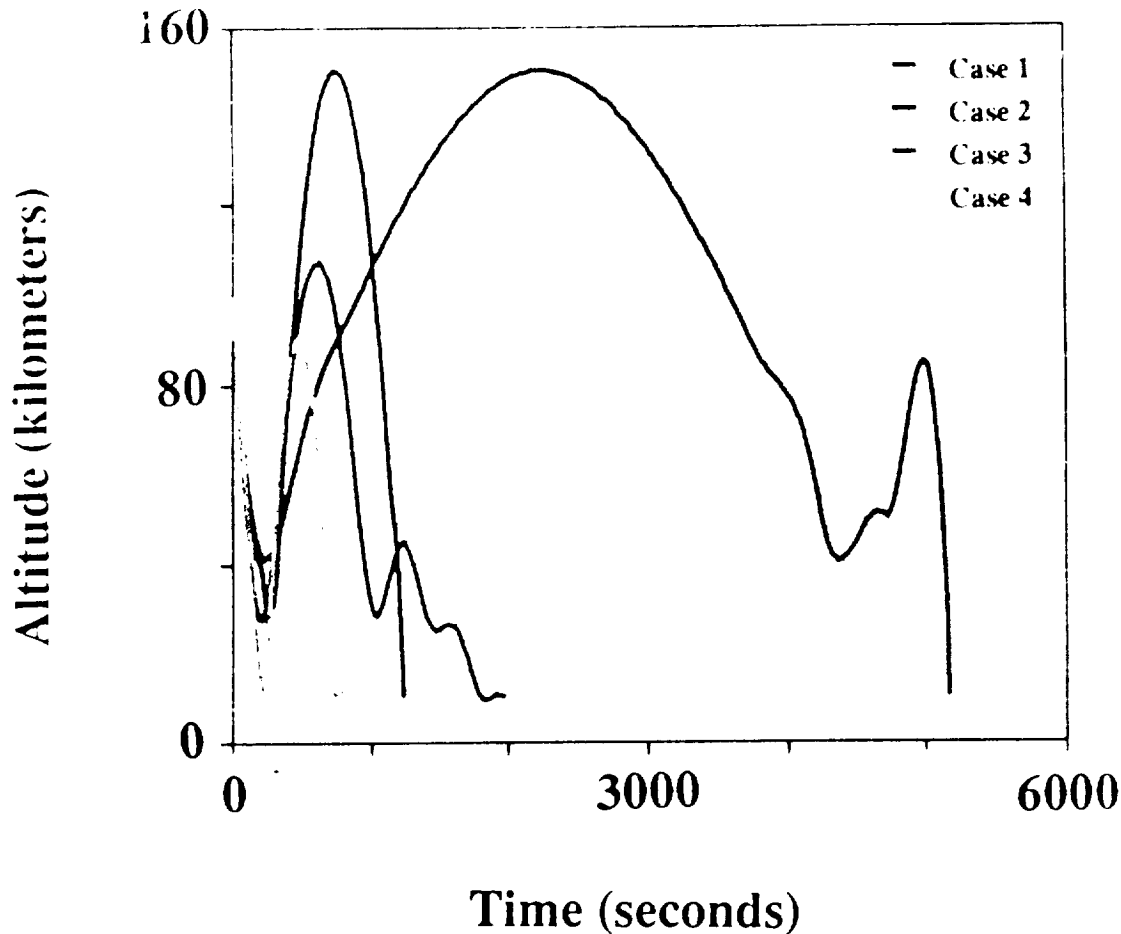


Figure 8-28. Altitude Time History

The dynamic pressure changes along the descent trajectory for Case 1 is illustrated in figure 8-32. The grid shows altitude, latitude, and longitude of the vehicle during descent. The twist of the ribbon (the ribbon is the multicolored surface associated with the descent of the vehicle) corresponds to the banking of the vehicle. The angle of attack of the vehicle is shown in the orientation of the vehicle along and above the ribbon. Similar plots for Cases 2, 3, and 4 are shown in figures 8-33 through 8-35. Maximum vehicle acceleration roughly corresponds to the maximum dynamic pressure shown in the ribbons. With the exception of Case 3, the maximum acceleration reached during the descent trajectories was 3 g. In Case 3, the maximum acceleration was 5.4 g; this higher acceleration is not significant as Case 3 was unable to meet final conditions (i.e., land) in the light. It is significant to note that those cases that successfully landed on the day side of the terminator experienced accelerations no greater than 3 g.

This page was intentionally left blank.

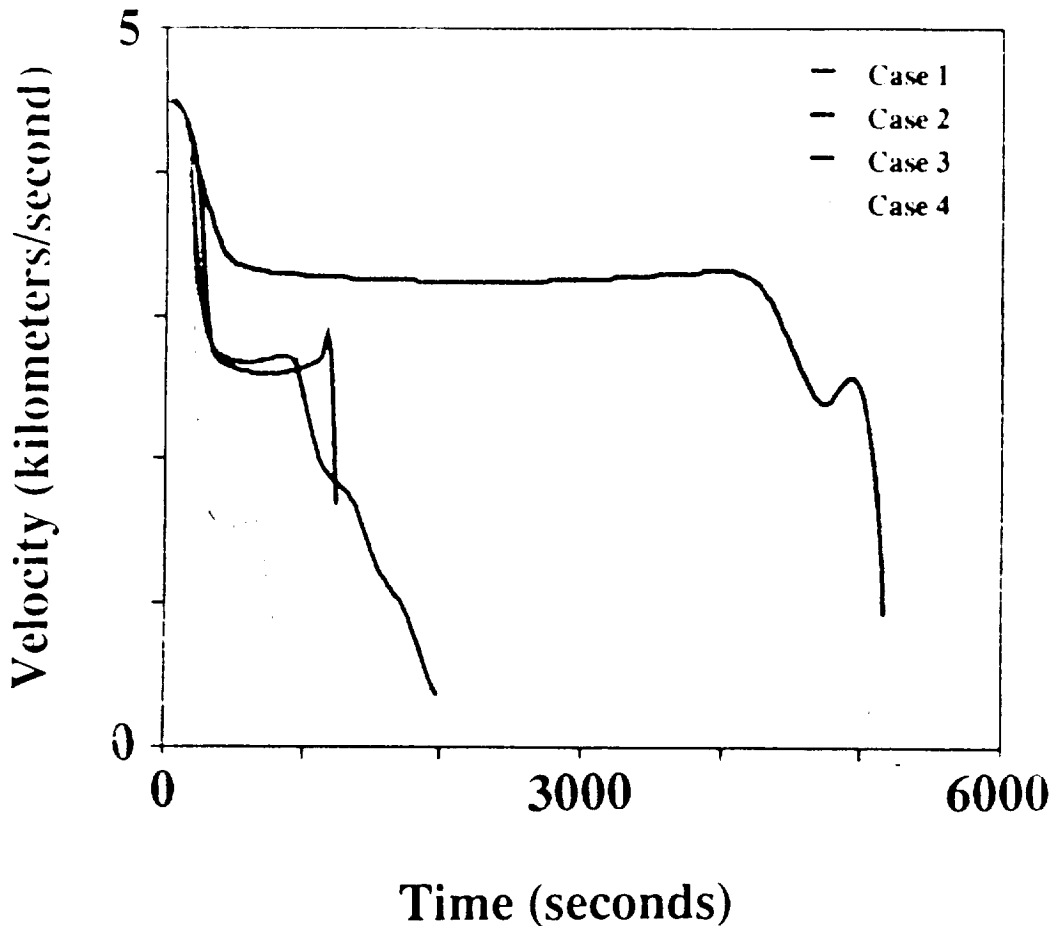


Figure 8-29. Velocity Time History

8.8 NUCLEAR REACTOR DISPOSAL

Provided below are options related to the disposal of spent nuclear reactor propulsion modules in a way that precludes or reduces the chances of Earth biosphere contamination with nuclear waste from the reactor. A spent reactor is defined as a nuclear thermal propulsion system reactor that has been operated over one or more Mars missions and has come to the end-of-life usefulness for mission purposes. The reactor may or may not have some propulsive abilities remaining. If the reactor does not have self-propulsive abilities and if it is in a safe Earth parking orbit, then it will be assumed that measures will be taken to affix a dedicated disposal vehicle to the spent reactor to facilitate appropriate delivery to safe disposal orbit.

Several nuclear safe disposal orbits have been proposed: circular orbit between Earth and Venus, circular orbit between Earth and Mars, and circular orbit about Earth. The most promising appears to be a circular orbit of .85 AU between Earth and Venus.

This page was intentionally left blank.

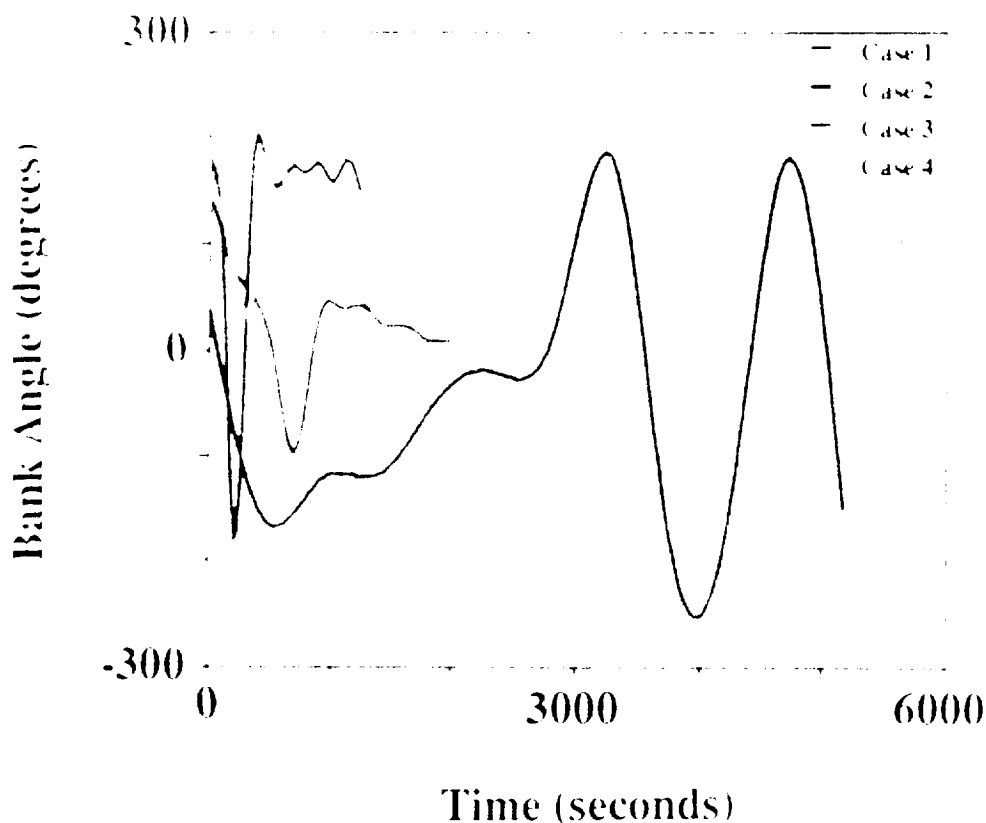


Figure 8-30. Bank Angle Time History

Listed below are some option scenarios for delivery of the spent nuclear reactor to a safe disposal orbit of .85 AU.

- a. A dedicated disposal vehicle delivers the reactor from safe Earth parking orbit to safe disposal orbit between Earth and Venus. The crew cab may be removed for reuse prior to disposal.
- b. The Nuclear Thermal Propulsion system delivers itself from safe Earth parking orbit to safe disposal orbit between Earth and Venus. The crew cab may be removed for reuse prior to disposal.
- c. The NTP vehicle performs an Earth gravity assist at Earth return. Subsequent maneuvers will be required to inject vehicle into a safe disposal orbit. For reuse purposes, crew habitat could be separated and aerocaptured (unmanned) at Earth.

Each of the above three options will be studied in greater depth to ascertain their impact on mission delta-V budgets.

This page was intentionally left blank.

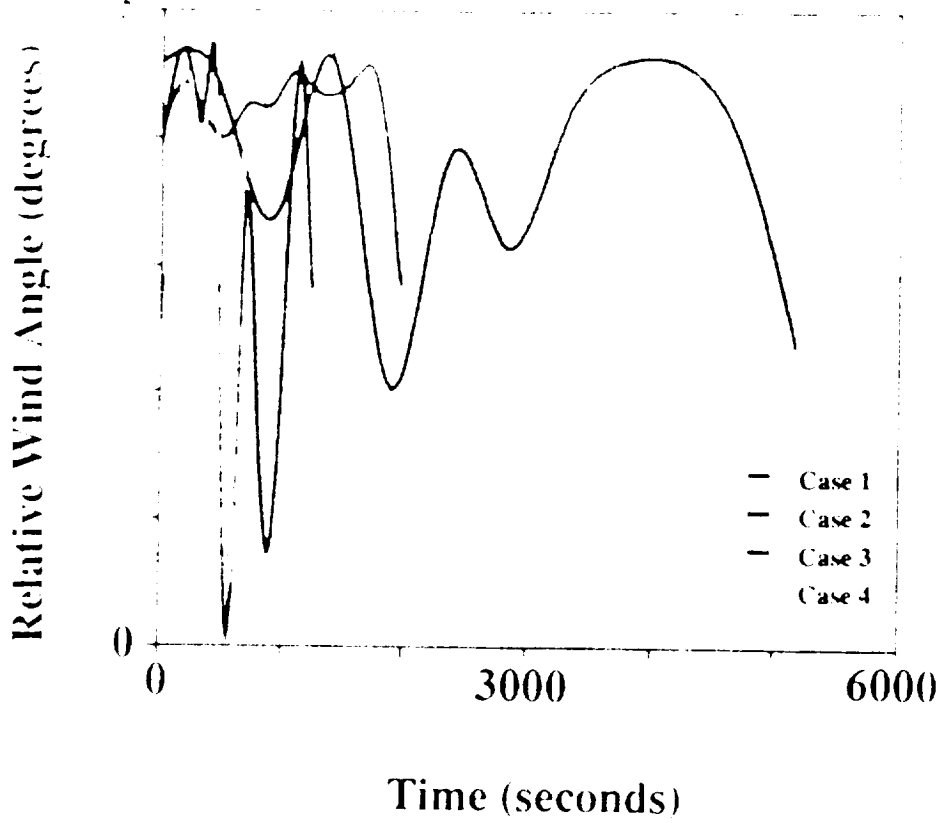
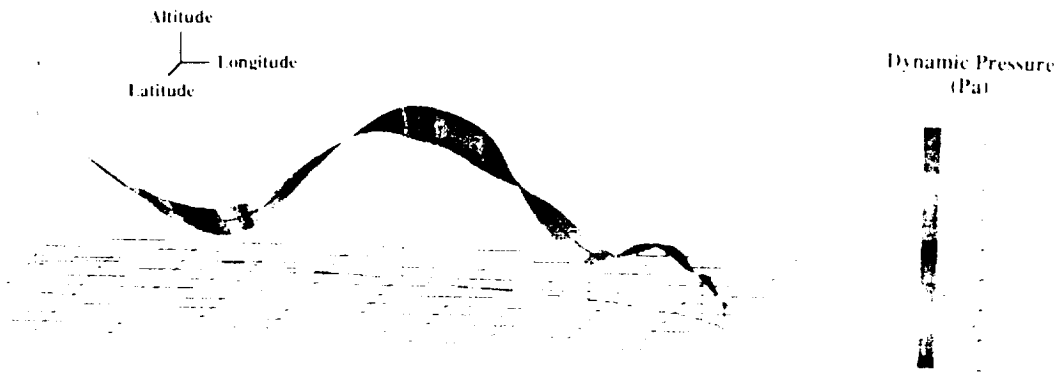


Figure 8-31. Relative Wind Angle Time History

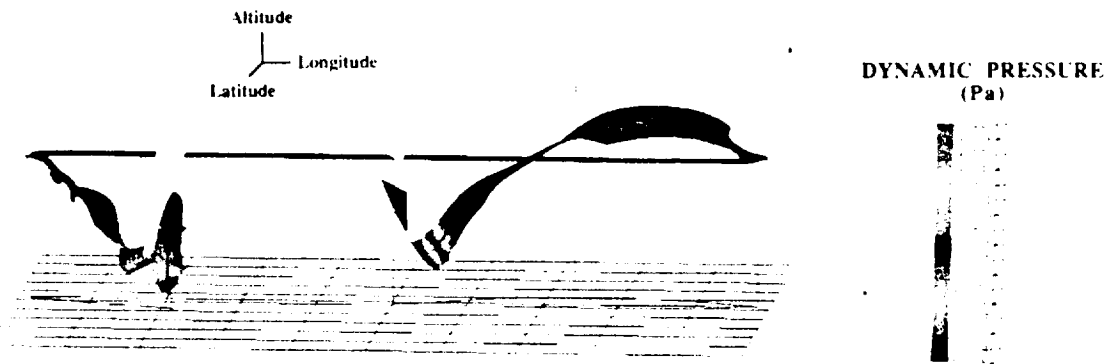
This page was intentionally left blank.



Trajectory endpoint in the dark
Final latitude = -20°
Final longitude = 24° (minimized)

Maximum acceleration = 2.7 g
Angle of attack and bank angle vary

Figure 8-32. Case 1 Descent Trajectory Dynamic Pressure

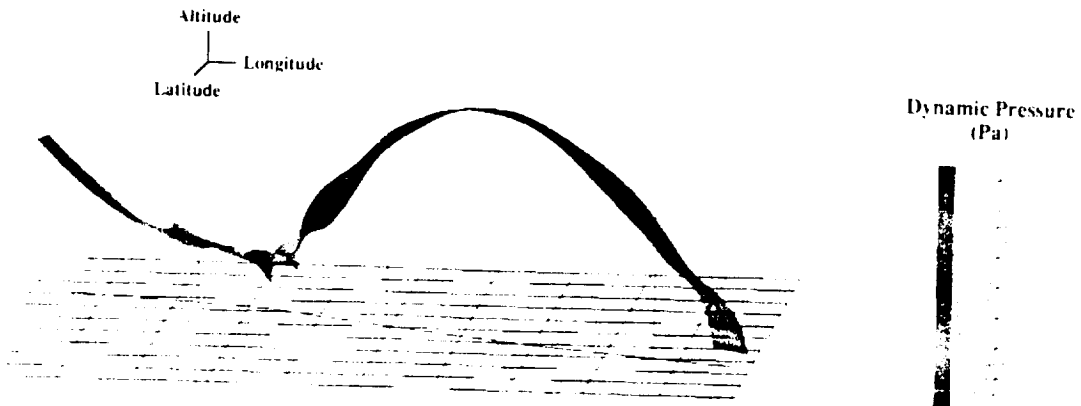


Trajectory endpoint in the light
Final latitude = -20°
Final longitude = 270° (maximized)

Maximum acceleration = 2.5 g
Angle of attack and bank angle vary

Figure 8-33. Case 2 Descent Trajectory Dynamic Pressure

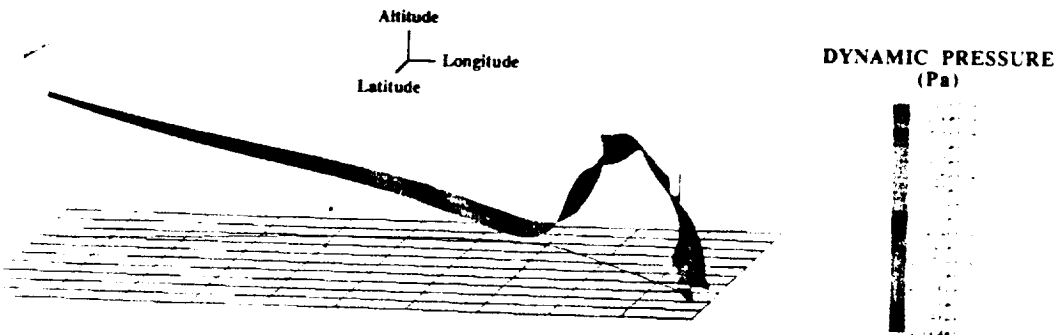
This page was intentionally left blank.



Trajectory endpoint in the dark
Final latitude = +20°
Final longitude = 67°(maximized)

Maximum acceleration = 5.4 g
Angle of attack and bank angle vary.

Figure 8-34. Case 3 Descent Trajectory Dynamic Pressure



Trajectory endpoint in the light
Final latitude = +20°
Final longitude = 12°(minimized)

Maximum acceleration = 3 g
Angle of attack and bank angle vary

Figure 8-35. Case 4 Descent Trajectory Dynamic Pressure

This page was intentionally left blank.

9.0 VEHICLE APPLICATION AND ABORT OPTIONS

9.1 VEHICLE APPLICATIONS AND ABORT OPTIONS TO THE SYNTHESIS GROUP REPORT MARS ARCHITECTURES

The Synthesis Group Report (ref. 2) outlines two nearly identical transportation implementations for its SEI Mars architectures, the two differing primarily in the date of the first manned mission. The architecture framework specifies the main features of the mission profiles but does not go to the level of detail of specifying preferences among the several trajectory suboptions that are available to the mission designer. In this study, these options are identified and their impact on individual missions evaluated. The objective of the work is to develop and characterize a comprehensive set of cargo and piloted vehicles that together would satisfy the goals outlined in the Synthesis report. Specific emphasis was put on the application of Mars transfer vehicles (in their transfer capability) to the set of missions given in the report. This section is not a critique of the architectures themselves.

Both Mars transportation implementations opt for a single 60 to 90 day stay opposition class mission as man's introductory mission to the planet, and follow with a series of long stay conjunction class missions more advantageous to a comprehensive exploration program. Cargo essential to the crew's surface habitation and exploration activities is in part delivered on lower energy one way Earth-Mars trajectories prior to the corresponding piloted mission. This split-sprint mission approach is being taken both to provide for on site validation of the crews surface habitation systems prior to occupancy and as a means of reducing total fleet IMLEO. A mission timeline is given in figure 9-1 for the primary architecture that provides for a first piloted mission in 2014. Flight profiles for cargo and piloted missions is illustrated in figure 9-2.

For all the piloted missions, the report mandates a crew of six and opts for Earth crew return via the CRV (regardless of vehicle recapture for reuse back at Earth). NTP was selected for all transfer vehicles. For this analysis an engine of 75,000 lbf thrust, T/W of 10:1, and 925 seconds specific impulse were selected. Two engines are utilized for the piloted vehicles to allow for a single engine out margin. For the cargo missions, single engine transfer vehicles are used for cargo only delivery flights. The expected operational lifetime of these engines is on the order of 10 hours.

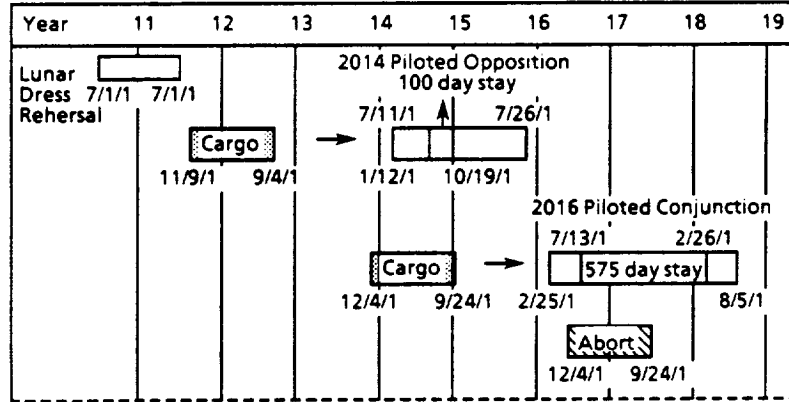


Figure 9-1. Synthesis Report Mars Architecture Timeline

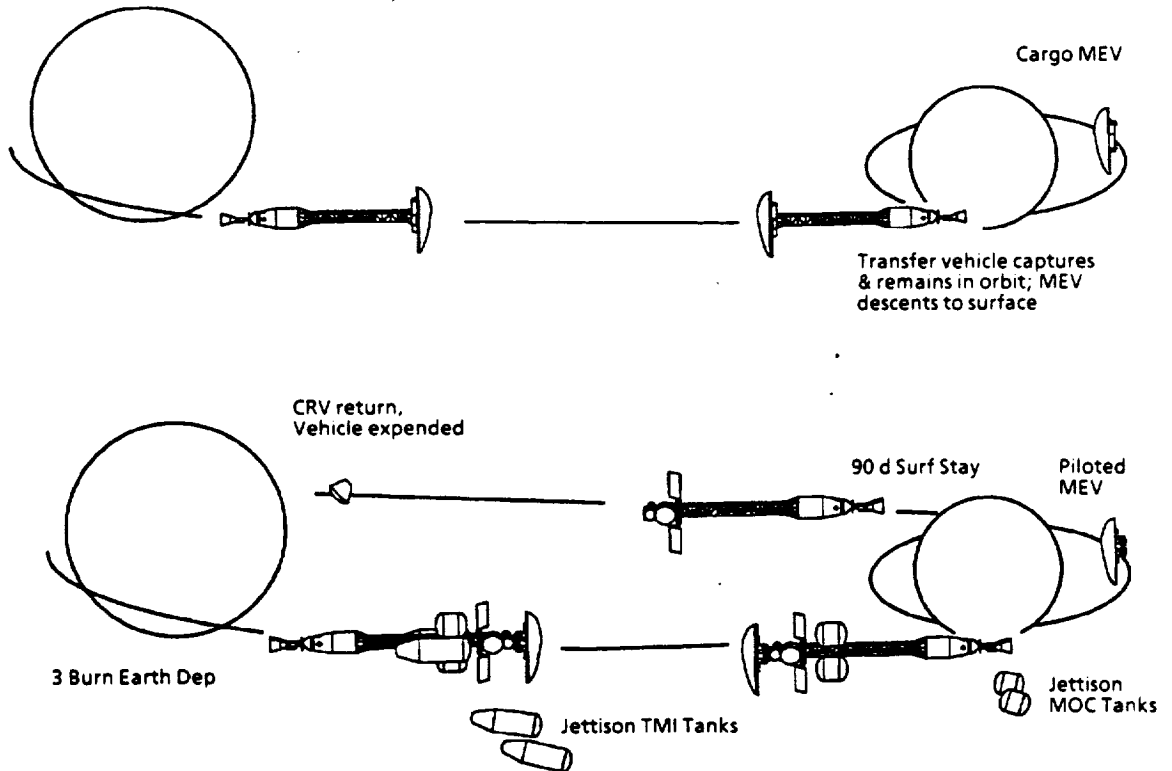


Figure 9-2. 2012 Cargo and 2014 Piloted Vehicle Mission Profiles

9.2 VEHICLE DESCRIPTIONS

The trips to Mars begin with the 2012 cargo mission, which provides a surface habitation module for the 90 day surface stay of the first piloted flight of 2014. A second cargo flight is also undertaken in 2014 to supply habitation modules and exploration hardware for the second piloted mission of 2016, which involves a 600 day surface stay. Prior to these missions a lunar dress rehearsal mission is flown in which the Mars transfer vehicle and surface habitation equipment is tested. The succeeding vehicle descriptions follow the chronological flight order given in figure 9-1, which begins with the systems checkout mission to the Moon.

9.2.1 Flight One: 2010 Lunar Dress Rehearsal Mission

This 2010 mission serves as a rehearsal for the first manned mission of 2014. Five key subsystems are validated over the course of this 175 day mission:

- a. MTV crew habitat module system.
- b. Mars surface habitat and exploration systems.
- c. Nuclear Thermal Propulsion systems.
- d. H₂ cryogenic propellant storage.
- e. CRV Earth return capsule.
- f. NTP unique H₂ gas (boiloff/tank pressurant) RCS.

Three key operational procedures are validated:

- a. In-space assembly of transfer vehicles.
- b. Three burn periapsis Earth departure burn.
- c. Outbound flight MEV descent engines checkout test prior to landing.

Because the Moon lacks atmosphere, MEV aerodynamic braking cannot be validated on this mission. A dual engine NTP propulsion system, identical to that of the Mars mission vehicles, is utilized for all major burns, including a three burn (periapsis) Earth departure to demonstrate the same startup/shut down cycling capability and post burn cool down operation that would be necessary for the later Trans-Mars Injection burns. A LEV equipped with a Mars surface habitat module, airlock, communication equipment and lab hardware is utilized to simulate those habitation and exploration activities to be accomplished on the initial Martian flights. The transfer vehicle is propulsively captured back to LEO for inspection. Because of the relatively short NTP engine burn time associated with a lunar mission (1.3 hr total), at least 80% of the expected engine operational life is still available. Because the recovery of the costly crew transfer

habitat module and NTP system elements is necessary for the post flight checkout, this lunar rehearsal vehicle stands as an excellent candidate for reuse 3 years later for the 2014 first manned mission or for subsequent missions. The additional resupply and reassembly required for reuse would be limited to providing and attaching the MEV and the new H2 propellant tanks. A representative sketch of the vehicle is given in figure 9-3. Also illustrated is a sketch of piloted/cargo LEV capable of delivering 30 mt to the surface. The surface cargo is held on the bottom of the lander, rather than on the top or on the sides. This facilitates off-loading of heavy habitat modules directly to the surface without the need for dedicated surface system off-loaders.

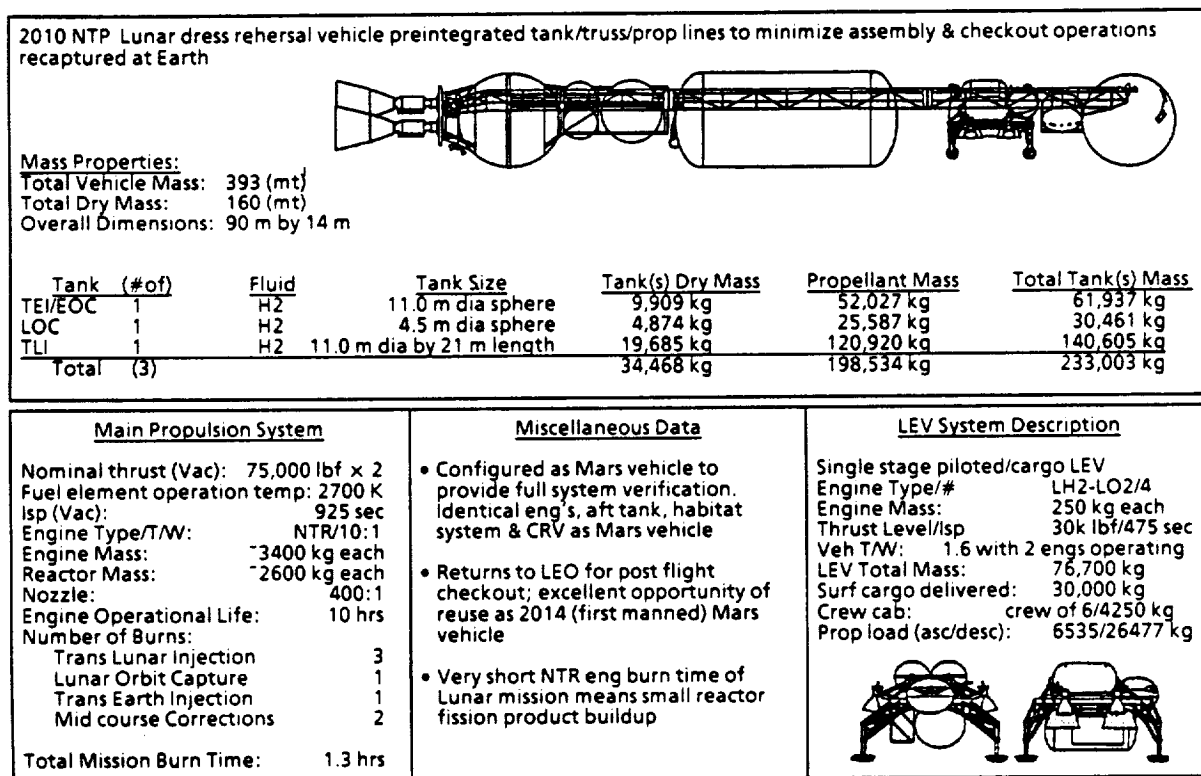


Figure 9-3. Lunar Dress Rehearsal Vehicle Data Set

9.2.2 Flight Two: 2012 First Cargo Mission

The first manned landing in 2014 is preceded by a 2012 unmanned cargo delivery flight. A low delta-V one way trajectory was chosen to minimize IMLEO. A single 72 t cargo MEV is propulsively captured into an elliptical Mars orbit. This MEV descends to the surface and awaits utilization in 2014.

9.2.3 Flight Three: 2014 First Piloted Mission - Opposition Class

The first manned landing in 2014 provides a 90 day stay time on Mars. Vehicle sizing analysis was done for transfer trajectories of 440 and 465 days, the latter utilized in the following discussion and represented by the sketch in figure 9-4. The vehicle carries a single 72 t piloted MEV and in the nominal case is expended at Earth with the crew returning via the CRV. Vehicle IMLEO is 681 t.

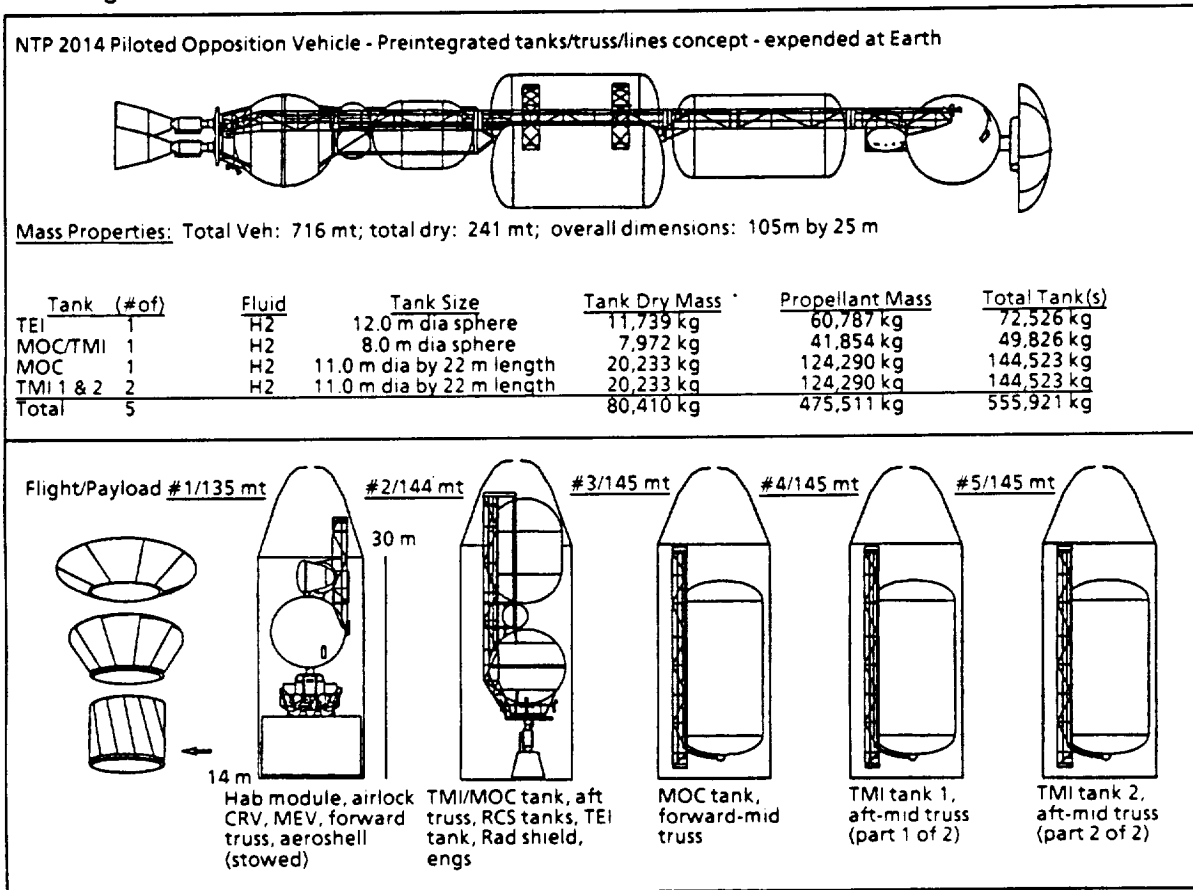


Figure 9-4. 2014 Piloted Vehicle Data Set and Representation 150 for Launch Vehicle Manifest

9.2.4 Mars Crew Transportation System Operational Description

About one month before the TMI window opens, a test crew will board the vehicle for final tests and pre-orbital-launch checkout. One week before the window opens the mission crew will board; after a tie-in period, the test crew will return to Earth on the shuttle that delivered the mission crew.

Trans-Mars Injection occurs in three burns of the NTP system. The first burn places the vehicle in a 72-hour elliptic orbit with apogee about halfway to the Moon's orbit.

The second burn occurs at apogee and makes the plane change required to access the trans-Mars velocity vector; orbit period is not changed by this burn. The third burn starts just before perigee and increases the vehicle velocity to that required for TMI. The crew spends the time during the first and third burns in the galley area to reduce radiation dose from van Allen belt passage.

Midcourse corrections during trans-Mars are divided into three maneuvers to reduce total delta-V, improve targeting, and also reduce the amount of hydrogen that must be stored in the attitude control propulsion system accumulators.

A few days before Mars arrival, terminal navigation and maneuvering begin. Navigation can use satellites in Mars orbit or radar ranging of Mars itself for approach state vector update. A test of the nuclear engines assures that both are ready for operation; if a failure is detected, or if other mission/equipment anomalies dictate, the approach path is retargeted by the attitude control system for a Mars flyby abort.

The Mars phase of the mission begins with a single-burn orbit insertion into an elliptic orbit. The state vector is updated by Earth track, and descent preparations begin, including orbital high-resolution imagery and viewing of the planned landing site. The MEV is checked out. Separation and de-orbit of the MEV occurs near apoapsis of the parking orbit. Atmosphere entry occurs 6 to 12 hours later, depending on the parking orbit period, and atmosphere braking begins. The MEV maneuvers towards the landing site and acquires one of the landing beacons delivered with the surface cargo mission. At about 10 km altitude, landing engines are started and the aerobrake is jettisoned. Terminal maneuvering to the landing site is done on rocket propulsion. The final approach is on a 15° descent "glide" slope so that the landing site is visible to the crew on approach.

During the descent, the crew occupies the crew module of the ascent stage to enable abort. Abort is possible during the terminal phase of the aero descent or after descent engines start; the ascent stage can start engines, separate and return to Mars orbit.

After landing the crew performs an ascent stage checkout, powers down and secures the MEV and initiates the surface mission. The MEV health management system remains active during the surface stay to alert the crew of any problem that might call for an abort to Mars orbit.

Upon completion of the surface mission, the crew returns to the MEV, boards the ascent stage, and prepares for ascent. Ascent windows occur at least twice per Mars day, whenever the surface base is in the parking orbit plane. At the first opportunity, ascent is initiated. The MEV ascent stage flies to a 100 km circular phasing orbit

coplanar with the parking orbit. Upon arrival at periapsis, burn to a transfer ellipse (apoapsis coincident with the parking orbit) occurs. At apoapsis the final phasing burn occurs followed by rendezvous and docking with the interplanetary vehicle. The crew transfers and the MEV ascent stage is jettisoned. This nominal ascent occurs about 10 days before the return-to-Earth window closes to allow contingency time.

Trans-Earth Injection occurs on a single burn. The coast to Earth is similar to the coast to Mars, with multiple midcourse corrections. Terminal navigation for Earth return is provided by the DSN.

About 16 hours before Earth arrival, the crew enters the CRV with the Earth return science. At entry minus 12 hours the CRV separates from the rest of the vehicle. Since the interplanetary vehicle is not on an Earth atmosphere intercept path, the CRV makes a burn of above 20 m/sec to place it on its entry path. The interplanetary vehicle passes by Earth and is abandoned. Earth gravity assist and final attitude control propulsion maneuvers place the vehicle on a trajectory which avoids a later Earth impact. The CRV enters Earth's atmosphere, decelerates, deploys parachutes, and makes a water landing to complete the mission.

A preliminary flight manifest sketch is given to illustrate a possible partitioning scheme applicable to a 150 t class NLS launch vehicle. Five 150 t class NLS flights are sufficient for complete delivery of the vehicle to the assembly platform. All flights excepting the first utilize a 30 by 10 m shroud. For this point design analysis, where the 150 t class lift capacity and a 30 m payload shroud length were fixed, there exists no advantage for propellant tanks of over 10 m in diameter, since this value allows the large TMI H2 tank to reach the 150 to 160 t lift capacity limit. If the tank diameter is increased beyond 10 m to provide more propellant capacity, the additional payload mass could not be accommodated by this size launch vehicle.

9.2.5 Launch Vehicle Flight 1

The MEV aeroshell is comprised of a center disk and 24 foldout petals that are hinged to the disk. Once delivered to orbit these petals are unfolded to form the low lift-to-drag shape as seen in the sketch, figure 9-4. When the aeroshell is in its folded position in the shroud, an empty center section between the petals of about 5 m in diameter is formed and may be occupied by another piece of hardware as a means of maximizing packaging shroud efficiency. Also packaged with the aeroshell in this flight is the MEV, with its landing legs folded, as well as the preassembled "core" unit, which consists of the MTV crew habitat module, airlocks and forward truss section. The forward truss system connects to the mid truss section. The combined mass of the MEV,

aeroshell, CRV preassembled MTV module-airlock-truss unit is about 135 t, and the unit fits into a single 14 m diameter by 30 m cylindrical length shroud.

9.2.6 Launch Vehicle Flight 2

The aft TEI propellant tank is carried up with the two engines, their radiation shadow shield, and the RCS propellant tanks, and a spherical excess MOC/TMI tank. The combined masses of the elements is 144 t, and this unit also fits into the the 14 m by 30 m shroud size.

9.2.7 Launch Vehicle Flight 3

The single 11 m by 22 m MOC tank with it attached truss section fits together into a single 14 by 30 m shroud. This large MOC tank, as well as the two TMI tanks are identical in size.

9.2.8 Launch Vehicle Flight 4 and 5

The two TMI propellant tanks for this 2014 mission each fit within the 14 m by 30 m shroud size. The truss sections for these two tanks are connected transversely; this unit is connected in-line with other truss sections as shown in figure 9-4.

9.2.9 Flight Four: 2014 Second Cargo Mission

The second manned landing in 2016 is preceded by a 2014 cargo delivery vehicle. A minimum delta-V one way trajectory was chosen to minimize IMLEO. Three 72 ton cargo MEVs are propulsively captured into Mars orbit and are landed autonomously. These landers supply the necessary habitation and exploration equipment for this 600 day surface stay mission and await utilization in 2016. An illustration is given in figure 9-5.

9.2.10 Flight Five: 2016 Second Manned Mission - Conjunction Class

The second manned landing in 2016 provides a 600 day stay time on Mars. The transfer vehicle is identical to the 2010 lunar rehearsal and 2014 manned vehicles in all respects except for differences in the total propellant requirement. A 72 t piloted MEV is taken. In the nominal case the vehicle is expended at Earth and the crew returns via the CRV.

9.3 MISSION OPTIONS DESCRIPTIONS

Several key trajectory options were evaluated to determine impact on vehicle IMLEO, operability and reusability. These are briefly described below:

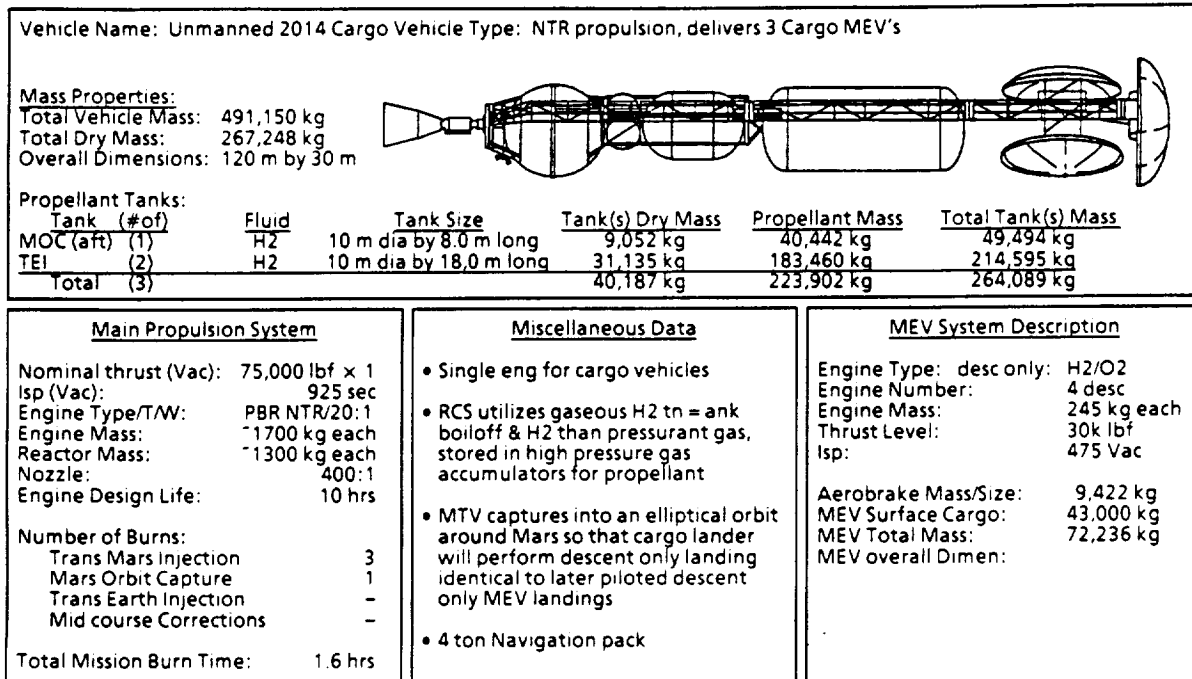


Figure 9-5. 2014 Second Cargo Mission, 3 MEV Transfer Vehicle

9.3.1 Option One: MEV Direct Entry vs MEV Descent Only Comparison

Mission: 2012 First Cargo Delivery Mission Only

The MEV descent from orbit only option requires transfer vehicle MOC propellant and thus increases IMLEO substantially over the MEV direct entry case. However, since the piloted MTV vehicles must utilize propulsive MOC, only the "lower energy" descent aerobrake is needed for the manned MEVs. If retaining cargo MEV aerobrake commonality with the piloted MEVs is essential, then the increased IMLEO is necessary. IMLEO variations with entry mode and Earth return option is given in figure 9-6.

9.3.2 Option Two: MEV Accommodation

Mission: 2014 Second Cargo Delivery Mission Only: 3 MEVs Are to be Delivered

- Each MEV is flown on a separate unmanned transfer stage, and arrives separately.
- All three MEVs are flown on the same unmanned transfer stage.

IMLEO variation with transfer vehicle number is given in figure 9-7.

Case 1 disadvantages: Three separate NTP propulsion and navigation systems are required.

Case 1 advantages: Concurrent vehicle assembly is eliminated with the 2014 piloted vehicle. If all three MEVs were taken on a single vehicle, in space assembly would

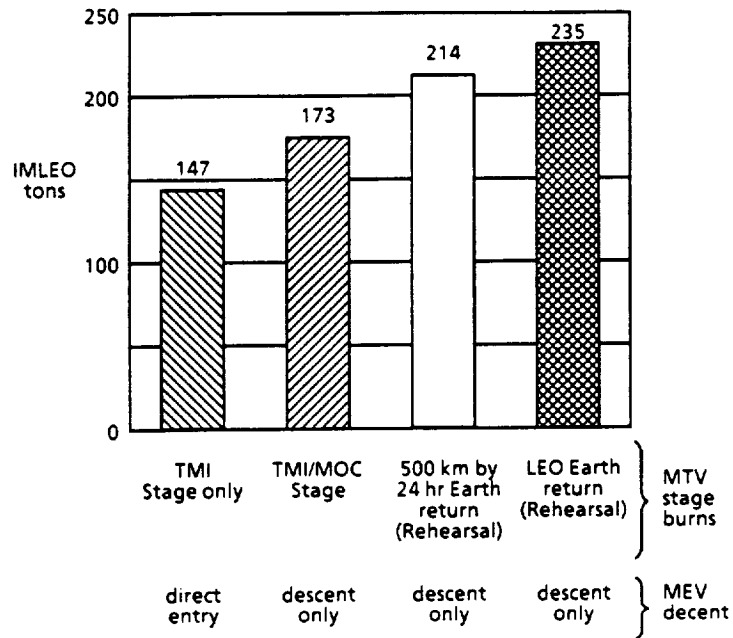


Figure 9-6. 2012 Cargo Vehicle IMLEO Variation with Entry Mode and Earth Return Option

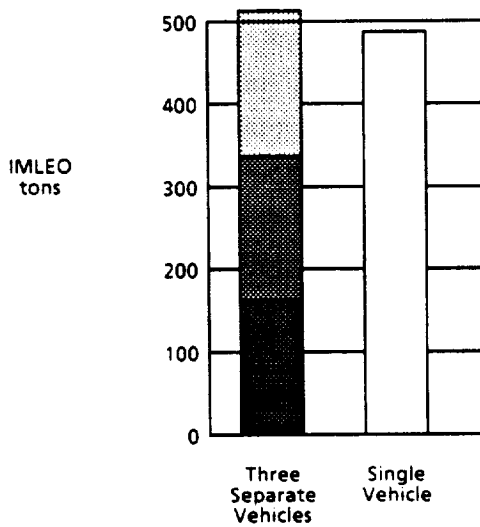


Figure 9-7. 2014 Cargo Mission IMLEO Variation with Transfer Vehicle Number

be required. The assumption was made that the 173 t single MEV cargo transfer vehicles could be delivered to LEO in one NLS launch as two pieces. The MEV would berth autonomously with the single tank transfer stage, eliminating on-orbit assembly.

9.3.3 Option Three: Aborts Comparison

Mission: 2016 Piloted Conjunction Mission Only

The objective of the aborts comparison analysis involved understanding the penalties associated with aborting the conjunction missions at various stages into the mission. Abort options available to the crew can be classified into two categories:

a. Early mission abort. This classification pertains to aborts occurring before Mars capture is attempted. During the outbound transfer leg, the crew has the option of maneuvering the vehicle in order to effect a Mars swingby gravity turn, with a propulsive delta-V addition, instead of capturing at Mars if a difficulty arises with the lander or surface habitation system in route. The cost to vehicle IMLEO is zero; the onboard MOC and TEI propellant is more than enough to provide the relatively low delta-V addition necessary at swingby for Earth return. This is true regardless of opportunity year, opposition or conjunction.

b. Abort from surface capability. This classification pertains to aborts occurring after Mars capture is completed. During the surface stay, the crew has the option of ascending directly to the orbiting MTV and effecting an immediate return to Earth. This is of particular concern to the conjunction missions due to their very long stay times. The conjunction mission total duration is on the order of 900 to 1000 days, of which the outbound leg, covered by case (1) above, is only about 150 days or roughly 20% of the mission. This abort from surface option is further divided into the following two subclassifications:

1. 0 to 30+ day surface abort. For aborts necessary within a few weeks of landing, it is sometimes possible to leave soon enough to take advantage of an inbound Venus swingby gravity assist. The gravity assist reduces the magnitude of the delta-V addition necessary for immediate Mars departure. In this case the total delta-V required of a vehicle providing this option would closely approximate a Venus swingby opposition trajectory of the same year.

2. 30+ and over surface abort. For aborts that occur after the first several weeks after landing, the inbound leg Venus swingby benefit is usually no longer available. A large propellant penalty is required for immediate Mars departure, and is a function of the opportunity year as well as the time into the mission when the abort becomes

necessary. For these cases, the minimum delta-V inbound return leg often requires a deep space burn of several km/sec in addition to the TEI burn delta-V.

In the data given on figure 9-8, the first three columns represent early mission abort cases (with differences in transfer time, and Mars parking orbit selection). The fourth column represents an abort from the surface case (0 to 30 days with Venus swingby inbound) and the fifth, sixth and seventh columns represent abort from surface cases in which the Venus swingby benefit could not be accommodated due to the delayed occurrence of the abort situation. The additional IMLEO required for providing these various abort capabilities are shown on the chart. Abort from surface reduction in trip duration is given for four surface abort options in figure 9-9.

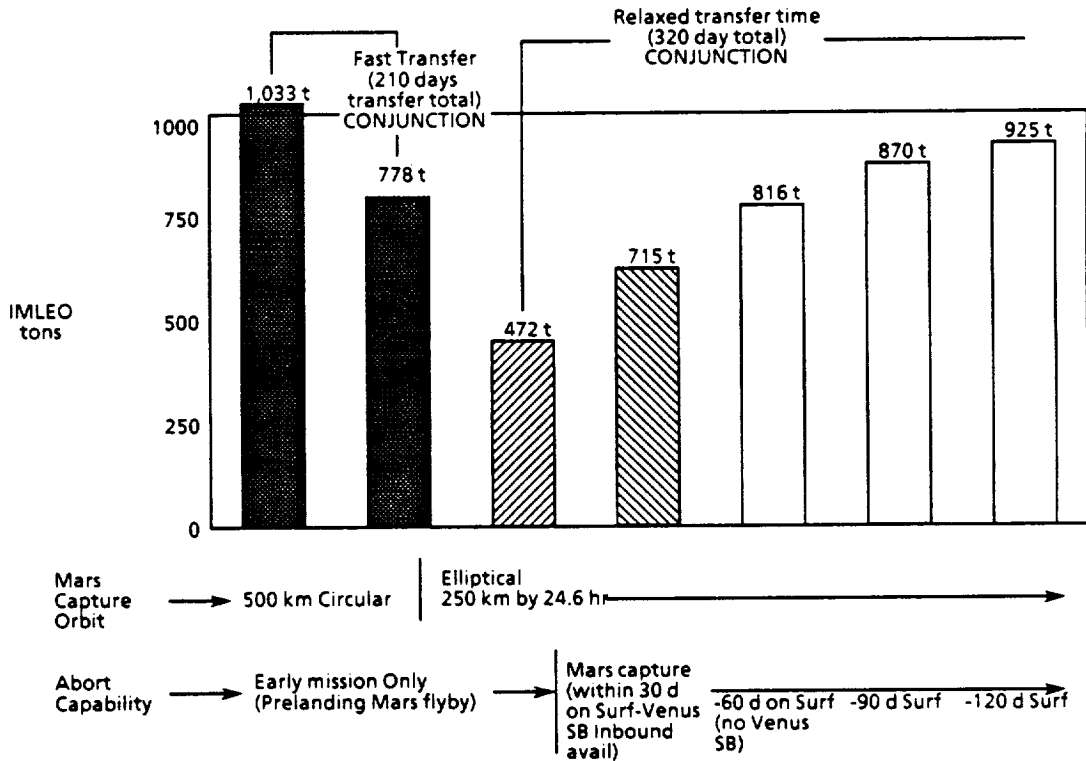


Figure 9-8. 2016 Conjunction Piloted Vehicle IMLEO Variation with Trip Time, Orbit Selection, and Surface Abort Period

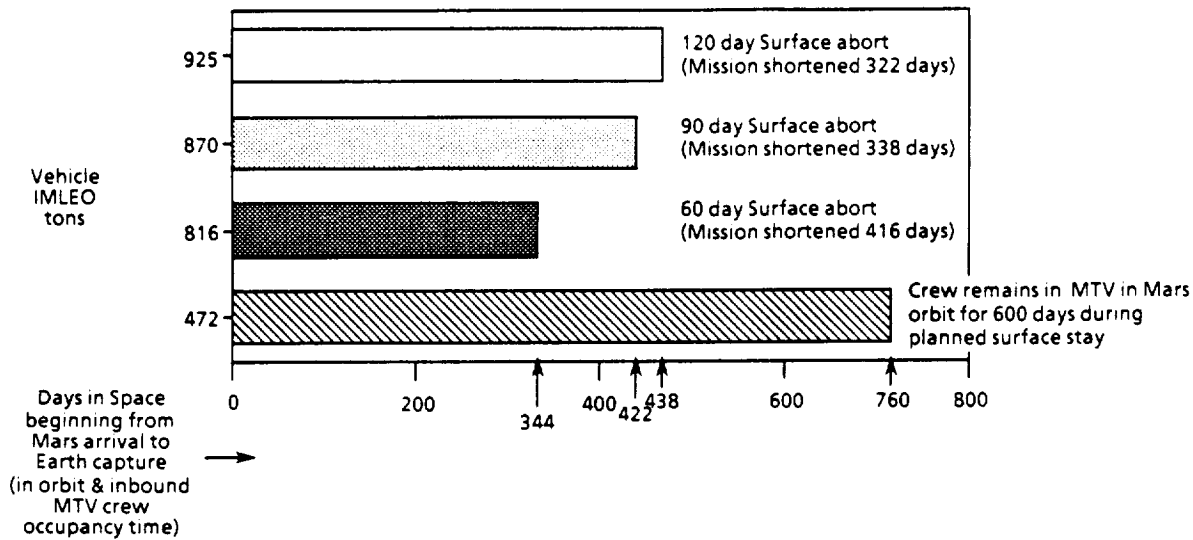


Figure 9-9. 2016 Conjunction Mission Abort Option Trip Reduction Analysis

9.3.4 Option Four: Mars Flyby Abort Options

Mission: 320 Day Transfer 2016 Conjunction Mission Was Chosen for Evaluation

Analysis indicates that for cases where the Mars flyby abort mode is in fact utilized, enough excess propellant (which would have been used for Mars capture) is still left in the MOC and TEI tanks after the flyby maneuver for the transfer vehicle to propulsively capture back at Earth. This would allow for a later reuse of the vehicle if desirable. The abort swingby delta-V is much less than the sum of the nominal MOC and TEI burn delta-Vs. This excess delta-V, if not used for Mars capture, can be used for Earth capture. Also considered in the Mars flyby abort case was retaining the MEV (rather than releasing it at the swingby), and carrying it back on the inbound trajectory leg for recapture with the MTV at Earth. It is apparent from the data given in figure 9-10 below that all but a MTV and MEV return down to LEO can be accommodated by the vehicle without adding propellant for Earth capture - that is, only if the Mars swingby is actually taken.

9.3.5 Option Five: Piloted MEV Placement

Mission: 2014 Opposition and a 2016 Conjunction

IMLEO vs MEV placement option is given in figure 9-11. In the first and third columns given below, the piloted MEV is carried with the crew on the piloted MTV. In the second and fourth columns, the piloted MEV is taken on an earlier cargo only flight, ahead of the piloted MTV. This later approach provides a slight total mission IMLEO saving, but adds the necessity of a Piloted-Cargo MTV Mars orbit rendezvous.

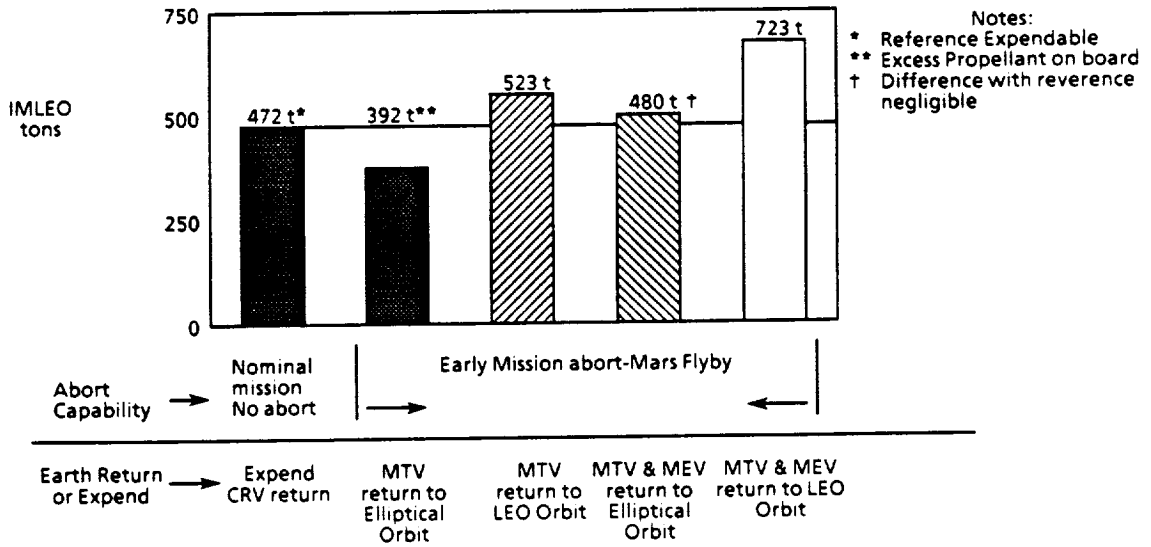


Figure 9-10. 2016 320 Day Transfer Conjunction Mission, Flyby Abort Mode, IMLEO Variation with Earth Return Mode

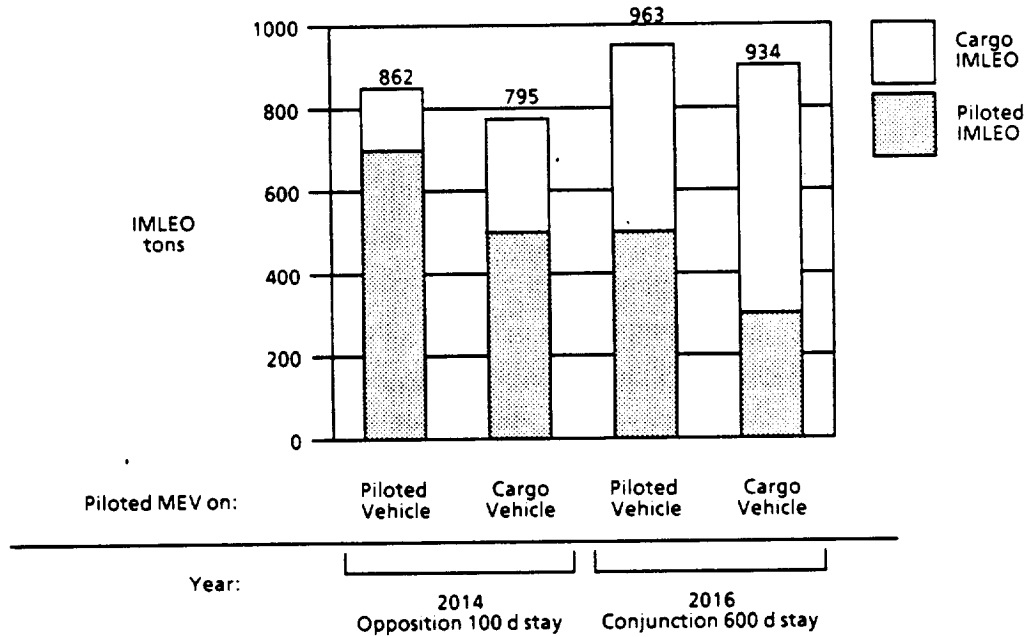







Figure 9-11. 2014 and 2016 IMLEO Variation with MEV Placement

9.3.6 Mars Architecture Vehicle Fleet Development

Five vehicles are illustrated in figure 9-12, with IMLEO figures for three mission options. All cases utilize 250 km by one Sol elliptical parking orbits at Mars. Only the early mission abort capability, discussed earlier, was considered for the last of the five, the 2016 piloted conjunction mission. The three mission options involved varying the piloted mission trip time, and reuse capabilities:

Illustration	Mission Description	Case 1 Fast Piloted transfers	Case 2A Relaxed Piloted transfers	Case 2B same as 2A except Manned Vehicles Reused
	210 Full Lunar Dress Rehearsal, 1 LEV	354	354	354 NTR burn time = 1.3 hr
	2012 One way Cargo to support 2014 1 MEV	173 [147]*	173 [147]*	173 [147]*
	2014 First Manned Mission 100 d stay Opposition, 1 MEV	781	689	2010 Lunar rehearsal veh reuse for 2014: 72 MEV 516 prop + tanks Burn time = 3.4 hr
	2014 One way Cargo Mission to support 2016, 3MEV's	440 d tot transfer 491 [411]*	465 d tot transfer 491 [411]*	491 [411]*
	2016 2nd Manned Mission 600 day stay Conj. swingby abort only	752 210 d transfer	472 320 d transfer	2014 Oppos veh reuse for 2016: 72 MEV 312 prop + tank Burn time = 1.9 hr
Total Fleet IMLEO		2551 [2445]*	2181 [2058]*	1990 [1884] total burn time = 6.6 hr

* Note: Cargo missions; xxx[yyy];
xxx = IMLEO using descent only MEV,
[yyy] = with direct entry MEV

Figure 9- 12. Vehicle Fleet Application to Synthesis Report Mars Architecture

Case (1): The two piloted missions fly fast transfers to and from Mars: 2014 - 440 day transfer opposition, 2016 - 210 day fast transfer conjunction.

Case (2a): The two piloted missions fly relaxed transfers to and from Mars: 2014 465 day transfer opposition, 2016 - 320 day transfer conjunction.

Case (2b): The lunar dress rehearsal transfer vehicle is reused for the piloted 2014 opposition mission, and for the piloted 2016 conjunction mission. The two piloted missions fly the relaxed transfer times as described in Case 2a.

The total fleet IMLEO is given at the bottom, and varies by about 20% between Case 1 and Case 2b. The 2010 lunar vehicle reused again in 2014 and 2016 accumulates approximately 7 hours of engine operation for the three missions. This is below its

estimated operational limit of 10 hours. Cost savings are accrued because the expensive MTV crew transfer habitat module is not expended in the 2010 and 2014 missions.

9.3.7 Identifying Avenues to Fleet Cost

The four elements of risk, IMLEO, capital and operations represent categories through which Synthesis Mars architecture program cost can be accounted. The objective is to illustrate basic cause and effect relationships among variables without utilizing the rather complex terminology found in other methods.

Risk involves structuring mission and vehicle design in order to provide a greater degree of ensured crew safety throughout the mission. Providing fast transfer times to reduce exposure time to solar and galactic radiation is an example. The cost of providing this benefit must be accounted through the element of risk.

IMLEO involves accounting for launch costs.

Capital involves the up front expenditures. One example of accounting cost through this element would be the reuse of costly hardware. By reusing the crew habitat module three successive times (2010, 2014 and 2016 missions), fewer habitat modules are necessary and thus less money is spent on these items.

Operations involves items like the kind and amount of on orbit assembly, scheduling, and testing.

For this evaluation, these four elements represent directions through which other, more specific parameters influence cost, or drive the cost parameter. The options (relating to vehicle applications) considered in this section primarily fall under the category of trajectory options, such as orbit selection, transfer time, etc. Five of these options are listed in figure 9-13 along with the arrow labeled "drivers", and each of these can have an input into cost through the four elements labeled cost "avenues". When each of the five trajectory "drivers" or inputs is considered, it is evident that these elements are primarily directed through the risk and IMLEO elements. That is to say, these five elements influence risk and IMLEO to a relatively large degree, and have little influence on cost through the capital and operations elements. Further evaluation of these five items shows that their influence on risk and IMLEO oppose one another. An example of this opposition between avenues could be taken from either of the five drivers. Reducing risk via decreasing transfer time, or by adding abort capability, increases IMLEO requirements because both of these techniques involve increased delta-V and thus increased propellant loading. However, capital or operations costs are relatively insensitive to variations in propellant loading - the number of costly habitat modules and reactors is not affected by variation in propellant loading. Therefore, decisions

regarding those options primarily influencing only risk and IMLEO can be accommodated later in the design cycle than those items that influence cost primarily via the capital or operations directions.

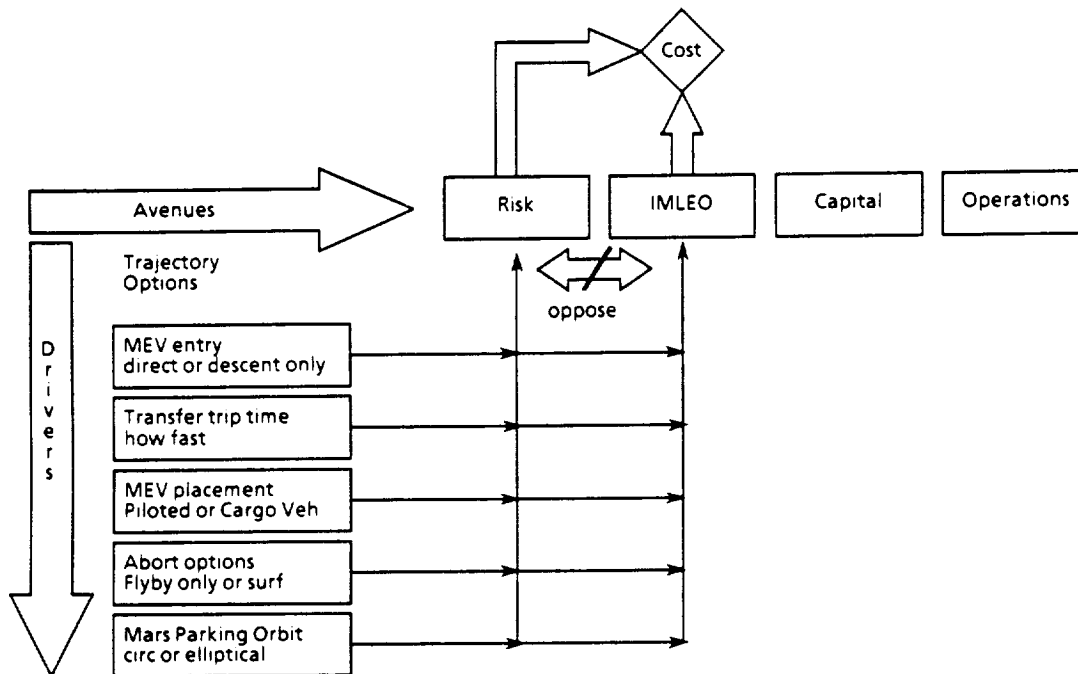


Figure 9-13. Avenues to Mars Architecture Fleet Cost: Trajectory Options

The options (relating to vehicle applications) that fall outside the category of trajectory options are labeled "non-trajectory options". These are vehicle reuse, in-orbit assembly, launch vehicle size and commonality. These are listed along with the arrow labeled "drivers" in figure 9-14, and each can have an input into cost through the four elements labeled cost 'avenues'. When each of the four non-trajectory "drivers" or inputs is considered, it becomes evident when cost is under consideration, that these elements are primarily directed through the capital and operations elements. That is to say, these four elements influence capital and operations costs to a relatively large degree, but have little relative influence to cost through the risk and IMLEO elements (as pertaining specifically to Mars transfer missions). Further evaluations indicate that their influence on cost through capital and operations avenues complement one another. An example of this complementary relationship between avenues could be taken from the vehicle reuse driver. As mentioned earlier, by reusing the lunar dress rehearsal crew habitat module for the following two missions (2014 and 2016), fewer habitat modules are necessary and thus less money is spent on these items. Decisions regarding those options (or items) primarily influencing capital and operations should be accommodated earlier in the

design cycle than those items that influence cost primarily via the risk and IMLEO directions.

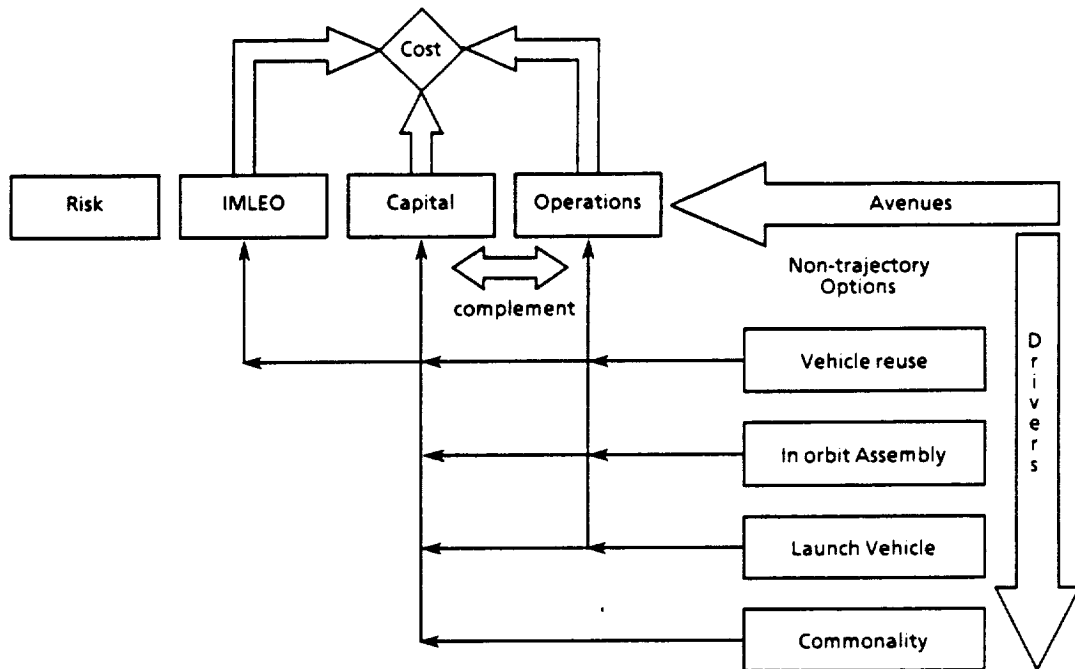


Figure 9-14. Avenues to Mars Architecture Fleet Cost: Non-Trajectory Options

9.4 NTP Baseline and Options

Several reference NTP concepts were developed during Phase 2 of the study. The underlying baseline was the Boeing baseline described in section 2. This baseline used the 2014 piloted mission with a Boeing delta-V set as reference; it had expendable and reusable options. The version illustrated in the figures of section 2 was expendable. A cargo version was derived from this baseline as described in this section.

Four additional reference options were created in support of MSFC ETO (launch vehicle) trade studies: crew and cargo options for 150 t and 250 t launch vehicles. These differed in several ways from the Boeing baseline as summarized in figure 9-15. Also, two further options were created for Architecture white papers. Two of the ETO trade study vehicles were applicable to Architecture No. 1; the Architecture No. 4 vehicles differed only in using oxygen-methane MEVs for compatibility with the *in-situ* materials focus of this architecture.

Attribute		ETO Trade Study Support					
				Architecture White Papers Arch. #1		Architecture White Papers Arch. #4	
Option Title	Boeing Baselines	150-t. Crew	150-t. Cargo	250-t. Crew	250-t. Cargo	250-t. Crew	250-t. Cargo
Mission Reference	2014 Piloted	2014 Piloted	2012 Cargo	2014 Piloted	2012 Cargo	2014 Piloted	2012 Cargo
Delta-V Set Expendable/ Reusable MTV	Boeing Both; drawing sized for reuse	Level 2 Exp.	Level 2 Exp.	Level 2 Exp.	Level 2 Exp.	Level 2 Exp.	Level 2 Exp.
No. of MEVs	1,72 t.	1,78 t.	2,78 t.	1,78 t.	2,78 t.		
Cargo	9 t. with crew 41 cargo cap.	5.7 t.	45 t.	5.7 t.	45 t.	5.7 t.	45 t.
Descent Prop	Cryogenic	Storable	Storable	Storable	Storable	Methane	Methane
Ascent Prop	Storable	Storable	Storable	Storable	Storable	Methane	Methane
MEV L/D	1.8	0.25	0.25	0.25	0.25	0.25	0.25
ETO Payload & Shroud Size	150 t. 12 x 32 m.	115-143 t. 7x35 to 14x30		230 t. 14x30	230 t. 14x30	230 t. 14x30	230 t. 14x30

Figure 9-15. Mars Nuclear Thermal Propulsion Baselines and Options

10.0 CONCLUDING REMARKS

During the early portion of this study, the results from the Stafford Synthesis Report became available. The current study found the Synthesis architectures to be a sound basis for Mars transportation analysis. The Synthesis mission profile strategy begins with an opposition mission, grows to conjunction fast transfer, delivers surface cargo separately, and includes abort requirements in the profile design.

Human lunar missions are an early development target for exploration. STCAEM found that a simple tandem-staged expendable system flying a direct lunar profile had the attributes of (1) fewest development projects for initial return to the Moon, (2) simplest operations, (3) easy access to any lunar landing site, (4) feasibility with a single 150-t-class ETO launch with modest cargo capability, (5) compatibility with a "campsite" early lunar surface mission system, and (6) straightforward evolutionary path to an efficient, economic reusable LOR system.

Because lunar missions are practical with one or two ETO launches, operating efficiency and simplicity demands that lunar missions be designed so that the transportation system operates efficiently. This turns around the usual process of setting somewhat arbitrary requirements and forcing the transportation system to adapt.

STCAEM has consistently identified nuclear thermal propulsion (NTP) as the best choice for Mars transfer propulsion, based on current estimates of performance and cost. Uncertainties associated with NTP performance and cost justify one or more backup technologies until technology advancement efforts reduce the uncertainties. SEP technology needs to be brought along for cargo delivery as a potential backup for Mars transfer propulsion. Aerobraking in some forms is essential to exploration missions: Mars precursors, crew return vehicles for Earth entry, and Mars excursion vehicles, both crew and cargo.

STCAEM investigated high L/D MEV concepts motivated by the view that Mars landing site access has not been adequately addressed as a mission requirement, and when it is, high L/D will be needed to meet the requirement. The high L/D concepts and analyses provide an initial database for highly flexible landing site access.

Significant advances in simplifying on-orbit operations for Mars vehicle assembly without reliance on very large launch vehicles were made. Small payoff in going larger than 150 t was identified for on-orbit operations.

REFERENCES

- 1 "Space Transfer Concepts and Analysis for Exploration Missions," Final Report Phase 1, Boeing Defense and Space Group, Huntsville D615-10030-2, March, 1991
- 2 "America at the Threshold, The Synthesis Group on America's Space Exploration Initiative, May, 1991
- 3 "Report on the 90-Day Study in Human Exploration of the Moon and Mars," NASA, November, 1989
- 4 Fay, J.A., Riddell, F.R., "Theory of Stagnation Point Heat Transfer in Dissociated Air," *Journal of the Aeronautical Sciences*, Vol. 25, February 1958, pp. 54-67
- 5 Tauber, M.E. and Sutton, K., "Stagnation Point Radiative Heating Relations for Earth and Mars Entries," *Journal of Spacecraft and Rockets*, Vol. 28, No. 1, Jan.-Feb. 1991, pp. 40-42
- 6 Pavlosky, James E. and St Leger, Leslie G., "Apollo Experience Report - Thermal Protection Subsystem," NASA TND-7564, January 1974
- 7 Hillberg, L.H., "The Convective Heating and Ablation Program (CHAP), User's Manual," Boeing Document D180-28494-2, Revision A, July 1986
- 8 "Aerotherm Charring Material Thermal Response and Ablation Program," (CMA87S), Acurex Report UM-87-13/ATD, Nov. 30, 1987
- 9 Peng, T.C. and Pindroh, A.L., "An Improved Calculation of Gas Properties at High Temperatures: Air," Boeing Document D2-11722, February 1962
- 10 Savage, R.T., Jaeck, C.L. and Mitchel, J.R., "Investigation of Turbulent Heat Transfer at Hypersonic Speeds," the Boeing Company, AFFDC TR-67-144, Vol III, December 1967
- 11 Engel, C.D., "Lunar Return Aerobraking Wake Flow Investigation, Final Report," REMTECH, RTR 242-02, Aug. 1991
- 12 Sambamurthi, J., Warmbrod, J., and Seaford, M., "Engineering Methodology to Estimate the Aerodynamic Heating to the Base of the Aeroassist Flight Experiment Vehicle," AIAA paper 89-1732, June 1989
- 13 Gnoffo, P.A., Price, J.M., and Brown, R.D., "On the Computation of Near Wake, Aerobrake Flowfields," AIAA paper 91-1371, June 1991
- 14 Hair, L.M., Engel, C.D., Shih, P., Bithell, R., and Bowman M., "Aerothermal Test Data Low L/D Aerobraking Orbital Transfer Vehicle at Mach 10, RTR 069-1, REMTECH, April 1983
- 15 Brant, D.N., and Nestler, D.E., "Development of an Afterbody Radiative and Convective Heating Code for Outer Planet Probes," AIAA Paper 78-862, May 1978
- 16 Engel, C.D., Praharaj, S.C., and Schmitz, C.P., "MINIVER II Upgrade for the AVID System," Volume I: LANMIN User's Manual, REMTECH RTR 123-01, Feb. 1988

